TAILORING THE ELECTRO-OPTICAL PROPERTIES OF Alq₃ DERIVATIVES FOR THE APPLICATION IN ORGANIC LIGHT EMITTING DIODES

Thesis Submitted for the Award of the Degree of

DOCTOR OF PHILOSOPHY

in

Physics

By

Mrinmoy Debsharma,

Registration Number: 11814235

Supervised By

Co-Supervised By

Dr. Alok Jain (12369) (Supervisor)

Associate Professor, Dept. of Physics

Lovely Professional University

Phagwara, Jalandhar

Punjab, India

Dr. Tanay Pramanik (Co-Supervisor)

Professor, Dept. of Chemistry

Institute of Engineering. and Management,

University of Engineering. & Management

Kolkata, W.B., India



LOVELY PROFESSIONAL UNIVERSITY, PUNJAB

2025

Dedicated to my loving parents, Mr.

Basanta Kumar Debsharma and Mrs.

Anjali Debsharma and My dearest better

balf & life partner Arpita and loving son

Mayukh

DECLARATION

In order to fulfil the requirements for a Doctor of Philosophy (Ph.D.) degree, I hereby declare that the work presented in my thesis, "Tailoring the Electro Optical Properties of Alg₃ derivatives for the Application in Organic Light Emitting **Diodes**," is the result of research I conducted under the direction of Dr. Alok Jain, an Associate Professor in the Department of Physics, School of Chemical Engineering and Physical Sciences, Lovely Professional University, Punjab, India. As is customary when reporting scientific observations, credit has been given whenever the work presented here was based on the findings of another researcher. My two mentors are Dr. Tanay Pramanik, Professor of Chemical Engineering at the University of Engineering and Management in Kolkata, West Bengal, India, and my other mentor and former supervisor, Dr. Rupam Mukherjee, Assistant Professor at the Presidency University in Bengaluru, Karnataka, India. No other university or institution has received this work in whole or in part for the purpose of awarding a degree.

Mrinmoy Debsharma

Date:

Reg. No: 11814235

Department of Physics

School of Chemical Engineering and Physical Sciences

Lovely Professional University (LPU)

Jalandhar-Delhi, G.T. Road (NH-1), Phagwara, Punjab (INDIA)-144411

CERTIFICATE

This is to certify that the work reported to the Ph.D thesis entitled "Tailoring the Electro-

Optical Properties of Alq3 derivatives for Application in Organic Light Emitting

Diodes" submitted in fulfillment of the requirement for the reward of degree of Doctor of

Philosophy(Ph.D) in the Department of Physics, School of Chemical Engineering and Physical

Sciences of Lovely Professional University, is a research work carried out by Mrinmoy

Debsharma (Reg. No.. 11814235), is a bonafide record of his original work carried out under

my supervision and that no part of the thesis has been submitted for any other degree, diploma

or equivalent course.

Dr. Alok Jain (Supervisor)

Date:

Associate Professors

Department of Physics

School of Chemical Engineering and Physical Sciences

Lovely Professional University (LPU)

Jalandhar-Delhi, G.T. Road (NH-1), Phagwara, Punjab (INDIA)-144411

(A)

Dr. Tanay Pramanik (Co-Supervisor)

Date: 28.10.2025

Dept. of Chemistry (Professor)

Institute of Engineering. & Management (IEM)

University of Engineering. & Management (UEM),

Kolkata, W.B., India

ABSTRACT

Throughout the past three decades, the most widely used, appealing, and constantly evolving electroluminescent display and solid-state lighting technologies have been small molecules Alq₃ [8-hydroxy quinolinato)aluminium(III)] and Alq₃-derivative-based organic light-emitting diodes, or OLEDs. These technologies operate on the electroluminescence principle. Since its discovery in 1987 by Tang and Van Slyke, organic electroluminescent n-type semiconducting tris (8-hydroxyquinoline) aluminium (Alq₃) powder, a metal chelated complex, has been the most popular OLED material selected for OLED applications. Alq₃'s exceptional blue-green bright luminescence, low cost, simple fabrication method, low operating voltage, and ability to fine-tune the emission wavelength have all contributed to its immense popularity. Alq₃ serves as both an OLED's emissive layer and electron transport layer (ETL). Alq₃ has experienced significant operational limitations, including lower-span durability and steep declines in photoluminescence (PL) and electroluminescence (EL) efficiency, despite its multifaceted applicability. This is primarily due to corrosion, joule heating-induced thermal instability, device deterioration from direct exposure to moisture, air, oxygen, and splashes of water, and the lack of an encapsulated protective shield.

In this study, pure mer-Alq³ was first created in a lab. After that, the following procedures were carried out: purification, collection, characterization, and analysis; thin film deposition, characterization, and analysis; and annealing in a hot-air oven, characterization, and analysis. Distinct from other published works, we discovered the cause of Alq³'s chemical degradation and its subsequent chemical fate. We discovered that after heating Alq³ from 50 to 200 degrees Celsius with an equivalent 50-degrees celsius temperature step in the ambient air, 8-Hq (8-hydroxyquinoline) recrystallizes and once more begins to fluoresce, even more intensely than it did at the annealing temperature of 150 to 200 degrees Celsius. We examined the surface morphology and thermal optical characteristics of the annealed Alq³ and contrasted the outcomes with those of the pristine Alq³. Developing a flexible, low-voltage-driven, full-colour, high-definition OLED with an Alq³ or Alq³ derivative emitter was my second objective. I also wanted to adjust the optical and electrical characteristics using different wavelengths and voltages to improve the device's performance, such as PL and EL efficiency and excellent EQE

and IQE. We created an OLED with a polymeric PEDOT: PSS(polyethylene oxythiophene) as the hole transport layer (HTL) and Alq₃ as the electron transport layer (ETL). Additionally, Alq₃ acts on the emissive layers (EML) of the previously mentioned OLED. We employ a metallic silver paste layer for our opaque cathode, and a transparent ITO- coated PET (polyethylene terephthalate) layer serves as both a high work function transparent anode and a flexible rollable transparent substrate. Our HBL was the V₂O₅ layer, which also served as a buffer layer to keep PEDOT: PSS from oxidizing. Additionally, I focused my attention on creating OLEDs with a longer lifespan, greater stability, and reduced susceptibility to chemical and atmospheric deterioration. Third and fourth, I wanted to dope transitional metal oxide ZnO (zinc oxide) nanoparticles and rare earth metals europium nitrate and neodymium nitrate onto the Alq3 host matrix. I wanted to see how the recombination rate, structural characteristics, electrical properties, and optical properties changed in comparison to pure Alq₃ emitters at three different concentrations: 0.1:1 wt%, 0.2:1 wt%, and 0.3:1 wt%. Additionally, we looked into the EL and PL efficiencies of the manufactured OLED using the three metal- Alq3 nanocomposites as the principal emitters, with the best-performing concentration being 0.3:1 weight percent. In comparison to 0.3 weight percent Nd/Alq₃ nanocomposites, which are three and two times better than pristine Alq3 emitter-based OLED devices, we discovered that the EL and PL intensities and device performances of 0.3 weight percent/Alq3 nanocomposites are the highest. These findings undoubtedly have the potential to expand the new research area in the areas of OLED materials, OLED applications and SSL(solid-state lighting) applications.

ACKNOWLEDGMENTS

I want to express my heartiest gratitude to the Almighty God and Goddesses, as well as to my beloved parents, Anjali Debsharma and Basanta Kumar Debsharma, for bringing me into the world as a human being, for their unending love and support, for their inspiration and bravery throughout my life, and for making it so wonderful, exciting, and joyful. Arpita Acharyya, my amazing spouse, has also been a blessing and the main driving force behind all of my accomplishments. Regarding the academic side of things, I am extremely blessed to have three humble and supportive doctors, Drs. Alok Jain, Rupam Mukherjee, and Tanay Pramanik, who have been like my parents' friends, mentors, and philosophers during my research journey to help me reach my fullest academic potential. Their relentless contributions to my dissertation making and theory understandings were invaluable. Dr. Goutam Pramanik, Dr. Souvik Chatterjee, and his research team at UGC CSR-DAE made our collaboration a highly instructive experience for my research visits. Specifically, the assistance from Presidency University's Dr. Hidayath Ulla in Bengaluru, Karnataka. India is definitely irreversible at any cost. I am grateful to many of my colleagues from the research group at Lovely Professional University in Phagwara, Jalandhar, Punjab, India, including Dr. Simrandeep Kaur, Dr. Bhumika Sharma, and Dr, Owais Amin Jibrin Mohammad, Pravjot Kaur, Rickky Singh, Asha Saini, and Dr. Hamnesh Mahajan, for their tremendous support and assistance as well as for fostering an exciting environment. I am very much grateful to Dr. Kailash Juglan for overcoming various challenges in the lab and academia, including administrative, academic, and lab-related ones. . Here I should mention our two Lab Assistant Nitin Yadav and Manoj Kumar and Ramesh Kumar for their untiring cooperation regarding chemical synthesis glassware make me understand the working procedure of new instrument in lab, chemicals and different logistic support urgently in Laboratory of LPU. Also, my gratitude goes to Anju Kumari, CIF, LPU and Dr. Goutam Pramanik and Dr. Souvik Chatterjee, UGC, CSR DAE, Kolkata and Dr, Hidayath Ulla Sir, Presidency University, Bengaluru, Karnataka for measurement of optical and electrical and electro-chemical properties of my materials. Last but not least, I am incredibly grateful to God for uplifting me, supporting me on his shoulders during my darkest hours, and keeping my spine strong and erect so that I could overcome all of my challenges at the hardest moments of my life.

LIST OF PUBLISHED PAPERS

- 1. Debsharma, M., Pramanik, T., Pramanik, G., Maity, A. R., Jain, A., & Mukherjee, R. (2024). Effect of growth temperatures on the structural and optical properties of bulk tris-(8-hydroxyquinoline) aluminium (III). Applied Physics A, 130(5), 281.
- 2. Debsharma, M., Pramanik, T., Maji, P. S., Maity, A. R., Jain, A., & Mukherjee, R. (2024). Effect of ZnO nanoparticle on morphology and optical properties of yellow emissive bulk Alq3 for OLED application. Optical Materials, 154, 115768.
- 3. Debsharma, M., Pramanik, T., Daka, C., & Mukherjee, R. (2022, May). Recent advances in the electrical and optical properties of Alq3 and Alq3 derivatives based OLEDS. In Journal of Physics: Conference Series (Vol. 2267, No. 1, p. 012159). IOP Publishing.
- 4. B. Sharma, R. Sharma, Simrandeep Kour, M. D. Sharma, O. Amin, A. R. Maity, and R. Mukherjee. "Fractional exponents of electrical and thermal conductivity of vanadium intercalated layered 2H-NbS2 bulk crystal." Indian Journal of Physics 96, no. 5 (2022): 1335-1339. https://doi.org/10.1007/s12648-021-02045-w

ORAL AND POSTER PRESENTATIONS

- Mrinmoy Debsharma presented a paper titled "Recent advances in the electrical and optical properties of Alq3 and Alq3 derivatives based OLEDS" at 2nd RAFAS held in 2021 at Lovely Professional University, Punjab, India.
- 2. Mrinmoy Debsharma presented a paper titled "Tuning structural, optical and thermal properties of bulk Alq3 nanoparticles by thermal annealing for OLED application" in 5th RAFAS held in 2024 at Lovely Professional University, Punjab, India

LIST OF CONTENTS

DECL	ARATION	ii
CERT	IFICATES	iii
ABSTR	RACT	<i>i</i> v
ACKN	OWLEDGMENTS	vi
LIST (OF PUBLISHED PAPERS	vii
ORAL	AND POSTER PRESENTATIONS	vii
LIST	OF CONTENTS	. viii
LIST (OFFIGURES	xiv
LIST O	OF TABLES	. xxii
Chapte	er 1:Introduction	1
1.1	Organic Electroluminescence (EL)	1
1.2	An OLED is used as an EL device	1
1.3	Architectural difference between OLED and LED	1
1.4	Alq3 as EL emitters in OLED	2
1.5	OLED application in flat and flexible full-color displays and as coloring	lights 2
1.6	History of organic electroluminescence	4
1.7.	The architectural design of an OLE8	7
1.8	The important materials or factors for organic electroluminescence	10
1.9	Reliability of OLEDs	20
1.10	Operation/Function of an OLED	21

1.11	Operating mechanism and device physics of an OLED21
1.12	Role of organic semiconductor in an OLED26
1.13	Why are organic semiconductors preferred over inorganic semiconductors for OLED construction?
1.14	Classification of OLED
1.15	Advantages of OLEDs
1.16	Ecological and societal impact/benefits
1.17	Disadvantages35
1.18	Comparison among the Incandescent bulb, CFL, LED, and OLED lights 36
1.20.	Comparison among the characteristics of TFT/LCD, LED, OLED, QLED & µLED displays and television and monitors
1.21.	Practical applications of OLEDs
Refe	rences
Chap	ter2: Literary review, Research gap and Research objective55
2.1	Literary review till date
2.2	Research gap64
2.3	Research Objective & Reference
Chap	ter 3: Materials and method of synthesis and fabrication techniques72
3.1.	Materials used for characterization of surface morphology, optical properties and electrical properties
Refe	rences

chem	ical and structural properties OLED materials93
4.1.	X-Ray Diffraction (XRD)94
4.2.	Fourier Transform Infrared Spectroscopy (FTIR)96
4.3.	Field Emission Scanning Electron Microscopy (FESEM)
4.4.	Energy dispersive X-ray spectroscopy (EDS)
4.5.	UV-VIS spectroscopy99
4.6.	Photoluminescence (PL) spectroscopy102
4.7.	Cyclic voltammetry (CV)105
4.8.	Differential Scanning Calorimetry (DSC)107
4.9.	Thermo gravimetric analysis (TGA)109
4.10.	Source measurement unit or source measure unit or source meter unit (SMU)
4.11.	Electroluminescence and Photoluminescence(EL and PL) analyzer instrument
4.12.	Chromaticity diagram analysis (on the basis of CIE 1931)118
4.13.	Integrating sphere121
4.14.	Instrument
Refe	rence122
Chaj	pter 5: Effect of growth temperatures on the structural and optical properties
of bu	ulk pristine tris-(8-hydroxy quino line) aluminiumIII)130
Abst	ract130
5.1.	Introduction130
5.2.	Experimental Methods132
5.3.	Result and discussion
	A. Morphology Study134

	B. Opti	cal Properties S	Study			138
5.4	Conclu	sion	•••••	•••••	•••••	145
Refe	rences	•••••	•••••	•••••	•••••	146
Cha	pter 6: Iı	nfluence of the	rmally annealed	d nano- crystal	line Alq3	thin film for
flexi	ble	WOLED	and	Solid-S	State	Lighting
appl	ication	• • • • • • • • • • • • • • • • • • • •	• • • • • • • • • • • • • • • • • • • •	• • • • • • • • • • • • • • • • • • • •	• • • • • • • • • • • • • • • • • • • •	152
Abst	ract	•••••	•••••	•••••	•••••	152
6.1.	Introdu	ction	•••••	•••••	••••••	152
6.2.	Experin	nental Methods	•••••	•••••	•••••	155
6.3.	Result a	and discussion	•••••	••••••	•••••	157
(A)	Morpho	ological study	•••••	••••••	•••••	157
(B)	Therma	al Properties	•••••	••••••	•••••	161
(C)	Optical	properties and	Photoluminescer	ice(PL) propert	ies Study	162
(D)	Electro	luminescence p	roperties study	and device per	formance	of the
	Fabrica	ted ITO/PEDO	Γ:PSS/Alq ₃ /Ag st	tructure-based (OLED dev	ice 165
6.4.	Conclus	sion	•••••	•••••	•••••	177
Refer	ences	•••••	•••••	•••••	••••••	178
Chap	ter 7: Eff	ect of ZnO nand	oparticle on moi	rphology and op	otical prop	perties of poly
cryst	alline	yellow	emissive	Alq ₃	for	OLED
appli	cation	•••••	•••••	• • • • • • • • • • • • • • • • • • • •	••••••	184
Abst	ract	•••••	•••••	•••••	••••••	184
7.1	Introdu	ction	•••••	•••••	••••••	184
7.2	Experin	nental Methods	•••••	•••••	•••••	187
7.3	Results	and discussion	•••••	•••••	••••••	189
Α.	Structu	ral and mornhol	logical study			189

B.	Optical property study	•••••	••••••	193
C.	Electroluminescence and device perfor	mance study	•••••	200
7.4. C	Conclusions	•••••	••••••	204
Refe	rences	•••••	•••••	205
Cha	pter 8: To Study the Structural, Optical	and Electrica	al Properties o	of Rare Earth
Eur	opium(III) and Neodymium(III) Ion D	oped Alq3 l	Based Emissiv	ve Layer for
OLE	ED Application and	Solid	State	Lighting
App	lication	• • • • • • • • • • • • • • • •	• • • • • • • • • • • • • • • • • • • •	210
Abst	ract	•••••		210
8.1.	Introduction	•••••	•••••	211
8.2.	What are the major differences betwe			0 0
8.3.	How lanthanides or rare - earth com and electroluminescence of OLEDs			
8.4.	Advantages of wide band gap semicone	ductor	••••••	215
8.5.	Experimental Methods	•••••	•••••	218
8.6.	Results and discussions	•••••	•••••	222
A.	Structural and morphological propert	ies study	•••••	222
В.	Thermal properties study	•••••	•••••	226
С.	Optical properties and photoluminesce	nce (PL) pro	perties	229
D.	Chromaticity diagram analysis (on the	basis of CIE	1931)	237
E.	Electroluminescence properties study	•••••	•••••	239
8.7.	Conclusion	•••••	•••••	245
Refe	rences	•••••	•••••	246
Chaj	pter 9: Conclusion and Scope for Future	Work	••••••	253
9.1 S	ummarv			253

9.1. Scope for a future work	256
9.2. Concise distillation of the thesis's main contributions	256
Bibliography/Abbreviations	258

	LIST OF FIGURES	
Sl. no	Caption/Title	Page No
1.	Figure 1.1: Basic Architecture of OLED	9
2.	Figure 1.2 :(A) Conjugate Bonding (B) energy diagram of π - π * molecular orbitals(C) and (D) conjugate system for conductive polymer	12
3.	Figure 1.3: The schematic representation of the spin pairing of singlet ground energy state, singlet excited state and triplet excited state	15
4.	Figure 1.4: Jablonski diagram	16
5.	Figure 1.5: Diagrammatic representation of outcoupling efficiency	19
6.	Figure 1.6: Schematic workings of an OLED	24
7.	Figure 1.7: Chemical structure of small molecule Alq ₃ and a polymer PEDOT:PSS	26
8.	Figure 1.8: Upper row: Images of AMOLED (first left corner), PMOLED (top row middle), architectural difference between WOLED and QD -OLED (right most corner) & lower row: images of difference between QD OLED and LCD (lower left), architecture of a QD-OLED display	31
9.	Figure 1.9: Comparison among incandescent bulb, CFL bulb, LED bulb and OLED light	36
10.	Figure 1.10: Comparisons among the characteristics of TFT /LCD, LED, OLED, QLED & μLED displays	37
11.	Figure 1.11: Applications of OLED as full color displays and coloring lights	43
12.	Figure 3.1: Chemical structure of Alq ₃ and PEDOT:PSS	74
13.	Figure 3.1A: molecular structure of vanadium pentoxide (left) and Zinc oxide nanoparticle (right)	75

14.	Figure 3.2: Amorphous powder forms of (a) neodymium nitrate hexahydrate, (b) europium nitrate hexahydrate, and (c) vanadium pentoxide	80
15.	Figure 3.3 . Schematic diagram of mer-Alq ₃ nano-particle synthesis (top picture) and Figure 3.4 : Conversion mechanism tris(8 -hydroxyquinoline-N-oxide)	81
16.	Figure 3.5. Schematic diagram of Zinc Oxide nano-particle synthesis	83
17.	Figure 4.1: The schematic-diagram / figure of a X-ray diffraction spectrometer to detect and determine the crystallographic morphological information through powder XRD of any samples.	95
18.	Figure 4.2: Schematic representation of FTIR spectrometer.	97
19.	Figure 4.3:(a) Schematic diagram of working of FESEM with all its components	98
20.	Fig 4.4: Schematic diagram of UV-VIS spectroscopy	100
21.	Fig 4.5: Schematic diagram of photoluminescence spectroscopy	102
22.	Figure 4.6: Block diagram of photoluminescence	103
23.	Figure 4.7.1: The image of agate mortar and pestle used for fine grinding of granular sample into powder	104
24.	Figure 4.7.2.: Image of Athena 500x500 cold press die set box with 12 mm. diameter (left) and KBr press instrument (right)	105
25.	Figure 4.7.3: Schematic diagram of spin-coating technique (left) and image of spin coater machine (right)	106
26.	Figure 4.8. Schematic diagram of cyclic voltammetry and cyclic voltameter	108
27.	Figure 4.9: Image of Differential Scanning Calorimeter (left) and block-diagram of heat flux Differential Scanning Calorimetric Instrument and working principle	110

28.	Figure 4.10: Image of Thermo gravimetric analyzer instrument (left) and schematic diagram of thermo gravimetric analysis technique (right)	112
29	Figure 4.11: Image of schematic diagram of Source Measurement Unit (SMU) (left) and image of Source measurement unit Keithley 2360	114
30	Figure 4.12: Image of Electroluminescence and Photoluminescence analysis scheme	116
31.	Figure 4.12A: Schematic block diagram of workings of EL and PL analysis scheme (right)	117
32	Figure 4.13.: Chromaticity diagram of pure Alq ₃ powder-based ITO/PEDOT: PSS/Alq ₃ /Ag	119
33	Figure 4.14: Block diagram of integrating sphere	121
34	Scheme 5.1 : Schematic diagram of wet-synthesis procedure of Alq ₃	133
34	Scheme 5.2 : Conversion of Alq ₃ to non-emissive polymer 8-hydroxy quinoline- N- oxide (NEP)	134
35	Figure 5.1: XRD spectra of as prepared bulk Alq ₃ (Sample A) and Alq ₃ pellets annealed at (1) 50 °C (Sample –B) (2) 100 °C (Sample- C) (3) 150 °C (Sample -D) and (4) 200 °C (Sample-E)	135
36	Figure 5.2(a): FESEM images of Alq ₃ powder annealed 50 °C having 7500x and 50000x magnification. The inset shows the image for as prepared Alq ₃ without annealing, (b)FESEM images of Alq ₃ annealed at 100 °C (40x & 50000x magnification), (c)FESEM images of Alq ₃ annealed at 150 °C (15000x & 25000x magnification) (d)FESEM images of Alq ₃ annealed at 200 °C (15000x & 25000x magnification)	137

37	Figure 5.3: The plot shows UV-Visible spectroscopy of as- prepared bulk	139
	Alq ₃ (Sample-A), Alq ₃ pellet annealed at 50 °C (Sample-B), Alq ₃ pellet	
	annealed at 100 °C (Sample-C), Alq3 pellet annealed at 150 °C (Sample -	
	D) and Alq ₃ pellet annealed at 200 °C ((Sample-E).	
38	Figure 5.4: FTIR spectra of Alq ₃ powder made pellet annealed at	141
	room temperature (Sample-A), 50 °C (Sample-B), 100 °C (Sample-	
	C), 150 °C (Sample-D) and 200 °C (Sample-E)	
39	Figure 5.5:(a) Fluorescence spectra (b) normalized PL spectra of pure	143
	bulk Alq ₃ at room temperature without annealed state and (c)	
	normalized PL spectra of sample B to E	
40	Figure 6.1: XRD spectra of as prepared bulk Alq ₃ annealed at room	158
	temperature (sample A) and Alq ₃ pellets annealed at (1) 50 °C (Sample B) (2) 100 °C (Sample C) (2) 150 °C (Sample B) and (4) 200 °C	
	B) (2) 100 °C (Sample C) (3) 150 °C (Sample D) and (4) 200 °C (Sample E)	
41	Figure 6.2: FESEM images of (A) without annealed bulk Alq ₃ and bulk	160
	Alq ₃ powder annealed at (B) room temperature (C) 50°C (D)100°C	
	(E)150°C (F) 200°C based on 5000X amplification	
42	Figure 6.3: DSC curves of bulk Alq ₃ powder annealed at (a) room	161
	temperature (b) 50 °C (c) 100 °C (d) 150 °C and (e) 200 °C.	
43	Figure 6.4(A): UV-Vis absorption spectra of Alq ₃ thin film without	163
	annealed at room temperature (RT) & annealed at (b) room temperature	
	(RT) (c) 50 °C (d) 100 °C (e) 150 °C and (f) 200 °C. Figure 6.4(B): the Tauc plot of the Alq 3 thin film(a) without annealed at room	
	temperature (RT) (b) annealed at 150 °C.	
44	Figure 6.5: Normalized photoluminescence (PL) spectra of Alq 3	164
	thin film (a) without annealed at RT & annealed at (b)RT (c)50°C	
	(d) 100°C and (e) 150°C	_
45	Figure 6.6: HOMO –LUMO energy level band gap of Alq ₃ and	166
	PEDOT: PSS based OLED	
46	Figure 6.7: Cyclic voltammogram of the (a) PEDOT: PSS and (b)	167
	Alq_3	

47	Figure 6.8A:(a)Current density vs voltage (J-V) characteristics curve of ITO/ PEDOT: PSS/Alq3 /Ag-based OLED (a) without annealed at room temperature[device1] and annealed at(b)RT (room temperature)[device2](c)50°C[device3](d)100°C [device4]and(e)150°C [device5]& Figure6.8(B)(right picture): L-V(luminance versus voltage) characteristics curve of ITO/PEDOT: PSS/Alq3/Ag-based OLED(a)without annealed at room temperature[device1] and annealed at(b)RT(room-temperature)[device2](c)50°C[device3](d)100°C [device4] and (e)150°C[device 5]	169
48	Figure 6.9(A)[(a)-(e)]: external quantum efficiency (EQE)a vs. current density(η _{ext} -J) characteristics plot of the five ITO/PEDOT:PSS/Alq ₃ /Ag-based OLED devices where emitter layers Alq ₃ were (a) without annealed at room temperature (device1) (b)annealed at room temperature(device2) c)50°C(device3) (d)100°C(device4) and (e)150°C(device 5), Figure 6.9(B) [(a)-(e)]: Power efficiency vs. luminance plot for device1 to device5 Figure 6. 9(C)[(a)-(e)]: Current efficiency vs. current density plot and Figure 6.9(D): EL intensity	172
49	Figure 6.10[(a)-(e)]: Chromaticity diagram of Alq 3 thin film emitter layer of ITO/PEDOT:PSS/Alq3 /Ag-based five OLED devices i.e., device1 to device 5, with greenish -white light emission	175
50	Figure7.1: XRD spectroscopy of (a) ZnO nanoparticles (b) Bulk Alq ₃ powder and (c)Zno:Alq ₃	190
51	Figure 7.2: FESEM images of (a) Pure Alq ₃ Nanorod powder (b) ZnO Nanoparticle (c) 0.1 wt % ZnO /Alq ₃ nanocomposites	192
52	Figure 7.3: UV –Vis spectroscopy of (a) ZnO-NP (b) Alq ₃ powder (c) 0.1wt % ZnO/Alq ₃ Nano-composites (d) 0.2wt % ZnO/Alq ₃ Nano-composites (e) 0.3wt % ZnO/Alq ₃ Nano-composites (f) 0.4 wt % ZnO/Alq ₃ Nano-composites	193
53	Figure 7.4:(A) Tauc plot of (a) Alq ₃ powder (b) 0.1wt % ZnO/Alq ₃ Nano-composites (c) 0.2wt % ZnO/Alq ₃ Nano-composites (e) 0.4 wt % ZnO/Alq ₃ Nano-composites (e) 0.4 wt % ZnO/Alq ₃ Nano-composites (B) Tauc Plot of (a) ZnO Nano-	195

	particles (b) pure Alq ₃ powder (c) 0.1 wt % ZnO/Alq ₃ Nano-composites	
54	Figure 7.5: Fluorescence spectroscopy of (a) ZnO Nano-particle (b) Alq3 and (c) 0.1 wt% ZnO/Alq3 Nano-composites (d) 0.2 wt% ZnO/Alq3 Nano-composites(e) 0.3 wt% ZnO/Alq 3 Nano-composites (c) 0.4 wt% ZnO/Alq3 Nano-composites	197
55	Figure 7.6: Integrated PL peak- intensity variation curve (λ _{ex} =385 nm) for variable ZnO NP concentration (weight percentage or wt%) incorporated over Alq ₃ molecules in ZnO/Alq ₃ Nano-composites	198
56	Figure 7.7: FTIR spectroscopy image of (a) ZnO NP (b) Alq ₃ powder (c) ZnO/Alq ₃ Nano composites	199
57	Figure 7.8: Stacked architecture of ZnO/Alq ₃ nanocomposites-based OLED	201
58	Figure 7.9: (A)chromaticity diagram (B)normalized EL intensity -wavelength plot) (C)Current efficiency vs. current density (η _c - J) plot (D) External quantum efficiency vs. current density (η _{ext} - J) plot (E)Power efficiency vs. Luminance (η _p - L) plot (F) Luminance vs-voltage(L-V) plot (G) Current density vs voltage (J- V) plot and (H) normalized PL intensity vs wavelength plot for ITO/PEDOT: PSS/V ₂ O ₅ /0.3wt% ZnO:Alq ₃ /LiF/Ag (device2)	203
59	Figure 8.1A: Photophysical processes of rare earth complexes	214
60	Figure 8.1: XRD spectroscopy of (a) Bulk Alq 3 powder (b) 0.3 wt%Eu(III)/Alq3Nano-composites(c) 0.3 wt% Nd(III)/Alq 3 Nano-composites	222
61	Figure 8.2: FESEM images of (a) Pure Alq 3 Nano-rod powder annealed at 150°C (inset pure Alq3 powder) (b) 0.3 wt% Eu(III)/Alq3 Nanoparticle (c) 0.3 wt% Nd(III) /Alq3 Nano- composites	224

62	Figure 8.2A: EDS Spectrum 1(left image) for 0.3 wt% Neodymium	226
	/Alq ₃ nano composites and EDS Spectrum 2 (right image for 0.3 wt%	
	Europium/Alq 3/nanocomposites	
63	Figure 8.3: TG curve of (a) Pure Alq ₃ Nano-rod powder annealed	227
	at 150°C(b) 0.3 wt % Nd(III) /Alq 3 Nano-composites and (c) 0.3 wt%	
	Eu(III)/Alq 3 Nanoparticle	
64	Figure 8.4: DSC curves of (a)bulk Alq 3 powder annealed at 150 °C	228
	(b) 0.3 wt % Nd(III) /Alq 3 Nano-composites and(c) 0.3 wt% Eu(III)/Alq3	
	Nanoparticle.	
65	Figure 8.5: (A) UV Vis absorption spectra of (a) Pure Alq ₃ Nanorod powder (b) 0.3 wt% Nd(III)/Alq ₃ Nanoparticle (c) 0.3 wt% Eu(III) /Alq ₃ Nano-composites and (B) Tauc plot of (a) Pure Alq ₃ Nano-rod powder (b) 0.3 wt% Nd(III) /Alq ₃ Nano-composites and (c) 0.3 wt% Eu(III)/Alq ₃ Nanoparticle	230
66	Figure 8.6: Normalized photoluminescence (PL)spectra of (a) Pure Alq ₃ Nano-rod powder (b) 0.3 wt% Nd(III)/Alq ₃ Nanoparticle (c) 0.3 wt % Eu(III) /Alq ₃ Nano-composites	232
67	Figure 8.7: FTIR spectroscopy of a) Pure Alq ₃ Nano-rod powder	233
	(b) 0.3 wt% Eu(III)/Alq ₃ Nanoparticle (c) 0.3 wt % Nd(III) /Alq ₃ Nano-composites	
68	Figure 8.8: Schematic architecture of (a) Device1: ITO/PEDOT:PSS/Alq ₃ /Ag based OLED (b) Device2: ITO/PEDOT:PSS/0.3wt%Nd(III)/Alq ₃ /Ag based OLED and (c) Device3:ITO/PEDOT:PSS/0.3 wt % Eu(III)/Alq ₃ /Ag based OLED	234
69	Figure 8.9: Schematic energy level of (a) Device1: ITO/PEDOT:PSS/Alq ₃ /Ag based OLED (b) Device2: ITO/PEDOT:PSS/0.3wt%Nd(III)/Alq ₃ /Ag based OLED and (c) Device3:ITO/PEDOT:PSS/0.3 wt % Eu(III)/Alq ₃ /Ag based OLED	235

70	Figure 8.10: Chromaticity diagram of pure Alq ₃ powder based	238
	TO/PEDOT:PSS/Alq ₃ /Ag	
71	Figure 8.11 :(A) Current density vs voltage (J-V) plot (B) Luminance vs-voltage(L-V) plot for (a) ITO/PEDOT:PSS/V ₂ O ₅ /Alq ₃ /Ag (device1) (b) ITO/PEDOT:PSS/V ₂ O/0.3wt% Nd(III):Alq ₃ /Ag (device2)and (c) ITO/PEDOT:PSS/V ₂ O ₅ /0.3wt%Eu(III):Alq ₃ /Ag (device 3)	240
72	Figure 8.12 :(A) Current efficiency vs. current density (η _c -J) plot (B)Power efficiency vs. Luminance (η _p - L) plot for (C) External quantum efficiency vs. current density (η _{e xt} -J) plot for (a) ITO/PEDOT:PSS/V ₂ O ₅ /Alq ₃ /Ag (device1) (b) ITO/PEDOT:PSS/V ₂ O/0.3wt% Nd(III):Alq ₃ /Ag (device2) and (c) ITO/PEDOT:PSS/V ₂ O ₅ /0.3wt%Eu(III):Alq ₃ /Ag (device 3)	242
73	Figure 8.13: Electroluminescence intensity versus wavelength(EL - λ) plot for different voltage ranging from 3V to 9V for (a) (b) ITO/PEDOT:PSS/V ₂ O ₅ /0.3wt% Nd(III):Alq ₃ /Ag (device2) and (c) ITO/PEDOT:PSS/V ₂ O ₅ /0.3wt%Eu(III):Alq ₃ /Ag (device 3)	243
74	Figure 9.1: PL intensity decay or fluorescence average lifetime plot	255

LIST OF TABLES

	LIST OF TABLES	
SL No.	Caption/Title	Pages
1.	Table1.1: Comparison among the Incandescent bulb, CFL, LED and OLED lights	38
2.	Table 1.2. Comparisons among the characteristics of TFT /LCD, LED, OLED, QLED & μLED displays	41
3.	Table 5.1: The morphological details of bulk Alq ₃ powder (Sample-A) and four annealed Sample-B, Sample-C, Sample-D and Sample-E	136
4.	Table 6.1 : Comparison table between HOMO- LUMO value of PEDOT:PSS and Alq ₃	168
5.	Table 6.2: EL properties and device performance related to summarized data of the ITO/PEDOT:PSS /V ₂ O ₅ /Alq ₃ /LiF/Ag-based five OLED devices i.e., device1 to device 5, with greenish-white light emission	173
6.	Table 6.3: Chromaticity diagram data of Alq ₃ thin film emitter layer of ITO/PEDOT:PSS/ V ₂ O ₅ /Alq ₃ /LiF/Ag-based five OLED devices i.e., device1 to device 5, with greenish-white light emission	176
7.	Table 7.1: Structural comparison table for Alq ₃ , ZnO NP, ZnO /Alq ₃ Nano-composites	191
8.	Table 7.2: comparative study of optical band gap with respect to concentration increase of Zno NP within Alq ₃	196
9.	Table 7.3: Comparative chromaticity data of Alq ₃ powder annealed at 150°C ITO/PEDOT:PSS/V ₂ O ₅ /Alq ₃ /LiF/Ag (device1) and 0.3 wt % ZnO nanoparticle incorporated Alq ₃ nanocomposites-based OLED devicesITO/PEDOT:PSS/V ₂ O ₅ /0.3wt% ZnO:Alq ₃ /LiF/Ag (device2)	204

10.	Table 7.4: Comparative electroluminescence and device performance oriented data of Alq 3 powder annealed at 150°C ITO/PEDOT:PSS/V ₂ O ₅ /Alq ₃ /LiF/Ag (device1) and 0.3 wt % ZnO nanoparticle incorporated Alq 3 nanocomposites- based OLED devices ITO/PEDOT:PSS/V ₂ O ₅ /0.3wt% ZnO:Alq ₃ /LiF/Ag (device2)	204
11.	Table 8.1 : Comparative data analysis of Eu(III) and Nd(III) ion's electronic configuration	216
12	Table 8.2 : Structural comparison table and crystallographic details of Alq ₃ , Eu(III)/Alq ₃ and 0.3 wt % Nd(III)/Alq ₃ nanocomposites respectively	223
13	Table 8.3 : Comparative data of EDS spectrum of 0.3 wt% Neodymium /Alq ₃ nano composites and EDS Spectrum 2 for 0.3 wt% Europium/Alq ₃ /nanocomposites	225
14	Table 8.4. Comparative analysis of TG and DSC curves of three samples	229
15	Table 8.5: Comparison table for device HOMO LUMO energy levels of each constituent charge carrier conducting and emissive layer materials of OLED device 1, OLED device 2 and OLED device 3	236
16	Table 8.6: Comparative chromaticity data analysis of four samples (a) (b) (c) and (d)]	239
17	Table 8.7: Comparative analysis of device performances of three OLED devices	244

Chapter 1: INTRODUCTION

1.1 Organic Electroluminescence (EL):

The electrical and optical phenomenon known as electroluminescence (EL) occurs when a substance or sample of interest is subjected to a strong electric field or to a strong electric current. When an electrical excitation bias (such as current or voltage) passes through a solid, light is released. This phenomenon is known as electroluminescence. In organic electroluminescence, light is produced only by organic molecules that contain hydrogen and carbon, along with other elements like nitrogen (N), sulphur (S), and oxygen (O). One noteworthy aspect of organic EL is that, unlike incandescence, which emits light from a hot filament in an incandescent lightbulb, organic EL does not cause the solid to change from ambient temperature [1-5].

1.2 An OLED is used as an EL device:

OLED (Organic Light Emitting Diode) is a contemporary opto-electronic electroluminescent device consisting of an organic emissive layer sandwiched between a high-function transparent anode (typically ITO) and a low-function metallic cathode. This technology is used in flat-panel displays found in Android smartphones, laptops, tablets and smartwatches. OLED displays have a full colour gamut, are lightweight, and consume little power or energy. OLEDs have a simpler structure than LCDs (liquid crystal displays). It can contain more than one organic layer to accelerate the flow of free charge carriers. The cathode and anode inject charge carriers, i.e., electrons and holes, when an electric current is applied, and these particles flow into the organic emissive layers before recombining to form extremely unstable neutral Frenkel excitons. This unstable exciton jumps to the ground energy state, releasing photon energy as light. Lights are thus emitted by the emissive layer. The emission of light energy subject to an electric field is known as Electroluminescence (EL) [1-3, 7, 9-10, 12].

1.3 Architectural difference between OLED and LED:

Although OLED refers to LED, their architecture fundamentally differs from each other.

A p-n junction diode structure serves as the foundation for LED formation. Trivalent or pentavalent atoms must be doped to alter the conductivity of the charge carrier in the host intrinsic semiconductor (germanium, silicon) in order to create n- and p-regions. OLEDs, however, do not adhere to the p-n junction diode structure of LEDs. In OLEDs, doping is used to change how quickly electrons and holes combine, which helps improve both their recombination rate and how efficiently they emit light. Furthermore, the wavelength of the released photon can be ascertained through doping. [7, 13, 14]

1.4 Alq₃ as EL emitters in OLED:

In this research study, we focused on creating flexible OLEDs made from Alq3 and its derivatives that are efficient in light emission and photoluminescence, require low voltage, and are cost-effective, while also examining the electro-optical properties of the new Alq3 material, particularly the emission layer, electron transport layer, and hole transport layer, in normal conditions. OLED material, especially EML, ETL, and HTL, under ambient conditions. Alq3 is an octahedral coordinated organometallic chelated compound, also known as Tris(8-hydroxyquinolinato) aluminium [Al(C9H6NO)3]. Using bidentate bonding, three 8-hydroxyquinoline ligands (Hq or HQ) stay linked to the core metal atom, aluminium, in Alg₃, a chelated salt of Al³⁺ cation and three 8-HQ[(C₉H₆NO-1)] anion. In Alq3 each hydroxyquinoline ligand has two aromatic functional groups: phenoxide and pyridyl groups. When we substitute the C-4, -5, -6, and -7 corners of the pyridine or phenoxide rings (benzene rings) with the right functional groups, like alkyl, aryl, amino, or any metal or radical (i.e., substituents), 8-hydroxyquinoline (or 8-HQ) ligands play a crucial role in the emission of different coloured lights in this scenario. In this case these type substitutions can tune the HOMO energy level as well as the emission wavelength of the emission spectrum. Alq₃ possesses a conventional bidentate [M(NO)₃] structure of chelated octahedral coordination complex salt in which M stands for metallic trivalent atom of the quinoline ring, N represents the nitrogen atom of the quinoline rings, and O is the oxygen atom of the quinoline ring [2, 3, 4, 5, 14].

1.5 OLED application in flat and flexible full- color displays and as coloring lights:

The development of OLED, or organic light-emitting diode, or organic electroluminescent diode-based displays have been able to bring the whole world to our fingertips. We can witness any event happening anywhere in the world being known in real time by pressing and scrolling on the OLED display screen of any electronic gadget, like a smartphone, tablet, laptop, or smart flat or curved OLED TV. All the electronic devices or technology used by people in their daily life, from waking up in the morning to going to bed at night, are unthinkable without any OLED display unit or OLED lighting. Flat full-colourproducing OLED displays are widely used in smartwatches, smart OLED TVs, smart Android phones, and smart windows. OLED base small displays have a variety of applications in our daily appliances, such as electronic digital display screens and indicators or sensors used in induction cookers in kitchens, geysers in bathrooms, modular switch indicators, music system indicators or party lights, indicators or sensors used in Bluetooth devices, displays and indicators used in cellphones, neckband Bluetooth headphones, earbuds, headphones, displays used in digital watches, thermometers, glucometers, oximeters, oscilloscopes, and treadmills for medical purposes, etc. OLED lights are used in architectural design lighting, car lighting, decorative lighting, spacesaving lighting, etc. OLEDs nowadays have achieved enormous popularity, leaving LCD, LED and other display counterparts of OLED for crispy pictures, perfect black and fullcolour high-definition images, quick refresh times, less voltage-driven operation, flexibility, less heat production, cost-saving fabrication and excellent EQE (external quantum efficiency) along with improved internal quantum efficiency (IQE) of the device. Constant research has been conducted to enhance the performance of QLED and micro-LED technologies. But still far away from reaching the benchmark set by the OLED market. But when OLED is used as a light source, it drives the incandescent bulb, CFL and halogen bulb but still could not beat the commercial market of LED light because of the lower cost. LEDs produce brighter, glare-free cool light. While OLED lights are limited to high-end automotive lighting, car or residential or commercial building's decorative light applications have higher manufacturing costs. The top OLED manufacturing company has been clinging to lowering the manufacturing cost by applying new organic emitters and new low-cost manufacturing techniques. Hence, undoubtedly, we can say that OLED will be the best choice for solid-state lighting for general purposes and also highend multi-dimensional applications. In the next section of this chapter 2 discuss the comparison or difference of OLED with their display as well as lighting counterparts [14-25].

1.6 History of organic electroluminescence:

In 1960, Martin Pope and his team witnessed the first injection of a dark hole into an anthracene crystal (organic compound). This groundbreaking discovery also described the energy requirements for injecting electron-hole connections [3]. The primary direct current electroluminescence (EL) of both single crystal and impurity-doped anthracene was detected by the same group three years later. The devices produced visible emissions over 400 volts and had a thickness of 10–20 μm [3]. The 10-20 μm thick EL devices were produced to emit visible emissions of more than 400 volts [3]. The history of organic lightemitting diodes (OLEDs) began in 1977, when Prof. Shirakawa and a colleague successfully synthesized the first semiconducting polymer by adjusting its chemical doping [2]. Prof. Shirakawa received the 2000 Nobel Prize in Chemistry for this discovery. Following this, Helfrich and Schneider successfully produced EL in the case of single organic anthracene crystals via doubly injected recombination utilizing electron- and holeinjecting electrodes, i.e., cathode and anode correspondingly. To obtain noticeable emission, the operating voltage was dramatically lowered to around 60 V. According to Child's law, the estimated electron mobility is about $0.4 \text{ cm}^2/(\text{V.s})$. The device's thickness of 1-5 mm limited the current to 10 A at 100 volts [3]. In 1982, Vincent and his associates used vacuum-deposition techniques to achieve EL using a 0.6 µm organic thin film. The operating voltage was substantially lowered to less than 100 V, accompanied by a low EQE (external quantum efficiency) of 0.05% [4]. Tang and his associates developed a new structure for electron and hole transport in the 1980s that consisted of two thin organic film layers (with a total thickness of approximately 135 nm). As amorphous and crystal organicbased EL systems advanced in the mid-1970s, researchers started studying polymers, probably because of their increased processability. Poly(vinylcarbazole) (PVCz) film was used in the UK's National Physical Lab's first successful attempt to produce polymer LEDs [6]. In 1990, Friend and associates reported a green electroluminescent, highly efficient poly(p-phenylene vinylene) (PPV) thin film (100 nm). via spin-coating When injected

electrons and injected holes were recombined mutually and underwent a radiative decay of singlet excitons, which was known as the EL of the EL device. A significant current injection threshold of 14 V with an EQE of 0.05% was reached [7]. Using platinum octaethylporphine (PtOEP), a phosphorescent dopant material, Baldo harvested triplet excitons, surpassing the 25% limitation of its internal quantum efficiency (IQE) limit [8]. A maximum EQE of 4% was achieved in 1998. This was yet another crucial turning point following Tang's revelation. Following that, using a phosphorescent dopant in a highbandgap host, Adachi et al. increased the EQE to roughly 22%, or nearly 100% IQE [9]. The small molecules, polymers, and dendrimers used in OLED materials have gained a lot of attention over the last ten years. Usually, a dendrimer consists of dendrons, surface groups and the core. It is possible to independently optimize the electrical and processing properties of surface groups and cores. The intermolecular interactions necessary for the device's operation are controlled by the number of dendrons. Furthermore, the cores make it easy to access fluorescence and phosphorescence. Lo et al. used phosphorescent conjugated dendrimers in 2002 [1-3] to achieve device performance comparable to evaporated molecules at the time and five times that of polymers [10]. In 1987, C.W. Tang et al. [4] described a bi-layered OLED thin film made of organic ETL layer Alq3 [Tris(8hydroxyquinolinato)aluminium(III)] and aromatic hole transport layer (HTL) layer diamine. Alq₃ has grown in popularity due to its exceptional blue-green dazzling luminosity, low production costs, simple manufacturing process, low operating voltage, and ability to fine-tune emission wavelength. Despite its versatility, Alq3 has significant operational limitations, including shorter lifespans and a sharp decline in photoluminescence (PL) and electroluminescence (EL) efficiency over time. The new OLED was impressive with an EQE of 1% photon/electron, a high luminous efficiency of 1.5 lm/W, and a luminance of over 1000 cd/m².

Over the last few decades, numerous intriguing discoveries have been made as a result of ongoing efforts to improve the efficiency of Alq₃-based OLEDs. Tang et al. [1, 3] also demonstrated that incorporating fluorescent organic dyes into the host organic Alq₃ matrix can significantly increase an OLED's efficiency by improving energy transfer from the host layer to organic dye layers, resulting in higher EL and PL quantum efficiency. At the C-5

position of the benzene (phenoxide ring), -SONR₂, a powerful electron-donating group in Alq₃, was described by Armstrong and his colleagues as having a higher blue shift of green luminescence at 580 nm than at 514 nm of parent Alq3.,Al(Meq)3[tris(4-methyl-8hydroxyquinoline)aluminum],Al(Cl₂q)₃[(tris(5,7-dichloro-8-hydroxyquinolinato) aluminium)],andB(Alq)2[bis-(2-methyl-8-hydroxyquinolinato)-4-(phenylphenolato) aluminium(III), and showed current densities of 4.3 cd/A, 8.7 cd/A, and 6.8 cd/A, and maximum luminance of 31839 cd/m², 35256 cd/m², and 33714 cd/m², respectively. In 2011, the 11H-indolo[3,4]quinolin-4-ol complex, the Alq3 derivative, was synthesized by J.P. Heiskanen et al. [19]. Its photoluminescence is 3.5 times better than that of parent Alq3. Paez-Sierra, B.A. et al. in 2016. Investigated the PL efficiency of MEH-PPV (poly(2-methoxy-5-(2'-ethylhexyloxy)-(p-henylenevinylene)) doped Alq3 nanocomposites by varying concentrations of MEH PPV dopant where the work function is 2.19 eV and energy band gap is nearly equal to 2.33 eV. A hetero junctionOLED based NPB(N,N'-di(naphthalene-1-yl)-N,N'-diphenyl benzidine)), (molybdenum oxide) was reported by Jiayi Song et al. in 2023. It had a brightness of 46040 cd/m². [12–14]. The reasons behind the decline and limitations of quantum efficiency are still up for debate, notwithstanding the reports mentioned above.

Furthermore, researchers have complicated and increased the cost of the synthesis process in an attempt to improve PL and EL efficiency. After 1987, researchers began using RE complex-dependent or RE coordination compound-based OLEDs in large numbers. [26-37]. Salah et al. [28-30] documented the integration of Alq³ thin-film nanostructures with various metals from 2013 to 2020, including silver (Ag), europium (Eu), copper (Cu), dysprosium (Dy), and terbium (Tb). To be more specific, the PL intensity of the lanthanides dye-incorporated Alq³ (Dy/Alq³) thin film was four times that of the pure Alq³ thin film. [27:28]. In 2002, Reyes, R. et al. [32] synthesized the complex of samarium, i.e., [Sm(TTA)³(TPPO)²] [tris(thenoyl trifluoro acetonate) bis(triphenyl phosphine oxide) samarium] to determine whether the samarium complex could be utilized as both an ETL (electron transporting layer) and EML (emissive layer) and then built the two devices. and used the following architecture to demonstrate how their EL performance varied. Here, Device 1 represents [Sm(TTA)³(TPPO)²] /ITO/MTCD/Alq³/Al, and Device 2 represents

Sm(TTA)₃(TPPO)₂]/[ITO/MTCD/A1. In 2002, they once again revealed the vacuum deposition approach for fabricating europium complex [Eu(TTA)₃(TPPO)₂]. OLED based on the, and they investigated the electroluminescence (EL) performance of the Eu³⁺ cationdoped Alq₃.source. In 2010.the introduction of a luminous silver(I) chalcogenide nanocluster that emits red light was demonstrated. The year "2011" saw the discovery of a hybrid material based on copper iodide that emits green light, also known as greenelectroluminescence. [18]. According to a 2011 study conducted by Muhammad Saleh Al Salhi et al., the electroluminescent conjugated polymer emits light when an electric current passes through it. It is a luminescent polymer. This posed a significant challenge for lightemitting diodes, polymer laser systems, and inorganic semiconductor materials [1]. Highly emissive hybrid white light emitters based on II-VI semiconductors were introduced in 2012. C.K. Pandey et al. (2018) investigated the impact of n-type doping on the electron transport of polyfluorenes and achieved trap-free electron transport for PFO-based diodes by deactivating the exponentially distributed deep energy traps [18]. In 2023, Myrid Ali Siddiq [31] developed two devices using the tris-(8-hydroxyquinoline)aluminium/yttrium oxide (Alq₃/Y₂O₃) nanocomposite and Alq₃.. These devices displayed the designs Ag/Alq₃/p-Si/Al and Ag/Alq₃:Y₂O₃/p-Si/Al. They then investigated these devices' electrical properties in both light and dark environments. Still, researchers from all over the world are looking for new OLED materials, such as organic semiconductors, emissive layers, metal-organic layer interfaces, conductive polymers, and various metal complexes of Alq₃ [1-8, 14-18, 25-37].

1.7. The architectural design of an OLED:

Basically, an ideal OLED is a stack of six successive layers. The topmost layer is a metallic cathode, and the bottom layer is a transparent substrate. Apart from these organic emitting material-based emissive layers (EML) or host layers, it lies in between two conducting layers: the electron transport layer (ETL) and the hole transport layer (HTL). The metallic cathode is a low work function metal, and the transparent anode is made up of indium tin oxide compound (ITO). The cathode and anode are directly connected to the battery for passage of current through the OLED circuit.

An ideal OLED possesses the following six successive stacked layers from top to bottom

- 1)Cathode layer: when electricity flows through an OLED device, the cathode layer (the top layer of the OLED) sends electrons into the host/emissive layer (EML) through the electron transport layer (ETL) and the blocking layer (BL). Depending on the kind and variation of OLED we need to manufacture, this layer can be either transparent or opaque. Typically, an OLED's opaque cathode layer is made of four metals with low work functions:
- 2)Electron transport layer (ETL): This layer aids in moving the cathode-injected electrons from the OLED's cathode layer to the blocking layer, which is the next layer. Stereotypical ETL uses both TPBI (1,3,5-tris(N-phenylbenzimidizol-2-yl)benzene and BCP (bathocuprene), PBD (2-(4-biphenyl)-5-(4-t-butylphenyl)-1,3,4-oxadiazole), and Alq₃ (tris(8-hydroxyquinoline) aluminium). In this case, NPB or Alq₃ might be used.[18] 3)Emissive layer (Host and PHOLED Emitter): The emissive layer of OLED drives electrons out of the anode layers. The core or heart of an OLED device is thought to be this
- electrons out of the anode layers. The core or heart of an OLED device is thought to be this layer. Light emission and the direct conversion of electrical energy to light energy occur only in this layer. Different colour-producing emitters that have been doped into the host layer make up this layer. These emitters are often phosphorescent and fluorescent dyes in terms of chemistry. Organic plastic and polymer molecules can emit light with a broad spectrum of wavelengths, intensities, and colours, depending on the processing factors and emissive materials utilized. We used Alq3 as our emissive material for the EML of our fabricated OLED in our research work. [18,19]
- **4)Hole transporting layer (HTL):** This layer moves the holes that are injected from the anode layer from the HIL layer to the OLED's emissive layer. Organic compounds based on triphenylamine functional groups are typically employed as hole transporting layers (HTLs) because of their exquisite optoelectronic characteristics, such as greater hole mobility and increased electron donating capacity. We used PEDOT: PSS as our HTL. It's an organic fluorescent dye. [35, 37-44]
- **5)Transparent anode layer:** This OLED layer is referred to as the active layer. This layer is composed of indium tin oxide (ITO), a material with a high work function that is optically transparent and conductive. This layer removes electrons and injects holes into

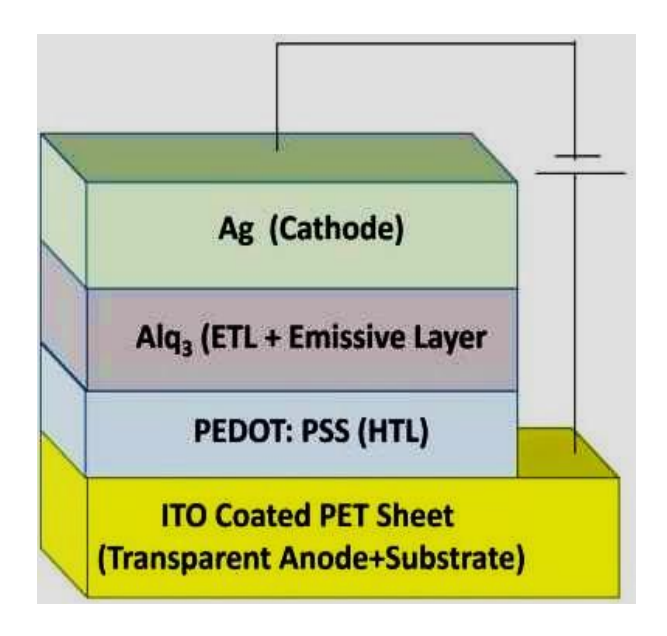


Figure 1.1: Basic Architecture of OLED

the emissive layer (EML) of the organic semiconducting layer at the highest occupied molecular orbital (HOMO) energy level. This layer removes electrons, which are then replaced by electron holes in response to electric current. The bottom layer of the anode is a transparent thin coating of ITO (indium tin oxide) that is applied to the substrate's surface, often a glass layer. These days, an organic conductive layer functions similarly to an optically transparent electrode that is transparent to visible light. The traditional ITO electrode, which uses conductive polymeric organic dyes PEDOT: PSS [poly(3,4-ethylene dioxy thiophene)poly(styrene sulphonate)], sulphonate)], by this transparent ITO electrode. This substance PEDOT: PSS energy level falls between the ITO's work function and the HOMO of other typical polymers. During the hole injection process, the polymer material's HOMO energy level aids in lowering the energy barriers. [35-44]

6)Substrate layer: This layer is composed of materials such as plastic, metallic foil, and glass (SiO₂) For OLED (synthesis and characterization of conductive polymers with increased solubility), this layer serves as a base, a supporting layer, or a foundation. The OLED device is referred to as a bottom emission device when the light it emits passes through its see-through substrate layer. In our research work we use transparent ITO-coated PET (poly tri ethylene terephthalate) sheet as substrate. In order to enhance the EL and PL efficiency of an OLED, two additional layers can be introduced:

In order to enhance the EL and PL efficiency of an OLED, two additional layers can be introduced:

7)Blocking Layer (BL): There are two types of blocking layers: EBL (electro- blocking layer) and HBL (hole-blocking layer). s layer confines injected electrons and holes within the EML and prevent them from returning back to ETL and HTL, respectively, and similarly confines injected holes from HTL into the host layer along with preventing them from backward flow to ETL and HTL, respectively. and thus, advancing OLED technology. Generally, EBL lies in between ETL and EML, and HBL lies in between HTL and EML. In our OLED we use Alq₃ as EBL and V₂O₅ as HBL layer

8)Injection layer (IL): There are two types of injection layer: electron injection layer (EIL) and hole injection layer (HIL). The HIL lies in between the transparent anode and the HTL. When an anode-injected hole reaches this layer, the holes take it in and then inject it again into the HTL layer. Similarly, the EIL layer lies in the middle of the cathode and ETL and helps to inject cathode-injected electrons into the ETL layer again. Your HIL was PEDOT: PSS, and the EIL layer was Alq₃.[18-25].

1.8 The important materials or factors for organic electroluminescence:

Basically, OLEDs are of two types: (1) small molecule-based OLEDs and (2) polymer-based OLEDs. Conductive polymers (or intrinsically conductive polymers, i.e., ICPs) are basically organic polymers which can be distinguished from other polymers for their lower mechanical properties but higher electrical conductivity due to the presence of a π -conjugated bond. Conductive polymers exhibit metallic conductivity, semiconducting characteristics, and processability through dispersion. Conductive polymers do not possess thermoformability properties like thermoplastics. Unlike other polymers, by using innovative dispersion techniques and organic synthesis, the electrical properties of organic conductive polymers can be finely tuned. [41]

1) Organic semiconductors: Organic semiconductors are the materials, which can be anything from tiny molecules to polymers, that have the ability to transfer charge. However, unlike conductors, which have free-flowing electrons, organic semiconductors depend on a structure mainly made up of hydrogen and carbon atoms and occasionally heteroatoms such as nitrogen (N), sulphur (S), and oxygen (O). For example, pentacene,

polythiophene, and polyacetylene. The polymeric molecular backbone chains of organic semiconducting materials exhibit π (pi)-conjugated bonding, which alternates between single and double bonds or single bonds. sp² hybridization is the process that creates these bonds. Three hybridized orbitals are created by the carbon atoms' two p-orbitals and one s-orbital during bond formation. Only one of the three hybridized orbitals can form a strong sigma (σ) bond with the polymerics' neighboring carbon atoms. In order to hold the entire polymeric backbone arrangement, the hybridized orbitals form a plane. The remaining Pz orbitals that are not hybridized stay perpendicular to the plane of the polymer molecular chain formed by those hybridized orbitals [35-44, 45, 46, 47].

Role of organic semiconductor in an OLED: The polymer chain's un-hybridized P_Z orbitals of two neighboring carbon atoms overlap sidewise to form a weak π (pi) bond, which causes the electrons to delocalize and flow freely inside the molecule along the polymeric backbone chain. In organic semiconductors, the unrestricted flow of electrons encourages semi-conducting characteristics. In our study, we employ PEDOT: PSS as a conjugated polymeric p-type polymeric semiconductor and Alq₃ as a small molecule n-type semiconductor [28, 44, 48-54].

- 2) Conjugated polymers: Conjugated polymers are organic macromolecular materials comprising alternating single and double bonds (or other types of pi (π) bonds) along their backbone chain, which results in delocalized pi (π) electrons for charge transport similar to that of semiconductors or even conductors. e.g., PVV, PEDOT: PSS, etc. Our study made use of poly(alkyl thiophene) (PEDOT) [14, 45, 54-60].
- 3) Conjugate bonding or conjugation: In organic conjugate polymers, there are alternating single and double bonds, along with each atom providing a p-orbital perpendicular to the molecular plane, which is known as conjugate bonding, and the process of bonding is known as conjugation (Figure: 1.2). Conjugation refers to the overlapping of one p-orbital with another across an adjacent sigma (σ) bond (d-orbitals are involved in transition elements). An organic molecule with conjugate bonding has a set of delocalized phenoxide rings (benzene rings) with the right functional groups, like alkyl, aryl, amino, or any metal or radical (i.e., substituents), 8-hydroxyquinoline (or 8-HQ) ligands play a crucial role in the emission of different coloured lights in this scenario. In

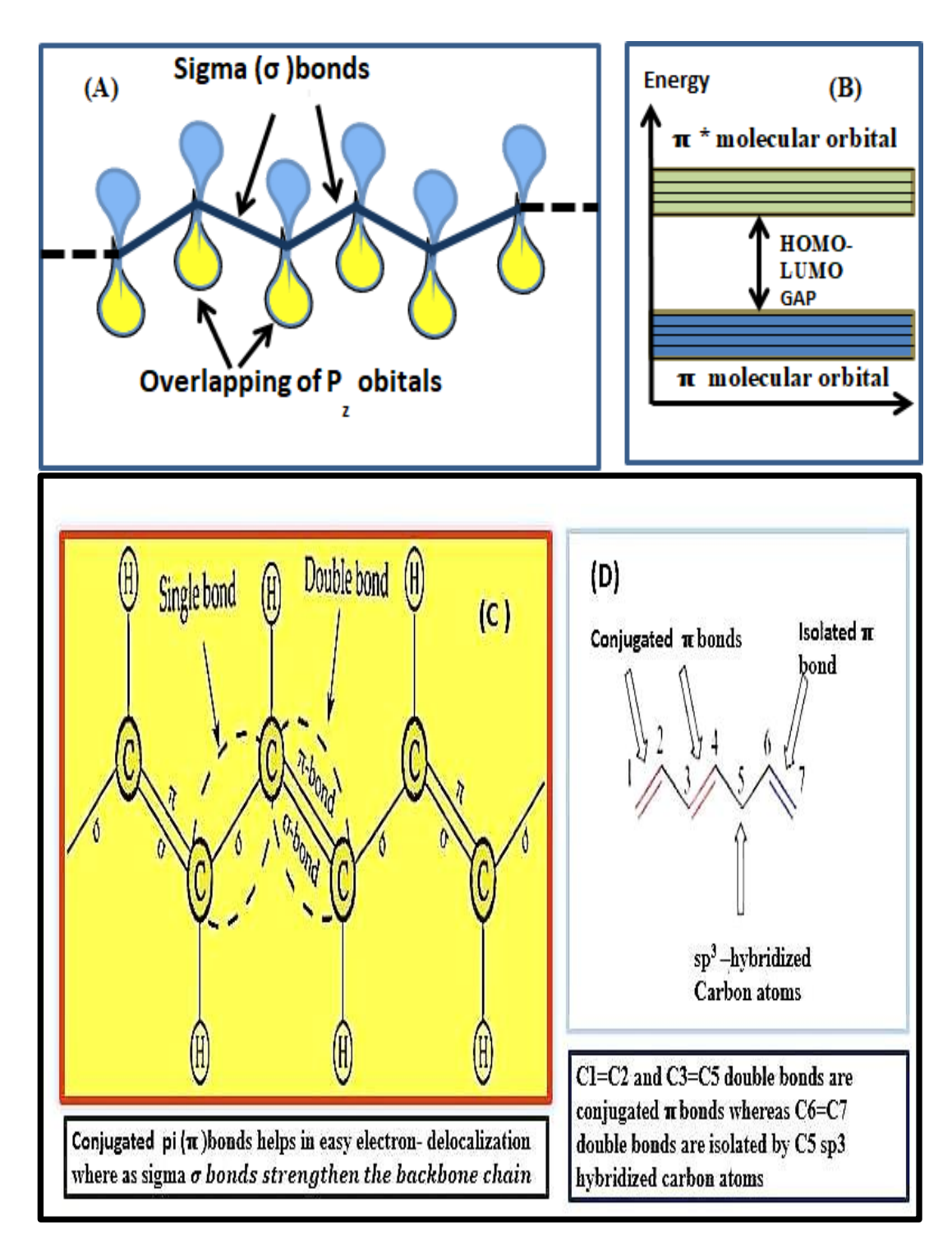


Figure 1.2: (A) Conjugate Bonding (B) energy diagram of π - π^* molecular orbitals (C) and (D) π -conjugate system for conductive polymer

this case these type substitutions can tune the HOMO energy level as well as the emission

wavelength of the emission spectrum. Alq₃ possesses a conventional bidentate $[M(NO)_3]$ structure of chelated octahedral coordination complex salt in which M stands for metallic trivalent atom of the quinoline ring, N represents the nitrogen atom of the quinoline rings, and O is the oxygen atom of the quinoline ring [2, 3, 4, 5, 14].

In conjugate molecules the 4 valence electrons of the carbon (C) atom along the molecular backbone chain undergo sp-hybridization, which form delocalized orbitals. Here, sp² hybridization means mixing 1 s electron with 2 p-electrons to form 3 sp² atomic orbitals. Three sp² electrons form a sigma bond with the other atoms to form the molecular structure, and the rest of the Pz is positioned in dumbbell-shaped molecular orbitals perpendicular to the plane of the three sp² orbitals. Here, according to the Pauli exclusion principle, these overlapping of P_Z orbitals with the adjacent other P_Z orbitals results in delocalization in the π - π * molecular orbitals (depicted in figure 12). The sigma bonds are the strongest covalent bonds within the material. Generally, hybrid orbitals form sigma bonds and nonhybrid orbitals form pi bonds. These carbon atoms have three sp² atomic orbitals which are used to form sigma bonds (a strong covalent bond formed within the molecules) which hold the backbone of the organic polymer molecules. A carbon atom has four valence electrons in its outermost shell. Only one electron that is not attached with covalent bonding can form a dumbbell-shaped Pz molecular orbital whose orientation is perpendicular to the plane of the chain molecules. According to the rules of quantum mechanics, specifically Pauli's exclusion principle, when the Pz orbital overlaps with a nearby Pz orbital, the energy levels of the electrons split into a sequence like 2, 4, 6, and so on. These two sets of split energies create two groups of energy levels that are very close together: one group at the top called π^* molecular orbitals (LUMO) and another group at the bottom called π molecular orbitals. These two distributed split energies form two sets of very densely spaced energy levels: on the top, π^* molecular orbitals (LUMO) and another at the bottom, π - molecular orbitals (HOMO) (according to the π -convention), and there is a HOMO-LUMO energy gap in between these two densely spaced energy levels. The HOMO-LUMO gap has no energy levels, which exhibits semiconductor behavior in organic conjugate polymers. In crystalline solid semiconductors, the valence band is similar to the π - molecular orbitals. (HOMO) and conduction band are also similar to the π^* molecular orbitals (LUMO) [4, 14, 28, 45, 46, 56-58].

- 4) Conductive polymers: The term "conductive polymers" refers to a subclass of polymers or a particular kind of conjugated polymer that has the ability to conduct electricity either naturally or through doping or reduction/oxidation of conjugated polymers because of overlapping pi-orbitals in their chemical structure and pi-bonds in their backbones. The conjugated backbone's delocalized pi electrons facilitate the flow of charge carriers, such as holes and electrons, which permits electrical conductivity. Doping is the process of introducing impurities or dopants into the structure of a polymer to adjust its electrical characteristics and boost conductivity. For instance, polythiophene, polypyrrole, and polyaniline (PANI). All conducting polymers are organic semiconductors, but not all organic semiconductors are conducting polymers. Although not all conjugated polymers are naturally conducting, doping or the reduction/oxidation of impurities called dopants can enable charge-carrier transport along the conjugated polymer's backbone. [58]
- 5) Spin pairing: Both holes and electrons have their spin, and the spin of the electron-hole pair is definite in nature. If in an electron-hole pair one electron is spin up (↑), the hole associated with that electron-hole pair should definitely be spin down (↓). For this reason, they unify. Another factor is momentum conservation. As both holes and electrons are mobile, they must have momentum. The conservation of their combined momentum during recombination can prevent certain electron-hole recombination. It is a complex phenomenon because it occurs in a condensed matter environment where there are many influences on such processes, such as lattice vibrations and various other types of quasiparticles. That's nothing; it can drive a specific electron to combine with specific holes. [25, 29, 31, 35-39]
- 6) Pauli Exclusion Principle: It states that two electrons in an atom cannot have the same four quantum numbers (n, l, ml, ms), and only two electrons can occupy each orbital where they must have opposite spin states. These opposite spin states are called spin pairing. [29,35-39]
- 7) Singlet and triplet state: There are three electronic spin states for the exciton or electron-hole pair: singlet, doublet, and triplet states (figure 2.3). When in a molecular electronic state, all the spins of its electrons are spin-paired, and their energy level does not get split by exposure to a magnetic field. A doublet state is formed when a spin-unpaired

electron splits into two feasible orientations with two different energy levels during exposure to a direct magnetic field. In a triplet molecular electronic state, there are two unpaired electrons that have the same and parallel spins ($\uparrow\uparrow$). When one ground state or lower energy state electron excites to a higher energy level, a singlet excited or triplet excited state. In the excited state, singlet-paired electrons retain the same spin-pair orientation as in their ground state ($\uparrow\downarrow$) [35-39, 56-63].

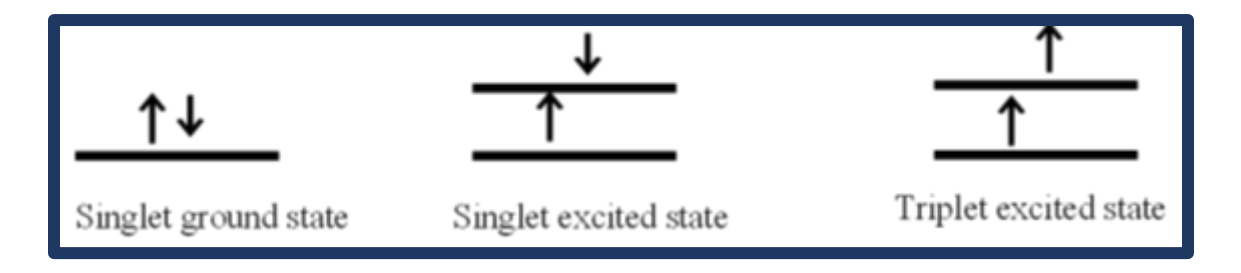


Figure 1.3: The schematic representation of the spin pairing of singlet ground energy state, singlet excited state and triplet excited state

8) Effect of spin pairing in organic materials: Due to spin pairing, most of the molecules are diamagnetic and do not get influenced with the application of a magnetic field, whereas free radicals are paramagnetic in character, meaning they respond accordingly to the influence of an external magnetic field due to the magnetic moment experienced by their unpaired electron. To calculate whether the spin multiplicity of the electron under investigation is a singlet state, doublet state, or triplet state, that can be ascertained using the spin multiplicity formula 2S + 1. In this case, S denotes the total spin angular momentum, and S = +1/2 represents the spin up, and S = -1/2 represents the spin down. For the singlet excited state, the value of the spin multiplicity will be 2S + 1 = 2. [(+1/2) + (-1/2)] +1=2(0) +1=1 That means only one excited spin multiplicity exists. For the triplet excited state, the spin multiplicity will be 2[(+1/2) + (+1/2)] + 1 = 2(1) + 1 = 3 That means three possible spin orientations can be obtained. Due to this, when molecular electrons exist in a singlet ground state (So) or in a singlet excited state (S1), the molecular electrons behave like a diamagnetic, while the molecular electrons that exist in a triplet ground state (To) or triplet excited state (T1) are paramagnetic in nature. The existence of triplet to singlet $(T \rightarrow S)$ transitions or singlet to triplet transitions $(S \rightarrow T)$ is invariably less likely

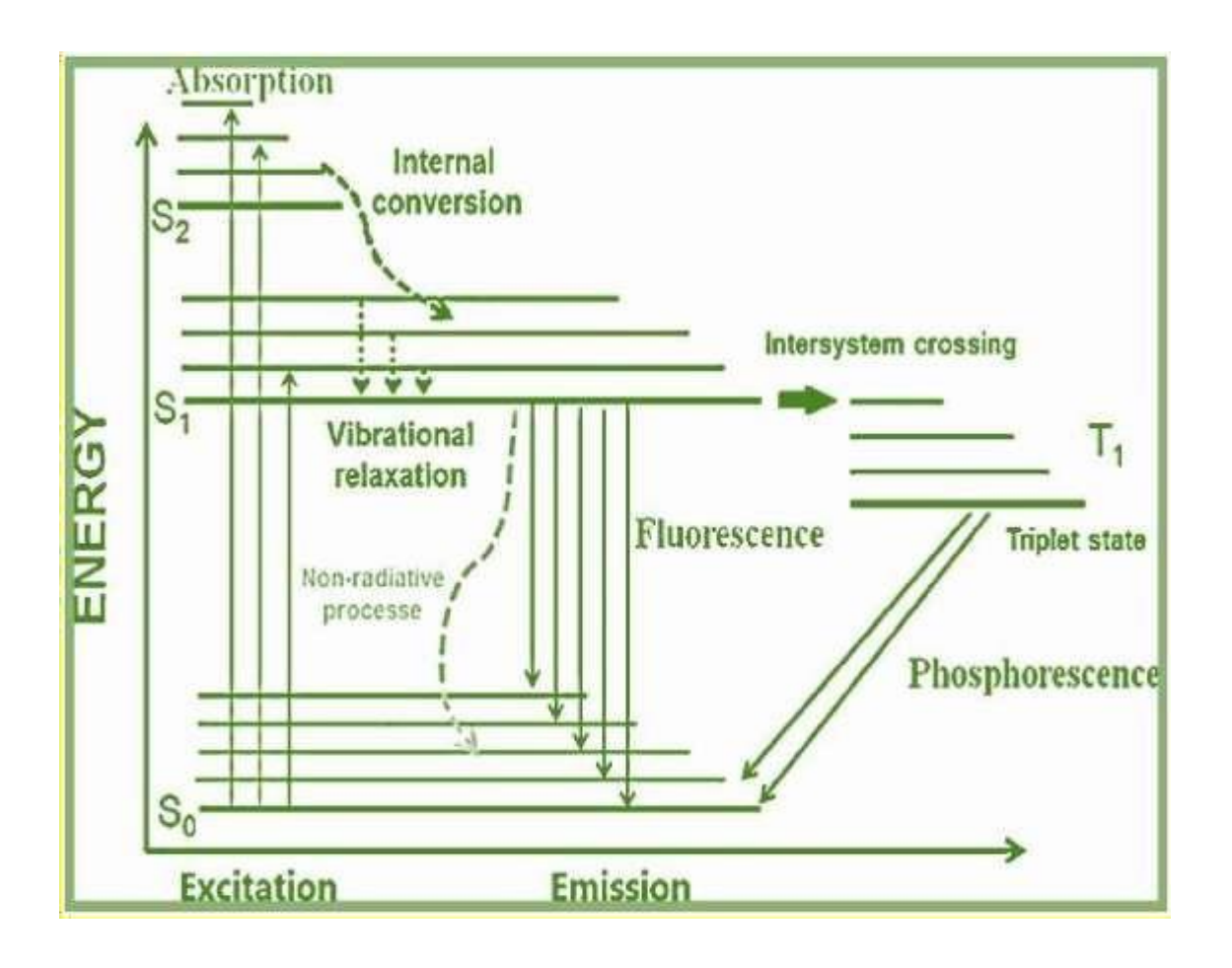


Figure 1.4: Jablonski diagram

due to this spin disparity of molecular energy states than singlet to singlet (S -> S) transitions. Using the Jablonski diagram, the transition that took place during a photoluminescence can be explained by singlet state, excited singlet state and excited triplet state the spin multiplicities of the excited state and ground states. The duration of the triplet state is therefore 10⁴ seconds bigger than that of the singlet state. The spin-electronic states are caused by singlet-to-triplet (S->T) or triplet-to-singlet (T->S) state transitions. Generally, singlet-to-singlet transition frequencies are probably more than transition frequencies from ground state to excited triplet state transitions. This occurs when induced radiation is applied. We get intense and sharp absorbance peaks when a ground-state to triplet excited-state transition occurs. When energy transition occurs from singlet excited state to triplet excited state, phosphorescence takes place. The transition that took place during a photoluminescence can be explained by the Jablonski diagram(figure:2.4) using

the spin multiplicities of the excited state and ground states. [8, 35-39]. When one ground state or lower energy state electron excites to a higher energy level, a singlet excited or triplet excited state. In the excited state, singlet- paired electrons retain the same spin-pair orientation as in their ground state $(\uparrow\downarrow)$ [35-39,56-61].

Luminescence, fluorescence and phosphorescence, electroluminescence: When a molecule absorbs energy as high-frequency radiation and that high-frequency radiation is re-emitted as visible light, then this phenomenon or property of that molecule is known as luminescence of that molecule. Luminescence is the reverse effect of absorption. If the molecule absorbs high-frequency radiation and, at the same time, emits light energy simultaneously, then the process is known as fluorescence. If after the absorption of high frequency radiation, the molecule emits light energy after 10⁻⁷ seconds or a longer time after the absorption, then the process is called phosphorescence, and the molecule of that substance is known as a phosphor. The phenomenon by which a molecule absorbs a photon of higher energy (higher frequency radiation or shorter wavelength) and simultaneously that molecules re-emit a photon of having a lower frequency or longer wavelength, i.e., lower frequency, is known as fluorescence. Photoluminescence (PL) is a phenomenon in which light energy is emitted from any form of matter after the matter absorbs electromagnetic radiation or photons. Electroluminescence (EL) is an electrical phenomenon as well as an optical phenomenon where a sample of interest or material emits light energy whenever it is exposed to a strong electric field or strong electric current passage. [2, 4, 14, 35-39,56.63]-

9)Conductivity doping: At room temperature, organic semiconductors contain very few inherent thermally produced charge carriers (less than 1011 cm⁻³ in number) [23, 34]. For this reason, organic semiconductors exhibit higher resistance, and thus it needs more plentiful operating voltage to emit photons than normal conditions. This problem can be sorted out by the conductivity doping method. For an OLED, HTL is being doped with strong electron-accepting molecules and ETL with electron-donating materials, which causes less operating voltage and minimum driving voltage [55, 57]. By doping conductive material into the organic semiconductor matrix, increasing the thickness of the doped devices is easily possible while maintaining a constant voltage drop. This process reduces the parasite-aided shorts of the electrodes for undoped, thinner devices used in large commercial displays. Due to photo-excitons,

electrons jump to the higher electronic states' vibration level vertically with the unchanged nuclear configuration. Then the electrons again jumped into the lowest multiple of excited energy state before jumping into the ground energy state with a new nuclear symmetric position (equilibrium position). Due to vertical photon emission, the spectrum will become red-shifted. This phenomenon is known as the Frank-Condon shift, which generates transparent emissions of 1 eV for some molecules. According to the Fermi-Golden rule, this electronic transition of molecules is directly proportional to the dipole moment acting between the initial states and the final states. Spin or symmetry between the adjacent transition states are the required conditions for allowing this type of transition [35-39]. become red-shifted. This phenomenon is known as transitions of molecules. According to the Fermi-Golden rule, this electronic transition of molecules is directly proportional to the dipole moment acting between the initial states and the final states. Spin or symmetry between the as the Frank-Condon shift, which generates transparent emission of 1 eV for some adjacent transition states are the required conditions for allowing this type of transition [35-39].

10)Enhancement of outcoupling efficiency or extract efficiency: Modern OLEDs are flat plane multilayered structures with different refractive indexes which play an important role for emission of photon and transmission of that photon through the transparent substrate (usually glass). The distribution of emitting dipoles of the small molecule —based OLEDs are isotropic which is not influenced by optical interference.

Outcoupling efficiency,
$$\xi = \frac{\text{Surface-escape cone}}{\text{hemispherical emission}}$$
 (1.1)

The outcoupling efficiency can be calculated by the following equation also:

$$\xi = \int_{0}^{\theta c} \sin\theta d\theta = 1 - \cos\theta c = 1 - \sqrt{1 - (1/n^2)} \approx 1/2n^2$$
 (1.2)

Where the value of n is large.

where n is the R.I. (refractive index) of the OLED's organic layers. Kim et al. [58] predicted that for the highest rate of emission from the emissive surface in isotropic emitters, the outcoupling efficiency, ξ (η extract) = $3/4(1/n^2)$ = $0.75(1/n^2)$, whereas ξ (η extract) varies as $1/(2n^2)$ for the flat even surface where the emitting dipoles are optimally placed. On the

basis of the above analysis, it can be concluded that out of 100% of the total number of photons that generate internally, only \sim 20% are able to come out from the front (anterior) viewing hemisphere [9], \sim 40-60% are confined within organic layers and the ITO anode, and at the same time they are wave-guided, and \sim 20-40% are lost due to total internal reflection occurring at the glass/air contact (or interface).

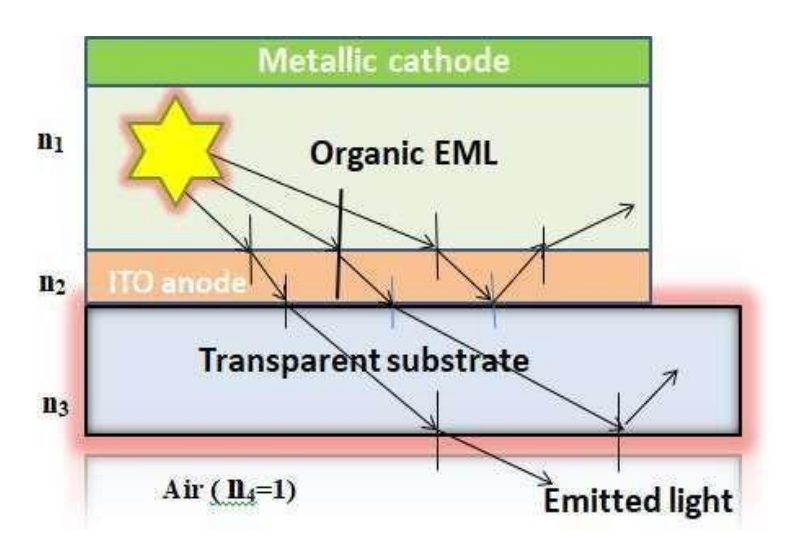


Figure 1.5: Diagrammatic representation of outcoupling efficiency

This is the reason for the low efficiency of OLED, where researchers worldwide are trying to optimize. Sun et al. [61] fabricated a micro-lens on the glass substrate through imprint lithography, which increased front emission by \sim 50% (Figure 1.5). This endeavor was the forerunner for the fabrication of a state-of-the- art white color–emitting OLED having the highest EQE of 34% with power efficiency as high as 68 lm/W. [39-49].

9) Four important factors to determine device performance: To determine device characteristics, amount of, light emitted from device, power output, light output these four terms are extremely important:

(a) Current efficiency=
$$\frac{(Luminance\ of\ OLED)\ (L)(cd/m^2)}{(Current\ density\ of\ OLED)\ (J)(A/m^2)}$$

(b) Power efficiency =
$$\frac{(Radiant\ power)\ (Lumen)}{(Electric\ power)(Watt)}$$

(c) External quantum efficiency (EQE) =
$$\frac{(\text{No. of photons escaped out/s})}{\text{No. of electron-hole pair injected /s}}$$
(d) Internal quantum efficiency (IQE) =
$$\frac{\text{No. of photons emitted}}{\text{witwithin an OLED /s}}$$
No of electron-hole pair injected/s

(e) Internal quantum efficiency (IQE) =
$$\frac{\text{No. of photons emitted within}}{\text{no of electron-hole pair injected/s}}$$
(f) Extraction efficiency (η extraction) =
$$\frac{\text{No of photons extracted/s}}{\text{No of electron-hole pair injected/s}} = 1/2n^2$$
= $1/(2x1.45x1.45)$
= $0.2378 = \approx 0.24$ (approx.)

where n=refractive index of the Alq₃ (host) is 1.45 (from published experimental data) Internal quantum efficiency (IQE) ($\eta_{internal}$)= (device characteristics of an OLED)

1.9. Reliability of OLEDs:

The small molecular- or polymer-based OLED suffers different kinds of operational Instability and storage instability, which results in efficiency reduction and performance degradation in OLEDs. which raises questions on the reliability of OLED operation. Principally, there are two types of operational degradation:

- Decay in luminance intensity over prolonged time.
- Gradual increase in operational voltage in response to constant current.
- Degradation of OLED materials is generally caused by chemical degradation of emissive material due to oxidation, water splash, moisture, impurities, etc. Chemical degradation also occurs due to the direct exposure of OLED material to ambient atmospheric conditions, excessive heat generation, absence of proper encapsulation and change in chemical properties of the emitter material due to ageing. Atmospheric nitrogen does not affect OLED [44-49]
- OLED can be short-circuited when excessive current passes through it damaging

it's hot and transport layers.

1.10. Operation/Function of an OLED:

Electrons travel away from the cathode, and holes from the anode follow in the opposite direction of the anode when an electric current flows through this circuitry. The photon produced by the recombination of electrons and holes has a frequency equal to the energy band gap (E = hv), or the difference between the HOMO and LUMO energy levels. In organic emitter molecules, the HOMO and LUMO stand for the highest occupied molecule orbital energy level and the lowest unoccupied molecule orbital energy level, respectively, of the photon or light energy that is released. The cathode's and anode's electrical power, also known as electrical energy, is thus transformed into light energy. The range of materials and dopants can yield a variety of light emission hues, and when these colours are combined, a white light source can be created. An OLED device's recombination rate and brightness are controlled by the physical and chemical characteristics of the EML layer and related additional effective layers. The anode and cathode can regulate the rate of electron and hole recombination by injecting carriers into the organic emissive layer. It is possible to enhance the rate of metallic cathode recombination by introducing an Alq3transformed into light energy. The range of materials and dopants can yield a variety of light emission hues, and when these colours are combined, a white light source can be created. An OLED device's recombination rate and brightness are controlled by the physical and chemical characteristics of the EML layer and related additional effective layers. The anode and cathode can regulate the rate of electron and hole recombination by injecting carriers into the organic emissions. It is possible to enhance the rate of metallic cathode recombination by introducing an Alq₃-doped layer between the active EML layer and the latter. The construction of the Alq₃-doped OLED depends critically on the influence of the necessary parameters, including mobility, band gap, and lifetime.

1.11. Operating mechanism and device physics of an OLED:

Inside an OLED, there is an organic material-based emitting layer, i.e., an organic layer. Basically, in this organic layer of OLED, there are few numbers of charged carriers, as these organic layers are not doped. That's why they cannot conduct current easily through

.it. To overcome this difficulty, the organic electroluminescence must perform those abovementioned six stages properly to emit light in response to current, i.e., organic electroluminescence (EL). We can summarize all the above-mentioned operating mechanisms of an OLED (Figure 1.5) in the following four ways:

1.Charge carrier injection (hole injection & electron injection): The first stage of the organic electroluminescence is to bring charge carriers into the OLED device. The charge carriers are negatively charged electrons and positively charged holes. These two charge carriers are injected into the organic layer with the application of electric current or voltage bias applied at the electrodes (cathode and anode of the correct polarity). We can inject electrons through metallic high work function cathodes like silver (Ag), magnesium (Mg), copper (Cu), Al, LiF/Al, etc. The holes can be injected by using low-function transparent Indium Tin Oxide (ITO). FTO, etc. By application of an electric field these charge carriers are injected into the organic layers.

Barrier lowering by image charge: when any electron is placed at an x distance from the surface of a metal electrode, an induced (+) or positive charge is produced on the opposite side at –x distance. This induced image charge lowers the potential barrier with the applied barrier as follows:

$$\phi_{\rm B} = \phi_{\rm m} - q/(Ex_m) - q^2/(16\pi\epsilon x_m)$$
where $\Delta \phi = \sqrt{(q^3 E/4\pi\epsilon x_m)}$ (1.3)

When electricity is applied, some electrons from the metallic surface transfer to the emissive or charge carrier transporting organic materials (maybe to the trap states) through diffusion only if the metal/organic layer contacts are energetically compatible for electron transfer. [20]. At room temperature, in an undoped intrinsic organic semiconductor, there are small numbers of thermally generated charge carriers. Electrons are confined within the molecules, and the extremities (tails) of the different energy states get widened due to disorders or structural imperfections formed. The widened, densely spaced (band-state) metallic electrode injects charge carriers into the organic molecule's localized polaronic energy state. [23]. On the basis of behavior, the carrier injection can be classified into two theoretical models, i.e., field-assisted tunnelling and thermionic emission. These two models are out of context with our research project. [20-24]

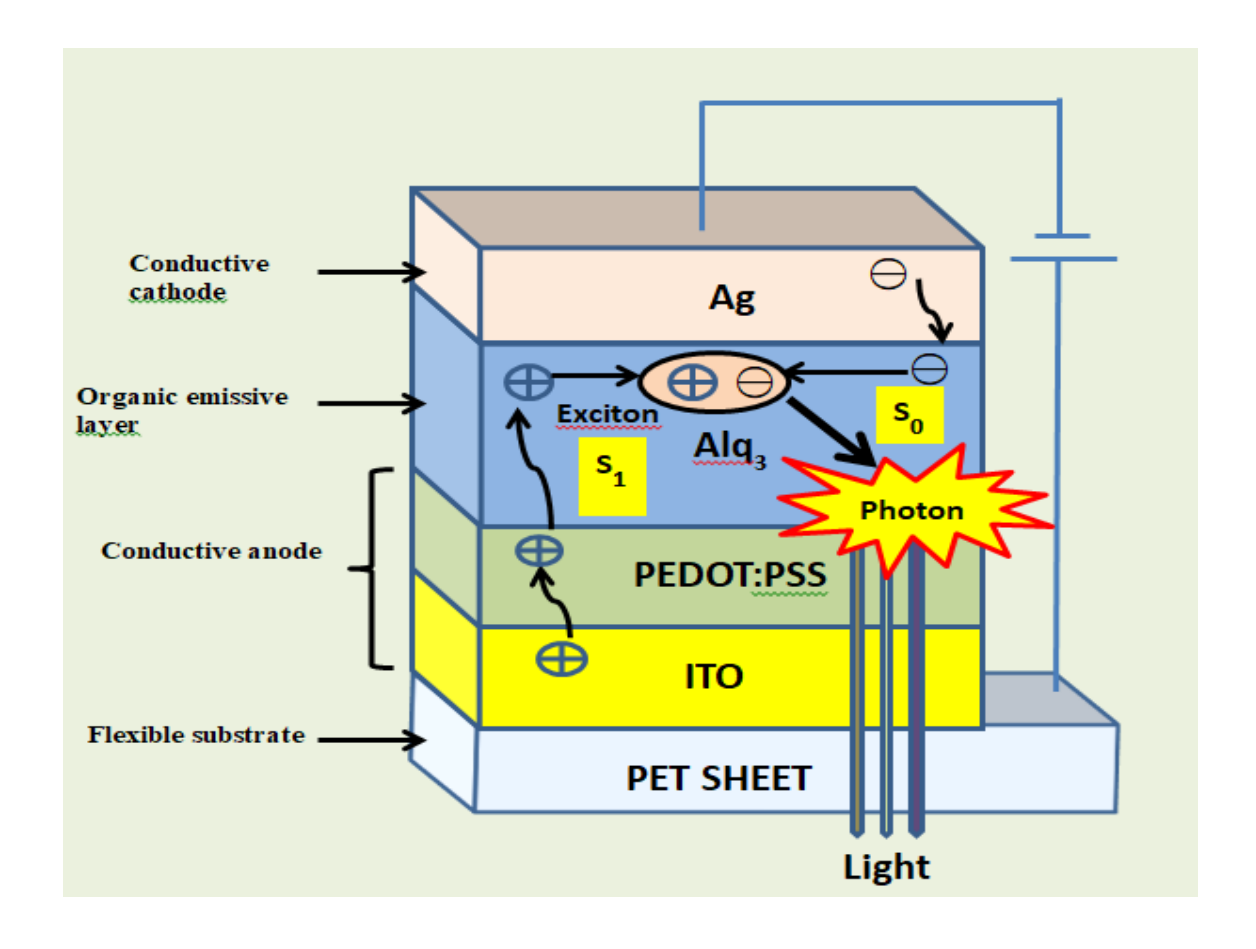


Figure 1.6: Schematic workings of an OLED

2. Charge carrier drift transport (hole drift transport & electron drift transport):

When these charge carriers reach the organic emitting layer, they experience an electric field (previously illustrated in the energy diagram of Figure). In organic layers electrons and holes undergo "drift transport. As the electrons and holes carry opposite nature of charges, i.e., they are pulled along by an electric field. The charge carrier drift diffusion equation is used to illustrate the behaviors of charged particles in an OLED. This equation is the sum of drift and diffusion, which is formulated by:

$$\overrightarrow{J_{n,p}} = \operatorname{qn}(or \, p) \mu_{n,p} \overrightarrow{E} \pm \operatorname{q} D_{n,p} \overrightarrow{\nabla_{n,p}}$$
(4)

Where $D_{n,p}=\mu_{n,p}\frac{TK_B}{q}=$ Einstein's law for diffusion constant for electron or proton, q=charge, $\mu_{n,p}=$ mobility of electron or hole, $\vec{E}=$ electric field, $\nabla_{n,p}=$ nabla operator , T= absolute temperature and $K_B=$ Boltzmann constant n=electron and p=hole.

There are three types of charge transport methods: multiple trapping and release theory, band-like transport, and hopping transport. In highly structurally imperfect or disordered amorphous or polycrystalline organic semiconductors or polymer-based semiconductors, such as polyaniline (PANI), poly(3,4-ethylenedioxythiophene) polystyrene sulphonate (PEDOT: PSS), etc., charge transport takes place by the hopping method or tunnelling through two consecutive localized sites or states due to its energetic and spatial disorder. The hopping method is a charge transport process where localized charge carriers are continuously transported for jumping from one localized site to another. Tunnelling between two adjacent localized sites occurs due to wave-function overlapping of two localized states or sites.

3.Recombination (electrons and holes combine with each other to form neutral Frenkel excitons): when independent electrons and holes, the free charge carriers with opposite charges, are statistically injected from the electrode (cathode and anode), they combine with each other at the emissive layer, which is known as the recombination process. This is a random process which can be explained through Langevin formalism. [38]. For electron-hole pair recombination, the Coulomb attractive forces should be greater than their thermal energy.

$$\frac{q^2}{4\pi s r e} > kT \tag{1.5}$$

Where r_c = Onsager radius=maximum distance of separation for electron hole pair capturing for exciton formation= ~ 17 nm at RT (room temperature). Within Onsager radius, electron –hole pair recombines and generate excitons. During this bimolecular process of capturing any one of the two charge carriers remain static and the other charge carrier moves towards the former one with resultant mobility, $\mu_m = \mu_h + \mu_e$

with where $r_c = \text{Onsager radius} = \text{recombination efficiency}, R = \left((epn) \frac{\mu_m}{\epsilon} \right)$ [where n and p=concentration of the electrons and holes]. In the Langevin model, the process of recombination depends on the spin of the singlet and triplet. The probability of triplet exciton generation from a triplet excited state is the same as the probability of singlet formation from a singlet excited state. The ratio of generated triplet and singlet excitons is 3:1 (75%:25%), which lowers the IQE (internal quantum efficiency) of OLEDs. The maximum IQE has been achieved at 25%, which could be improved to a higher magnitude than 25%. By converting triplet excitons into singlet excitons, thus raising he numbers of emissive singlet exciton generation [8, 27, 38-42, 56-61] 4. Radiative decay of singlet Frenkel exciton and photon (light) generation: The electrons and holes eventually encounter each other, forming neutral excited states called Frenkel excitons. Frenkel excitons are one of three types of excitons. In organic materials we observe the generation of small-sized Frenkel excitons only, which is represented by S1 in figure 2.3. S1 represents two subcategories of Frenkel exciton: singlet-type and triplet- type Frenkel excitons. The generation of singlet Frenkel excitons is very significant, as they are emissive in nature, thus helping OLEDs to emit light in response to electricity. These singlet excitons are designated by S1 in the diagram. Below the S1. state there is another state. So, the ground state is shown by an arrow in the diagram. This stage is the last stage of the organic electroluminescence process. The neutral excited Frenkel excitons are very unstable in nature. After some time of its generation, it undergoes radiative decay of its higher energy and transit to the ground energy state, releasing its energy, which is then emitted as photon energy in the form of light emission. The energy of the released photon or emitted light is equal to the energy gap value between the HOMO and LUMO energy bands (E=hv). [1, 2, 42-46, 56-61]. state there is another state. So, the ground state is shown by an arrow in the diagram. This stage is the last stage of the organic electroluminescence process. The neutral excited Frenkel excitons are very unstable in nature. After some time of its generation, it undergoes radiative decay of its higher energy and transit to the ground energy state, releasing its energy, which is then emitted as photon energy in the form of light emission. The energy of the released photon or emitted light is equal to the energy gap value between the HOMO and LUMO energy bands ($E=h\nu$). [1, 2, 42-46, 56-62]

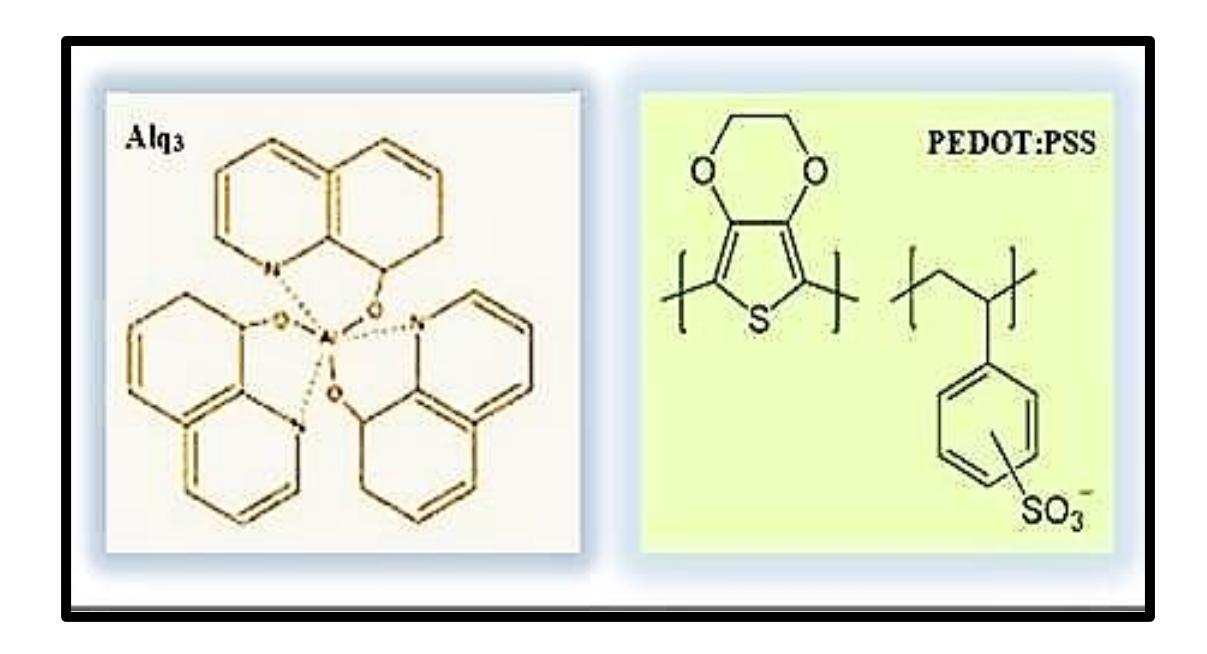


Figure 1.7: Chemical structure of small molecule Alq₃ and a polymer PEDOT: PSS

1.12. Role of organic semiconductor in an OLED:

Organic semiconducting materials possess π -conjugated bonding, i.e., alternating single and double bonds or single or triple bonds throughout their polymeric molecular backbone chains. These bonds are formed through sp² hybridization. During bond formation, two p- orbitals and one s-orbital of carbon atoms develop three hybridized orbitals. Out of three hybridized orbitals, only one orbital can create a strong sigma (σ) bonding with the adjacent carbon atoms of the polymeric backbone chain. The hybridized orbitals form a plane which holds the whole polymeric backbone arrangement. The rest of the unhybridized Pz orbitals remain perpendicular to the plane of the polymer molecular chain created by the hybridized orbitals. The unhybridized Pz orbitals of two adjacent carbon atoms of the polymer chain overlap sidewise to generate a feeble π (pi) -bond, resulting in the delocalization of the electrons, causing

those electrons to move spontaneously inside the molecule. This free movement of electrons promotes semi-conducting properties in organic semiconductors. In our research we use Alq₃ as a small molecule n-type semiconductor and PEDOT: PSS as a polymeric p-type organic semiconductor. (Figure 2.6) [35-39,45,46.]

1.13. Why are organic semiconductors preferred over inorganic semiconductors for OLED construction?

Usually, organic semiconducting materials used in OLEDs are found in amorphous forms. The organic polymers or small molecules used in OLEDs interact with each other by means of weak Van der Waals forces. Whereas for inorganic semiconductors, the constituent molecules are attracted by strong covalent bonding. In consequence, the free charge carriers are being transported through polymer segments or molecules by using the place- to-place hopping method in place of bank-type transport in inorganic semiconductors, causing lower mobility of ~10⁻⁶ to 10⁻³ cm²/(V.s) [46] compared to the high mobility of 102-103 cm²/(V.s) in the case of inorganic semiconductors. The HOMO (highest occupied molecular orbital) and LUMO (lowest unoccupied molecular orbital) for organic semiconductors are analogous to the valence and conduction energy bands of the inorganic semiconductors. The dielectric constant of organic semiconductors is near about 3, while it's 10 for inorganic counterparts. In organic semiconductors, the magnitude of dielectric constant influence in dielectric screening for exciton binding which moderately ascertains the binding energy of excitons. In organic semiconductors Frenkel excitons are formed with exciton binding energy within 0.2 to 1 eV, whereas in organic semiconductors support Mott-Wannier excitons have an exciton binding energy of about ~10 meV. [21, 27-29,]

1.14. Classification of OLED:

OLEDs are principally classified into seven types based on their manufacturing types and nature of usage: On the basis of material characteristics and size, OLED can be divided into the following categories:

1.Small molecules OLED (SM-OLED): The term "OLED "specifically and technically refers to SM-OLED. In 1987, Ching W. Tang and Van Slyke of Eastman Kodak Company for the first time developed an efficient OLED utilizing small molecules (SM-OLED). To fabricate an OLED, generally four kinds of molecules are used: fluorescent dyes (e.g., perylene, quinacridone derivatives and rubrene), phosphorescent dyes, organometallic chelates (e.g., Alq3) and conjugated dendrimers. Various kinds of fluorochromes, anthracene, coumarin derivatives, aluminium complexes and biphenyl acetylene aryl derivatives are the common examples of small molecule electroluminescent organic materials. Electroluminescent organic small-molecule materials are chosen for their easy purification procedure, robust chemical modification method and extensive variety. Unsaturated groups or chromophores as luminescent materials (e.g., benzene rings or alkene bonds) are usually incorporated in the design of the molecular structure to alter and engineer the conjugation range size of the material in such a way that the material's photophysical properties change. Generally, for the larger π - electron conjugation range, the materials emit light of longer wavelength. The more benzene rings in benzene, anthracene, butyl and naphthalene, the more gradual the red shift of emission peaks occurs within the range of 283-480 nm. Charge transport materials such as Alq₃ are popular electron transport materials which also act as green emitters and hosts of red and yellow- coloured light-illuminating dyes. Triphenylamine and its derivative are the most common hole transport materials

Some key properties of small-molecule OLED materials:

- As electroluminescent small-molecule OLED materials have morphological flexibility, their thin film can be made using an expensive vacuum-vapor deposition method which restricts their use for larger-area or big-size devices. Instead, the vacuum-coating system is skillfully used in fully operational ambience for getting stable and uniform thin film which uplifts the OLED's device performance greatly.
- In solid form, organic small molecular dyes are susceptible to quenching in their fluorescence, which lowers the OLED's luminescence rate and device efficiency.
- The doped small molecule organic OLED material often crystallizes, thus

- lowering the luminescence value and device-efficiency.
- The application of small-molecule organic OLED material in device formation is limited due to its shorter life span, higher manufacturing cost, and lower stability.

2. Polymer or plastic light emitting diodes (P-OLED or PLED) or light-emitting polymers (LEP): P-OLED is an OLED composed of electroluminescent organic conductive polymer, which emits light when electricity is being passed through the P-OLED and that conductive polymer." Polymer" or "Polymer Group" represents that material which has long repetitive chain of same specified group of molecules having molecular weight greater than 10.000gm/mol. POLED uses plastic or polymer substrates. Polymers are more complex in structure heavier than small molecules. In 1990, POLED was discovered by researchers at Cambridge University, and P-OLEDs are used to form thin films for full-colour OLED-based displays. P-OLED can emit light even while consuming comparatively less power; thus, PLEDs are highly efficient. Usually side-chain substitution, by using the ring-opening metathesis-polymerization technique, onto the backbone of polymeric PPV [poly(p-phenylene vinylene)], PF [polyfluorene], and their derivatives are used in P-OLED to tune the colour of the illuminated light, level of solubility in water or organic solvent, processability, and device performance, as well as efficiency. These conjugated poly electrolytes (CPEs) or water- soluble polymers can be utilized as HIL (hole injection

layer) of P-OLED alone or blending with different nanoparticles such as grapheme. The vacuum vapour-deposition method is not suitable for thin film formation of conductive polymeric materials, as it cuts off the chain elements, resulting in degradation in its photophysical properties. As conjugate polymers are processible in solution, so spin coating (without vacuum) is the appropriate method for thin film formation, even for large-area deposition of polymeric thin films.

Applying the inkjet printing method, these emissive materials can be deposited over the substrate. During multi-subsequent layer deposition, spin coating or inkjet printing techniques using solvents of the different substrate strata are more acceptable techniques,

which again are prone to dissolve the preceding deposited layers, so metal cathodes are deposited using the vacuum thermal evaporation method. Another solution is the vacuum-free Langmuir-Blodgett film deposition technique.

Apart from these, on the basis of characteristics of emitter materials used in OLED, OLED can be classified as follows:

1.Active-matrix OLED (AMOLED): Basically, AMOLED consists of three layers: anode, organic molecules made up of either small molecules or polymer or both, and cathode. It uses glass substrates, unlike POLEDs. The anode layer contains a parallel thin film transistor (TFT) layer array which acts as a matrix and circuitry. This TFT layer governs which pixel will be turned "ON" or "OFF" to produce an image on an AMOLED TFT screen. AMOLED creates a black image when pixels are "OFF" and a bright image on TFT-based displays when pixels are "ON". Thus, AMOLED has a longer battery life. AMOLED exhibits a faster refresh rate and the lowest power consumption ability, which is suitable for brighter and crisp images as well as video. As TFT array consumes less power than its external circuitry, AMOLED is more effective for large-display units. AMOLEDs are mostly used in Android smartphones, large-screen TVs, smart TVs, computer monitors, electronic billboards and electronic advertising signs.

2.Passive-matrix OLED (PMOLED): PMOLEDs consist of organic molecular layers and a mutually perpendicular array of cathode strips and anode strips. Light-emitting pixels are formed at the intersecting point of each pair of cathode strips and anode strips. The applied current will be passed through which selected pair of anode strips and cathode strips are mainly determined by external circuitry, and thus PMOLED can illuminate specific pixels through external circuitry. PMOLED consumes the highest amount of battery power for its external circuitry compared to other counterparts but less than an LED and an LCD, which currently powers a PMOLED. PMOLED's fabrication is a cost- effective and easy process. The more lines appear on the TFT screen of a PMOLED, the more voltage will be needed; thus, the size and resolution of a PMOLED are restricted. Generally, PMOLEDs are the best choice for small 2-3 inch wide (diagonally) small screen displays where text, small icons, small symbols, and character data are displayed, like in PDAs, cell phone sub-displays, MP3 players, etc.

3.Quantum Dot OLED (QD-OLED): Quantum dot OLED, or QD-OLED, uses an analogous stacked configuration of WOLED with an important difference. In QD-OLED, one inkjet-printed conversion layer is made up of quantum OLED. All stacked layers jointly produce blue light to excite green quantum dots and red quantum dots to illuminate green and red light, and the rest of the blue light passes across the blue colour sub-pixels. During this excitation of green and red QD by blue light, no intensity loss along with



Figure 1.8: Upper row: Images of AMOLED (first left corner), PMOLED (top row middle), architectural difference between WOLED and QD -OLED (right most corner) & lower row: images of difference between QD OLED and LCD (lower left), architecture of a QD-OLED display

quantum efficiency loss occurs. In QD-OLED, a white sub-pixel is not required to improve its brightness. QD-OLED display exhibits exquisite efficiency, wide colour volume and

high brightness within the range of near-black regions of illumination.

4.Phosphorescence **OLED** (PHOLED): Phosphorescence **OLEDs** have phosphorescent green and phosphorescent red emitter along with fluorescent blueemitters. PHOLED emits light because of electroluminescence occurring in the organic emissive semiconductor layer on application of electric current. Electrons and holes recombine in the organic EML layers, thus forming excitons which emit photons after losing their energy during their movement from excited energy state to the ground state. PHOLED is a kind of OLED which shows internal quantum efficiency higher than fluorescent OLED following the theory of phosphorescence. This is a developing technology. In phosphorescent OLED organometallic complex compounds are doping into the host organic semiconductor molecules. PHOLED generates both singlet and triplet excitons to emit light, resulting in ~100% internal quantum efficiency in it. In the organometallic complex there is a heavy metallic atom at the center of the organic molecule (like iridium in Ir(mppy)₃). This central atom of heavy metal experiences a strong spin-orbit interaction with the adjacent molecules leading to the mixing of the singlet and triplet excited states (intersystem crossing), and thus the reduction of the triplet state lifespan happens. For this reason, phosphorescence is seen at once.

5.Foldable OLED (FOLEDs): FOLEDs possess a flexible thin plastic substrate or metallic foil substrate. Because of this flexible substrate, FOLEDs are thin, flexible, durable and light in weight but stronger in stability. That's why FOLED is used in those appliances which are very precious, delicate and fragile in nature. FOLED display offers higher contrast, higher resolution images, quicker refresh time and crispy pictures. Thus, FOLEDs are a prime choice for cell phones, GPS gadgets, curved large TV screens, etc. Smart outdoor clothing, which incorporates FOLED displays into fabrics, is the most remarkable application of FOLED technology.

6.White OLED (WLED): White OLED is the essential tool for large-screen or large-area AMOLED displays. WOLED is a potential candidate for futuristic solid-state lighting. In WOLED is successfully applied in OLED TV panels where phosphorescent green units, phosphorescent red, yellow and fluorescent blue emitter layers are fabricated one

after another and sandwiched between transparent ITO anodes (adjacent to the substrate) and cathodes (Al or Ag, LiF/Al, etc.), and the whole systems are encapsulated. White OLED was reported for the first time by J. Kido et al. from Yamagata University of Japan in the year 1995. They commercialized the OLED-based lighting and backlit displays. Generally, cool white OLED structures mainly can be divided into two types: single stacked structure and three-stacked tandem structure. The three-stacked configuration is mostly used for display usage for its longer durability and higher efficiency. In this three-stacked configuration, two blue-emitting layers are used as emissive layers (EML), leading to longer device durability, high-intensity blue fluorescence emission and emission of cool, higher-efficiency white light. The white OLED can be (i) top-emitting, (ii) bottom- emitting, (iii) vertically stacked, (iv) pixelated monochrome-based, (v) single-emitter- based, (vi) single-layer OLED having sub-layers within the EML layer, or (vii) blue OLED having a down-conversion layer.

We can witness white OLED displays in OLED televisions. Generally, white OLEDs possess four coloured sub-pixels: red, green, blue and white. Any three subpixels remain active for any specified time interval. White OLEDs have no separate emitters for each subpixel, unlike OLED displays used in our Android phones or tablets. In WOLED, stacked emissive layers were utilized to emit white light through each and every pixel. These emissive layers make RGB sub-pixels using a colour filter. LG Displays manufactured tandem stacks for WOLEDs which have two emissive layers containing blue, green, yellow-green and red. These emissive colours produce white light unitedly, which must pass through a colour-filter layer for producing blue-green-red-white subpixels. The 3rd generation cutting-edge WOLED displays are known as MLA OLEDs (micro lens array OLED) as they use a micro-lens array along with meta-booster technology from LG for improving the brightness by 60% and increasing the viewing angle by 30%.

1.15. Advantages of OLEDs:

OLEDs are the most popular display technology in commercial display markets. OLEDs are now used in different large-area displays as well as in small-area displays such as flat full-colour displays, flexible or rollable displays, curved displays, transparent displays, touch screens and even low-information displays used for smartphones, MP3 players,

laptops, PDAs, digital cameras, etc. The reasons for OLED's extensive applicability are only because of these different advantages mentioned below:

- **Self-luminescent OLED** is self-luminous, and it does not need any backlight, polarizer or diffuser to illuminate its screen. Each pixel and sub-pixel itself illuminate and is turned ON or OFF to form a desirable, brighter, higher-resolution picture on the screen.
- Low voltage driven: The turn-on voltage of an OLED is very low. It can be driven within 2-10 DC volts.
- Easy and low-cost fabrication procedure: The fabrication and manufacturing cost of an OLED (especially polymer-OLED) is very low, and it can be easily fabricated using a low-cost fabrication method, e.g., spin coating, inkjet printing, screen printing, or roll-to-roll technique.
- **Desirable colour emission:** There are plenty of organic materials available in the market to emit the full gamut of visible coloured light.
- Thin, lightweight and compact form factors: Usually OLEDs are thin and have a compact form factor, which causes their lightweight
- Flexible, transparent rollable displays: Nowadays transparent flexible transparent rollable OLEDs have attracted viewers' extreme attention, and these OLEDs can be fabricated easily on plastic or fiber substrates with a cost-saving fabrication procedure and open up the new research avenue of flexible electronics.
- Forms brighter, high-resolution images: OLEDs can form brighter, crispy, full-black, high-resolution images at low operating voltages. OLED, e.g., WOLED, can produce bright images of ~150000 cd/m² brightness.
- **Supports wide viewing angle:** The OLED supports Lambertian emission; that's why it allows a wide viewing angle of 160°.
- Fast response time: OLED screens have an extremely fast response time of less than $1 \mu s$ (=10⁻⁶ S) which causes fast electroluminescence decay in OLED.

1.16. Ecological and societal impact/benefits:

- OLEDs need less power and can be recyclable; hence, they are energy efficient.
- OLEDs have a great impact on the environment by the following means:
 - It emits a lesser amount of greenhouse gas.
 - It consumes less electricity, resulting in energy savings and lesser use of nonrenewable sources of energy.
 - It causes less air pollution.
 - It is recyclable and biodegradable.
- OLED has a long battery life.
- OLED displays exhibit excellent visibility and readability.
 - OLED SSL lighting technology helps in decorative lighting, automobile lighting, space-saving lighting, corner critical angular lighting, and architectural designs.
 - OLED displays produce excellent images, videos, and graphics with pure black and full colour, high resolution, and fast refresh rates.
 - OLED technology is a continuously developing technology which yields variations of products according to market demand and viewers' choices.
- OLED growing industry creates opportunities for multi-dimensional employment.

1.17. Disadvantages:

The following are the existing disadvantages which lower its application efficiency:

- Prone to atmospheric degradation: OLED materials are made up of organic small molecules or polymers, which are extremely susceptible to atmospheric moisture (H₂O or water molecules) and atmospheric oxygen. In consequence, the OLED devices undergo chemical degradation or chemical failure, which results in gradual degradation in device performance and efficiency and shortens the life span of the OLEDs.
- Low operating temperature: As the small molecule-based OLED has low glass transition temperature (Tg) less than 70°C, it cannot be operation more than its Tg
- Low electron and hole mobility: Amorphous organic molecules possess low

- electron mobility and low hole mobility, which is a big problem for increasing the recombination rate.
- **Instability due to high brightness:** when OLED is forced to produce a higher brightness image, it loses its stability. This is a significant problem with OLED technology.
- Complexity of OLED devices: The complexity of OLED devices results in high manufacturing and fabrication costs.
- Fabrication difficulties for uniform and large-area lighting resources: Inconveniences occurred to fabricate large-area-based uniform lighting panels, and lighting sources are another big issue for solid-state lighting.

1.18. Comparison among the Incandescent bulb, CFL, LED, and OLED lights:

We have highlighted the fundamental differences between incandescent bulbs in this section. LED (light-emitting diode), OLED (organic light-emitting diode), and CFL (fluorescent bulb). We can quickly learn about the features of those four lights from

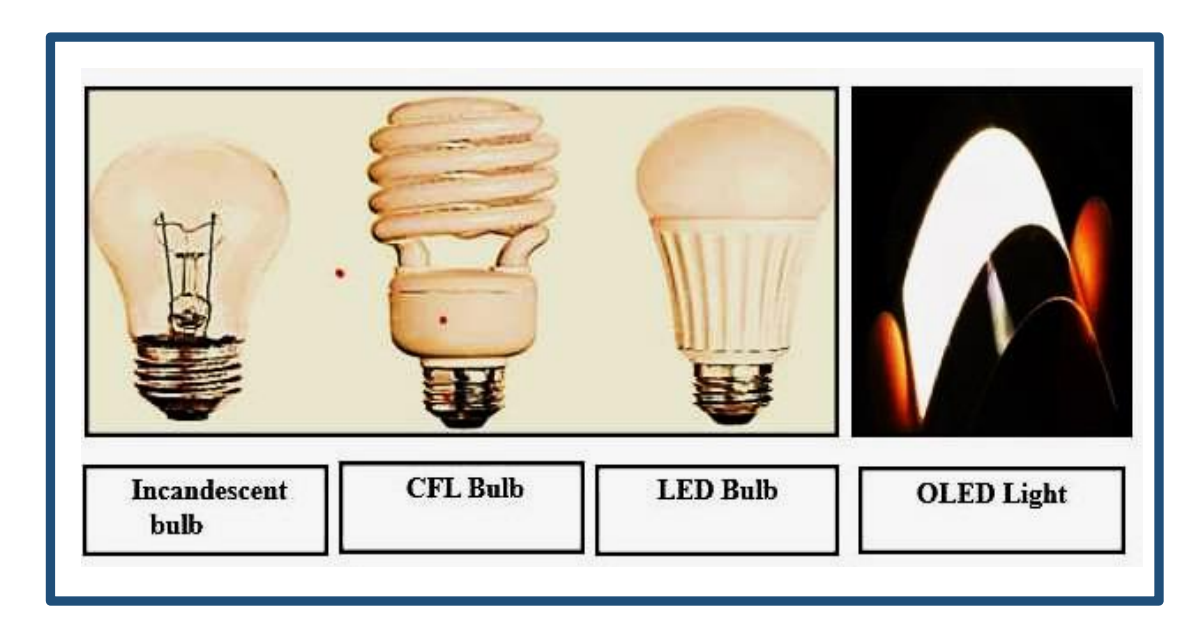


Figure 1.9 : Comparison among incandescent bulb, CFL bulb, LED bulb and OLED light

this tabular comparison, and we can also see how OLED technology has advanced to its current state after leaving all its competitors far behind. Because of its versatility, flicker-free brilliant light generation, cool touch, ability to be utilized in any acute angle, increased brightness, low voltage driven, etc. There are distinct tables for the displays and light to help



Figure 1.10: Comparisons among the characteristics of TFT /LCD, LED, OLED, QLED & μ LED displays

with comprehension. OLED screens are listed in table 1.2 and light in table 1.1. For displays, we have contrasted the features of OLED with those of LCD, TFT, micro-LED, and LED. In the field of display units used in smartphones, tablets, Android phones, mobile phones, daily-used devices, and electrical or electronic appliances, OLED has achieved breakthrough optimization.

1.19. Comparison among the Incandescent bulb, CFL, LED and ED light character wisely

Table1.1: Comparison among the Incandescent bulb, CFL, LED and OLED lights

Sr. No.	Comparative characteristics	Incandescent light	CFL	LED	OLED
1.	Average life	1000-1,200 hours	8,000 hours	25,000-50,000 hours	100,000 hours
2.	Mercury used as gas	No	Yes	No	No
3.	Electric power needed	60 Watts	13-15 watts	6-8 watts	6 watts
	for operation (On				
	the basis of 60 W				
	incandescent bulb)				
4.	Energy Efficiency	90% energy is	It uses 75% less	It uses 84% less	It consumes 40% less energy
	(% Loss of energy)	lost due to heat	energy	energy	compared to other displays
5.	Annual cost	~\$ 11.00 (916.98 INR)	~\$ 2.50 (208.41 INR)	~\$ 1.80 (150.05 INR)	For panel \$300-500 /klm
6.	Bulbs needed for 50,000	50	5	1	1
	hours of use				
7.	Existence of filaments	Yes	No	No	No
8.	Current passes through	The current passes through wire filament and results in heating of filament until	Tube containing argon gas and a little amount of mercury vapour. So no filament is there	The forward biased current passes through the inorganic semiconducting	The forward biased current passes through the organic semiconducting layers (ETL and HTL)

		the filament		layers of p-n junction	of p-n junction diode
		glows		diode and causing	and causing electron-
				electron-hole	hole recombination
				recombination	in EML to emit light
				to emit light	
9.	Burnt out due to	Yes	Generally, no but	No	No
	passage of current and		excessive current		
			and extreme		
	voltage fluctuation		voltage variation		
			can cause burntout issues in CFL		
10	Heat consumtion during	Vashishan		No	No
10.	Heat generation during	Yes higher amount of heat	Yes, but less heat generation than	NO	NO
	light emission	generation	incandescent bulb		
11.	Realignment and	No	No No	Yes	Yes
11.		110	110	163	1 63
	dissembling of electron				
	due to starting and				
	stopping				
	of current passage				
12.	Decaying of filaments	Yes	No	No	No
13.	High Versatility	Bigger in size as	Bigger in size as	A single LED is	An OLED is
		compared to	compared to solid	very small in size –	thinner than and
		solid state	state lighting	It can form any	smaller in size
		lighting	resulting in less	desired size and	compared to LED
		resulting in less	versatility	shape grouping	. Many OLED can

		versatility		with many of its	be incorporated in
				prototypes	a flat surface to
				including clusters,	form OLED panel
				Bigger in size as	as LED
				compared to solid	is flexible and
				state lighting	rollable
				resulting in less	
				versatility bars,	
				dots, ropes and	
				many	
14.	Multiple color option	Need different	Need different	Only single RGB	Only single OLED
		colour lamps for	CFL	LED can produce	can produce with
		multi colour		with varying	varying voltage and
		emission apartly		voltage	passing current
					through different
					organic layers

1.20. Comparison among the characteristics of TFT /LCD, LED, OLED, QLED & μLED displays and television and monitors.

Table1.2: Comparisons among the characteristics of TFT /LCD, LED, OLED, QLED & μ LED displays

Sl.	Parameters	TFT/LCD	LED	OLED	QLED	μLED
No.						
1.	Technology	LCD	LED/OLED	Self-Emissive	Trans- missive	Self-Emissive
		Backlight+	Backlight			
		Colour filter				
2.	Contrast and Black levels	Low	Good	Great (Perfectly	Light bleeding	Perfect
				Black and	occurs	
				dark)		
				,		
3.	Colours	Good	Fantastic	Fantastic	Excellent	Good
4.	Refresh rate, Response	Low (ms)	Low(ms)	High (µs)	2-8 ms	Very High (ns)
	time					
5.	Life time	Long	Long	Moderate	Long	Long
6.	Screen burn- in	No	No	Can occur	Not susceptible	High
					to	
					burn -in	
					Colli III	

7.	Price	low	High but less	Highly	Less expensive	Average
			than OLED	expensive	compared to	
					OLED	
8.	Power consumption	High	More	Less (60%-	More	More (30%-
	1 over consumption	Ingii	1,1016	80%	1,1010	40%
				of LCD)		of LCD)
9.	Brightness	Low	Higher but	Low- medium	Separate	High
			less than OLED		Backlight	
10.	Efficiency	Low	High	Medium	High	High
11.	Flexibility	Low	Low	High	Low	Medium
12.	Operating	-20 to 80°C	-20 to 80°C	-30 to 70°C	-20 to	-100 to
	temperature				100°C	120 °C
13.	Luminous	Low	High	Medium	High	High
	Efficacy					
14.	Luminance	> 3000	8000-10000	>500	<3000	>100,000
	(cd/m^2)					
15	Encapsulation	No	No	YES	No	No
	Needed					

1.21. Practical applications of OLEDs:

The applications of the OLEDs mainly can be categorized into two types:

- (1) as full color high resolution high-definition displays and (2) as full colored brighter solid-state lighting (SSL)
- (1) As high resolution full- color display: OLED is as thin as less than 0.4 µm (apart from its substrate) and attuned with flexible or rollable substrates. OLED fabrication is a very cost- effective solution-dependent procedure which leads to roll-to-roll processing and efficient bulk production. OLED displays are self-luminous, low power consuming, self responsive at the same time they have fast refresh rate, wide viewing angle as large as 160° large contrast-ratio. The flat OLED screen supports Lambertian emission which maintains



Figure 1.11: Applications of OLED as full color displays and coloring lights constant brightness irrespective of viewing angle. The full range of colour of OLED displays can be possible varying the emissive organic material These advantages widen the dimension of OLED application as follows:

In mobile phones or smart phones: From 2016 all leading mobile companies like Apple, Samsung, Gionee, Xiomi, LG, OPPO began to Active matrix (AMOLED) displays in their mobile phones e.g., iPhone X, Samsung A8+, Google pixel 2, Gionee S11S, etc.

In digital cameras or viewfinders: OLED displays are widely used in digital cameras as well as in viewfinders. In 2003, Kodak introduced world's first digital camera Kodak LS633.each and every leading digital camera producing company use OLED displays for SLR, DSLR or different prototype of these cameras e.g. Sony A99 Mark II, Canon PowerShot G1 X Mark III, Fuji film GFX 50S Panasonic DMC- FZ2500, Nikon DL24-85, etc.

In smart watches or wearable devices: Generally Wearable devices or smart watches utilize curved, flat and flexible OLED displays. They generally contain multi-functional advanced sensing tools which can recognize voice- command, face-gesture, fingerprint, systole and diastole pressure, blood-oxygen amount, BMR rate, step counting, amount of calorie burn Diesel used OLED displays in their smart watch of model DZ-7086 and Fossil used OLED displays in JR-965 Model, LG, AU optronics and many more manufacturers use OLED displays for their watch production Some wearable devices are Xioami Mi Band 2 In car stereo and car dashboards-OLEDs are used in car dashboard displays, car –music system car-radios, GPS devices (to see the traffic situation, to detect the right path or accurate direction and to see the destination map and locations of the car) etc. Pioneer Electronic Corporation first produced car stereos by using monochrome OLED. The world's first automotive OLED display was incorporated in 2004 by Aston Martin DB9, produced by Yazaki. Then Jeep. Chevrolet followed its path. In 2015, Hyundai and Kia used 3.5' wide PMOLED display in their vehicle. Nowadays Audi Marcedes, Volvo, B.M.W. Maruti-Suzuki and the rest of all automobile manufacturers incorporated use of OLED displays in their vehicles.

In kitchen appliances: OLED displays are used in micro-oven, induction cooker Airfrier, turn on "on", "off" switches and other dedicated workwise individual buttons fry cooker, electric kettles, geysers, water-purifiers where OLED display panels are used to regulate temperature.

Illuminated clothing in fashion technology: In the fashion world OLEDS are

incorporated into textiles such as fibers, fabrics and cotton wears are amazing innovations. They open a new spectrum of fashion to illuminate inert things like textiles with lights. The idea behind this is to combine low energy consuming cool light emitting property of OLED with the low-cost comfortable properties of textiles. The illuminating clothes and photonic textiles are the developing research fields.

In Transparent OLED panels: Transparent OLED panels are widely used in Smart Window replacing glasses. TOLED can be used in the car-windscreen and back rear screen. Transparent OLED is used in transparent OLED smart TVs

Foldable Screen displays: FOLED is widely used in foldable display devices like foldable mobile phones, laptop, display unit, curved displays here two flexible or foldable OLED are used. Comparatively thick and sturdy one gives compactness while the softer on is used for foldable display. Harder OLEDs are connected to a hinge which helps it to bend. **In medical instruments, surgery instruments**: OLEDs have multipurpose application in **oscilloscope**, surgery—monitors, glucometer, oximeter, flexible fiber optics cameras, sphygmomanometer (blood pressure measuring instrument), thermometer etc.

In sports instruments: OLED displays are incorporated into all sports or gym equipment like treadmills, different pressing machines, acrobatics machines, etc. Recently in tennis, cricket football, there are wide applications of OLED displays for big display panels, third referee monitoring, TVs, high density telescopic cameras, OLED TV used for VAR technology in footballs to detect offside, foul in football and baseline call in lawn-tennis and badminton. table tennis etc.

In security devices: OLED displays are used in CCTV, CC camera, display monitor, computers used **in** traffic control room or different security surveillance services

In computers, Laptops tablets, PDAs: Nowadays OLED displays are top choice to produce the monitor or screen of laptop, desktop, tablet, personal digital assistance (PDA) devices etc.

In communicatory devices: OLED displays are widely utilized in telecommunication devices and monitors, computers, In satellite communication, the observatory and the surveillance all remote sensing monitors are made up of OLED displays.

(2) As full colored brighter solid-state lighting (SSL):

- 1. OLED light provides homogeneity in colour and brightness which eases obtuseangular visibility. OLED light can be customized easily.
- 2. As OLED light can be recycled and sustained easily it has become an automatic selection for eco-friendly light sources for the automobile industry
- 3. As OLED is ultra-thin, roll-able and flexible, it allows convex or concave bending and hence can be used for various curved designs and shape in exterior or interior decoration of car, car headlight and taillight etc.
- 4. An OLED light has a longer lifespan. It is a light weight and higher energy-efficient light.
- 5. An OLED possesses higher resistance of temperature, so it does not get heated much.
- 6. OLED light does not emit harmful blue light.
- 7. As an OLED has defined segmentation with glare free, flicker-free properties and needs marginal finish for cars' interior decoration and hence, it also can be used for desirable dimming and focusing of OLED.

1.22. Conclusion

In this research work our principal aim was to fabricate Alq₃ derivative-based OLED devices with novel annealed emitting materials which remain functional even at higher temperature as well as low voltage without compromising its EL and PL performances. The other challenges were to fabricate all the stacked layers one upon another at ambient condition and on ITO coated PET sheet substrate as transparent anode and substrate. Which is novel as we did in-depth study of chemically degraded Alq₃ and found that after oxidation Alq₃ gives more fluorescence. This finding motivated us to create device with this annealed oxide of Alq₃ In order to tune the annealed emitting material we doped ZnO nano particles and rare earth nitrate of europium and neodymium for investigating the possible changes occurred after doping compared to pristine Alq₃. We also tried to investigate our device for prospective SSL applications such as automotive dashboard lighting, high-end cars backlight and indicators, sensor lights, sharp angular lighting applications along with its flat, full color display applications. We will discuss it in detail in our next chapters sequentially. In this project our central aim were to find out oxidative

derivatives of a thermally annealed Alq₃ at,150°C, a degraded non emissive polymeric bye product, Al(q-N-O)₃ [tris (8-hydroxyquinoline -N-oxide)] which is our novel finding. This emissive polymer can exhibit higher photoluminescence (PL) and electroluminescence (EL) compared to bulk Alq₃ powder. Which is also a novel finding. In addition to this if we doped rare earth ion (Eu(III), Nd(III) it will escalate its PL and EL 3 to 4 times compared to our novel non emissive polymer. Our principal aim was to form a flexible transparent rollable low-cost high EL and PL exhibiting, low turn on voltages, higher EQE% performing WOLED and green or yellow OLED. I have explained all the sequential procedures, a characterization technique, and device formation clearly to achieve our research goal in my forthcoming chapters. I have designed low cost flexible high EL and PL emitting OLED successfully through this research product which can open different avenues of new prospects in this field.

References:

- [1.] Kallmann,H., & Pope, M. (1960). Bulk conductivity in organic crystals. Nature, 186(4718), 31-33.
- [2.] Shirakawa, H., Louis, E. J., MacDiarmid, A. G., Chiang, C. K., & Heeger, A. J. (1977). Synthesis of electrically conducting organic polymers: halogen derivatives of polyacetylene,(CH) x. *Journal of the Chemical Society, Chemical Communications*, (16), 578-580.
- [3.] Tang, C. W. (1987). S, A. VanSilyke. *Appl, Phys, Lett*, 51(913), 2
- [4.] Pope, M., Kallmann, H. P., & Magnante, P. (1963). Electroluminescence in organic crystals. *The Journal of Chemical Physics*, 38(8), 2042-2043..
- [5.] Chou, J. H., Kosal, M. E., Nalwa, H. S., Rakow, N. A., & Suslick, K. S. (2000). Applications of porphyrins and metalloporphyrins to materials chemistry. *The porphyrin handbook*, *6*, 43-131.
- [6.] Helfrich, W., & Schneider, W. G. (1965). Recombination radiation in anthracene crystals. *Physical Review Letters*, *14*(7), 229.
- [7.] Vincett, P. S., Barlow, W. A., Hann, R. A., & Roberts, G. G. (1982). Electrical conduction and low voltage blue electroluminescence in vacuum-deposited organic

- films. Thin solid films, 94(2), 171-183.
- [8.] Burroughes, J. H., Bradley, D. D., Brown, A. R., Marks, R. N., Mackay, K., Friend, R. H., ... & Holmes, A. B. (1990). Light-emitting diodes based on conjugated polymers. *nature*, 347(6293), 539-541.
- [9.] Baldo, M. A., O'Brien, D. F., You, Y., Shoustikov, A., Sibley, S., Thompson, M. E., & Forrest, S. R. (2023). Highly efficient phosphorescent emission from organic electroluminescent devices. In *Electrophosphorescent Materials and Devices* (pp. 1-11). Jenny Stanford Publishing.
- [10.] Anthopoulos, T. D., Markham, J. P., Namdas, E. B., Samuel, I. D., Lo, S. C., & Burn, P. L. (2003). Highly efficient single-layer dendrimer light-emitting diodes with balanced charge transport. *Applied physics letters*, 82(26), 4824-4826.
- [11.] Adachi, C., Baldo, M. A., Thompson, M. E., & Forrest, S. R. (2001). Nearly 100% internal phosphorescence efficiency in an organic light-emitting device. *Journal of Applied Physics*, 90(10), 5048-5051
- [12.] Lo, S. C., Male, N. A., Markham, J. P., Magennis, S. W., Burn, P. L., Salata, O. V., & Samuel, I. D. (2002). Green phosphorescent dendrimer for light-emitting diodes. *Advanced Materials*, 14(13-14), 975-979.
- [13.] Brütting, W., Berleb, S., & Mückl, A. G. (2001). Device Physics of Organic Light-Emitting Diodes Based on Molecular Materials. Organic Electronics, 2, 1-36.
- [14.] Debsharma, M., Pramanik, T., Daka, C., & Mukherjee, R. (2022, May). Recent advances in the electrical and optical properties of Alq3 and Alq3 derivatives based OLEDS. In *Journal of Physics: Conference Series* (Vol. 2267, No. 1, p. 012159). IOP Publishing
- [15.] Tang, C. W., & VanSlyke, S. A. (1987). Organic electroluminescent diodes. *Applied physics letters*, 51(12), 913-915.
- [16.] Chen, Y., & Ma, D. (2012). Organic semiconductor heterojunctions as charge generation layers and their application in tandem organic light-emitting diodes for high power efficiency. *Journal of Materials Chemistry*, 22(36), 18718-18734
- [17.] Van Slyke, S.A., Chen, C.H., & Tang, C. W. (1996). Organic electroluminescent devices with improved stability. *Applied physics letters*, 69(15), 2160-2162.

- [18.] Pandey, C. K., Bajpai, M., Srivastava, R., Malik, R., Shukla, G. P., Katiyar, A. K.,... & Dhar, R. (2018, December). Effect of n-type doping on the electron transport of polyfluorene. In *National Conference on Advanced Materials and Devices for Futuristic Applications* (Vol. 2050, No. 1, p. 020024).
- [19.] Tang, C. W., VanSlyke, S. A., & Chen, C. H. (1989). Electroluminescence of doped organic thin films. *Journal of applied physics*, 65(9), 3610-3616..
- [20.] Burrows, P. E., Gu, G., Bulovic, V., Shen, Z., Forrest, S. R., & Thompson, M.E. (1997). Achieving full-color organic light-emitting devices for lightweight, flat-panel displays. *IEEE Transactions on electron devices*, 44(8), 1188-1203.
- [21.] Kim TS, Kim DH, Im H-J, Shimada K, Kawajiri R, Okubo T, Murata H, Mitani T (2004) Improved lifetime of an OLED using aluminum(III) tris (8-hydroxyquinolate)
- [22.] Salleh, M. M., Hasnan, T., Azis, T., Sepeai, S., & Yahaya, M. (2007). Fabrication of organic light emitting diodes (oleds) for flat panel displays. *Berkala Ilmiah MIPA*, 17(3).
- [23.] J. S., & Song, C. K. (2019). Textile display with AMOLED using a stacked-pixe (2006) Study on photoluminescence from tris-8-hydroxyquinoline aluminium thin films and influence of light. *Appl Phys Lett* 89:082106–3
- [24.] Colle M, Gmeiner J, Miliu W, Hillebrecht H, Brutting W (2003) Preparation and characterization of blue-luminescent Tris(8-hydroxyquinoline)- aluminum (Alq3). *Adv. Funct. Mater.13(2)*, 108–112 (2003)
- [25.] Jou, J. H., Kumar, S., Agrawal, A., Li, T. H., & Sahoo, S. (2015). Approaches for fabricating high efficiency organic light emitting diodes. *Journal of Materials Chemistry C*, 3(13), 2974-3002.
- [26.] Craford, M. G. (2005, September). LEDs for solid state lighting and other emerging applications: status, trends, and challenges. In *Fifth International Conference on Solid State Lighting* (Vol. 5941, p. 594101). SPIE the organic semiconductor Alq3. *physica status solidi (a)*, 201(6), 1095-1115.
- [27.] Salah, N., Habib, S. S., & Khan, Z. H. (2013). Highly luminescent material based on Alq 3: Ag nanoparticles. *Journal of fluorescence*, *23*, 1031-1037.

- [28.] Langevin, P. (1903). Recombinaison etmobilitds des ions danslez gaz. *Ann. Chim.Phys*, 28, 433.
- [29.] Kahn, A., Koch, N., & Gao, W. (2003). Electronic structure and electrical properties of interfaces between metals and π -conjugated molecular films. *Journal of Polymer Science Part B: Polymer Physics*, 41(21), 2529-2548.
- [30.] Pauli, W. (1925). "Über den Zusammenhang des Abschlusses der Elektronengruppen im Atom mit der Komplexstruktur der Spektren". Zeitschrift für Physik.31 (1): 765–783.Bibcode:1925ZPhy...31..765P.doi:10.1007/BF02980631.S2CID 122941900.
- [31.] Salah, N. A. J. (2018). SA), Memic, Adnan (Jeddah, SA), Al-ghamdi, Attieh A. Jeddah, SA), Algarni, Sabah Eid (Jeddah, SA), Khan, Zishan H.(New Delhi, IN), Method of making doped Alq3 nanostructures with enhanced photoluminescence, KING ABDULAZIZ UNIVERSITY (Jeddah, SA), United States.
- [32.] Salah, N., Habib, S. S., Khan, Z. H., & Alharbi, N. D. (2013). Synthesis and characterization of pure and Tb/Cu doped Alq3 nanostructures. *Journal of luminescence*, *143*, 640-644.
- [33.] Johansson, N., Osada, T., Stafström, S., Salaneck, W. R., Parente, V., Dos Santos, D. A., ... & Bredas, J. L. (1999). Electronic structure of tris (8-hydroxyquinoline) aluminum thin films in the pristine and reduced states. *The Journal of chemical physics*, 111(5), 2157-2163.
- [34.] Siddiq, M. A., Sopaih, M., & Elgazzar, E. (2023). Impact of Y2O3 nanosheets on the photodiode performance. *ACS omega*, 8(28), 24883 microstructural characteristics of Alq3 prepared via the co-precipitation route for enhancement of -24892.
- [35.] Reyes, R., Hering, E. N., Cremona, M., Da Silva, C. F. B., Brito, H. D., & Achete, C. A. (2002). Growth and characterization of OLED with samarium complex as emitting and electron transporting layer. *Thin Solid Films*, 420, 23-29.
- [36.] Xu MS, Xu JB (2005). Visualization of thermally-activated degradation pathways of tris(8- hydroxyquinoline) aluminum thin films for electroluminescence

- application. Thin Solid Films 49:317-22
- [37.] D. Ammermann, A. Böhler, W. Kowalsky(2009) *Multilayer Organic Light Emitting Diodes for Flat Panel Displays* Archived at the Wayback Machine, Institut für Hochfrequenztechnik, TU Braunschweig, 1995.
- [38.] Holmes, Russell; Erickson, N.; Lüssem, Björn; Leo, Karl (2010). "Highly efficient, single-layer organic light-emitting devices based on a graded-composition emissive layer". Applied Physics Letters. **97** (1): 83308. Bibcode:2010 ApPhL.. 97a3308S. doi:10.1063/1.3460285.
- [39.] Carter, S. A.; Angelopoulos, M.; Karg, S.; Brock, P. J.; Scott, J. C. (1997). "Polymeric anodes for improved polymer light-emitting diode performance". Applied Physics Letters. 70 (16):Bibcode:1206997ApPhL..70.2067C. doi:10.1063/1.118953.
- [40.] Friend, R. H.; Gymer, R. W.; Holmes, A. B.; Burroughes, J. H.; Marks, R. N.; Taliani, C.; Bradley, D. D. C.; Santos, D. A. Dos; Brdas, J. L.; Lgdlund, M.; Salaneck, W. R. (1999). "Electroluminescence in conjugated polymers". Nature. 397 (6715): 121–128. Bibcode:1999Natur.397..121F. doi:10.1038/16393. S2CID 4328634.
- [41.] AlSalhi, M. S., Alam, J., Dass, L. A., & Raja, M. (2011). Recent advances in conjugated polymers for light emitting devices. *International Journal of Molecular Sciences*, 12(3), 2036-2054
- [42.] Davids, P. S.; Kogan, Sh. M.; Parker, I. D.; Smith, D. L. (1996). "Charge injection in organic light-emitting diodes: Tunneling into low mobility materials". Applied Physics Letters. 69 (15):2270. Bibcode:1996 ApPhL..69.2270D. doi:10.1063/1.117530.
- [43.] Crone, B. K.; Campbell, I. H.; Davids, P. S.; Smith, D. L. (1998). "Charge injection and transport in single-layer organic light-emitting diodes". Applied Physics Letters. 73 (21): 3162.Bibcode:1998 ApPhL..73.3162C. doi:10.1063/1.122706.
- [44.] Crone, B. K.; Campbell, I. H.; Davids, P. S.; Smith, D. L.; Neef, C. J.; Ferraris, J.P. (1999). "Device physics of single layer organic light-emitting diodes". Journal

- of Applied Physics. **86** (10):5767. Bibcode:1999JAP. 86.5767C. doi:10.1063/1.371591.
- [45.] Shah, Bipin K.; Neckers, Douglas C.; Shi, Jianmin; Forsythe, Eric W.; Morton, David (1 February 2006). "Anthanthrene Derivatives as Blue Emitting Materials for Organic Light-Emitting Diode Applications". Chemistry of Materials. 18 (3): 603–608. doi:10.1021/cm052188x. ISSN 0897-4756.
- [46.] Sato, Y.; Ichinosawa, S.; Kanai, H. (1998). "Operation Characteristics and Degradation of Organic Electroluminescent *Devices"*. *IEEE Journal of Selected Topics in Quantum Electronics*. 4 1): 40–48.Bibcode:1998IJSTQ...4...40S.
- [47.] Arik, M., Petroski, J., & Weaver, S. (2002, May). Thermal challenges in the future generation solid state lighting applications: light emitting diodes. In *ITherm 2002*. Eighth Intersociety Conference on Thermal and hermomechanical Phenomena in Electronic Systems (Cat. No. 02CH37258) (pp. 113-120). IEEE..
- [48.] Burrows, P. E., Bulovic, V., Forrest, S. R., Sapochak, L. S., McCarty, D. M., & Thompson, M. E. (1994). Reliability and degradation of organic light emitting devices. *applied physics letters*, 65(23), 2922-2924.
- [49.] Lee, S. T., Gao, Z. Q., & Hung, L. S. (1999). Metal diffusion from electrodes in organic light-emitting diodes. *Applied Physics Letters*, 75(10), 1404-1406.
- [50.] Aziz, H., Popovic, Z. D., Hu, N. X., Hor, A. M., & Xu, G. (1999). Degradation mechanism of small molecule-based organic light-emitting devices. *Science*, 283(5409), 1900-1902.
- [51.] Sun, Y., & Forrest, S. R. (2006). Organic light emitting devices with enhanced outcoupling via microlenses fabricated by imprint lithography. *Journal of applied physics*, 100(7).
- [52.] Debsharma, M., Pramanik, T., Maji, P. S., Maity, A. R., Jain, A., & Mukherjee, R. (2024). Effect of ZnO nanoparticle on morphology and optical properties of yellowemissive bulk Alq3 for OLED application. *Optical Materials*, 115768.
 - [53.] Cai, M., Xiao, T., Hellerich, E., Chen, Y., Shinar, R., & Shinar, J. (2011). High- efficiency solution-processed small molecule electrophosphorescent organic light- emitting diodes. *Advanced Materials*, *23*(31), 3590-3596.

- [54.] Gessmann, T., & Schubert, E. F. (2004). High-efficiency AlGaInP light-emitting diodes for solid-state lighting applications. *Journal of applied physics*, 95(5), 2203-2216
- [55.] Schubert, E. F., Kim, J. K., Luo, H., & Xi, J. Q. (2006). Solid-state lighting—a benevolent technology. *Reports on Progress in Physics*, 69(12), 3069.
- [56.] Lee, S., Kim, B., Jung, H., Shin, H., Lee, H., Lee, J., & Park, J. (2017). Synthesis and electroluminescence properties of new blue dual-core OLED emitters using bulky side chromophores. *Dyes and Pigments*, *136*, 255-261.
- [57.] Sudheendran Swayamprabha, S., Dubey, D. K., Shahnawaz, Yadav, R. A. K., Nagar, M. R., Sharma, A., ... & Jou, J. H. (2021). Approaches for long lifetime organic light emitting diodes. *Advanced Science*, 8(1), 2002254.
- [59.] Rajeswaran, G., Itoh, M., Boroson, M., Barry, S., Hatwar, T. K., Kahen, K. B., ... & Takahashi, H. (2000, May). 40.1: Invited Paper: Active Matrix Low Temperature Poly-Si TFT/OLED Full Color Displays: Development Status. In SID Symposium Digest of Technical Papers (Vol. 31, No. 1, pp. 974-977). Oxford, UK: Blackwell Publishing Ltd.
- [60.] Cao, Y., Parker, I. D., Yu, G., Zhang, C., & Heeger, A. J. (1999). Improved quantum efficiency for electroluminescence in semiconducting polymers. *Nature*, *397*(6718), 414-417.
- [61.] Baldo, M. A., O'brien, D. F., Thompson, M. E., & Forrest, S. R. (1999). Excitonic singlet-triplet ratio in a semiconducting organic thin film. *Physical Review B*, 60(20), 14422.
- [62.] Dwivedi, A. D. D. (2014). Numerical simulation and spice modeling of organic thin film transistors (OTFTs). *International Journal*, 1(2), 15.

Chapter2: Literature review, Research gap and Research objective

2.1. Literature review till date

- Martin Pope et al. (1960) witnessed the first injection of a dark hole into an anthracene crystal (organic compound). This groundbreaking discovery also described the energy requirements for injecting electron-hole connections. The primary direct current electroluminescence (EL) of both single crystal and impurity-doped anthracene was detected by the same group. The devices produced visible emissions over 400 volts and had a thickness of 10–20 μm. These 10-20 μm thick EL devices were produced to emit visible emissions of more than 400 volts [1]
- Helfrich and Schneider (1965) successfully produced EL in the case of single organic anthracene crystals via doubly injected recombination utilizing electronand hole-injecting electrodes, i.e., cathode and anode correspondingly. To obtain noticeable emissions, the operating voltage was dramatically lowered to around 60V. According to Child's law, the estimated electron mobility is about 0.4 cm²/(V.s). The device's thickness of 1-5 mm limited the current to 10 A at 100 volts [2].
- Hideki Shirakawa and colleagues (1977) synthesized electrically conductive organic polymers, specifically halogen derivatives of polyacetylene [(CH)x]. Upon exposure to chlorine, bromine, or iodine vapours, silvery films of the semiconducting polymer trans'polyacetylene' (CH)x undergo halogen uptake, resulting in a significant increase in conductivity (exceeding seven orders of magnitude with iodine). The degree of halogenation yields silvery or silvery-black films, some exhibiting exceptionally high conductivity at ambient temperature.[3]

- C.W. Tang et al. (1987) described a bi-layered OLED thin film made of organic ETL layer Alq₃ [Tris(8-hydroxyquinolinato)aluminium(III)] and aromatic hole transport layer (HTL) layer diamine. Alq₃ has grown in popularity due to its exceptional blue-green dazzling luminosity, low production costs, simple manufacturing process, low operating voltage, and ability to fine-tune emission wavelength. Despite its versatility, Alq₃ has significant operational limitations, including shorter life-spans and a sharp decline in photoluminescence (PL) and electroluminescence (EL) efficiency over time. The new OLED was impressive with a luminance of over 1000 cd/m² an EQE of 1% photon/electron, and a high luminous efficiency of 1.5 lm/W. [4]
- Tang et al. (1989) also demonstrated that incorporating fluorescent organic dyes into the host organic Alq₃ matrix can significantly increase an OLED's efficiency by improving energy transfer from the host layer to organic dye layers, resulting in higher EL and PL quantum efficiency.[5]
- Friend and associates (1990) reported a green electroluminescent, highly efficient poly(p-phenylene vinylene) (PPV) thin film (100 nm). via spin-coating When injected electrons and injected holes were recombined mutually and underwent a radiative decay of singlet excitons, which was known as the EL of the EL device. A significant current injection threshold of 14 V with an EQE of 0.05% was reached [6]
- **Keith A. Higginson et al. (1998)** examined the thermal and morphological influences on the hydrolytic stability of Alq₃.A study was conducted on the physical and chemical properties of Alq₃ as both potent ETL materials and EML materials for small-molecule organic light-emitting diodes (OLEDs), The thermal stability of Alq₃ in the presence of atmospheric moisture was examined by tracking the release of volatile 8-hydroxy quinoline (8-Hq), employing TGA(thermogravimetric analysis) along with GC/MS(gas chromatography/mass spectrometry). The stability of more crystalline annealed Alq₃ sample was shown to be significantly influenced by sample morphology. Annealed samples, which

are more crystalline, demonstrated enhanced stability to hydrolysis compared to freshly sublimed films, albeit with a reduction in photoluminescence efficiency. The potential ramifications of these phenomena are examined concerning the failure mechanisms of Alq₃-based OLEDs.[7]

- Reyes. R. et al. (2002) synthesized the complex of samarium, i.e., [Sm(TTA)₃(TPPO)₂][tris(thenoyltrifluoroacetonate)bis(triphenylphosphine oxide) samarium] to determine whether the samarium complex could be utilized as both an ETL (electron transporting layer) and EML (emissive layer) and then built the two devices. and used the following architecture to demonstrate how their EL performance varied. Here, Device1represents [Sm(TTA)₃(TPPO)₂]/ITO/MTCD/Alq₃/Al, and Device2 represents Sm(TTA)₃(TPPO)₂]/ITO/MTCD/Al. In 2002, they once again revealed the vacuum deposition approach for fabricating europium complex [Eu(TTA)₃(TPPO)₂]. OLED based on the, and they investigated the electroluminescence (EL) performance of the Eu₃₊ cation-doped Alq₃.source.[8]
- M. Colle et al. (2005) presented the initial findings regarding the electronically excited triplet state in Alq3. They examined the ISC (intersystem crossing) behavior of it. They recorded phosphorescence spectrum. They also found that in δ-Alq3 the diminished population of triplet states is attributable to intersystem crossing. It is a distinctive feature of the facial isomer. Additionally, they discovered that intersystem crossing is responsible for the decreased number of triplet states in δ- Alq3. This was shown for a variety of morphologies, including diluted material in a frozen glass matrix, crystalline phases, and amorphous films. They observed two separate bands in the delayed luminescence phases of Alq3: (1) delayed fluorescence (for crystalline phases), and (2) phosphorescence (for amorphous thin films). They discovered that the energy levels of the triplet vibrations changed from 2.16 eV to 0.1 eV in the case of facial isomer (or δ-Alq3) and from 2.11 eV to 0.1 eV on the case of meridional isomer (α-Alq3). They also observed a phosphorescence band in the case of temperature-

- dependent delayed luminescence between 6K and 150K. For yellowish green Alq₃, the temperature-dependent triplet lifespans, varying from about 17 ms (@ 6 K) to 4 ms (@ 120 K), were also confirmed. Additionally, they showed that Alq₃ underwent a phase transition at about 50 K. [9]
- Knox et al. (2005) utilized Alq₃ as an electron transport layer (ETL) and an emissive layer (EML) in their organic light-emitting diodes (OLEDs). One important mechanism of failure for Alq₃-based OLEDs has been found to be the reaction between Alq₃ and trace H₂O. They used hybrid DFT (density functional theory) calculations to outline the hydrolysis process of Alq₃. For the neutral and oxidized Alq₃/Alq₃⁺ systems, they offered extensive information on atomistic and thermochemical reactions. Neutral hydrolysis reaction pathway is a thermally activated process with a conventional barrier width of 24.2 kcal mol⁻¹. Alq₃ and its hydrolysis product, Alq₂OH, are further characterized by comparing electronic absorption infrared and spectra obtained from first principles. The activation energy of the neutral reaction is 8.5 kcal mol⁻¹ higher than that of the cationic Alq₃ hydrolysis pathway, indicating that charge imbalance may play a role in the chemical failure modes of OLED devices.[10]
- Norlida Kamarulzaman et al (2011) synthesized Poly[2-methoxy-5-(2'-ethylhexyloxy)-(p-phenylenevinylene)] (MEH-PPV) using three consequential (3) steps of modified Gilch route. The 19.5% polymer was yielded where the transition temperature of glass (Tg) is 85 °C, melting point of the polymer is 330 °C and on- set temperature of decomposition is 720 °C.[11]
- César Pérez-Bolívar et al. (2011) reported a study to tune Alq₃-complexes' electroluminescence (EL) and the emission ranging from green light region to blue light region. They found that on C4 and C6, the electron –donating substituents exist in combined forms, beginning with the compounds 1 to compound 6, They observed that emission tuning ranges in between 478 nm to 526 nm whereas quantum of fluorescence ranging 0.15 to 0.57. they used

Compound 2 to compound 6 as OLED's hosts and emitters. They used compound 3 to compound 5 for the host of red phosphorescent dopants of WOLEDs (white OLEDs) having 19% EQE (higher external quantum efficiency) and higher purity of white colour with colour rendering index was near about 85, Whereas the highest EQE for compounds 2 to 6 was 4.6 %.[12]

- **Zubair Ahmad et. al (2013)** reported MEH-PPV /Alq₃ –based organic bulk heterojunction photodiode (BHJ) and they characterized its optical properties for different illumination intensities and got a fair amount of Photo-current responsivity at 3V which is ~8 mA/W and value of *I*Photo/*I*Dark ratio is 1.24. By using UV-Vis spectroscopy and Photo-luminescence (PL) they studied optical properties of blended thin films of MEH_PPV and Alq₃ thin films. For fabrication MEH- PPV/Alq₃/PEDOT: PSS (40 nm thickness)/LiF/Al. At first, they spun coated PEDOT: PSS(poly(3,4-ethylendioxythiophene):poly(styrene sulfonate) on an ITO coated glass substrate and then fabricated MEH-PPV and Alq₃ photosensitive blending part by spin coating method. After that LiF (Lithium Fluoride) and Al cathode thin-films are deposited using thermal-evaporation method.[13]
- Salah et al. [2013] documented the integration of Alq₃ thin-film nanostructures with various metals, including silver (Ag), europium (Eu), copper (Cu), dysprosium (Dy), and terbium (Tb). To be more specific, the PL intensity of the lanthanides dye-incorporated Alq₃ (Dy/Alq₃) thin film was four times that of the pure Alq₃ thin film. [14]
- Cuba et al. (2014) synthesized pure tris-(8-hydroxyquinoline)aluminum (Alq₃) and Alq₃/ZnO nanocomposites with varying weight percentages (5 wt%, 10 wt%, 20 wt%, 30 wt%, 40 wt%, and 50 wt%) of ZnO in Alq₃, which were subsequently coated onto a glass substrate via the dip coating method. In Alq₃ films, they found that the highest luminescence yield was obtained at the ideal ZnO concentration. The amorphous nature of the pure Alq₃ film is revealed by

the XRD pattern. There is crystalline ZnO in the Alq₃/ZnO nano composite thin films of Alq₃ films with different wt% of ZnO. Quinoline's synthesis is confirmed by the FTIR spectrum, which showed absorption between 600 and 800 cm⁻¹. Both the corresponding Alq₃ band and a Zn⁻O vibration band are present in the Alq₃/ZnO nano composite thin films. The band gap (HOMO–LUMO) of Alq₃ film was determined from absorption spectra, yielding a value of 2.87 eV for pristine films, while composite films with 5–50 wt% of ZnO exhibited band gaps of 3.26 -3.20 eV. When Alq₃ films are excited at 390 nm, their photoluminescence (PL) spectra show a peak PL intensity at 514 nm. The ZnO-containing composite films (Alq₃/ZnO) exhibit emissions at 485 and 514 nm. The composite films with 30 wt% ZnO demonstrate the highest luminescence yield.[15]

Cuba et al. (2014) synthesized Tris-(8-hydroxyquinoline)aluminum (Alq₃) and applied it onto a glass substrate utilizing the dip coating technique. When the Alq₃ thin film was thermally annealed from 50°C to 300°C, they investigated its optical and surface morphological characteristics. They fabricated Alq₃ thin films consisting of 2 to 16 layers (42 nm to 324 nm in thickness) to achieve the maximum luminescence intensity. The quinoline anion's presence and formation during absorption in the 700-500 cm⁻¹ range were verified by the FTIR spectrum. Alq₃ films, when subjected to annealing at 300°C, exhibited decomposition and partial sublimation of the quinoline anion. The amorphous nature of the Alq₃ thin films annealed between 50°C and 150°C was determined using X-ray diffraction patterns. The Alq₃ film annealed at temperatures exceeding 150°C exhibited a crystalline structure. After being annealed at temperatures higher than 150°C, the Alq₃ film showed a crystalline structure. When energized at 390 nm, film annealed at 150°C exhibits a photoluminescence intensity peak at 512 nm. The Alq₃ thin film, which was deposited at 150°C and consisted of 10 layers (each about 220 nm), showed the best luminescence

yield.[16]

- **Po- Ching Kao et al.,(2015)** demonstrated that when MoO₃ or CS₂CO₃ and, a high work function p-type dopant are doped with host Alq₃ and ITO coated glass substrate and with Al cathode to make an monolayered hybrid OLED device with p-i-n homojunction their hole mobility becomes 9.76 x10⁻⁶ cm²/Vs and their electron mobility becomes 1.26 x10⁻⁴cm²/Vs respectively with turn on voltage is about 4.3 volt at 1 cd/m², and at 11.4 volt maximum luminance is 5860 cd/m² and at 100 mA/ cm² maximum luminous efficiency is 2.53 cd/A which is more higher than bi-layered hetero-junctional OLEDs and exhibit extraordinary electroluminescence.[17].
- **B.A. Paez-Sierraa et al.(2016)** formulated toluene soluble MEH-PPV (hole transport polymer and Alq₃ (electron transport polymer) blended semiconducting ink by doping intentionally at room temperature resulting in lower switch—on voltages required OLED display as well as additional state of bandgap occurred for MEH-PPV. For 30% Alq₃ doping concentration the emission occurs for band of 565 nm with work function 2.19 eV and for 60% concentration Alq₃ emissions are observed at 530 nm with work function of 2.33 eV (blue shifted) and as a result charge transfers from LUMO of Alq₃ to HOMO of MEH-PPV.[18]
- **Derkowska and Zielinska**(2017) reported that Alq₃ has two absorbance bands, band-A and band-B, which results in ligand oriented electronic shift. A-band is seen in the 350–450 nm spectral range when charges are transferred from the oxygen- containing quinolinolate ring to the nitrogen-containing pyridyl ring, resulting in a π–π* transition of the qH^{2.+}, or when electronic transitions originate from the ground energy state to the excited energy state. However, within the spectral range of 210 nm to 280 nm we can observe band-B. This begins when electrons are moved from electronic orbitals to π* molecular orbitals and strong p–π* transitions are facilitated by the central metal-containing p-band of aluminium (Al) [19].

- C.K. Pandey et al. (2018) investigated the impact of n-type doping on the electron transport characteristics of polyfluorenes and electroluminescence (EL) in conjugating polymer polyfluorene. They also deactivated exponentially spread deep energy traps by doping of a n-type dopant, DMC(decamethylcobaltocene) which results trap free electron transport for PFO based diodes [20].
- I. M. Ibrahim et al. (2019) demonstrated that if in an OLED if MEH-PPV/TiO2 nanocomposites materials are used as an emissive layer (amounts of TiO2 incorporation onto MEH-PPV are 0.002 g/ml and 0.008 g/ml) higher value of current about 7430 μA/m² and higher value of electroluminescence are found at the same time the TiO₂ anatase phase is observed, They also do characterization and gave different application of TiO₂ thin films. They also compared these results with the pristine Alq₃.[21]
- Wei Liu et al. (2019) explained that developing a high performance giving luminescent material for solid state lighting (SSL) technology and its application in LED and especially OLED has become a great interest for researchers. These luminescent materials can be developed by two methods: first by phosphors and second by emissive layers. These two methods are used to make light emitting diodes and organic light emitting diodes.[22]
- HemlataBisht et al. (2020) reported that the excitation energy, between the donor Alq₃(donor) and MEH-PPV (acceptor), can be transferred using time-domain and steady state operating fluorescence-techniques. This transferred excitation energies are non-radiative, Long-ranging Förster- resonance and also occurred because of dipole—dipole coupling. This causes fluorescence intensity and decay time to increase and decrease for the acceptor and donor, respectively, depending on the higher acceptor concentration that is given. Strong donor-acceptor interactions are more important than donor-donor interactions.[23]

- Liangfei Duan et al. (2021) prepared nano films of green OLED material Tris(8- hydroquinoline) on glass substrates applying vapor deposition method for variable surface-states and the luminescent properties of the green OLED The structural and surface-morphologies of Alq₃ nanofilms were investigated using XRD and SEM They created Alq₃, emitters -based green OLED devices containing architecture: Mo/2-TNATA(20 nm)/NPB(10 nm)/Alq₃(25 nm):Ir(ppy)3 (5%)/Bphen (10 nm)/LiF (5 nm)/Mg:Ag (10%) (10 nm). They characterized the photoelectric properties of the green OLED device employing Photo Research PR655 spectrometer. The observed that the during physical vapor deposition method Alq₃ forms nanotubes, nanowire, nanospheres and also nanosphere containing chains due inter-molecular weak van-der-waals force and mutual weak interaction π - π bond resulting in molecular self-assembling of Alq₃ molecules. The vapor deposition temperature regulates the surface control of Alq₃ thin film. Enhancing the green OLED's performance. They found that Alq₃ nanotubes made OLED, among all the different morphologies created, was the best green-OLED device, which exhibited CIE coordinate (3358, 0.6302) i.e., chromaticity, 20.24 cd/A current efficiency, and 11,490 cd/m² brightness at 5V. [24]
- having architecture: Alq₃/TAZ:Ir(ppy)3-BCP/HMTPD to study the mechanism of light generation via electron hole pairs (EHPs) recombination in the OLED. They studied J-V characteristics plot and I-V characteristics plot of the OLED following the Langevin model. They evaluated the threshold voltage of the OLED was ~3.25 Volt. They also investigated the changes in the and transmitted and from OLED reflected lights for different thickness of the ETL layer of developed OLED. They also observed recombination pre-factor for EML and ETL layers and found photon- emission at wavelength ~560 nm [25]
- <u>Ritu</u> et al. (2023) explained about the structure-development of an ITO/NPD/Alq₃/TPBi/Bphen/LiF/Al based OLED. They investigated I-V

characteristics, J-V characteristics, charge density for the electrical properties and recombination rate following the Richardson Shockley –Hall formula drift and diffusion equations, Poisson equations and carrier continuity equation. Their OLED showed ~3.5 operating (threshold) voltage with highest e-h recombination rate of ~ $4.5 \times 10^{28}/\text{m}^3$) within the wavelength range of ~ 260 nm-275 nm. maximum intensity wavelength of ~ 475 nm (visible region) of in emissive (EML) region of Alq₃. They also studied IQE at different voltages, efficiency drop at particular voltage and recombination pre-factors $\theta1$ and $\theta2$ for different voltages. [26].

Małgorzata Sypniewska et al. (2024) utilized Tris(8-hydroxyquinoline) aluminium integrated into polymeric matrices, specifically poly(Nvinylcarbazole) (Alq3: PVK) and polystyrene sulfonate (Alq3: PSS), as the active layer for green- colored OLEDs, which were accumulated via spin-coating method on silicon- and glass-substrates. Employing SEM plot they discovered that comparatively thin Alq3: PSS and Alq3: PVK thin films were produced. They verified the samples' composition via FTIR spectrum. They studied optical characteristics of these three thin films utilizing UV-VIS absorbance spectroscopy & spectroscopic ellipsometry. They found 4(four) absorption bands and three absorption bands within the absorption spectrum of Alq3: PVK and Alq₃: PSS nano composites respectively. The peak intense light emission of the examined thin layers was seen at approximately 500 nm wavelength. Cyclic voltammetry of Alq₃ and two other nanocomposites were also presented. Their theoretical DFT (density functional theory) calculations were investigated to elucidate the interactions and characteristics of the excited states of Alq3: PVK and Alq3: PSS. They also constructed OLED (organic light-emitting diode) structure utilizing Alq3: PVK which exhibited a robust electroluminescence with a green emission at 520 nm wavelength. The EL and PL efficiency of the device indicate that the

ITO/PEDOT: PSS/Alq₃: PVK/Ca/Al configuration is advantageous for the fabrication of economical OLEDs, utilizing Alq₃: PVK as the active layer for prospective lighting applications.[27]

• Yukang Zhao et al. (2025) incorporated a MoO₃ layer onto N,N'-diphenyl-N,N'-bis(1-naphthyl)(1,1'-biphenyl)-4,4'-diamine or NPB (HTL) to improve the performance of Alq₃-based OLEDs, Despite an improvement in the J-V characteristics, the addition of MoO₃ to the NPB layer causes a noticeable electroluminescence quenching effect in their OLED device. At a current density of 20 mA/cm², the MoO₃-blended NPB (50 weight percent) OLED device shows 5.83 V driving voltage while the device without MoO₃ shows a 6.6 driving voltage The latter's brightness (735 cd/m²) or current efficiency (3.68 cd/A) is much higher than former's brightness (54.3 cd/m²) and current efficiency (0.27 cd/A) This was caused due to charge-transfer occurred between MoO₃ and NPB or Alq₃ followed by formation of energy gap states among them. [28]

2.2 Research gap:

There are huge research gap prevails in the case of Alq₃ and Alq₃ derivative -based OLED device regarding device performances, stability, chemical degradation due to moistures, temperature, oxidation, reductions etc., PL and EL efficiency's degradation, emitter material's degradation, variable architecture, higher manufacturing cost, operation life-span, turn- on voltage, driving voltage, charge transport, charge injection, doping concentration of different materials. Different substrate materials, synthetic procedures, metallic organic interface, and different factors that can tune the emission colour and characteristics of light etc. Here all afore- mentioned research gaps can be categorized into four principal classes as follows:

1. **Stability and Degradation:** Over time, Alq₃-based OLEDs are susceptible to deterioration, particularly when exposed to environmental conditions or operated at high brightness for extended periods of time i.e., on account of ageing effect.

Common causes of this deterioration include:

- Hole- accumulation and oxidative degradation: As Alq₃ has comparatively low electron mobility in comparison to many materials that transport holes, holes can accumulate at the Alq₃ interface, which can result in oxidative degradation.
- **Photo-oxidation:** Alq₃'s electronic structure and luminescence efficiency may alter as a result of photooxidation.
- **Hydrolysis:** Breaking down of Alq₃ through chemicals reaction with water or moisture is known as hydrolysis of Alq₃, and it can have detrimental effect on the stability and functionality of the OLED device. As the emitters and other materials undergo chemical hydrolysis, those materials are degraded which negatively affects its PL and EL efficiency of OLEDs
- Self-luminous-quenching and charge trapping: Due to production of non-radiative triplet excitons compared to less radiative singlet exciton production (3:1), Alq₃-based OLED usually lose their energy and encounter self- luminous-quenching and charge trapping. These result in reduction of brightness of emitted light along with its PL-& EL- efficiency.

2. Enhancing Performance: The main goals of research are:

- Constructing new derivatives of Alq₃: Degradation and mobility problems can be resolved by investigating altered Alq₃ molecules with better stability or electron transport characteristics.
- Optimizing device architecture: To reduce hole accumulation and enhance charge transport, including additional materials, such as MoO₃, V₂O₅ in hole-transporting layers (HTL) or use charge-balancing copolymers.
- Analyzing new materials: Examining substitutes like different functional groups

such as alkyl, amine, aryl, benzyl, addition of different metals such as rare earth element such as neodymium(Nd), europium(Eu) etc. transitional elements, Zn, different alkali metal like lithium(Li),sodium(Na),potassium(K) etc or combinations of materials, polymers, co-polymers that can be used with different corners and side chains of benzene and pyridile rings of Alq₃ to improve OLED performance and stability. Relentless research is still a ongoing process to incorporate new materials with new characteristics into Alq₃ matrix.

- **3. Particular Topics of Research:** Creating different Alq₃ derivatives broadens various arenas of specific fields of research. We can summarize those arenas into the following principal classes:
- **Molecular engineering:** Developing Alq₃ derivatives with specific electronic configurations to improve their electron transport and/or stability characteristics.
- Interface engineering: Improving charge injection and transport efficiency by optimizing the interfaces between the OLED device's various layers such as HTL and ETL. It also minimizes energy loss occurred inside an OLED.
- Tuning of colors, PL and EL efficiency by doping and co-doping: In order to improve the material's qualities, color-tuning ability, PL- & EL-efficiency and boost device performance of an Alq₃ -based OLED device, doping and co-doping are introduced into Alq₃ matrices. E.g., ZnO/Alq₃ nanocomposites can tune the green emission of pristine Alq₃into yellow emission.
- **Solvent -free synthesis:** Using techniques for Alq₃ synthesis without the use of organic solvents, or solvent-free synthesis, can help lower contamination and increase stability
- **4. Research gap of semiconducting conductive polymers:** From the available literature the following shortcomings are detected: when conductive polymers are used as semi-conducting OLED materials then the following drawbacks are prevalent:
- Conductive polymers possess poor processibility which limits their large –scale applications.
- The manufacturing cost of conductive polymer is very high

- The conductive polymers suffer material inconsistencies
- The conductive polymers are toxic in nature
- The Conductive Polymer shows poor solubility in solvents.
- The conductive polymer cannot be melted by direct melting processes.
- OLED displays last for very short time

Apart from these Alq₃ based OLED materials and devices encounter different shortcomings as follows:

- In the early forms of OLEDs were suffering four times rapidly wearing out problems while compared to conventional LEDs Or LCD displays.
- Organic molecules are highly hydro sensitive which could be detrimental when it is exposed to water molecules, splashing water, rainwater, moisture etc.
- p-type doped semiconducting OLED materials and devices have a numerous number of published papers, but n-type doped polymeric semiconductor OLED material is few as it is difficult to synthesis and double doping also a difficult to produce.
- When insulators like polymers are doped or administered by organometallic material; or metallic material its electrical and thermal conductivity increases but mechanical property of it gets decreased. The conversion from insulator to metallic or semiconducting properties is a very time-consuming method.
- Although significant progress has been made in raising OLED's internal quantum efficiency to almost 100%, optical losses continue to cause the external quantum efficiency to lag.
- One common substance that emits light is tris-(8-hydroxyquinoline)aluminum (Alq₃). In organic light-emitting devices (OLEDs), it also serves as an electron-transporting layer. However, one of these devices' biggest issues is degradation. Factors like air, moisture, and light exposure have an impact on the device's

performance [1,2].

• Alq₃ has very poor levels of processibility

The main area of research for Alq₃-based OLEDs is addressing the limitations of Alq₃, specifically its low electron mobility, photooxidation susceptibility, and degradation vulnerability. Realizing the full potential of Alq₃-based OLEDs in solid state lighting and display applications requires more research in these areas.

2.3 Research Objective:

- 1) To develop voltage tunable OLEDs with wide wavelength of emission spectrum.
- 2) Tuning the bandgap of emissive layers to improve the recombination rate.
- 3) To investigate the role of rare earth ions in electronic and optical properties.
- 4) To find possible application in solid state lighting industry.

Reference:

- [1.] Pope, M., Kallmann, H. P., & Magnante, P. (1963). Electroluminescence in organic crystals. *The Journal of Chemical Physics*, 38(8), 2042-2043.
- [2.] Helfrich, W., & Schneider, W. G. (1965). Recombination radiation in anthracene crystals. *Physical Review Letters*, 14(7), 229. Shirakawa, H., Louis, E. J., MacDiarmid, A. G., Chiang, C. K., & Heeger, A. J. (1977).
- [3.] Synthesis of electrically conducting organic polymers: halogen derivatives of polyacetylene,(CH) x. *Journal of the Chemical Society, Chemical Communications*, (16), 578-580.
- [4.] Tang, C. W., & Van Slyke, S. A. (1987). Organic electroluminesecnt diodes. Appt.Phys. Leu, 51(12), 913-915.
- [5.] Tang, C. W., VanSlyke, S. A., & Chen, C. H. (1989). Electroluminescence of doped organic thin films. *Journal of applied physics*, 65(9), 3610-3616

- [6.] Friend, R. H.; Gymer, R. W.; Holmes, A. B.; Burroughes, J. H.; Marks, R. N.; Taliani, C.; Bradley, D. D. C.; Santos, D. A. Dos; Brdas, J. L.; Lgdlund, M.; Salaneck, W. R. (1999). "Electroluminescence in conjugated polymers". Nature. 397 (6715): 121–28. <u>Bibcode</u>: 1999 <u>Natur.397..121F</u>. doi:10.1038/16393. S2CID 328634.
- [7.] Higginson, K. A., Thomsen III, D. L., Yang, B., & Papadimitrakopoulos, F. (2004). Chemical Degradation and Physical Aging of Aluminum (III) 8- Hydroxyquinoline: Implications for Organic Light-Emitting Diodes and Materials Design. In *Organic Light-Emitting Devices: A Survey* (pp. 71-101). New York, NY: Springer New York.
- [8.] Reyes, R., Hering, E. N., Cremona, M., Da Silva, C. F. B., Brito, H. D., & Achete, C. A. (2002). Growth and characterization of OLED with samarium complex as emitting and electron transporting layer. *Thin Solid Films*, 420, 23-29.
- [9.] Cölle, M., & Brütting, W. (2004). Thermal, structural and photophysical properties of the organic semiconductor Alq3. *physica status solidi (a)*, 201(6), 1095-1115.
- [10.] Knox, J. E., Halls, M. D., Hratchian, H. P., & Schlegel, H. B. (2006). Chemical failure modes of AlQ3-based OLEDs: AlQ3 hydrolysis. *Physical Chemistry Chemical Physics*, 8(12), 1371-1377
- [11] AlSalhi, M. S., Alam, J., Dass, L. A., & Raja, M. (2011). Recent advances in conjugated polymers for light emitting devices. *International Journal of Molecular Sciences*, 12(3), 2036-2054.
- [12] Kamarulzaman, N., Aziz, N. D. A., Subban, R. H. Y., Hamzah, A. S., Ahmed, A. Z., Osman, Z., ... & Shaameri, Z. (2011, June). Poly [2-methoxy-5-(2';- ethylhexyloxy)-(p-phenylenevinylene)](MEH-PPV) synthesized via a modified Gilch method and the electrical conductivities of MEH-PPV/MCMB films. In 2011 3rd International Symposium & Exhibition in Sustainable Energy & Environment (ISESEE) (pp. 63-68). IEEE

- [13.] Pérez-Bolívar, C., Takizawa, S. Y., Nishimura, G., Montes, V. A., & Anzenbacher Jr, P. (2011). High-Efficiency Tris (8-hydroxyquinoline) aluminum (Alq3) Complexes for Organic White-Light-Emitting Diodes and Solid-State Lighting. *Chemistry—A European Journal*, 17(33), 9076-9082.
- [14.] Ahmad, Z., Suhail, M. H., Muhammad, I. I., Al-Rawi, W. K., Sulaiman, K., Zafar, Q., ... &Shaameri, Z. (2013). MEH-PPV/Alq3-based bulk heterojunction photodetector. *Chinese Physics B*, 22(10), 100701.1\
- [15.] Salah, N., Habib, S. S., & Khan, Z. H. (2013). Highly luminescent material based on Alq 3: Ag nanoparticles. *Journal of fluorescence*, 23, 1031-1037
- [16.] Cuba, M., & Muralidharan, G. (2014). Enhanced luminescence properties of hybrid Alq3/ZnO (organic/inorganic) composite films. *Journal of luminescence*, 156, 1-7.
- [17.] Cuba, M., & Muralidharan, G. (2015). Effect of thermal annealing on the structural and optical properties of tris-(8-hydroxyquinoline) aluminum (III)(Alq3) films. *Luminescence*, 30(3), 352-357.
- [18.] Kao, P. C., & Chiu, C. T. (2015). MoO3 as p-type dopant for Alq3-based p-i-n homojunction organic light-emitting diodes. *Organic Electronics*, *26*, 443-450.
- [19.] Paez-Sierra, B. A., & Marulanda, D. M. (2016). Luminescence Tuning of MEH-PPV for Organic Electronic Applications. *ActaPhysicaPolonica A*, 129(6), 1187-1190
- [20.] Derkowska-Zielinska, B. (2017). Enhancement of third-order nonlinear optical susceptibility of Alq 3 in polar aprotic solvents. *Optics Letters*, 42(3), 567-570.
- [21.] Pandey, C. K., Bajpai, M., Srivastava, R., Malik, R., Shukla, G. P., Katiyar, A. K.,...&Dhar, R. (2018, December). Effect of n-type doping on the electron transport of polyfluorene. In *AIP Conference Proceedings* (Vol. 2050, No. 1, p. 020024). AIP Publishing LLC. Abbas,
- [22.] W. A., Abdullah, I. H., Ali, B. A., Ahmed, N., Mohamed, A. M., Rezk, M. Y.,...&Allam, N. K. (2019). Recent advances in the use of TiO 2 nanotube powder in biological, environmental, and energy applications. *Nanoscale*

- Advances, I(8), 2801-2816.
- [23.] Liu, W., Lustig, W. P., & Li, J. (2019). Luminescent inorganic-organic hybrid semiconductor materials for energy-saving lighting applications. *EnergyChem*, 1(2), 1008.
- [24.] HemlataBisht, GopalRawat, SatyabrataJit&Hirdyesh Mishra(2020), Excitation Energy Transfer/Migration between Tris(8-hydroxyquinoline) Aluminum and Poly[2-methoxy-5-(2-ethylhexyloxy)-1,4-phenylenevinylene] in Chloroform, *The Journal of Physical Chemistry C* 2020, 124, 12, 6486-6494
- [24.] Duan, L., Yang, H., Wang, G., & Duan, Y. (2021). Preparation of 8-hydroxyquinoline aluminum nanomaterials to enhance properties for green organiclight-emitting diode devices. *Journal of the Society for Information Display*, 29(6), 466-475.
- [25.] Sharma, G., Ritu, Quraishi, A. M., Kattayat, S., Josey, S., Hashmi, S. Z., ... & Alvi, P. A. (2022). Structure optimization and investigation of electrical and optical characteristics of Alq3/TAZ: Ir (ppy) 3-BCP/HMTPD OLED. *Optical and Quantum Electronics*, 54(5), 284
- [26.] Ritu, Quraishi, A. M., Kattayat, S., Muqri, A. K., Hashmi, S. Z., Ezzeldien, M., ... & Alvi, P. A. (2023). Optimization of NPD/Alq3/TPBi/Bphen OLED structure and investigation of electrical characteristics along with allied parameters. *Optical and Quantum Electronics*, 55(8), 698.
- [27.] Sypniewska, M., Pokladko-Kowar, M., Kaczmarek-Kedziera, A., Brumboiu, I. E., Figà, V., Apostoluk, A., ... & Derkowska-Zielinska, B. (2024). Tris (8-hydroxyquinoline) aluminium in a polymer matrix as an active layer for green OLED applications. *Opto-Electronics Review*.
- [28.] Zhao, Y., Su, J., Zou, W., Wu, Y., Zhang, C., & Shao, M. (2025). Influence of MoO3's blend in hole transporting layer on the performance of Alq3-based OLEDs. *Next Materials*, 6, 100426.

Chapter 3: Materials and method of synthesis and fabrication techniques

3.1. Materials used for characterization of surface morphology, optical properties and electrical properties:

In this research project my principal aim was to fabricate a transparent flexible low turn on voltage driven low cost unoptimized OLED which will exhibit excellent photoluminescence (PL) and electroluminescence (EL). For this purpose, I chose PEDOT: PSS as HTL, Alq₃ as ETL and EML. V₂O₅ as HIL, ITO coated PET sheet as transparent anode as well as transparent flexible substrate, and metallic high work function metallic silver as cathode. In this research work, I have followed ten basic stages to achieve our goal: (1) synthesis of mer-Alq₃,(2) annealing this pristine Alq₃ from RT to 200°C under ambient condition and made its thin film and amorphous powder(3) Synthesis of ZnO nano-particle and synthesis of ZnO/Alq₃ nanocomposites with three different concentrations of ZnO nanoparticle into Alq₃ matrix i.e., 0.1wt% ZnO NP/Alq₃, 0.2 wt% ZnO NP/Alq₃ and 0.3 wt% ZnO NP/Alq₃ nanocomposite powder and solutions,(4)synthesis of homogeneous PEDOT:PSS solution from its coloring dye sample,(5) synthesis of V₂O₅ solution from V₂O₅ powder sample.(6) synthesis of europium nitrate solution from europium oxide; [Eu₂O₃] powder, (7) synthesis of neodymium nitrate solution from neodymium nitrate[Nd(NO₃)₃] crystalline powder(8) synthesis of 0.1wt% Eu/Alq₃ nano composite,0.2 wt% Eu/Alq₃ nano composites, and 0.3 wt% Eu/Alq₃ nanocomposites powder and solutions, and (9) 0.1 wt% Nd/Alq₃, 0.2 wt% Nd/Alq₃ and 0.3 wt% Nd/Alq₃ nanocomposite powders and solutions.(10) fabrication of EML. ETL, HTL layer on ITO- coated flexible substrate employing spin coating techniques with all aqueous samples. I have characterized all the samples under investigation to investigate the structural, thermal, optical and electrical properties of them. Alq₃ is a n-type semiconductor that can be used both as an electron transporting layer and emissive, and PEDOT:PSS is a popular fluorescent dye used as a layer hole transporting layer for OLED,ITO (Indium tin oxide) is a transparent high work function anode and metallic silver as low work function cathode PET or poly tri ethylene terapthalate is polymeric transparent rollable substrate. V_2O_5 is used as a hole blocking layer. In this chapter, the structure of these materials and its characteristics and role in OLED functionality are given in the following sections alongside a brief explanation of their function in charge transport, OLED application, solid stat lighting application. We will discuss all the measurement, required materials for synthesis in this chapter and its subsequent chapter clearly.

The following are important materials that we used for different purposes relating to our research goals from time to time. We also have described shortly why these materials were utmost important for achieving goal and their physical and chemical properties. We also have discussed in this section how many materials we bought directly from the local market and how many chemicals we synthesized during our entire research project. The required materials are described as follows:

A. Material selected for OLED stacked layers of flexible transparent OLED preparation:

1. Alq₃ (tris (8-hydroxyquinoline) aluminum):

Organic electroluminescent n-type semiconducting tris (8-hydroxyquinoline) aluminum (Alq₃) powder, a metal chelated complex has been the prime-picked OLED material chosen for OLED applications since its discovery in 1987 by Tang and Van Slyke [1,3]. Alq₃ has achieved enormous popularity for its excellent blue-green bright luminescence, low cost, easy fabrication technique, less operational voltage, and fine-tuning ability of emission wavelength (Figure 3.1). Hence, metal quinolates Alq₃ has proved itself as a promising organic light emitting diode (OLED) material where Alq₃ plays a dual role of electron transport layer (ETL) and emissive layer of an OLED. Despite its multi-dimensional applicability, Alq₃ has encountered serious shortcomings in their operations such as smaller-span durability and severe deterioration in photoluminescence (PL) and electroluminescence (EL) efficiency. This is mainly because of corrosion, thermal

instability because of joule heating, device degradation on direct exposure to moisture, air, oxygen, water splash, and the absence of an encapsulated protection shield. Besides, the electrical conductivities of Alq₃, luminescence performances of OLED are also characterized by the existing percentage of the highly conductive thermodynamic crystalline phase [1-13].

2.PEDOT: PSS [poly(3,4-ethylenedioxythiophene), polystyrene sulphonate)]:

PEDOT: PSS (poly(3,4-ethylenedioxy thiophene), polystyrene sulphonate) is a p-type conjugate polymeric organic dye [6,7,8,9,10]. It is the combination of two different kinds of polymers: PEDOT (poly(3,4-ethylenedioxy thiophene) and PSS (polystyrene

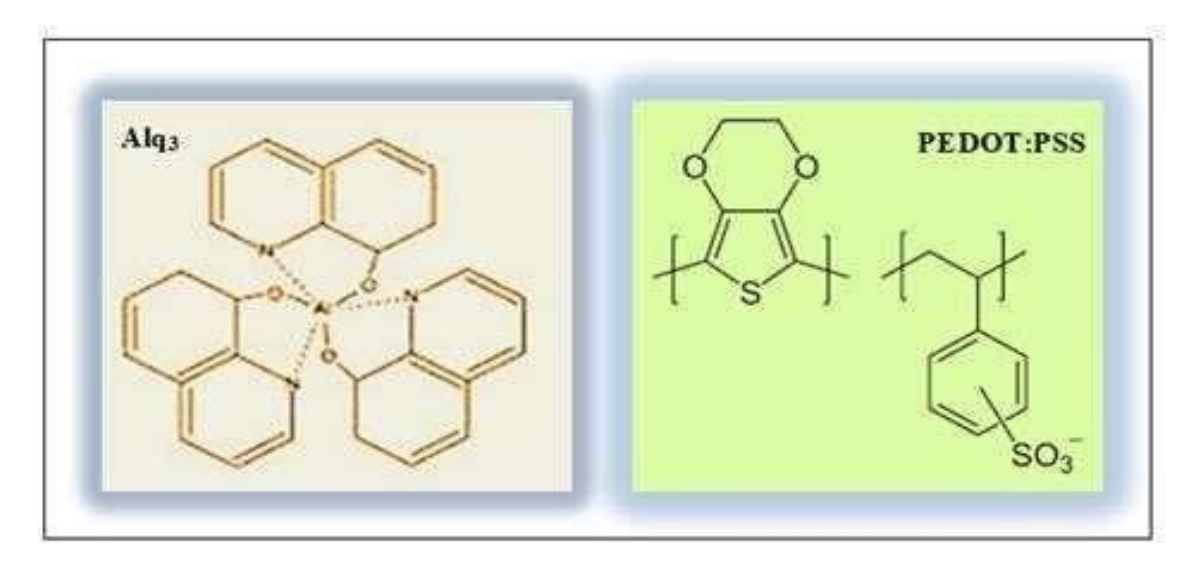


Figure 3.1: Chemical structure of Alq₃ and PEDOT: PSS

sulphonate). PEDOT is a conductive conjugated polymer consisting of poly(3,4-ethylenedioxy thiophene) monomer at 2,5 positions of each thiophene whereas PSS is a non-conductive polymeric stabilizing surfactant having styrene as the backbone and pending unit of sulphonate group (-SO₃H) (Figure 3.1). PSS is doped into PEDOT to stabilize and disperse PEDOT into water and other solvent. Thus, insoluble PEDOT forms stable colloidal dispersion i.e., solution processing is possible for PEDOT. PEDOT: PSS

is popularly used due to its higher mechanical stability, easy thin film production method, coarseness, higher optical transparency, lower surface, higher work function, higher hole injection, low processing cost, and high conductivity (10⁻⁴ to 10⁻³ S/cm) [14-19].

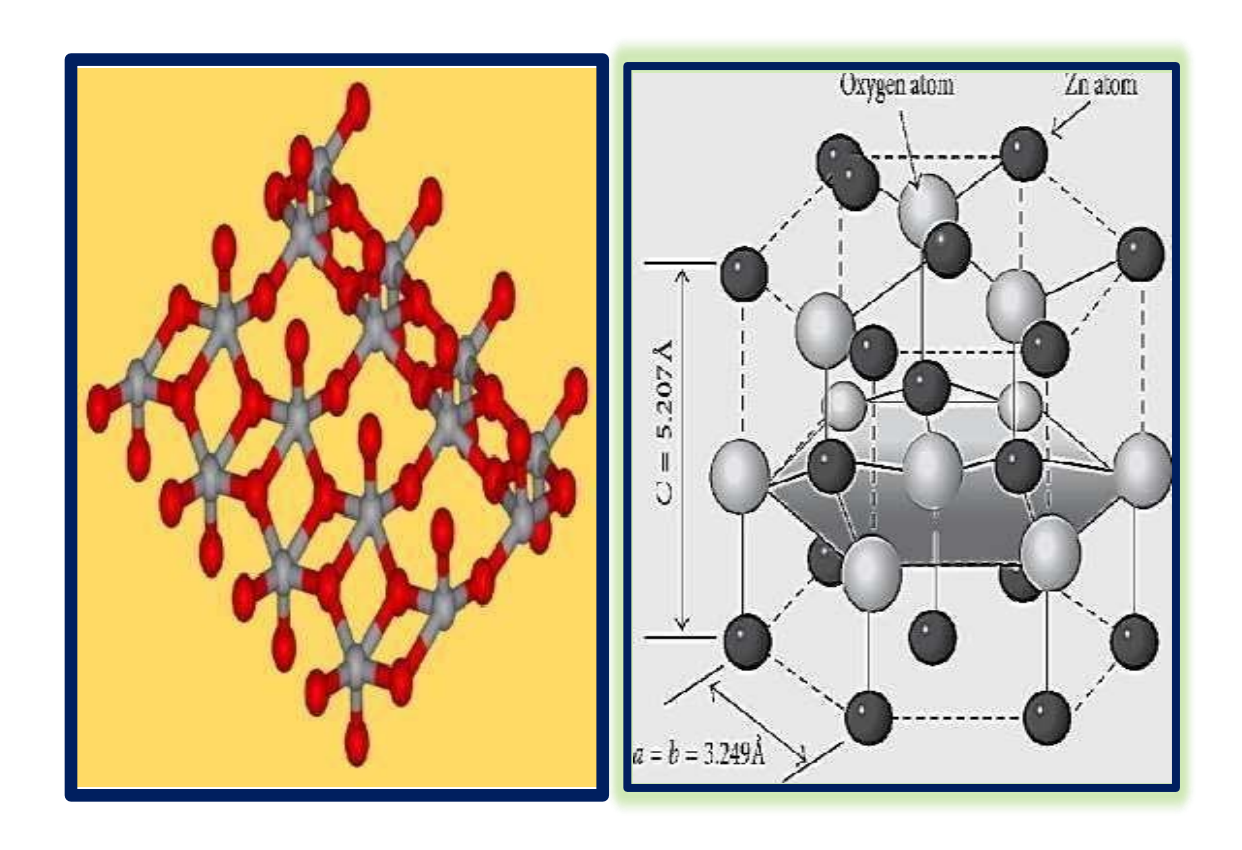


Figure 3.1A: molecular structure of vanadium pentoxide(left) and Zinc oxide nanoparticle (right)

2. Zinc Oxide Nanoparticles (ZnO NP):

Zinc oxide (ZnO) is a transition metal oxide with n-type semiconductor characteristics, biodegradability, excellent optical properties, spintronic properties and electrical properties. ZnO is a non-toxic material (Figure 3.1A) having direct wide band gap as high as ~3.37 eV and exciton binding energy of~ 60 MeV, high electron mobility and an excellent optical transmittance. Though Alq₃ has multi-dimensional advantages still it suffers many disadvantages like low chemical and physical stability over time, often suffers photo-oxidation, chemical degradation and performance degradation due to exposure to

atmospheric oxygen gas, nitrogen gas hydrogen gas and water splash or moisture leading to reduction in prolonged life-span of Alq $_3$ and its derivative aided devices like OLED, photodiodes, OLETs, Solar OPV cells etc. [18,19,20,21,22,23] .To overcome this our target was in this to tune the photoluminescence(PL) and electroluminescence(EL) property of Alq $_3$ by using organometallic /inorganic hybrid nanocomposites(Alq $_3$ /ZnO) with varying concentrations where ZnO:Alq $_3$ =0.1:1, 0.2:1, 0.3:1 and 0.4:1 respectively, to overcome the above-mentioned limitations thereby improving efficiency , longevity, stability of chemical and physical property etc.[20-26].

3. Vanadium pentoxide (V_2O_5) :

The yellow to red orthorhombic crystalline powder known as vanadium pentoxide (V₂O₅) (Figure 3.1A) has a density of 3.35 g/cm³, which is higher than that of water, and it dissolves somewhat in it. It decomposes at 1750°C, while its melting point is 690°C. Because of its strong chemical and thermal stability, broad band gap (2.3 eV), and electrochromic characteristics, it has a wide range of applications. V₂O₅ is typically regarded as an n-type semiconductor. Its primary characteristic is that of an n-type material, though it can also display p-type behavior in certain specific situations or under specific conditions. The material's fluorescent and transparent qualities are also well known. Vanadium is in the (+5) oxidation state (V^{5+}) . It can act as an oxidizing agent as well as an amphoteric oxide. Under typical storage circumstances, it is stable. Because it reacts with a variety of gases, it is used in gas sensors. Because of its high crystallinity, affordability, and resistance to photo-corrosion, it is used as a photocatalyst for photocatalytic degradation. Transitional metal oxides, such as MoOx, V₂O₅, ReO₃, and WO₃, are frequently employed as HTL and HIL for stack layered OLEDs to improve device performance. These transitional metal oxides significantly enhance the performance of OLEDs by acting as buffer layers between HTL and EML and as HTL or HIL (or electron acceptor) dopants for the creation of p-doped devices. To prevent holes from backtracking towards PEDOT: PSS (HTL) of our manufactured OLEDs, we employed V₂O₅ as both our HIL and buffer layer. Additionally, V₂O₅ guards against chemical deterioration, etching or corrosion of the ITO anode layer through oxidation by acidic PEDOT: PSS layer. In comparison to the device performance of OLEDs without a V_2O_5 layer, we obtained a notable improvement in EL and PL characteristics when employing V_2O_5 as HIL, which is consistent with other published results. In this case, we spin-coated the V_2O_5 layer over the PEDOT: PSS layer rather than doping it to improve its hole injection and electron blocking properties, which are essential for our OLED [27-30].

4. Lithium fluoride (LiF):

LiF is an inorganic solid that is colourless and mildly insoluble in water; when the crystal size decreases, it turns white. It resembles sodium chloride in structure. from the elements releasing one of the highest energies per mass of reactants, second only to BeO. Despite not being the main cathode material in OLEDs, LiF is frequently utilized as a buffer layer an OLED's organic layer and a metal cathode (such as silver or aluminium).to improve electron injection at the cathode interface. LiF contributes to improved electron injections by reducing the energy barrier that prevents electrons from moving from the cathode into the organic layers of the OLED. LiF may also serve as a barrier, preventing organic layers from being harmed during the cathode deposition procedure. LiF can help OLEDs have higher luminance and current efficiency by enabling better electron injections. LiF has the ability to alter the cathode material's work function, improving its suitability for electron injection. [27-35]

6.Metallic Silver Paste (Ag-Paste): To improve certain qualities, conductive silver paste is usually made by mixing 60 weight percent silver powder, 10 weight percent(wt%) lead-free glass powder, and 30 weight percent(wt%) organic carrier (which contains terpineol, ethyl cellulose, and organic additives like polyamide wax, KH-570 silane coupling agent, and soy lecithin). To create a uniform paste with the required viscosity and conductivity, these ingredients are mixed, occasionally with ultrasonic treatment and grinding. Because of its low cost, high conductivity and efficient electron injection in the visible zone of spectrum of light, reflectivity, minimum resistive loss, improved power efficiency and suitability for solution processing—especially in top-emitting devices—metallic Ag paste is utilized as the cathode in certain OLEDs. By modifying the surface of the Ag cathode, researchers can enhance hole injections from the cathode while maintaining high reflectivity. Using Ag as a cathode, particularly when combined with an alkali-metal

doped electron transport layer, can lead to a reduction in the driving voltage of the OLED, improving its power efficiency. [27-35]

7. Neodymium Nitrate hexahydrate [Nd(NO₃)₃·6H₂O]:

Neodymium nitrate hexahydrate(Figure 3.2 (a)) is a purple, crystalline powder that dissolves in both alcohol and water. It is hygroscopic, meaning it easily takes in moisture from the atmosphere. With a molecular weight of 438.35 g/mol, the compound has a melting point of 69 °C. When it comes into contact with combustible materials, this oxidizing agent has the potential to cause fire. Both optical and electrical characteristics are present in neodymium nitrate hexahydrate [Nd(NO₃)₃·6H₂O]. It is well-known for its optical characteristics, especially the way it absorbs visible light. Furthermore, neodymium nitrate is well-known for its electrical characteristics, which include the ability to behave like a semiconductor, particularly when doped with other elements. Neodymium nitrate is not a transparent substance. The 10% neodymium nitrate aqueous solution is purple in colour but clear, meaning it doesn't scatter light. When added to glass, neodymium nitrate can produce a range of colors. This type of glass absorbs light at very specific wavelengths, resulting in unusual absorption-bands in the light transmitted through it. Neodymium doping can be used to adjust a material's optical band gap, which will increase its absorption of light in the visible spectrum. Low activation energies found in studies on neodymiumdoped materials suggest that charge carrier mobility is comparatively simple. [31-40]

8. Europium nitrate hexahydrate [Eu(NO₃)₃·6H₂O]:

Europium nitrate hexahydrate [Eu(NO₃)₃·6H₂O](Figure 3.2(b)) is a white, transparent crystalline solid that exhibits luminescent qualities. It dissolves very easily in water. The compound is utilized as a precursor in the production of different nanomaterials and in applications such as white light-emitting diodes and bioimaging. The electronic structure of the Eu³⁺ ion and its interaction with the environment is what gives europium nitrate [Eu(NO₃)₃] its distinct electrical and optical characteristics. Eu³⁺ ions are particularly helpful in optoelectronic applications because they show distinct, narrow fluorescence lines in the red portion of the spectrum. Furthermore, materials' semiconducting behavior and electrical conductivity can be affected by europium doping. By raising the concentration of

free charge carriers, doping materials with Eu³⁺ can improve electrical conductivity. This is so that electron transport can be facilitated, and the electronic structure changed by substituting Eu³⁺ ions for other metal ions in the lattice. Semiconducting material's bandgap and electron transport characteristics can be altered by Eu³⁺ doping. While carrier concentration and hopping conduction processes can affect electrical conductivity, Eu³⁺ doping can also affect a material's dielectric characteristics. Because of their strong and sharp red-region luminescence, Eu³⁺ ions are useful for a variety of applications, such as displays, LEDs, and phosphors. In materials such as ZnS and SnO₂, Eu³⁺ doping can increase photoluminescence, which can be advantageous for sensors and optoelectronic devices. Eu³⁺ doping can alter a material's absorption characteristics. For instance, the transmittance and absorption index of Eu-doped PEO- PVA blends are dependent on the amount of Eu present. The photoconductivity of materials can also be affected by Eu³⁺ doping. Eu-doped ZnS, for instance, has enhanced photoconductivity, which qualifies it for use in photo detectors. As a result of their special electrical and optical characteristics, europium nitrate [Eu(NO₃)₃] and its derivatives are useful for a wide range of applications, particularly in optoelectronics and semiconducting devices. [38-45] conditions of chemical reactions to produce a desired product are called wet chemical synthesis. By providing a flexible and regulated method of producing materials with particular qualities, this technique is extensively employed in materials science, especially for the synthesis of nanoparticles and functional materials. Using chemical reactions in solutions, wetchemical synthesis techniques create target materials from specific precursors. The wet chemical synthesis to create nanoscale materials like nanoparticles, quantum dots, and 2D materials. The final product's size, composition, and shape can be customized using this method by adjusting the temperature, PH, pressure, and type of additives or surfactants. method uses a bottom-up approach, meaning that smaller molecules or atoms are used. Wet chemical methods are frequently superior to other synthesis techniques because they are more affordable, simpler to use, and can yield materials with particular qualities. Metal oxide nanoparticles, semiconductors, OLED materials, catalysts, sensors, and energy storage devices are just a few examples of the materials that can be created using these techniques. [41-46]

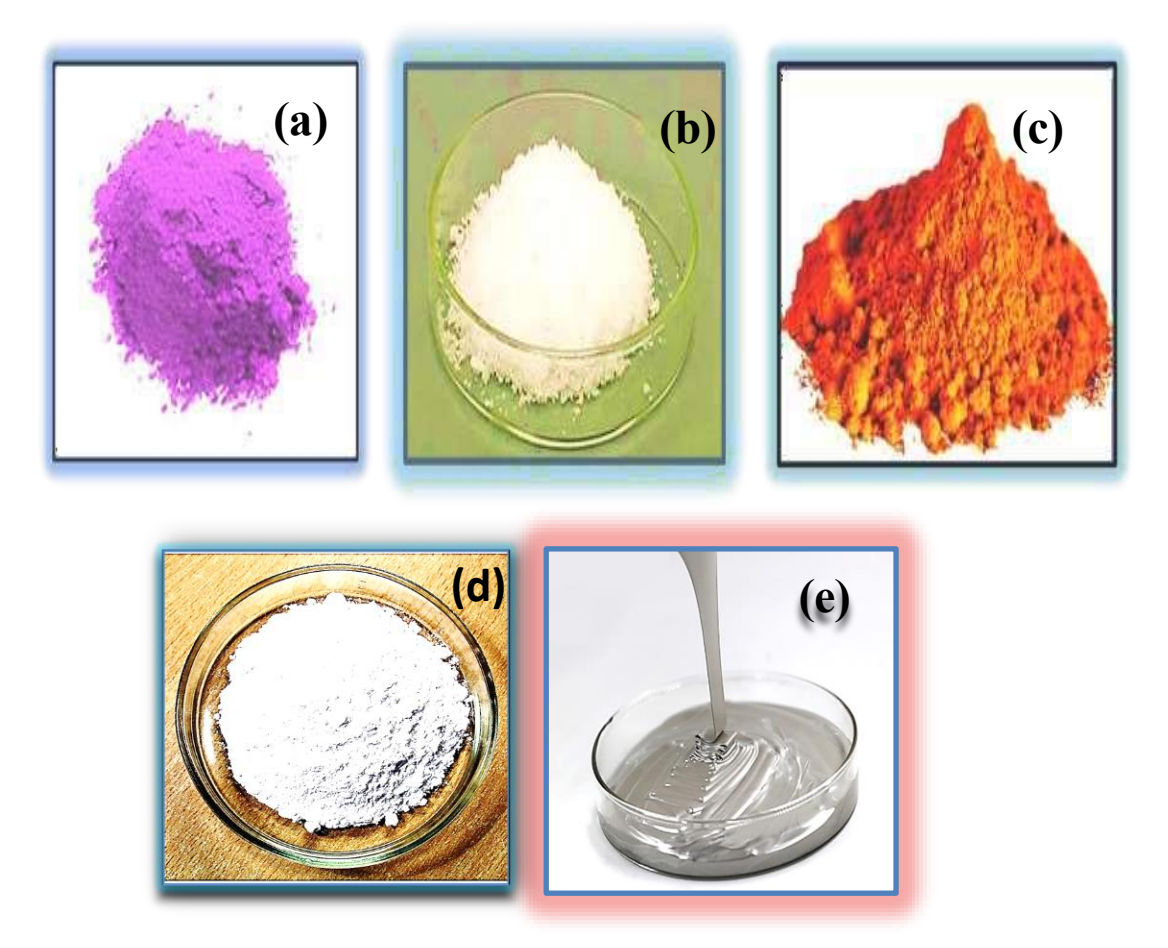


Figure 3.2: Amorphous powder forms of (a) neodymium nitrate hexahydrate, (b) europium nitrate hexahydrate, and (c) vanadium pentoxide (d) lithium fluoride (e)metallic silver paste

3.2. Synthesis of powders and their aqueous solutions, and thin film fabrications:

A. Synthesis of materials in powder form:

In this section we have illustrated how our synthesized materials are synthesized in the laboratory and also demonstrated the route of synthesis, purification, collection, annealing, grinding, thin film preparation

1. Synthesis of bulk polycrystalline mer-Alq3 and its oxide in powder form:

Electroluminescent material Alq₃ is synthesized through a wet-synthesis method using the procedure reported by J.G. Mahakhode, et al. [35] where we deviated some steps keeping

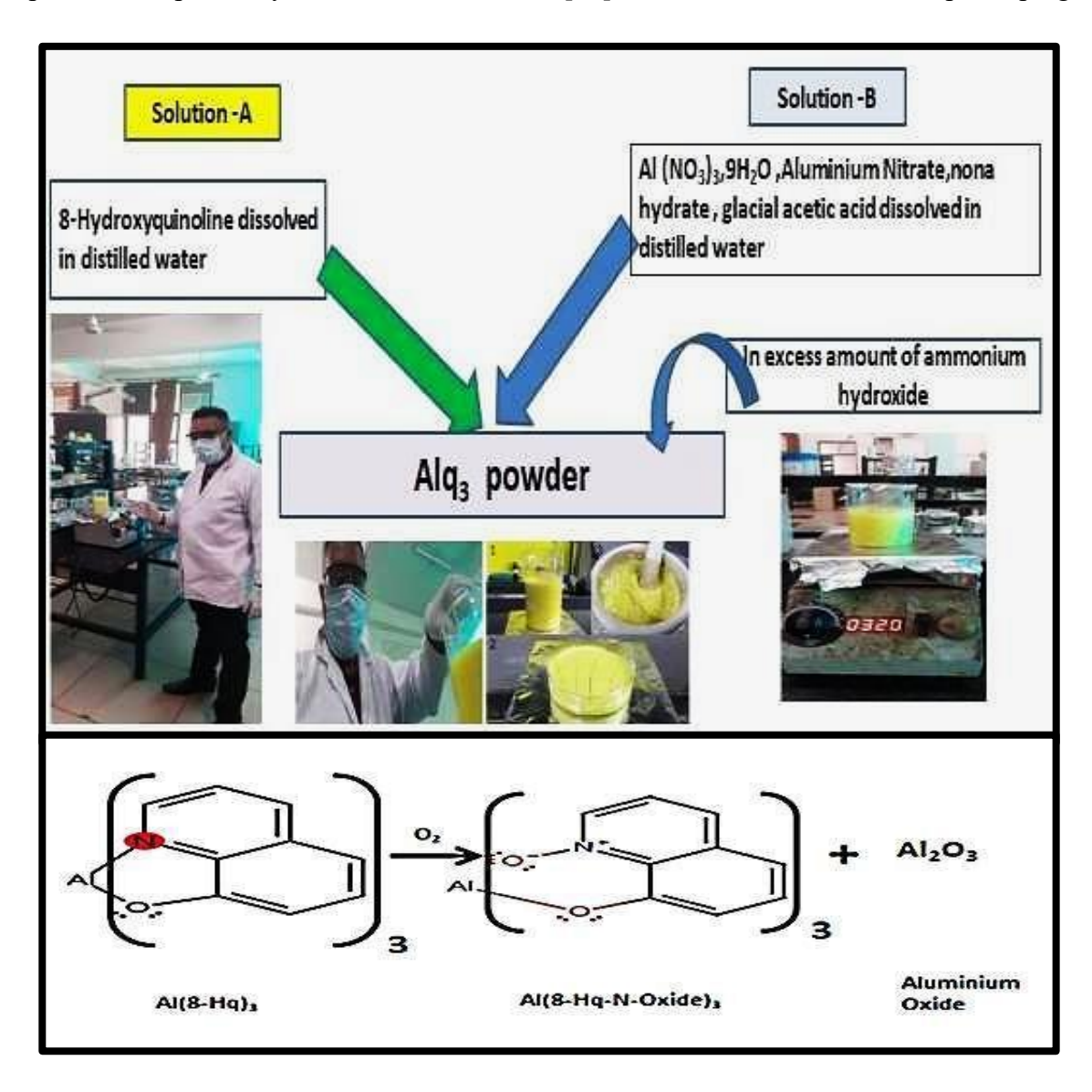


Figure 3.3. Schematic diagram of mer-Alq₃ nano-particle synthesis (top picture) and

Figure 3.4: Conversion-mechanism of tris(8-hydroxyquinoline- N-oxide aluminium(III)[Al(q-N-oxide)₃],a non-emissive polymer (NEP) from tris(8-hydroxyquinoline)aluminium [Alq₃]the original synthetic procedure intact on the basis of experimental needs (Figure 3.3 and 3.4). At first 5 gm 8-hydroxyquinoline(8- HQ) was dissolved in the mixture of 25 ml distilled water (H₂O) and 25 ml of acetic acid

(CH₃COOH) and then the mixture was heated to 50 °C with continuous stirring for 30 minutes resulting a transparent orange colored solution (Solution –D). Then 4.306 gm. of aluminium nitrate[Al(NO₃)₃] powder was dissolved in 100 ml of distilled water(H₂O) and then the mixture was heated to 50 °C with continuous stirring for 30 minutes resulting a transparent colorless solution (solution– E). Then solution-D was poured into solution-E (Solution–F). Then ammonium hydroxide (NH₄OH) solution (precipitating agent) was added drop wise to the mixed solution-F and stirred for 10 minutes. Then, yellow–green colored precipitate of mer-Alq₃ was yielded. Then that yellow precipitate was filtered and washed 8-10 times with warm water. Then, the yellow green precipitate was heated to 60°C for 2 hours. The dried yellow –green colored Alq₃ powder was then crushed into fine powder using a mortar pestle and a crucible pot. That fine yellow green powder of Alq₃ was used for our ZnO/Alq₃ Nano-composite formation.

Chemical reactions occurred during synthesis are summarized as follows:

$$3(C_9H_7NO) + A1(NO_3)_{3,..}9H_2O \longrightarrow A1(C_9H_7NO)_3 + 9H_2O + 3(NO_2)$$
 (3.1)

$$8-Hq+O_2 \longrightarrow 8-Hq-N \text{ oxide (NEP)}$$
 (3.2)

$$Alq_3+3O_2 \longrightarrow Al(q-N-oxide)_3 + Al_2O_3$$
 (3.3)

2. Synthesis of Zinc Oxide nanoparticles powder:

ZnO Nano-particles (NP) are synthesized through the aqueous sol-gel method mentioned by Bolla G Rao et al (2017) [33]. At first 12.00 gm. NaOH pellet were dissolved in 150 ml of [Zn(CHCOO)₂.2H₂O] was dissolved in 100 ml distilled water and stirred for 5 minute (solution-B). Then solution-A was mixed with solution-B to get solution-C. After that 150 ml of aqueous ethanol (C₂H₅OH) solution was added drop wise to the solution-C and heated at 80°C with continuous stirring for 15 minutes. After the reaction was

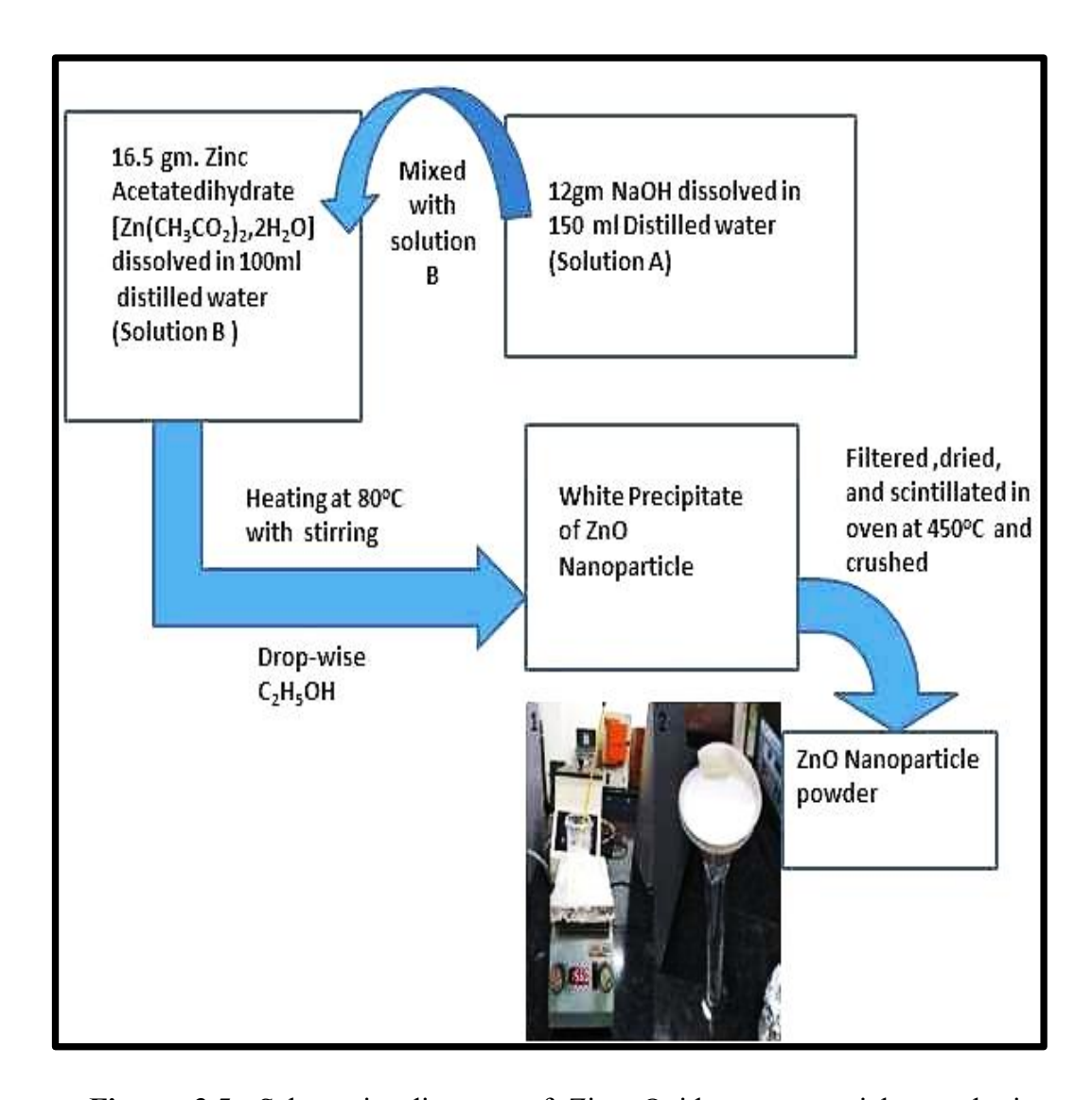


Figure 3.5. Schematic diagram of Zinc Oxide nano-particle synthesis

completed, the white precipitate of zinc oxide (ZnO) Nanoparticle was obtained. (Figure 3.5) This white precipitate was collected using filter paper and washed in distilled water for 6 to 8 times and then allowed to dry at room temperature. Thereafter, white colored dried powder was scintillated at 450°C in an oven for 5hrs. Finally, the distilled water and stirred for 5 minutes (Solution- A). Then 16.5 gm. of zinc acetate di hydrate scintillated ZnO Nano-particle powder was crushed into fine powder using mortar and pestle. Later on that fine ZnO NP powder was utilized for our ZnO-Alq₃ composite-

fabrication [20-26]

3. Preparation of Alq₃/ZnO Nanocomposites powder:

ZnO/Alq₃ Nanocomposites were fabricated through a novel and low-cost easy procedure via solution intercalation and exfoliation adsorption method [30,31,32]. At first, 0.50 gm. of Zinc oxide Nanoparticle (ZnO NP) was added in the mixed solution of 10 ml distilled water and 10 ml ethanol (C₂H₅OH) solution (taken in 1:1 volumetric ratio) along with stirring for 20 minutes and was thereafter ultra-sonicated for 30 minutes. An opaque white solution was formed to give solution -G. Then 0.50 gm of Alq₃ powder was mixed with 10 ml of ethanol (C₂H₅OH) and 10 ml of distilled water and stirred for 20 minutes which was then ultra-sonicated for 30 minutes. A yellow-green opaque solution (solution-H) was obtained. Thereafter, solution-G was added into Solution-H and the resulting mixture (solution-I) was then ultra-sonicated again in sonication bath for 4 hours. A light white mixed green-yellow precipitate was obtained at the bottom of the transparent colorless solution. The excess liquid was decanted, and the remaining viscous yellow white solution was put in a water-bath with heating at 50°C for 8 hours and then left it in open air at room temperature overnight to settle down and to dry. The dried yellow ZnO/Alq₃ (1wt%:1wt% ratio) Nano-composite powder is finally formed which were collected and crushed into fine powder with the help of crucible pot and a mortar and pestle. In another attempt we filtered the yellow-white solution using filter paper and the yellow-white precipitate was collected over filter paper. The yellow precipitate was collected in a petri dish and allowed to be dried overnight. Then the dried powder was heated at 50 °C for 2 hours to remove moisture absorbed in it. Finally, the dried powder was collected and crushed into fine powder using mortar and pestle to form the composite pellets [20-26].

B. Preparation of aqueous solution of materials for thin film fabrication:

1.Preparation of V₂O₅ solution for thin film formation:

At first 0.542 gm V₂O₅ powder , bought from market(Sigma Aldrich) was dissolved in 10 ml of monoethylamine(99.8% purity, Sigma Aldrich) and 20 ml of ethanol (98% pure),Sigma Aldrich)dilute hydrogen peroxide(H₂O₂) (15 mol%, Sigma Aldrich)solution resulting a whitish pink transparent solution which was then ultrasonicated for 45 minutes in a ultra sonicator bath at room temperature .as a result, a pinkish white transparent

solution was produced. This yielded solution was used for OLED fabrication. [33-36]

2. Preparation of LiF slurry solution:

First, 10 ml of isopropyl alcohol solution was used to dissolve 1 gm of white, 99% pure LiF (lithium fluoride) powder. The mixture was then ultrasonically agitated for ½ hours, and the resulting bluish solution was filtered through 0.45 μm-diameter filter paper until a white slurry solution was obtained. which was utilized for spin coating for 30 minutes at 3000 rpm. It is then utilized for vacuum-assisted spin coating at 3000 rpm for 30 seconds after silver paste (Ag) solution is created by dissolving silver paste (99% purity, Sigma Aldrich) in acetone solution with a 1:0.5 volumetric proportion [41].

3. Synthesis of Europium Nitrate from Europium oxide (Eu₂O₃) powder:

At first 2.14 gm. europium oxide bought from market was dissolved in 5 ml distilled water and the resultant opaque milky white solution was treated with conc. HNO₃ (1:6 volumetric ratio) to yield soluble europium nitrate [Eu(NO₃₎₃] which showed pH value 3 which confirmed that the resultant solution was acidic. The yielded white solution was heated at 60°C for ½ hr. with constant stirring. As a result, a white translucent solution of europium nitrate was obtained which was allowed to settle down. The white precipitate was filtered and collected after drying at 50°C for 15 minutes. [31-40]

4. Synthesis of Eu³⁺doped Alq₃ nanocomposites:

At first 100 mg europium nitrate as prepared powder is dissolved in double distilled water on which Alq₃ powder was added with different wt% ratios: 1:0.1.1:02 and 1:0.3. The resultant solutions are individually ultrasonicated for 4 hrs. Then the mixture was heated to 50°C for 8 hrs to get dried Eu³⁺ doped Alq₃ nanocomposites powder. [41-47]

5. Synthesis of Nd³⁺doped Alq₃ nanocomposites:

At first 0.186 gm neodymium nitrate [Nd(NO₃)₃](Sigma Aldrich) as prepared powder was dissolved in the 5 5 ml acetone and 10 ml double distilled water on which 0.502 gm. Alq₃ powder dissolved in 10 ml was added with different wt% ratios: 1:0.1:02 and 1:0.3. The resultant solutions are individually ultrasonicated for 4 hrs. Then the mixture was heated to 50°C for 8 hrs to get dried Nd³⁺ doped Alq₃ nanocomposites powder. [31-40]

The associated chemical reactions occurred during rare earth metallic nitrate solutions:

$$Eu_2O_3 + 6HNO_3 \longrightarrow 2Eu(NO_3)_2 + 3H_2$$
 (3.4)

$$Al(C_9H_7NO)_3+Eu(NO_3)_3 \longrightarrow Eu(C_9H_7NO)_3+Al_2O_3$$
 (3.5)

$$Al(C_9H_7NO)_3+Nd(NO_3)_3$$
 $\longrightarrow Nd(C_9H_7NO)_3+Al(NO_3)_3$ (3.6)

C. Fabrication technique:

At first the ITO coated PET sheet was cleaned with acetone and ethanol alternately several times. It was dried at room temperature by using a hot plate at 27 °C under an ambient atmosphere. The solution of PEDOT: PSS was then spin-coated for HTL layer on the PET coated sheet. After drying it for 15 minutes, thin film of tris (8- hydroxyquinolinilato (aluminium (III) was deposited through spin coater machine under vacuum condition. This process helped us to fabricate an OLED device where the stacked layers are constructed like: ITO (175 nm/PEDOT: PSS (48 nm)/V₂O₅(12 nm)/Alq₃(83 nm)/LiF (3 nm)/Ag (100 nm). In this hetero structure, ITO (Indium tin oxide) acts as an transparent anode, PEDOT: PSS is an organic dye acts as a transparent bulk hole transport layer (HTL), Alq₃, an ETL layer acts as an emissive green layer and silver-paste used at the perimeter of the Alq₃ layer acts as metallic cathode. The thickness of Alq₃ and PEDOT: PSS layers are 83 nm and 48 nm, respectively. All the measurements of the constructed OLED were performed without any encapsulation and subjected to experimental measurement at room temperature. [14-19]

References

- [1.] Tang, C. W., & Van Slyke, S. A. (1987). Organic electroluminesecnt diodes. Appt. Phys.Leu, 51(12), 913-915.
- [2.] Jeong, E. G., Kwon, J. H., Kang, K. S., Jeong, S. Y., & Choi, K. C. (2020). A review of highly reliable flexible encapsulation technologies towards rollable

- and foldable OLEDs. Journal of Information Display, 21(1), 19-32.
- [3.] Fukushima, T., & Kaji, H. (2012). Green-and blue-emitting tris (8-hydroxyquinoline) aluminum (III)(Alq3) crystalline polymorphs: Preparation and application to organic light-emitting diodes. *Organic Electronics*, *13*(12), 2985-2990
- [4.] Cölle, M., & Brütting, W. (2004). Thermal, structural and photophysical properties of the organic semiconductor Alq3. *physica status solidi (a)*, 201(6), 1095-1115.
- [5.] Painuly, D., Mogha, N. K., Masram, D. T., Singhal, R., Gedam, R. S., & Nagpure, I. M. (2018). Phase stability and transformation of the α to ε-phase of Alq₃ phosphor after thermal treatment and their photo-physical properties.

 *Journal of Physics and Chemistry of Solids, 121, 396-408.

 [6.]

Raje swaran, M., Blanton, T. N., Tang, C. W., Lenhart, W. C., Switalski, S. C., Giesen, D. J., ... & Young, R. H. (2009). Structural, thermal, and spectral characterization of the different crystalline forms of Alq3, tris (quinolin-8- olato) aluminum (III), an electroluminescent material in OLED technology. *Polyhedrn*, 28(4), 835-843

- [7.] Debsharma, M., Pramanik, T., Daka, C., & Mukherjee, R. (2022, May). Recent advances in the electrical and optical properties of Alq3 and Alq3 derivatives based OLEDS. In *Journal of Physics: Conference Series* (Vol. 2267, No. 1, p. 012159). IOP Publishing.
- [8.] El-Nahass, M. M., Farid, A. M., & Atta, A. A. (2010). Structural and optical properties of Tris (8-hydroxyquinoline) aluminum (III)(Alq3) thermal evaporated thin films. *Journal of alloys and compounds*, 507(1), 112-119.
- [9.] Fong, H. H., & So, S. K. (2006). Hole transporting properties of tris (8-hydroxyquinoline) aluminum (Alq3). *Journal of applied physics*, 100(9).
- [10.] Dalasiński, P., Łukasiak, Z., Wojdyła, M., Re, M., & Bała, W. (2006). Study of optical properties of TRIS (8-hydroxyquinoline) aluminum (III). *Optical Materials*, 28(1-2), 98-101.
- [11.] Debsharma, M., Pramanik, T., Pramanik, G., Maity, A. R., Jain, A., & Mukherjee, R. (2024). Effect of growth temperatures on the structural and

- optical properties of bulk tris- (8-hydroxyquinoline) aluminium (III). *Applied Physics A*, 130(5), 281.
- [12.] Duvenhage, M. M., Ntwaeaborwa, M., Vis Khantham, S., Tunhoo, B., Onlaor, K., Thiwawong, T., & Nukeaw, J. (2012). Electrical properties of dye-doped colour tunable organic light emitting diode. *The Canadian Journal of Chemical Engineering*, 90(4), 903-908.
- [13.] Cuba, M., & Muralidharan, G. (2015). Effect of thermal annealing on the structural and optical properties of tris-(8-hydroxyquinoline) aluminum (III)(Alq3) films. *Luminescence*, 30(3), 352-357
- [14.] Groenendaal, L.; Jonas, F.; Freitag, D.; Pielartzik, H.; Reynolds, J. R. (2000). "Poly(3,4-ethylenedioxythiophene) and Its Derivatives: Past, Present, and Future". AdvancedMaterials. 12 (7): 481–494.
- [15.] Yoo, Dohyuk; Kim, Jeonghun; Kim, Jung Hyun (2014). "Direct synthesis of highly conductivepoly(3,4-ethylenedioxythiophene):poly(4-styrenesulfonate) (PEDOT:PSS)/graphene composites and their applications in energy harvesting systems" (PDF). Nano Research. 7 (5): 717–730.
- [16.] Sakunpongpitiporn, Phimchanok; Phasuksom, Katesara; Paradee, Nophawan; Sirivat, Anuvat (2019). "Facile synthesis of highly conductive PEDOT:PSS via surfactant templates". RSCAdvances. 9 (11): 6363–6378. Bibcode:2019 RSCAd. 9.6363S. doi:10.1039/C8RA08801B. PMC 9060941. PMID 35517248.
- [17.] Kim, Yong Hyun; Sachse, Christoph; Machala, Michael L.; May, Christian; Müller-Meskamp, Lars; Leo, Karl (2011-03-22). "Highly Conductive PEDOT: PSS Electrode with Optimized Solvent and Thermal Post-Treatment for ITO-Free Organic Solar Cells". Advanced Functional Materials. 21 (6): 1076–1081. doi:10.1002/adfm.201002290. S2CID 136583700.
- [18.] Kim, J. Y.; Jung, J. H.; Lee, D. E.; Joo, J. (2002). "Enhancement of electrical conductivity of poly(3,4-ethylenedioxythiophene)/poly(4-styrenesulfonate) by a change of solvents". Synthetic Metals. **126** (2–3): 311–316. doi:10.1016/S0379-6779(01)00576-8.

- [19.] Ouyang, J.; Xu, Q.; Chu, C. W.; Yang, Y.; Li, G.; Shinar, J. (2004). "On the mechanism of conductivity enhancement in poly (3,4-ethylenedioxythiophene): poly (styrene sulfonate) film through solvent treatment". Polymer.45(25):8443–8450.
- [20.] Boeckler, C., Feldhoff, A., & Oekermann, T. (2007). Electrodeposited Zinc Oxide/Phthalocyanine Films—An Inorganic/Organic Hybrid System with Highly Variable Composition. *Advanced Functional Materials*, 17(18), 3864-3869.
- [21.] Duvenhage, M. M., Ntwaeaborwa, M., Visser, H. G., Swarts, P. J., Swarts, J. C., & Swart, H. C. (2015). Determination of the optical band gap of Alq3 and its derivatives for the use in two-layer OLEDs. *Optical Materials*, 42, 193-198
- [22.] Cuba, M., & Muralidharan, G. (2014). Enhanced luminescence properties of hybrid Alq3/ZnO (organic/inorganic) composite films. *Journal of luminescence*, 156, 1-7.
- [23.] Makki, A. H., & Park, S. H. (2021). Yellow emissive tris (8-hydroxyquinoline) aluminum by the incorporation of ZnO quantum dots for OLED applications. *Micromachines*, *12*(10), 1173.
- [24.] Sypniewska, M., Szczesny, R., Popielarski, P., Strzalkowski, K., & Derkowska-Zielinska,B. (2020). Structural, morphological and photoluminescent properties of annealed ZnO thin layers obtained by the rapid sol-gel spin-coating method. *Opto-Electronics Review*, 28(4)
- [25.] Kapustianyk, V., Turko, B., Kostruba, A., Sofiani, Z., Derkowska, B., Dabos-Seignon, S., & Sahraoui, B. (2007). Influence of size effect and sputtering conditions on the crystallinity and optical properties of ZnO thin films. *Optics Communications*, 269(2), 346-350.
- [26.] Daka, C., & Mukherjee, R. (2022). Synthesis and Characterization of ZnO Nanoparticles and Alq3 for Fabrication of Alq3/ZnO Nanocomposites.120-133,

- [27.] Lee, H., Kim, Y. K., & Lee, C. (2012, June). Improved Performances in Phosphorescent Organic Light-emitting Diodes using Solution-processed Vanadium Pentoxide as a Hole Injection Layer. In *SID Symposium Digest of Technical Papers* (Vol. 43, No. 1).
- [28.] Sharma, B., Sharma, R., Kour, S., Sharma, M. D., Amin, O., Maity, A. R., & Mukherjee, R. (2022). Fractional exponents of electrical and thermal conductivity of vanadium intercalated layered 2H-NbS2 bulk crystal. *Indian Journal of Physics*, *96*(5), 1335-1339.
- [29.] Bauer, Günter; Güther, Volker; Hess, Hans; Otto, Andreas; Roidl, Oskar; Roller, Heinz; Sattelberger, Siegfried (2000). "Vanadium and Vanadium Compounds". *Ullmann's Encyclopedia of Industrial Chemistry*. doi:10.1002/14356007.a27_367. ISBN 3-527-30673-0.
- [30.] Zhang, H., Zhu, W., Wu, M., Feng, Z., Huang, L., Chen, Y., ... & Yang, Y. (2024). A stepwise bilayered hole-injection layer composed of vanadium oxide and PEDOT: PSS for simultaneously enhancing efficiency and stability of organic light-emitting diodes. *Optical Materials*, 152, 115509.
- [31.] Mahakhode, J. G., Bahirwar, B. M., Dhoble, S. J., & Moharil, S. V. (2006). Tunable Photoluminescence from tris (8-hydroxyquinoline) aluminum (Alq3). *Proc of ASID, New Delhi*, 237-239.
- [32.] Lu, J. G., Ye, Z. Z., Zhang, Y. Z., Liang, Q. L., Fujita, S., & Wang, Z. L. (2006). Self-assembled ZnO quantum dots with tunable optical properties. *Applied physics letters*, 89(2).
- [33.] Debsharma, M., Pramanik, T., Maji, P. S., Maity, A. R., Jain, A., & Mukherjee, R. (2024). Effect of ZnO nanoparticle on morphology and optical properties of yellow emissive bulk Alq3 for OLED application. *Optical Materials*, 115768.
- [34.] Ma, C. G., Brik, M. G., Liu, D. X., Feng, B., Tian, Y., & Suchocki, A. (2016) Energy level schemes of fN electronic configurations for the di-, tri-, and

- tetravalent lanthanides and actinides in a free state. *Journal of Luminescence*, 170, 369-374.
- [35.] López-Romero, S., García-Hipólito, M., & Aguilar-Castillo, A. (2013). Bright green luminescence from zirconium oxide stabilized with Tb 3+ ions synthesized by solution combustion technique. *World Journal of Condensed Matter Physics*, 2013.
- [36.] Khreis, O. M., Curry, R. J., Somerton, M., & Gillin, W. P. (2000). Infrared organic light emitting diodes using neodymium tris-(8-hydroxyquinoline). *Journal of Applied Physics*, 88(2), 777-780.
- [37.] He, P., Wang, H., Liu, S., Hu, W., Shi, J., Wang, G., & Gong, M. (2008). An efficient europium (III) organic complex as red phosphor applied in LED. *Journal of the Electrochemical Society*, 156(2), E46.
- [38.] Wei, C., Ma, L., Wei, H., Liu, Z., Bian, Z., & Huang, C. (2018). Advances in luminescent lanthanide complexes and applications. *Science China Technological Sciences*, 61, 1265-1285.
- [39.] Wang, L., Zhao, Z., Wei, C., Wei, H., Liu, Z., Bian, Z., & Huang, C. (2019). Review on the electroluminescence study of lanthanide complexes. *Advanced Optical Materials*, 7(11), 1801256.
- [40.] Gorai, T., Schmitt, W., & Gunnlaugsson, T. (2021). Highlights of the development and application of luminescent lanthanide-based coordination polymers, MOFs and functional nanomaterials. *Dalton Transactions*, 50(3), 770-784.
- [41.] Evans, R. C., Douglas, P., & Winscom, C. J. (2006). Coordination complexes exhibiting room-temperature phosphorescence: Evaluation of their suitability as triplet emitters in organic light emitting diodes. *Coordination chemistry reviews*, 250(15-16), 2093-2126.
- [42.] Weissman, S. I. (1942). Intramolecular energy transfer the fluorescence of complexes of europium. *The Journal of Chemical Physics*, 10(4), 214-217.

- [43.] Fangfang, C., Zuqiang, B., & Huang, C. (2009). Progresses in electroluminescence based on europium (III) complexes. *Journal of rare* earths, 27(3), 345-355
- [44.] Xu, H., Sun, Q., An, Z., Wei, Y., & Liu, X. (2015). Electroluminescence from europium (III) complexes. *Coordination Chemistry Reviews*, 293, 228-249.
- [45.] Trusova, Elena A.; Vokhmintcev, Kirill V.; Zagainov, Igor V. (2012). "Wetchemistry processing of powdery raw material for high-tech ceramics". NanoscaleResearchLetters.7(1):11.
- [46.] Bi, H., Zhang, H., Zhang, Y., Gao, H., Su, Z., & Wang, Y. (2010). aluminium(III)[Al(q-N-oxide)₃],a non-emissive polymer (NEP) from tris(8- hydroxyquinoline)aluminium [Alq₃}Fac-Alq3 and Mer-Alq3 Nano/Microcrystals with Different Emission and Charge-Traporting Properties. *AdvancedMaterials*, 22(14), 1631-1634.

Chapter 4: Characterization techniques to determine electro-optical, electro- chemical and structural properties OLED materials

To achieve my research goal, the foremost thing is the selection of OLED material and their characterization. After selecting my appropriate materials, I synthesized Alq₃ as our parent material for preparation of my electron transport material (ETL) and host or emissive layer (EML). I also synthesized PEDOT: PSS solution, and for making our hole transport layer (HTL)or HIL and V₂O₅ solution for making EBL layer. I prepared LiF slurry for my ETL and EIL and Ag-paste for my low function cathode. But for energy- transfer and proper tandem layer-stacking of OLED, at first cyclic-voltammetry is used to determine the HOMO and LUMO. Then powder form, aqueous solution and thin film and of those selected material were synthesized. Then to ensure the structural property, thermal property of the materials for determining surface-morphology, stability, crystalline structure, crystalline phases, particle size, particle characteristics, presence of specific chemical bond, fingerprint about materials, presence of specific functional group, I used FTIR, XRD and FESEM characterization techniques. To know the optical properties of the synthesized material I used UV-VIS spectroscopy, PL spectroscopy, Fluorescence spectroscopy. To determine the thermal stability, thermal properties and change in state of the material due to heating, boiling point, melting point, thermal degradation, I used TGA and DSC. To determine electrical properties, electronic properties and electroluminescence properties as well as device performance I used CV, ,J-L-V characteristics plot, EL intensity-wavelength plot, EQE, CE, PE,EL& CIE characteristics plot via cyclic voltammeter, source measurement unit, integration sphere, El/PL measurement unit and CIE calculating software given by OSRM. So characterization techniques are the most important part of a research project to substantiate its aim.

4.1. X-Ray Diffraction (XRD):

The most effective characterization technique or way to determine the crystallographic structural details of materials being studied is XRD. Through XRD of a chemical compound, chemical properties, physical properties different crystal phases of the identical molecular planes, crystal structure, (h k l) values, crystal- planes, nature of crystal can easily, XRD is a multifunctional non-destructive investigative method where constructive interference of electromagnetic X-ray radiations and crystal plane of the samples takes place. XRD is a high energetic short wavelength electromagnetic radiated beam. When a moving electron with high speed is passed through a high voltage accelerator and compelled to bombard with a metal target, X-ray begins to generate. In this case, the K.E. of the fast-moving electron decelerates swiftly and transforms into Xray radiation. The wavelength of the X-ray is $0.02A^{\circ}$ to $100A^{\circ}$ (0.002 nm to 10 nm). The XRD operates according to Bragg's law principle. For two reflected beams of light, constructive interference will occur if the path difference between them is an integral multiple of wavelength (λ)[2,3]. The minimum intensity requirement is:

$$2d\sin\theta = n \lambda [n=1,2,3...]$$
(4.1)

Where n=1 denotes the first order of spectrum, n=2 denotes the second order of spectrum, θ =angle of the diffracted ray, d=separation of lattice- points. Bragg's law regulates the elementary principles of X-ray diffraction in the sample's crystalline structure. Here a monochromatic beam of X-ray incidents on a sample surface kept in flat circular sample holder at an angle θ but diffracted with an angle of twice the angle θ i.e., 2θ , which is detected by a detector and a computer software program draws the X-ray diffractogram of the samples on a monitor using specified software. X-ray pattern is the characteristics plot of the samples of a material under analysis.

The relation between accelerating voltage of the fast-moving electrons and the wavelength of the radiated X-ray beam can be expressed by the following equations [1-5]:

$$\lambda = (1.2398 * 103)/V \tag{4.2}$$

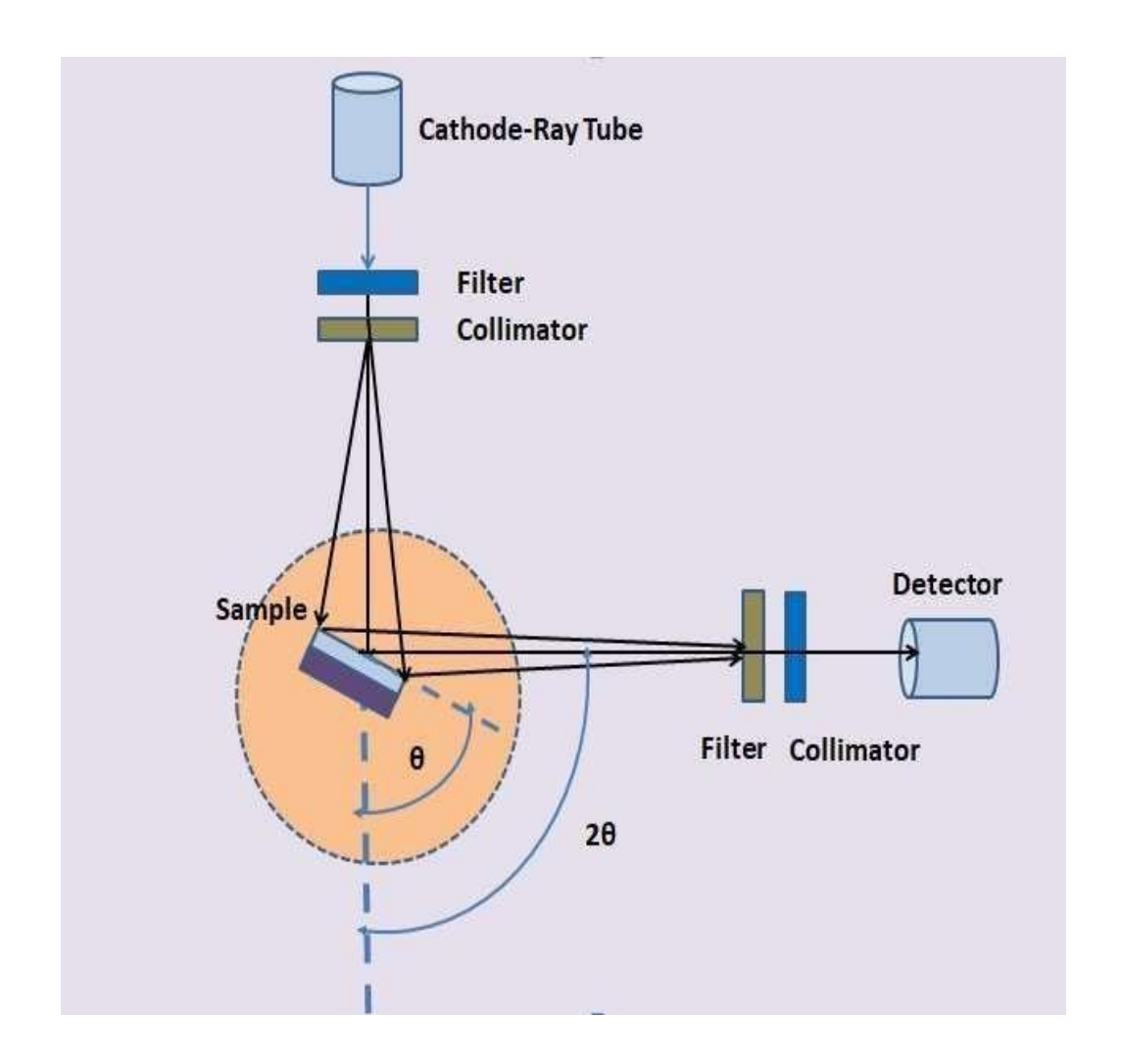


Figure 4.1: The schematic-diagram / figure of a X-ray diffraction spectrometer to detect and determine the crystallographic morphological information through powder XRD of any samples.

For producing X-rays, an X-ray tube is foremostly required. We have illustrated the schematic diagram of the total XRD technique through figure 4.1. An XRT contains two metal electrodes, and a jet of accelerated electrons encapsulated into vacuum tube. When a strong higher voltage is applied across these two electrodes: cathode and anodes then accelerated electrons bombard on the hard metal target made up of chromium, iron,

copper, molybdenum etc and emanate X-ray beams. The generated X-ray beams are guided by XRT window to hit accurately at the collision–site. In spite of to produce different wavelength off X-ray by XRT tube, For XRD methodology only monochromatic X-ray beam is required. A nickel filter is used to cut off the other spectrum of wavelengths of X- ray beam. In a X-ray-diffractometer X-ray diffractogram is formed for a specified current and voltages by Cu-K α X-rays where wavelength of X-rays is used as 0.15406 nm where the range of diffracted angle 2 θ is from 10 $^{\circ}$ to 100 $^{\circ}$ with 0.01 steps and performed at room temperature. The sample is kept in a quartz-made sample holder.

XRD technique provides different decisive information on crystal orientation or texture of the crystal, crystal structures, crystal phases, average grain size, crystal defects, strains, and crystallinity. Amorphous samples give broad peaks, and crystalline samples give sharp pointed higher peaks. Peaks are formed from the X-ray diffracted from sample planes.

By JCPDS (Joint Committee on Powder Diffraction Standards.) card number or ICCD (International Centre for Diffraction Data) database, phase and crystal structure of the samples under observation can be determined using d-spacing values and (h k l) values of the peaks. [1-5]

4.2. Fourier Transform Infrared Spectroscopy (FTIR):

Fourier transform infrared spectroscopy is a non-destructive analytical method that uses infrared (IR) absorption to measure the surface spectroscopy of a sample. In a FTIR spectrometer or interferometer (Figure 4.2) spontaneous alignment of the dipole moment is characterized by using IR aided tool. FTIR provided important information regarding inter or intra-atomic forces of the material's crystal -lattice. Any inorganic or organic compound vibrates by six different techniques: twisting, wagging, scissoring, rocking, symmetrical stretching and anti-symmetrical stretching. In our experiment we use Perkin Elmer made FTIR spectrometer. The mutual correlation among the inter-atomic forces and the infra-red vibrational frequencies are truly outstanding thus IR vibrational

frequencies are used to detect the existence of the particular functional group in the sample under observation. We can find the value of energy transfer occurred between two adjacent energy states by following Planck-Einstein relations.:

$$\Delta E = E_1 \sim E_2 = h\nu \tag{4.4}$$

where v represents the frequency, h=Planck's constant and ΔE = change in energy respectively. When ΔE is positive the molecule is able to absorb energy but when ΔE is

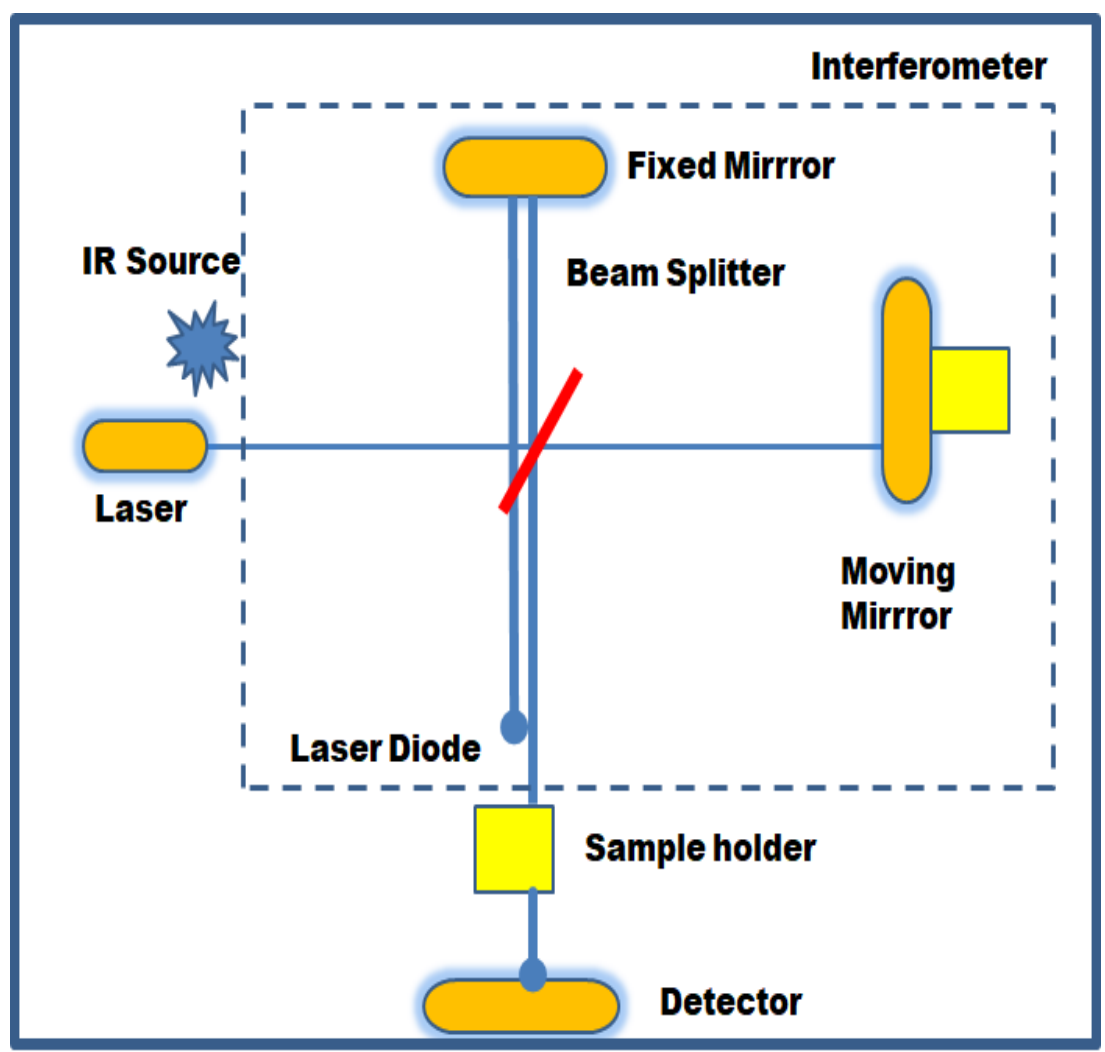


Figure 4.2: Schematic representation of FTIR spectrometer.

negative, the molecule radiates its energy, and an emission spectrum is observed. For getting absorption of a particular molecule the above Equation (3.4) should be satisfied The IR spectrum is usually plotted as intensity vs frequency and exhibit absorption peaks when the above equation (4.4) satisfies. Within a small region of the visible spectrum (10 nm to 1 mm), UV-VIS portion and IR portions remain active for production of absorption level transition among allows atomic electronic transitions. peaks during our spectroscopic observations. The different atomic or molecular energy between two orbitals due to absorption or release of energy. It is worth saying that the atoms of the molecules vibrate and absorb energy resulting in an atomic orbital energy level shift. In addition to this it also involves different energy transitions such as vibrational, rotational and electronic transitions. As translational energy is very small it is ignored for energy-transition calculations. Out of the six methods vibrational spectrums exhibit unmatched molecular physical properties or characteristics. Hence, FTIR spectrum is considered to be as fingerprint identification of a material [6-8].

4.3. Field Emission Scanning Electron Microscopy (FESEM):

Field-emission scanning electron microscopy (FESEM) is a characterization technique which produces a detailed high-resolution image of the surfaces of the samples under investigation using a stream of electron beams [9]. FESEM (Figure 4.3) produces electrons by utilizing its field emission gun, hence it is named so. In this method for higher focusing the electrons are driven through an electric field created by the electron gun and allowed to incident on the sample's surface. Those electrons are directed to the sample-surface. The FESEM produces high-density high-resolution images of the sample's surface area as electron beams are focused directly on specified small areas thus showing detailed images of the surface. In Figure 4.3, the various parts of the FESEM instrument are schematically represented. The electron gun creates a jet of electrons which are allowed to focus on the

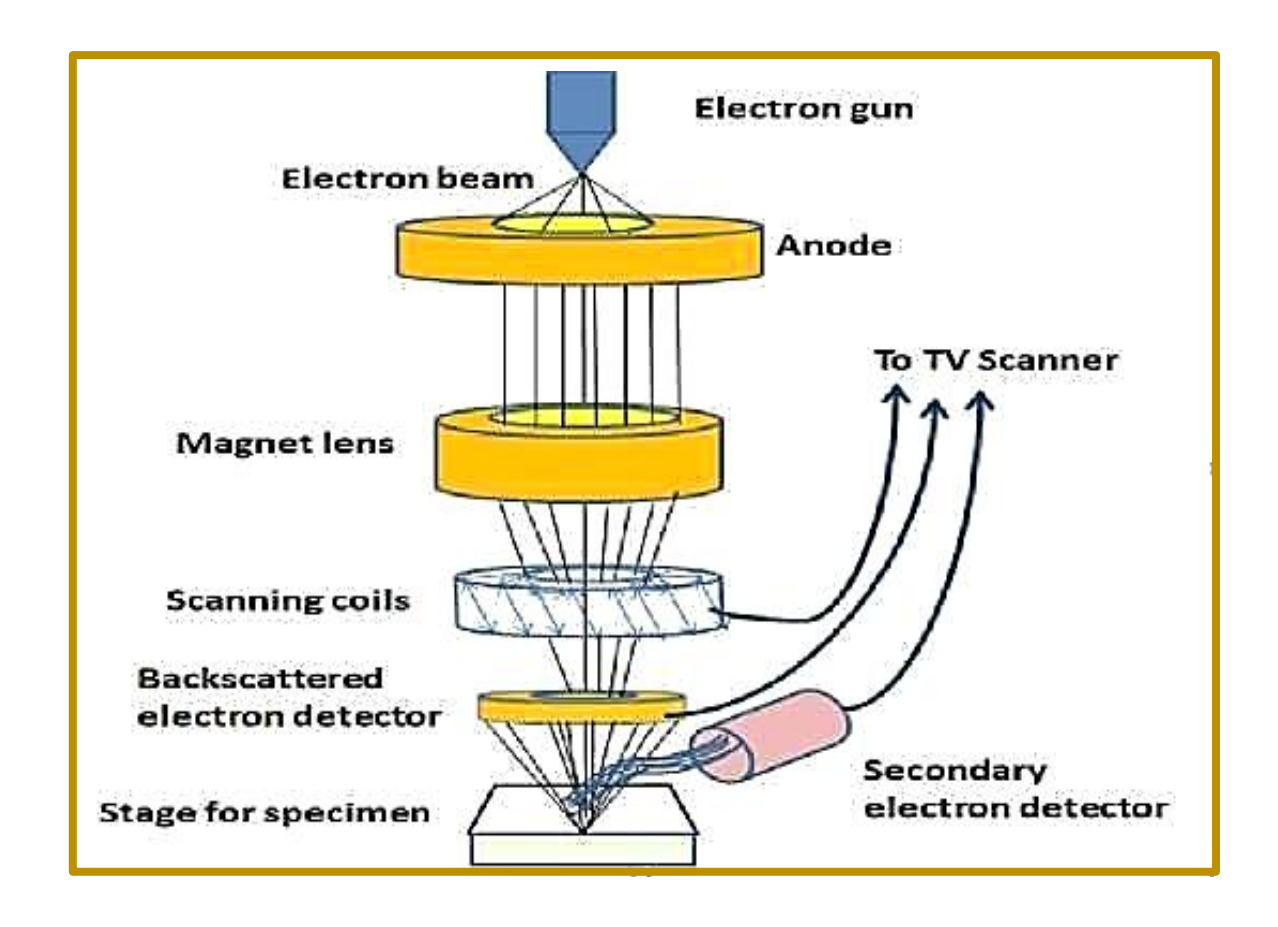


Figure 4.3:(a) Schematic diagram of working of FESEM with all its components surface

specified small area of the sample's surface. In this case an electron gun contains condenser lens and apertures. The objective lens streamlines or guides the incident to an incident accurately on the target site on sample surface filtering unwanted beams to prevent beam's broadening. To raster small surface area of the sample a scanning coil is used. By FESEM we can analyze the image and can detect the topology, morphology, porosity, particle size and particle's shape. For this reason, FESEM is an excellent analytical method. [9-12]

4.4. Energy dispersive X-ray spectroscopy (EDS):

X-rays, secondary electrons (SEs), and backscattered electrons (BSEs) are produced when electrons come into contact with solid materials. Of them, X-rays only can quantify,

analyze and detect the compositional elements of the sample under investigation. All these three signals provide significant information about the samples on the basis of how an electron encounters with a material. The EDS measurements (Figure 4.3) also identify the chemical composition, atomic and molecular distribution in the different parts of the sample.Fig.4.3. illustrates the workings of the schematic diagram of EDS systems. At 3-5nm.depth from the upper surface the Auger-electrons are generated while at 50 nm secondary electron and at 500 nm of depth secondary electrons and backscattered electrons are generated. At 1-2 μm. depth, continuous and characteristics electrons are emitted [11-12]. EDS measurement encounters some sensitivity-limitations. If the samples under investigations have elements with low concentration, we cannot be able to determine the accurate elemental composition in the samples. The challenges of the EDS measurements are: EDS cannot measure low atomic number elements which comprise of only one outermost shell (n=1) elements like hydrogen, helium. These elements have no required core electrons to emit X-ray. The EDS measurement of low atomic number containing elements such as beryllium and lithium which cannot be able to produce required energy for accurate EDS measurements. During EDS measurements to find the existence of these aforementioned elements is quite a big challenge. [11-12]

4.5. UV-VIS spectroscopy:

Ultraviolet-Visible s within the spectroscopy is an analytical methodology for measuring the light absorbance by the material within the range of ultraviolet as well as the visible region of the electromagnetic spectrum. UV-VIS spectrophotometry or UV- VIS spectroscopy represents the reflectance spectroscopy or absorbance spectroscopy. It is a complementary spectroscopical process of fluorescence. It follows the principle of Beer-Lambert's law. [12-14]

$$A=Log10 (Io/I) = \epsilon 1 c$$
 (4.5)

Where A=absorbance, c = concentration, l=path length and (Io/I) = 1/T = reciprocal of the transmittance=(intensity of light before it passes through the sample) / (intensity of

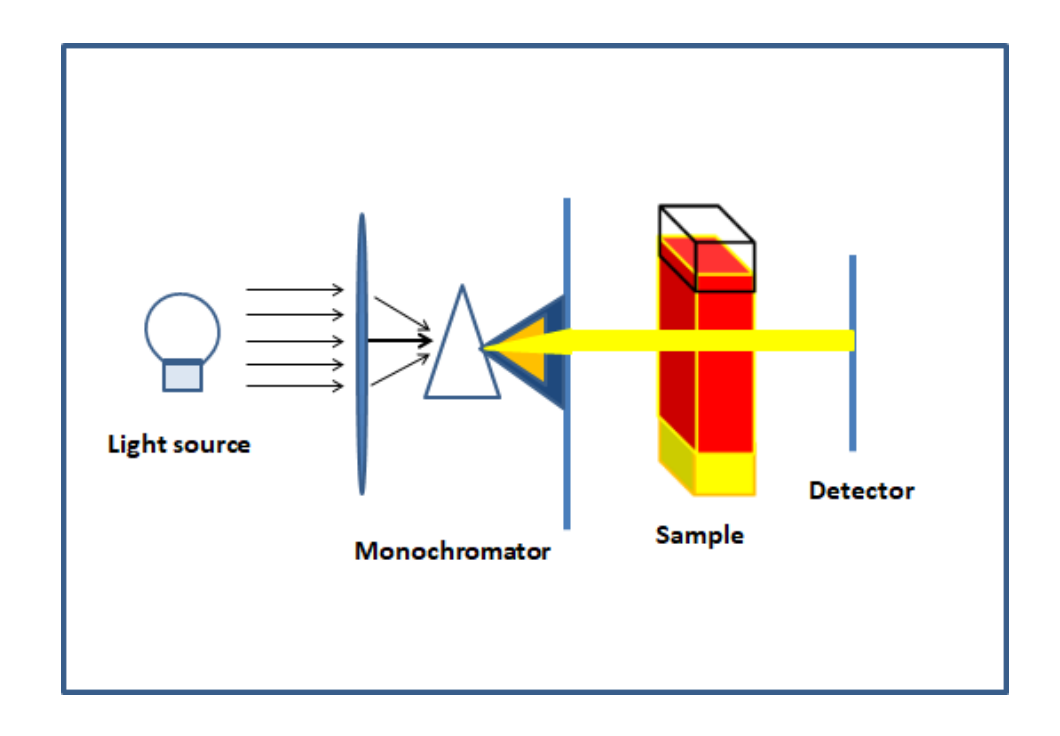


Fig 4.4: Schematic diagram of UV-VIS spectroscopy

The light after it passes through the sample). According to Beer Lambert's law, the amount of the light absorbed is directly proportional to the product of the distance that light travels across the sample's surface, the sample's concentration, and path length. Figure 4.5 clearly depicts the schematic diagram of a UV-VIS spectrophotometer (Figure 4.4). A monochromatic light source with tungsten filament or Xenon lamp is used as the required light-resource. The light source's radiated light travels through the scanning monochromator. Scanning monochromators filter the light beam so that only one wavelength of light can reach the detector at a time using single photo diode detectors and photomultiplier tubes. The function of a monochromator is to split source light into narrow bands of wavelength using diffraction grating prism. The monochromator splits each wavelength meticulously such that the intensity of the selected wavelength can be enumerated by function of wavelength. The selected wavelength of light passes through the sample solution kept in a transparent rectangular quartz made cuvette with 1 cm internal width) and a reference cuvette with liquid solvent of the samples under investigation. The internal width of the cuvette is considered as the path length of the

Beer–Lambert law. The light passes through the transparent cuvette and is being directed to the photo detector here at first the process is performed with solvent solution for calibration then it is performed with the sample dissolved in a solvent. A common reference solution is taken acetone. Dimethyl formide, benzene as they have high UV absorbance cut off, below that cut off all light will be absorbed by the reference solvent. The photo detector received that selected wavelength of light ,once for reference solvent and second time for sample's solution dissolved into same solvent, determines how much selected light are absorbed by the solvent and sample's solution, the difference of absorbance can be visualized through a computer monitor attached with it as an analyzed graphical report .This graphical report is the actual UV-VIS absorbance spectrogram actually tells about how much light is absorbed the sample under investigation at specified wavelength. Thus UV-VIS spectroscopy measures how much UV

-light or visible light is absorbed by a certain molecule for determining its chemical composition. UV-VIS spectrum acts throughout the Ultraviolet waves' range (200-400 nm) and entire visible light range (390 nm -700 nm). The electro-magnetic radiation range is 200-1000nm. UV-Vis. is used as an important measuring-tool for biotechnology, academic research, pharmaceutical, bacterial culturing, drug identification, to know bonding anti-bonding, optical transition, nucleic acid purity checking, for maintaining quality-control in the chemical research as well as in beverage industry. [12-14]. The relation between transmittance and absorbance [14]:

$$A = \epsilon lc = log 10(I0/I) = log 10(I/T) = -log 10 (T)$$
 (4.6)

4.6. Photoluminescence (PL) spectroscopy:

Photoluminescence spectroscopy or PL spectroscopy is a non-contact, non-destructive technique for examining materials or samples. Photoluminescence is measured by the spectrophotometer (Figure 4.5 and 4.6). A spectrophotometer is a measuring instrument which can measure the absorbed amount of light by sample under investigation. PL spectroscopy is a non-contact, non-destructive technique for examining materials. A spectrometer and a photometer are the two instruments that make up a spectro-photometer.

While the photometer gauges the light's intensity, the spectrometer can generate light at any desired wavelength. The sample, liquid, or solution in a spectro-photometer is positioned between the photometer and the spectrometer. A voltage signal is sent to the computer monitor or detector display connected to a spectrophotometer in this case by the photometer, which measures the amount of light that passes through the sample being observed. Any changes occurred in the light-absorption, the voltage signals change

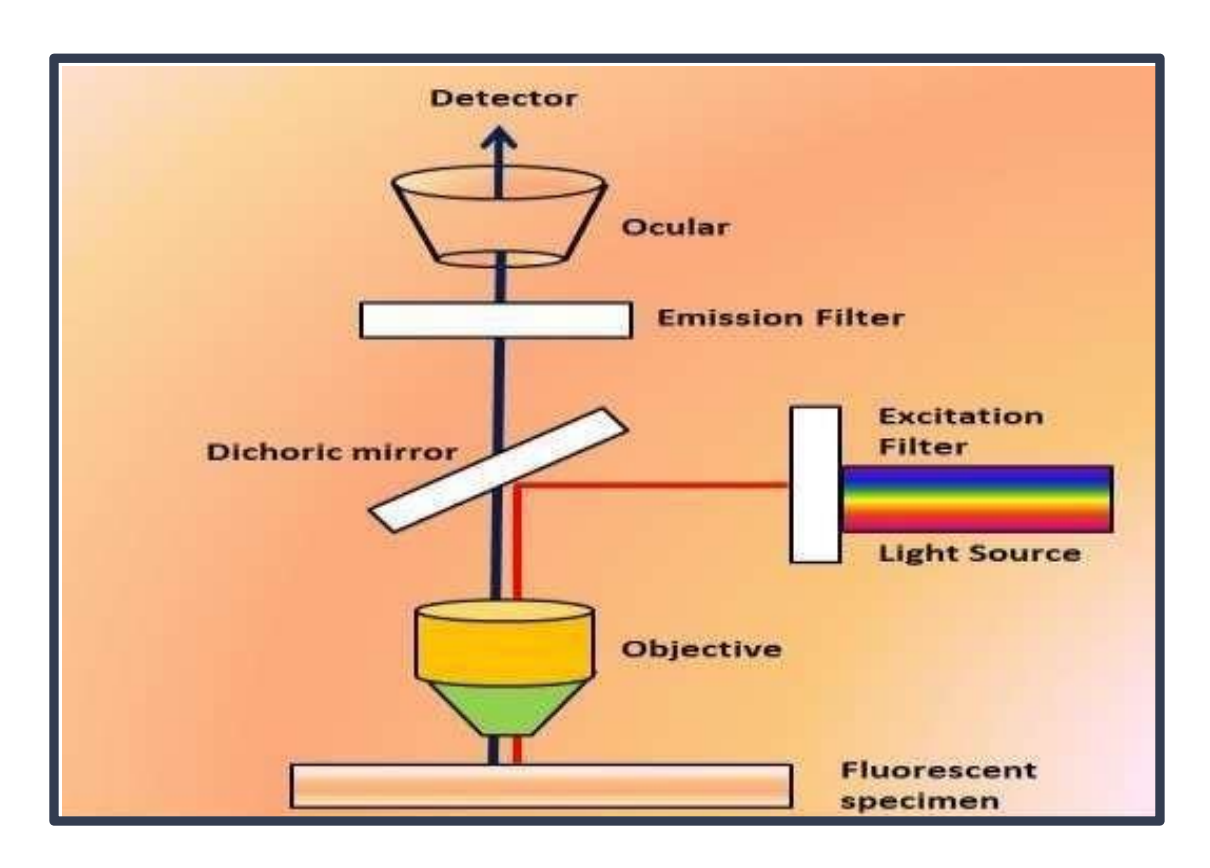


Fig 4.5: Schematic diagram of photoluminescence spectroscopy

accordingly resulting in multi-shaped or multi-sized plotting which has multipurpose determinant application. Spectroscopy measures the light intensity of the source light along with its absorption. A spectrophotometer's fundamental parts include a monochromatic

light source, a monochromator, a collimator to transmit light in a straight line, a quartz

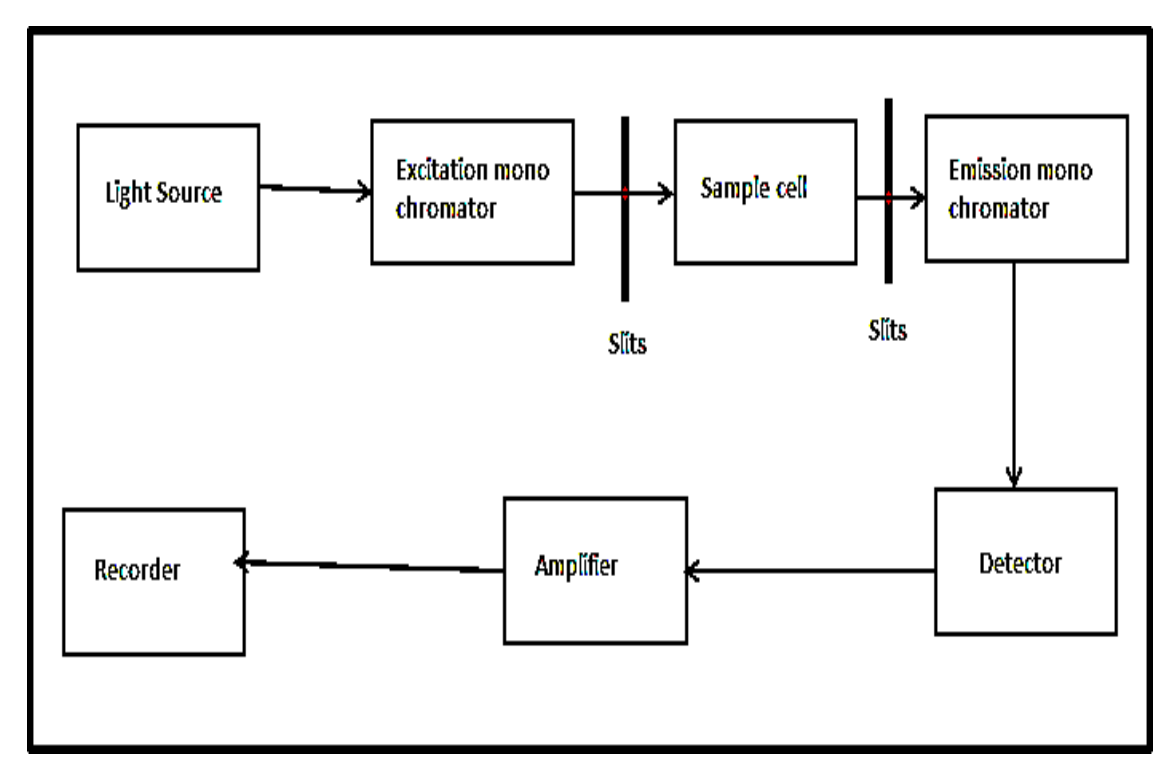


Figure 4.6: Block diagram of photoluminescence

cuvette, a digital display, a wavelength sector that sends a laser beam with the desired wavelength through the sample, and a photoelectric detector that is connected to a computer monitor. The spectrophotometer compares two light intensities when light is passed through blank solution before calibration is "Io" and the intensity of light after calibration is "I". Sample's fluorescence is recorded and evaluated through an analytical device which is known as spectrofluorometer. It can measure fluorescence through scanning emission wavelength and excitation wavelength or both. In a fluorescence spectrometer laser source of light is allowed to pass through a wavelength-splitter tool or monochromator or excitation monochromator and an emission monochromator using slits. Then, at first the selected wavelength for excitation and then emission wavelength is driven towards a detector which amplifies the signal through an amplifier and then recorded using a recorder attached to the system. We can observe different kinds of plot which confirm different physical and chemical properties. [14-20]. In our research

photoluminescence properties of mer-Alq₃ have played a crucial role. Alq₃ is a transparent highly fluorescent organic small molecule n-type semiconductor. To tune its photoluminescence is our one of the important pre-requisites. The result of photoluminescence plot gives a rough idea of the nature of light it reflects, and this information also helps to find CIE chromaticity co -ordinates or chromaticity characters of extracted light from Alq₃ emitter-based devices,

4.7. Cyclic voltammetry (CV):

A type of potentio-dynamic electrochemical technique called cyclic voltammetry is used to measure the HOMO and LUMO energy levels of the sample under consideration as well as to observe the redox behavior, or the reduction and oxidation processes of molecular species. During oxidation process (potential) electrons are being removed from the HOMO energy level whereas reduction process (potential) represents the material's LUMO energy level. By the help of cyclic voltammetry, we can determine the E_{OX} (Oxidation potential) and can know the energy transfer feasibility and also get a better idea about the relativeenergy of the molecular orbitals of the composite polymers under observation. For this, dip-coated film on glassy carbon electrodes is considered for cyclic voltammetric analysis. The primary parts of a CV system (Figure 4.8) include a potentiostat, an electrochemical cell for electrolysis that also has three electrodes: a reference electrode, a counter electrode, a working electrode, and a current to voltage converter. Additionally, there is a system for recording data. All three electrodes remain sunk in the electrolytic solution. A potentiostat produces a constant potential by using dc power supply and maintained that voltage until it is changed at the same time it allows a small amount of current without any voltage change. Cyclic voltammetry works on the principle of Nernst equation.CV measures the amount of current generated in an electrochemical cell under where excess voltage is developed compared to the prediction of Nernst Equation -----

-

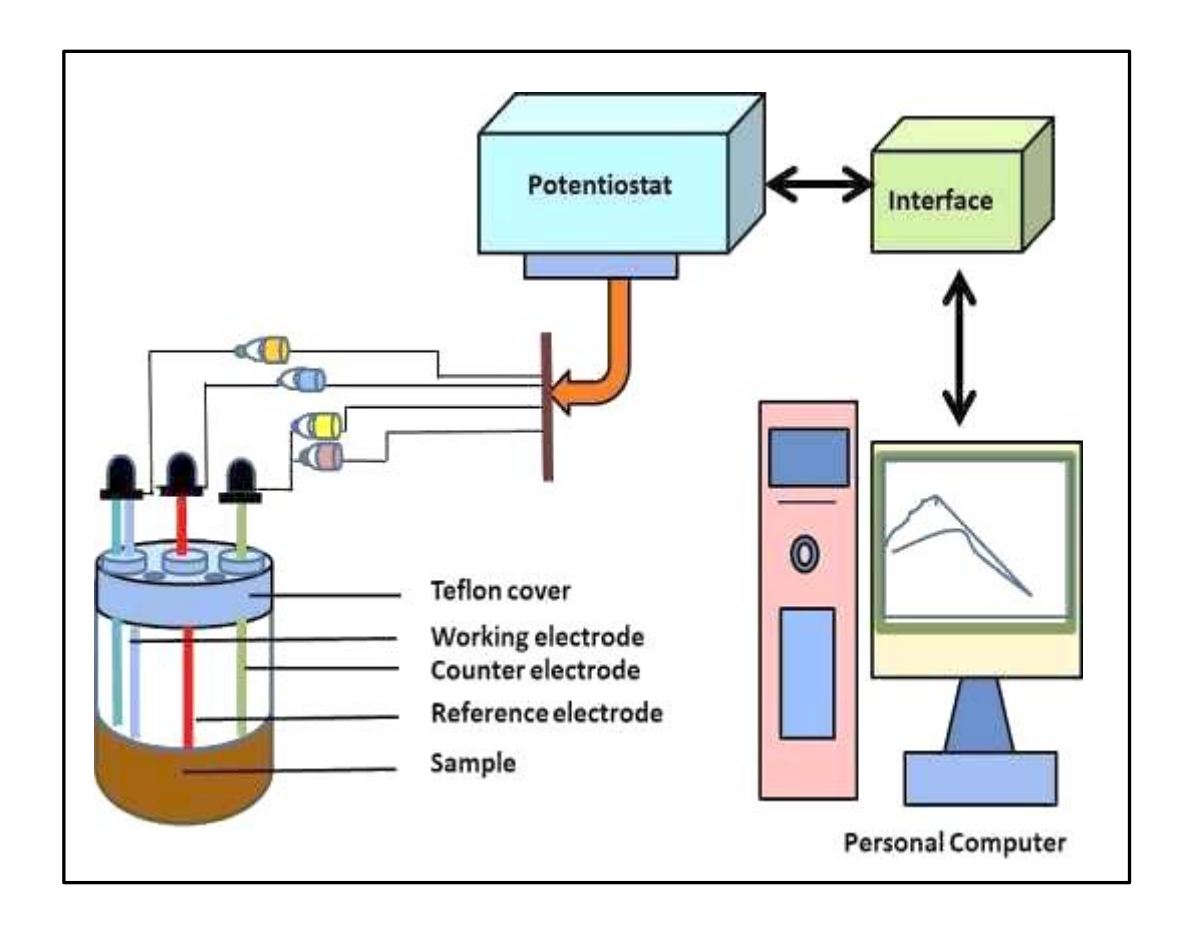


Figure 4.7. Schematic diagram of cyclic voltammetry and cyclic voltameter

for the reversible electrochemical electron transfer of $X + e^- \subseteq X$

$$E=E^{\circ} - \frac{RT}{nF} \ln \left(\frac{c_{X^{-}}}{c_{X^{+}}} \right) = E^{\circ} + 2.3026 \log_{10} \left(\frac{ox}{red} \right) = E^{\circ} + 2.3026 \log_{10} \left(\frac{c_{X^{-}}}{c_{X^{+}}} \right)$$
(4.7)

where E is the potential of an electrochemical cell, E^o is a species' standard potential, T is temperature, n is the number of electrons, R is the universal gas constant, and F is Faraday's constant.

In CV, a potentiostat is swept linearly between the working electrode potential and reference electrode potential until it gets its present condition or magnitude. Then, in this way the same process should be replicated many times. During each single and reverse scan changes of current between those probes (electrodes) are noted immediately. A duck shaped diagram is created on the potential (V) vs reference electrode graph. [21-24]

4.8. Differential Scanning Calorimetry (DSC):

We can perform thermal analysis of a sample under investigation via Differential Scanning Calorimetry, an important thermal—analysis technique. Through DSC we can calculate the exchange of heat energy that occurred at the time of physical change or chemical change of any material under constant applied pressure. The DSC instrument (Figure 4.9) can measure the changes in thermal property of a sample on the basis of heating a thermally inert reference sample within a fixed range of temperatures. High precision and controlled heating rate based thermal analysis can be analyzed within a wide extent of temperatures. All these measurements are studied under the influence of the inert environment by flowing nitrogen (N₂) gas. In DS calorimeter, oxygen or air is flowed to investigate the oxidative properties of samples. DS Calorimeter is a single furnace -based equipment which works on the principle of heat-flux measurement. It consists of temperaturesensors made up of thermo-couples. It also allows photo-calorimetric measurement using photo-calorimetric accessory with DS calorimeter. A DS calorimeter can also measure different applications as follows: melting point, glass transition temperature, crystallization time, crystallization temperatures, percentage of crystallinity, heat capacity, oxidative stabilities, thermal stabilities, thermal curing, polymorphism, quality of the product, purity analysis etc. According to measurement methods DSC mainly are of two types: (1) Heat Flux DSCs: and (2) Power Compensation DSC. Heat Flux DSC is basically a methodology used for measuring temperature difference as a function of temperature between the reference material and the sample material (called as sample unit all together) when the temperature of that sample unit is altered in a specific program. However, when the temperature of that sample unit is changed in a particular program, the Power Compensation DSC technique measures the thermal energy difference per unit time between reference material and sample material as a function of time to match their temperature The following parts make up a heat flux DSC: heater, heat sink, heat resistor, reference holder, and sample holder. through the use of a heat resistor and a heat sink. The heater transfers its thermal energy into reference and sample holders. The amount of heat flow is directly proportional to the heat differential between the sample unit and

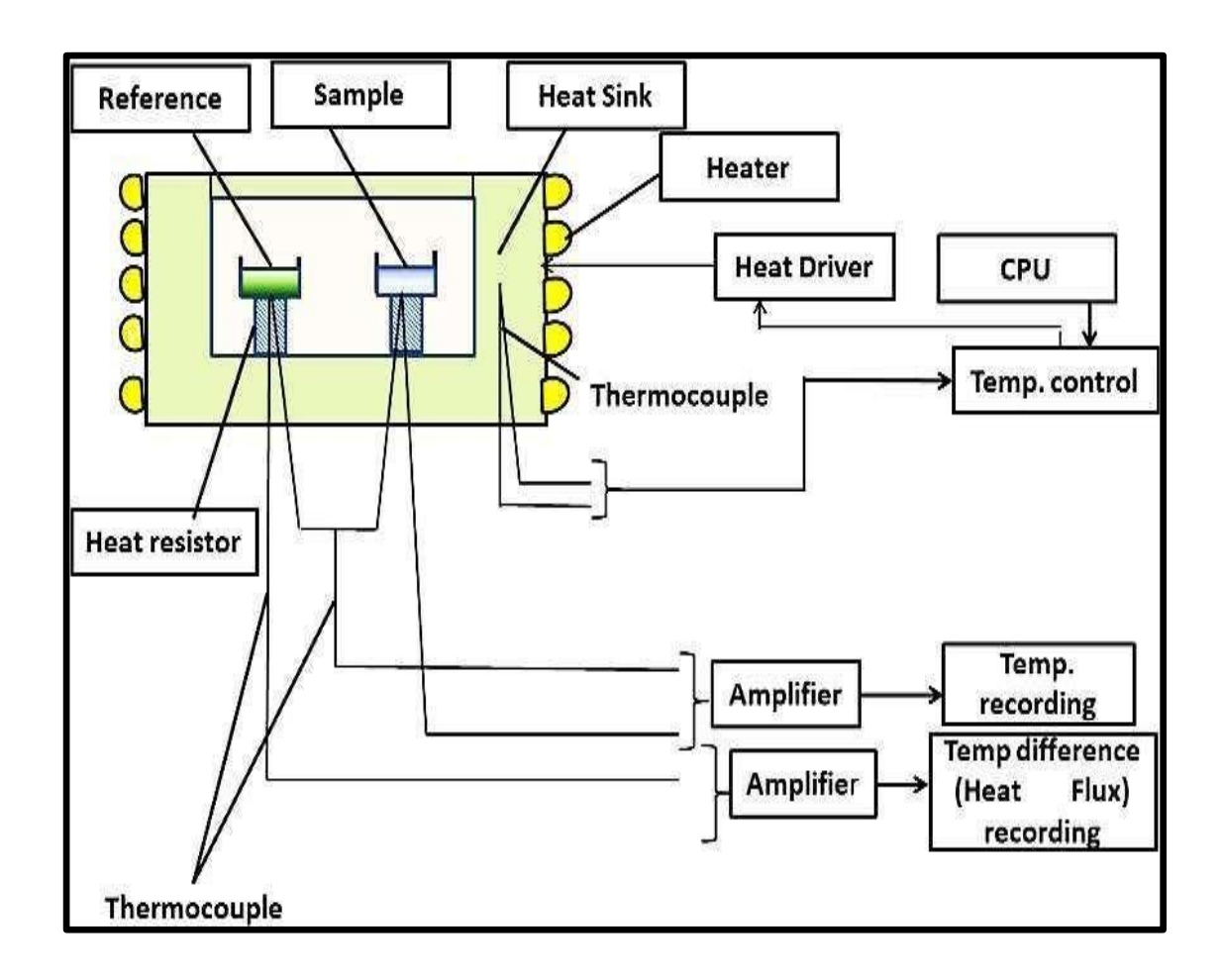


Figure 4.8: Image of Differential Scanning Calorimeter (left) and block-diagram of heat flux Differential Scanning Calorimetric Instrument and working principle

the heat sink. The amount of heat-flow is directly proportional to the heat differential between the sample unit and the heat sink. The heat sink's heat capacitance in this system is higher than the sample material's heat capacitance. Heat sink compensates for the exothermic or endothermic phenomena such as reaction, transition etc. occurred in the sample. In this way the temperature difference between reference and the sample remains constant. A direct proportionality exists between the temperature differential between the reference and sample holders and the quantity of heat-energy supplied to each holder separately. We can use DSC to calibrate any standard material so that we can perform quantitative measurements on any unknown sample. [29–31]

4.9. Thermo gravimetric analysis (TGA):

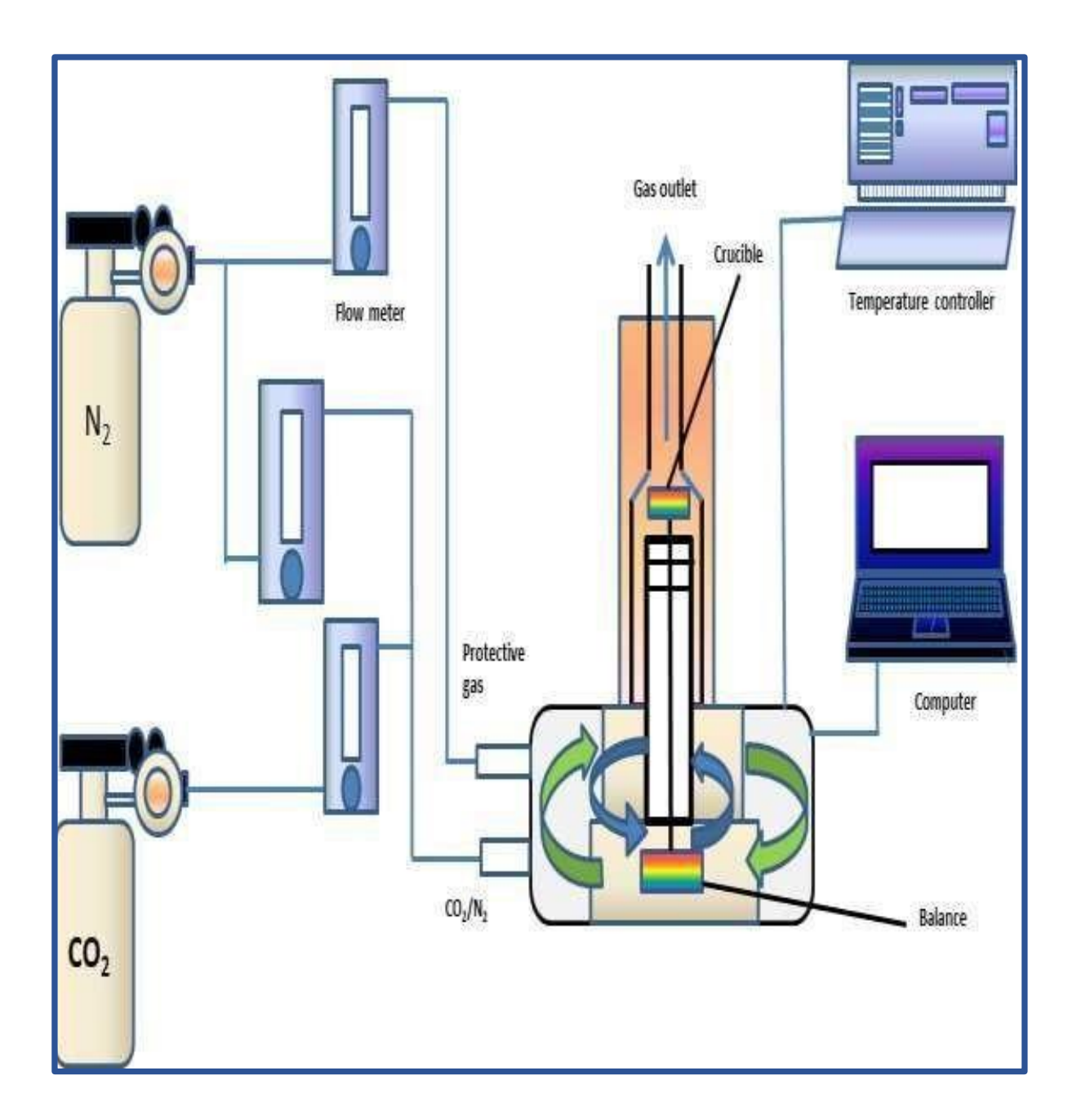


Figure 49: Image of Thermo gravimetric analyzer instrument (left) and schematic diagram of thermo gravimetric analysis technique (right)

Thermogravimetric analyzer is an instrument which evaluates the change in weight% or mass % of any sample-material due to different physical changes

or chemical changes occurred with the variation of temperature of that sample.TG analyzer senses change in mass during all these thermal events like absorption, desorption, vaporization, sublimation, reduction, oxidation, decomposition etc. In thermogravimetric analysis, the sample-material is heated under the given environment (environment of CO₂, N₂, air, Ar, He etc.) at regulated rate. As time and temperature change, the mass or weight change of the material being studied is noted. For a predefined initial weight or a mass of fundamental principle of TGA. A software program of the TG analyzer instrument studies all thermal events that occurred in the substance over a specified range of temperature. This TG analyzer instrument (Figure 4.10) is compatible with outstanding temperature reproduction capability as well as it can be fully functional over wide iso-thermal range. Tap water is used to cool down the heating furnace quickly. In this equipment, many samples can be studied easily even in less time by using integral forced air. Balance purge gas is used to maintain a balance environment inside the equipment and protects the balance from the materials as well as reactive purged gas from sample-material. The change in mass or weight of the sample is measured through a microbalance. This instrument also contains an anti- corroded substance to protect the furnace from corrosion. An integrated mass - flow controller system is used for controlling and monitoring purge -flow rates and switching over between two gases used TGA is used for the following important functions: for experiments. measurement of volatile substances, oxidative-stabilities, thermal-stabilities, flammability-studies, compositional-analysis, catalyst-studies, coking-studies, decomposition- temperatures, engine-oil volatility [32-33].

4.10. Electroluminescence and Photoluminescence (EL and PL) intensity vs wavelength plot and its measurement and analysis using EL/PL analyzer:

An EL/PL measurement system (Figure 4.12 and 4.12A) consists of following components: Spectrometer, Laser, Lock-in amplifier, PMT/CCD, Optical Chopper,

Optical fiber, EL/PL Sample Holder, Sample Chamber ,low temperature Refrigerator, Vacuum generator, Optical optics and related other accessories The sample-wafer under test is kept on an in-built aluminium chuck, attached with multi-directional (with typical XYZ configuration)

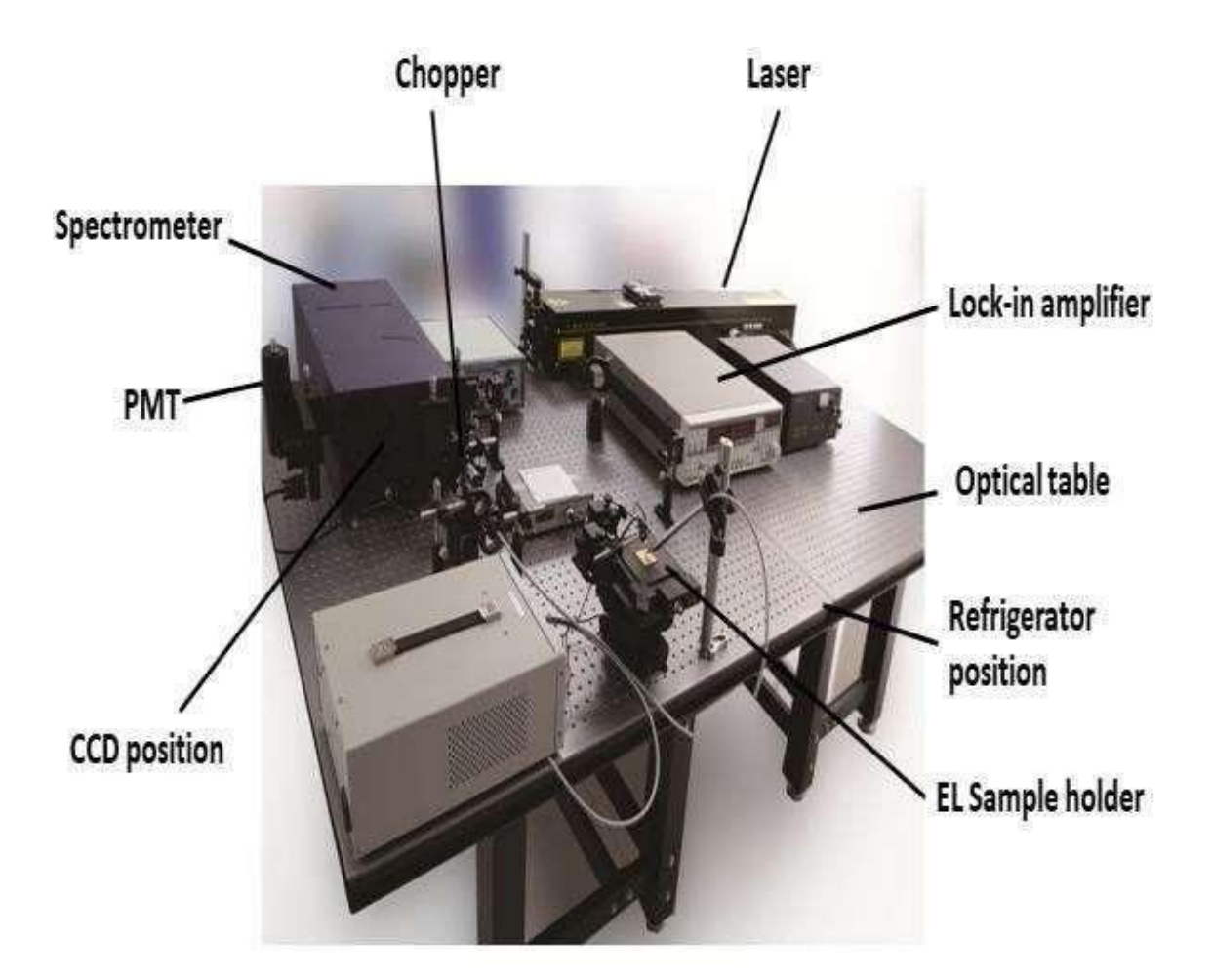


Figure 4.10: Image of Electroluminescence and Photoluminescence analysis scheme movable platform by means of three step motors (made by Micos VT- 80), under vacuum atmosphere. There is one (or two) position adjustable tungsten-made probes for biasing the samples. A source-meter (Keithley2430) is utilized to set up voltage- difference amid the chuck and probe/probes and to measure the change in current simultaneously. It also facilitates simple mode pulse operation and also measures the voltage for fixed v

current. A microscope and a camera attached with the microscope are used for appropriate placement of the probe/s and for capturing the images of the wafer of the sample under test respectively. Three separate detection techniques are used to capture the amount of emitted light from the sample surface. Likewise biasing an optical fiber is put just on the top of the wafer with the help of a probe to collect and measure the amount of emitted light by the sample and to measure and analyze the spectrum formed due to this through a spectrometer aided by Perkin Elmer. A sensitive PMT (photomultiplier tube) biased with a voltage source is used to measure arbitrary units of power and improve the degree of signal to noise ratio. The output of PMT is linked with a lock-in amplifier. The output of the source-meter sends reference signal which is converted into pulsed-mode signals. A software program (Lab view) of a computer controls the

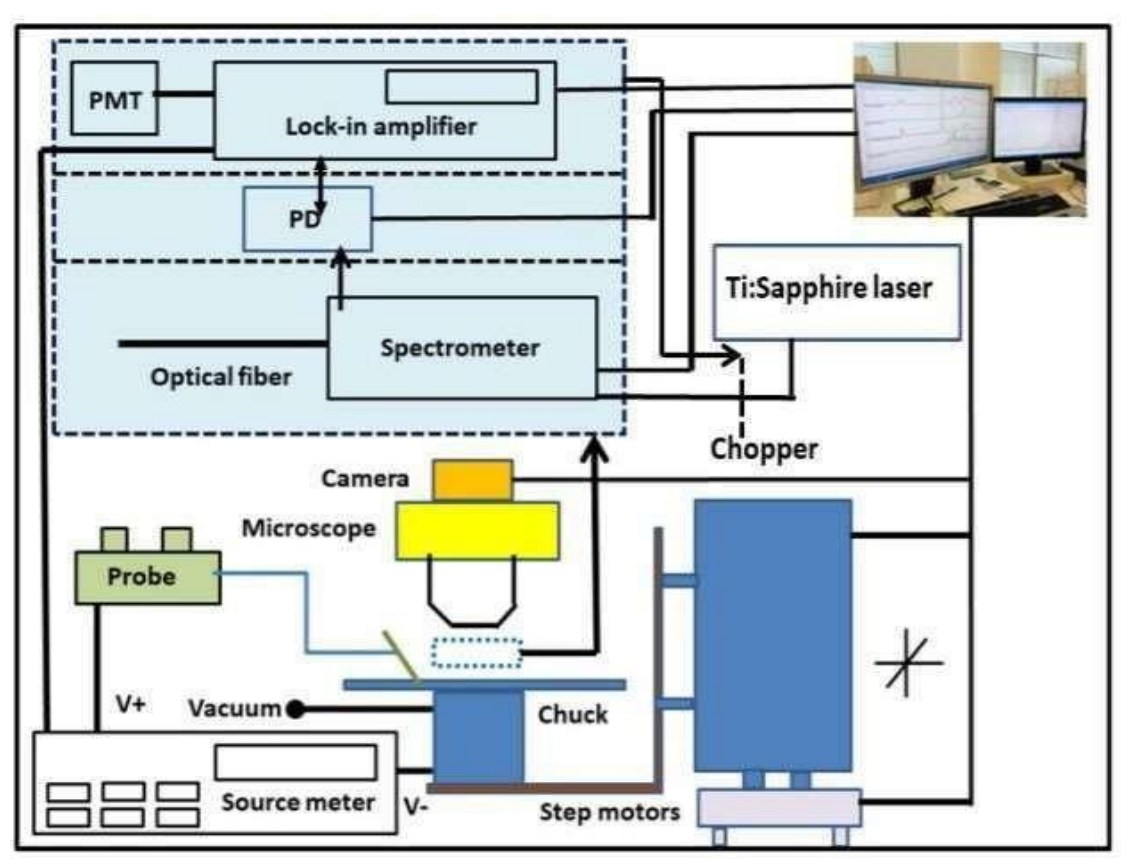


Figure 4.10A: Schematic block diagram of workings of EL and PL analysis scheme (right)

operations of source meter, step motors and chosen detection system altogether. This software program also helps to measure voltage-current or current – voltage (I or V) sweeping and EL or PL spectrum or EL or PL intensity simultaneously. This also correlates electrical characteristics of the sample with the EL signal. The amount of power density or emitted total power output per unit area of the emitters and per unit solid angle is dependent on the emission profile as a function of observation angle followed by Lambert's cosine law as:

$$I(\theta, \varphi) = I\max \cos(\theta) \text{ W sr}^{-1} \text{ m}^{-2}$$
(4.8)

Where φ = angle of revolution lying within the range of $[0, 2\pi]$ and θ =azimuthal angle created with the normal drawn to the emitter which lies within the range of $[0, \pi/2]$. [37-38]

4.11.J-L-V(current density-luminance-voltage or I-L-V(current-luminance-voltage) plot, power efficiency(PE) plot and current efficiency(CE)plot using Source measurement unit or source measure unit or source meter unit (SMU):

An electronic automated test device or tool that can simultaneously measure and source voltage and current is called a source measure unit, SMU, or source-measurement unit. It has the ability to measure source voltage, source current, and their resource precisely. Four- quadrant source and sink power measurement is provided by a source meter unit (SMU). It also gives 5- in-1 functions that can be performed in single instruments. An SMU is a five- in- one device that combines the practical features of a digital multimeter (DMM), pulse generator electronic load, power supply, and current source into a single small package. These four functions are: source voltage, source current, measure voltage and measure current. Thus, these four instruments provide a 5-in-1 source-function which includes sink capability. For this reason, these instruments can be utilized as electronic loads.

A source measure unit (Figure 4.11) integrates a DC aided stable power source as a steady voltage source or a steady current source and an accurate multimeter. (Figure 4.11) Typically, this SMU consists of four (4) terminals, 1 (one) for measurement and 1 for source, 1 for remote sense or kelvin and 1 for 1 for connection. DC power is passed simultaneously through a pair of terminals, positive (source) and negative(sink), at the same time for sourcing and sinking as well as for measuring the amount of voltage or current passed across through those two terminals. Here both sourcing current and sourcing voltage spins across the positive values and negative values via both positive and negative terminal. So. a SMU always contains 4- quadrant based outputs. A SMU have ability: to measure resistance versus, voltage characteristics or resistance vs. current characteristics, to precise source as well as to measure current-voltage characteristics individually or simultaneously, can measure current source in the range of 100aA to 50A current and also a volt source in the range of 100nV to 3kV voltage with resolution of 6½ digits. It also runs the production tests comparatively 60% faster than its other counterparts. A SMU can gain more than 10X throughput. Thus, a SMU performs its job very fast thus saves time with its maximum speed. It can measure current densityluminance-voltage characteristics plot and luminance-current-voltage and I-V characteristic- plot of a semiconductor based electronic device like diode, LED, transistor, OLED etc. It is bench equipment which works like a curve tracer does. It also has a USB or GPIB interface facility for establishing connectivity between a PC and SMU. and luminance-current-voltage and I-V characteristic- plot of a semiconductor based electronic device like diode, LED, transistor, OLED etc. It is bench equipment which works like a curve tracer does. It also has a USB or GPIB interface facility for establishing connectivity between a PC and SMU.

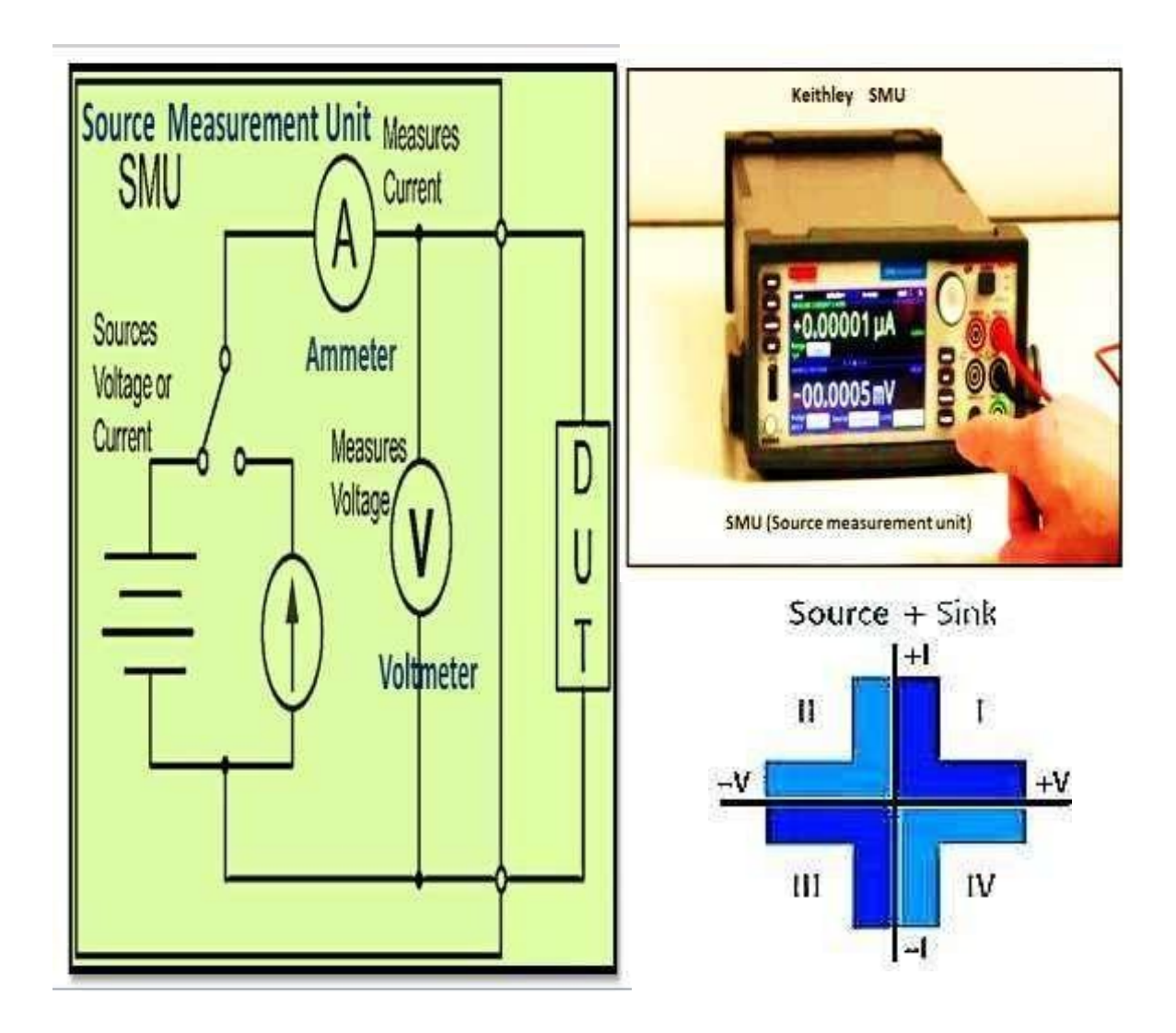


Figure 4.11: Image of schematic diagram of Source Measurement Unit (SMU) (left) and image of Source measurement unit Keithley 2360

Some notable features of SMU are as follows:

On-board processing- SMUs have capability of adding user defined on board script processors to improve test time, communication time and also instrument integration-time additionally apart from its basic functionalities. A SMU can control test flow, test sequencing, instrument autonomy and decision-making ability by on-board script performance technique.

Current- and voltage (I&V) sweeping: The sweeping characteristic of a SMU helps it

to test DUT (devices under test) to measure different characteristics with respect to different range, different conditions, different sources, delay and different measuring criteria. A SMU allows pulsed sweeps, fixed level/valued sweeps linear sweeps and logarithm-based sweeps.

Contact checking-SMU can check the quality of connections made with the testing device before its test. Thus, A SMU can measure the following characteristics of a testing device, connection breakage, current/voltage leakage, loose connections, short circuit, contact fatigue, corrosion, contamination, broken connections, relay failure etc. [34-36].

4.12. Chromatic diagram analysis (on the basis of CIE 1931):

C.I.E. diagram is usually used to find out the physical value of a colour within a range or gamut. C.I.E diagram typically represents all average person's perceivable chromaticity. It also evaluates the range of the colours under test and finds its allied complementary and dominant colours. CIE is the acronym of Commission Internationale de I'Eclairage. This is a organization which brought the concept of CIE diagram in the year 1931. CIE chromaticity diagram is used to characterize colours using Y, a luminance parameter, and x and y, two color co-ordinates for specifying a point on CIE chromaticity space diagram. These three parameters are basically influenced by the measurement of sensitivity curves for the human eyes and dependent of the spectral power distribution of emitted light from the surface of colored objects. The Human eyes have three different kinds of colour-sensitivity cones cells i.e., eye-responsive tri-stimulus values. Thus, any colour can be represented by two colour coordinates i.e., x and y respectively. In chromatic diagram a triangle is drawn to join the coordinates of three primary colours or RGB colours to represent any matching colours by combining those RGB colours.

The Chromaticity diagram represents the colours of spectrum and also their mixtures on the basis of three existing primary colours i.e., RGB (Red, Green and Blue) in them. Chromaticity is established on the basis of two parameters: saturation and hue. Chrominance is another parameter formed due to the combination of two parameters i.e.

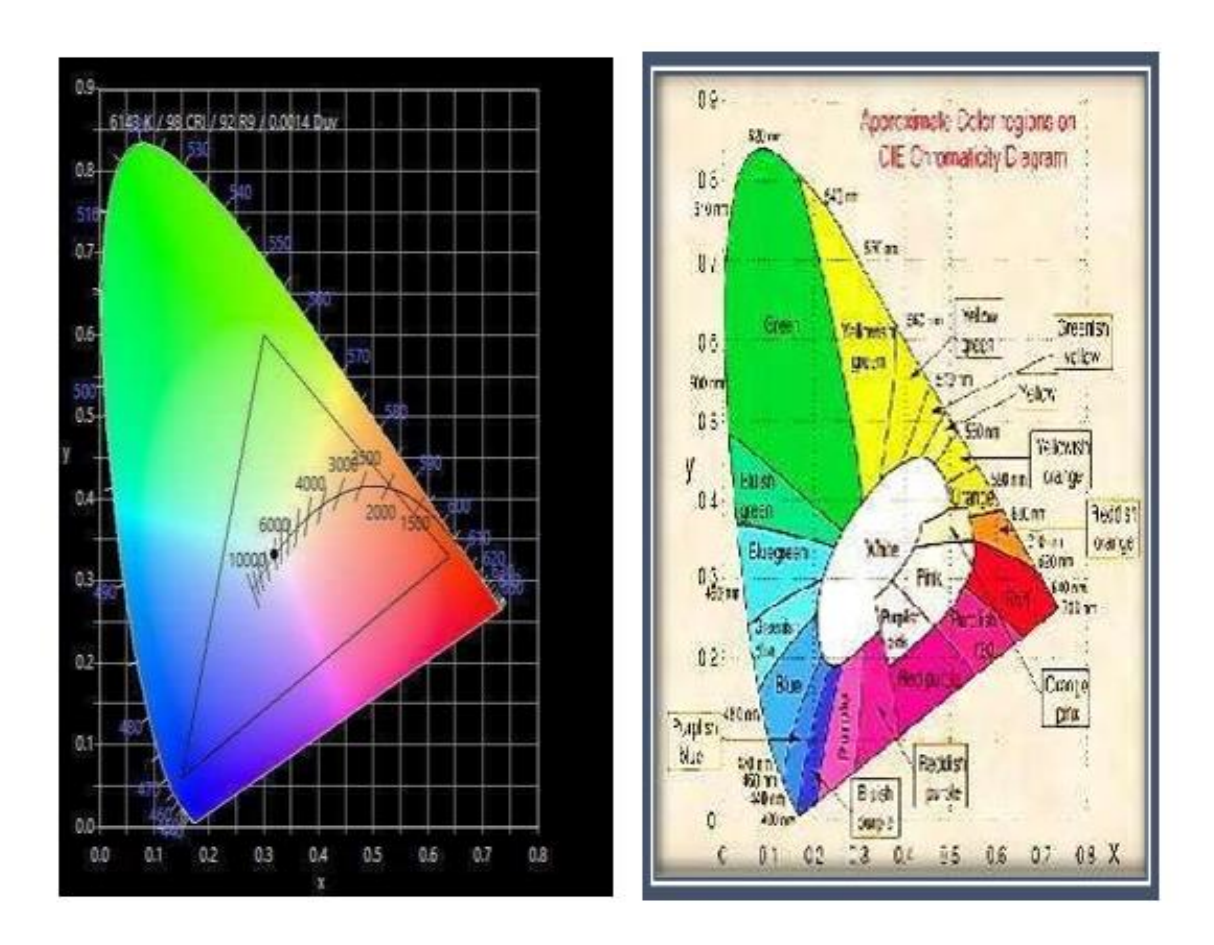


Table 4.12: Chromaticity diagram of pure Alq₃ powder -based ITO/PEDOT:PSS/Alq₃/Ag

saturation and hue. In chromatic diagram visible colours of spectrum are represented by (x,y) coordinates where horizontal and vertical axis are represented by x and y. Various pure saturated colours of the spectrum on the basis of RGB colours are recognized along the perimeter of the MacAdam ellipse. In the middle portion of the curve pure white colours are found which is represented by point C. The white colour region is formed by admixing three spectral primary colours (RGB) of the spectrum with the following wavelength: Red=700 nm, Green=546.3 nm and Blue=438.8 nm. The corners and the boundary of the MacAdam ellipse or chromaticity diagram represent three primary colours and are completely saturated.

Table 4.1: Chromaticity data of pure Alq₃ powder

Compound	CCT	CRI	R9	X	y	CIE	λemission
						coordinates	
Pure Alq ₃	6143 K	98	92	0.29891	0.32621	(0.29891,	520.1nm
powder						0.32621)	
annealed at							
150 °C							

The CRI CIE chromaticity diagram is another important term for chromaticity

determination of a light source. CRI CIE diagram is the visual demonstration of CIE color, where the location of the light source on the CIE chromaticity diagram denotes its CRI (Color Rendering Index). CIE CRI represents how it renders the color of the substance in comparison with a reference or known light source. The higher CRI means better color fidelity while lower CRI will describe lower fidelity color of the substance. [41-53].

4.13. Integrating sphere for external quantum efficiency (EQE) determination:

Integrating sphere or Ulbricht sphere is an important optical instrument consisting of a spherical hollow cavity (Figure 4.14) having a diffused white colored reflective layer in its interior wall and also contains a light-entering small holes and an exit port. The working principle of an integrating sphere is uniform diffusing or scattering effect of

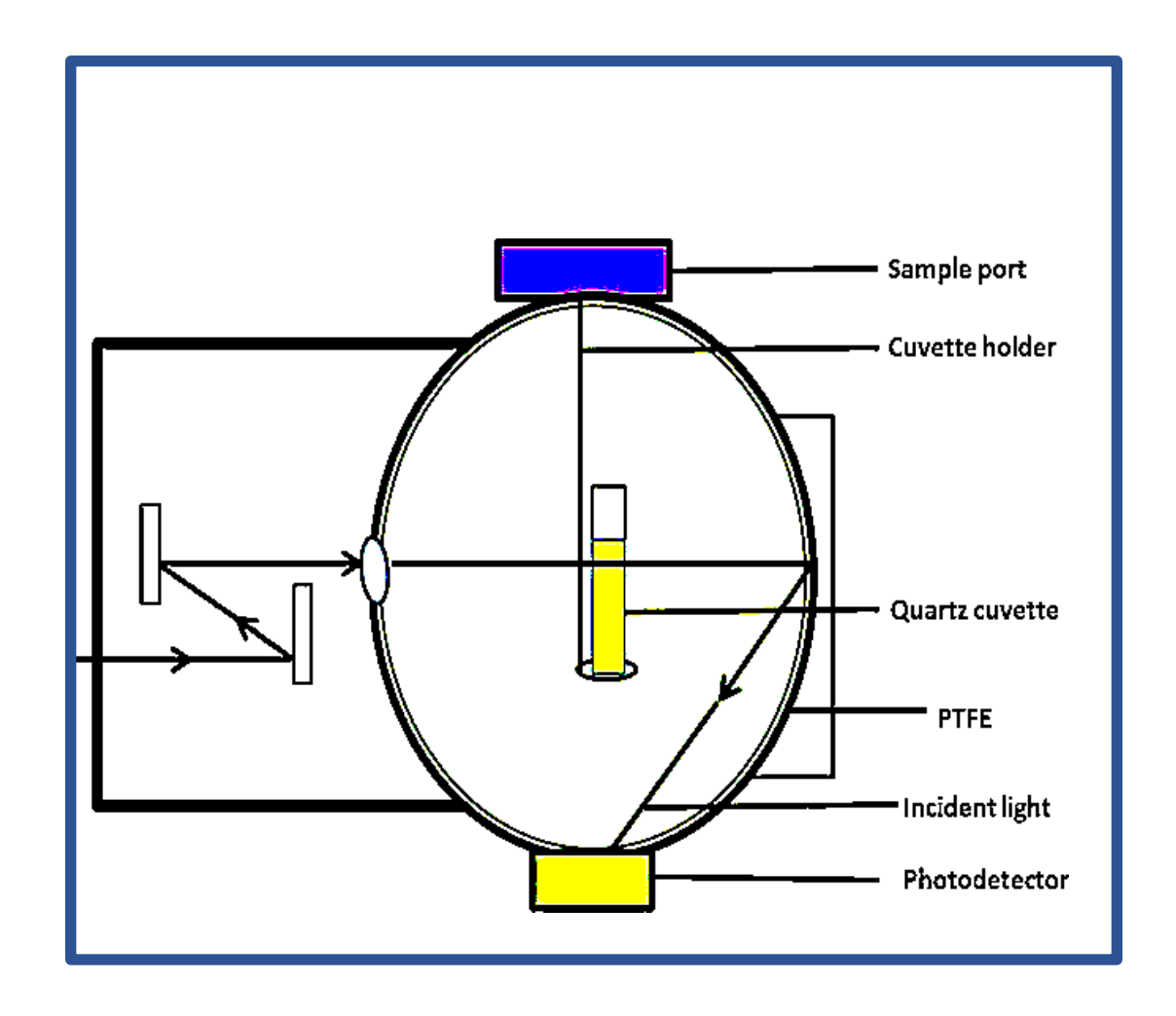


Figure 4.13: Block diagram of integrating sphere

light rays entering through the entrance-hole. Incident light rays are reflected or scattered multiple times from a point on the inner layer by the reflective white inner layer of the integrating sphere and equi- distributed to other points. [54-63]

4.14. Instruments used for grinding powder, pellet making, spin-coating and thin film fabrication:

Apart from characterization techniques three important instruments were used for different purposes: (1) agate mortar and pestle set for crushing and grinding amorphous irregular or crystalline powder into fine powder preparation (2) cold dye set and KBr press instruments for circular pellet formation and (3) spin-coater for spin-coating and fabrication of uniform stacked layer of OLED materials one after another vertically over

PET coated ITO anode and substrate. The following three instruments are discussed with figures as follows:

1. Mortar and Pestle: Generally, agate porcelain mortar and pestle-these (Figure 4.7.1)

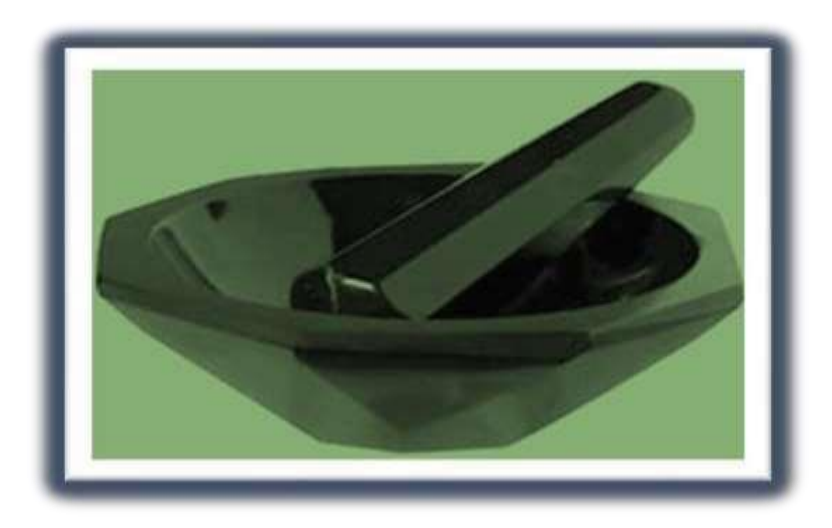


Figure 4.14.1: The image of agate mortar and pestle used for fine grinding

2. two tools (Figure 4.7.1.) together are used in laboratory to grind and crush the amorphous powder or crystalline materials into fine powder or uniformly dense paste. The hard unglazed high temperature-resistant porcelain made mortar, and pestle can crush or grind most of the powder or crystalline materials into evenly distributed fine powder. In the laboratory polished agate mortar and pestle set are used preferentially due to contamination-free, low porosity and cost-effective polished hard layer of agate. These keep the purity of the powder materials during crushing and grinding powders.

3. Cold press die set and KBr press instrument:

In our project at first, we synthesized mer-Alq₃ powder. Then we dried the powder after heating at 40 °C through heating plate. We made desired number of Alq₃ and Alq₃ – derivative based dry circular pellets with 12 mm. diameter applying hydraulic pressure on the amorphous or crystalline powder in KBr Press instrument (Figure 4.7.2) along with the help of cold press die-set. KBr press is a mini efficient hydraulic press for exerting



Figure 4.14.2.: Image of Athena 500x500 cold press die set box with 12 mm. diameter (left) and KBr press instrument (right)

pressure on the powder specimens up to 15 Tons. On the other hand, cold powder pelleting press die set is a velveted teakwood made box. This box contains plunger rod, die-sleeves, spacers (2x), a release ring having a viewing slot and a base plate. This circular pellet pressing die sets are essential tools for producing circular pellets with desired diameters meticulously in the range of mm. to inch.

4. Spin coating using spin-coater:

Spin coating (Figure 4.7.3) is considered as one of the cost-effective industry-spearheading methods that is used for depositing uniform thin film of liquid or asprepared sample- materials over a uniformly planar functional-substrate by applying centrifugal force. No chemical constraints are placed in this case on thin films; the deposited thin films are the simple thin uniform layer of sample-materials having thickness ranging from few nm (nanometers) to few μ m (micrometer). In this case, a uniform planar substrate or electronic

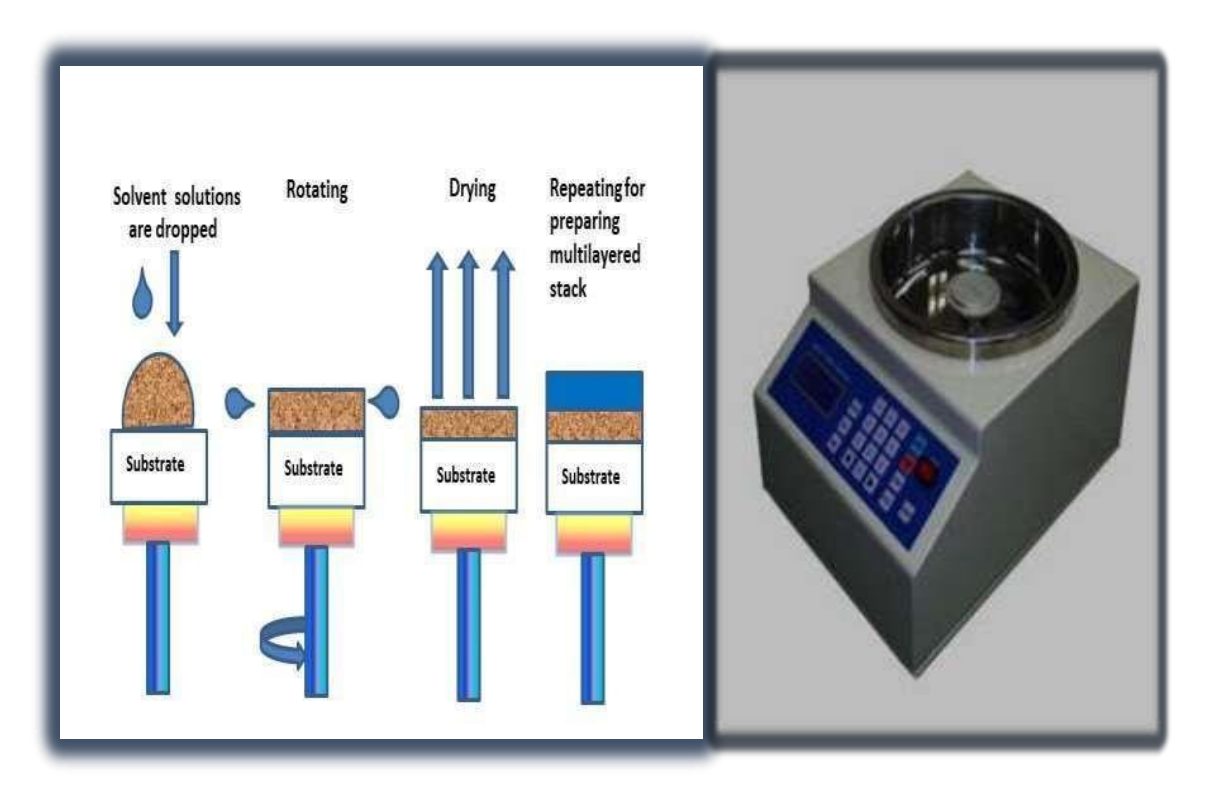


Figure 4.14.3: Schematic diagram of spin-coating technique (left) and image of spin coater machine (right)

wafer is tightly fastened on a circular chucker or work piece. This circular chucker contains a hole at the center of it. A rotating spindle remains attached to the chucker. The planar substrate remains tightly fastened over the circular chucker by using vacuum pressure through a vacuum pump. The liquid sample of interest is poured drop- wise through a syringe or dropper onto the center of planar substrate for thin film deposition. Then, the planar substrate placed on circular chucker is accelerated centripetally. This results in the uniform spreading and deposition of uniform thin film surface of samplematerial across the planar substrate through centrifugal force. That rotating planar substrate throws off the excess liquid or sample- material from its circular surface-edge thereby leaving uniformly spread thin film on the planar substrate surface. In a typical spin-coating process, the speed of the rotating work piece is controlled on the basis of the substance- properties of the sample-solution. Here the viscosity of the sample governs the resistance to flowing uniformly to get homogenous surface-texture. The speed of

rotation varies from 500 rpm (rotation per minute) to 12000 rpm based on solution's viscosity. The flow characteristics of the sample's solution are also controlled by its surface tension. The percentage (%) amounts of solid particles present in solution controls the electrical -mobility or end-use properties (or wettability) of deposited thin film. In our project, we form four (4) Alq₃ and Alq₃ derivative or Alq₃-nano- composites based vertically stacked architecture of OLEDs i.e., ETL, EML, HTL, HIL, Cathode, by using spin-coating method over a transparent planar ITO-coated PET sheet anode cum substrate .Our solutions of interest were mer-Alq₃ annealed at 150°C, ZnO:Alq₃ nano-composites,Eu:Alq₃ nano-composites and Nd:Alq₃ composites as EML and ETL ,PEDOT:PSS as HTL, V₂O₅ as HIL for fabrication of our four devices: device-1, device-2, device-3 and device-4 respectively. [25-28]

Reference

- [1.] Sarita Kango, Susheel Kalia, Annamaria Celli, James Njuguna, Youssef Habibi, and Rajesh Kumar. Surface modification of inorganic nanoparticles for development of organic–inorganic nanocomposites—a review. Progress in Polymer Science, 38(8):1232–1261, 2013.
- [2.] D Cullity and SR Stock. Elements of x-ray diffraction, prentice hall. Upper Saddle River, NJ, page 388, 2001.
- [3.] GEM Jauncey. The scattering of x-rays and bragg's law. Proceedings of the national academy of sciences, 10(2):57–60, 1924.
- [4.] LRB Elton and Daphne F Jackson. X-ray diffraction and the bragg law.American Journal of Physics, 34(11):1036–1038, 1966.
- [5.] AL Patterson. The scherrer formula for x-ray particle size determination. Physical review, 56(10):978, 1939.
- [6.] Griffiths, P.; de Hasseth, J. A. (18 May 2007). Fourier Transform Infrared Spectrometry (2nd ed.). Wiley-Blackwell. ISBN 978-0-471-19404-0. Brault, James W. (1996). "New Approach to high-precision Fourier transform

- spectrometer design". Applied Optics. **35** (16):2891–2896. Bibcode: 1996ApOpt...35.2891B. doi:10.1364/AO.35.002891. PMID 210854
- [7.] Chamberain, J.; Gibbs, J.E.; Gebbie, H.E. (1969). "The determination of refractive index spectra by fourier spectrometry". Infrared Physics. 9 (4): 189–209. Bibcode:1969InfPh...9..185C. doi:10.1016/0020-0891(69)90023-2.
- [8.] Baker, Matthew J.; Trevisan, Júlio; Bassan, Paul; Bhargava, Rohit; Butler, Holly J.; Dorling, Konrad M.; Fielden, Peter R.; Fogarty, Simon W.; Fullwood, Nigel J.; Heys, Kelly A.; Hughes, Caryn; Lasch, Peter; Martin-Hirsch, Pierre L.; Obinaju, Blessing; Sockalingum, Ganesh D. (2014). "Using Fourier transform IR spectroscopy to analyze biological materials". Nature Protocols.
 9 (8): 1771–1791. doi:10.1038/nprot.2014.110. ISSN 1750-2799. PMC 4480339. PMID 24992094
- [9.] Karen D Vernon-Parry. Scanning electron microscopy: an introduction. III-Vs Review, 13(4):40–44, 2000.
- [10.] M Abd Mutalib, MA Rahman, MHD Othman, AF Ismail, and J Jaafar. Scanning electron microscopy (sem) and energy-dispersive x-ray (edx) spectroscopy. In Membrane characterization, pages 161–179. Elsevier, 2017.
- [11.] David C Joy and James B Pawley. High-resolution scanning electron microscopy. Ultramicroscopy, 47(1-3):80–100, 1992. Cole, Kenneth; Levine, Barry S. (2020), Levine, Barry S.; Kerrigan, Sarah (eds.), "Ultraviolet-Visible Spectrophotometry", Principles of Forensic Toxicology, Cham: Springer International Publishing, pp. 127–134, doi:10.1007/978-3-030-42917- 1_10, ISBN 978-3-030-42917-1, retrieved 19 October 2023
- [12.] Vitha, Mark F. (2018). "Chapter 2". Spectroscopy: principles and instrumentation. Hoboken, NJ: John Wiley & Sons. ISBN 978-1-119-43664-5.
- [13.] Edwards, Alison A.; Alexander, Bruce D. (1 January 2017), "UV-Visible Absorption Spectroscopy, Organic Applications", in Lindon, John C.; Tranter, George E.; Koppenaal, David W. (eds.), Encyclopedia of Spectroscopy and Spectrometry (Third Edition), Oxford: Academic Press, pp. 511–519,

- doi:10.1016/b978-0-12-803224-4.00013-3, ISBN 978-0-12-803224-4,retrieved 19 October 2023.
- [14.] Metha, Akul (22 April 2012). "Derivation of Beer–Lambert Law". PharmaXChange.info.
- [15.] Tebyetekerwa, Mike; Zhang, Jian; Xu, Zhen; Truong, Thien N.; Yin, Zongyou; Lu, Yuerui; Ramakrishna, Seeram; Macdonald, Daniel; Nguyen, Hieu T. (24 November 2020). "Mechanisms and Applications of Steady-State Photoluminescence Spectroscopy in Two-Dimensional Transition-Metal Dichalcogenides". ACS Nano. 14 (11): 14579–14604,
- [16.] Kira, M.; Koch, S. W. (2011). Semiconductor Quantum Optics. Cambridge University Press. ISBN 978-0521875097.
- [17.] Haug, H.; Koch, S. W. (2009). Quantum Theory of the Optical and Electronic Properties of Semiconductors (5th ed.). World Scientific.p.216. ISBN 9812838848
- [18.] Chatterjee, S.; Ell, C.; Mosor, S.; Khitrova, G.; Gibbs, H.; Hoyer, W.; Kira, M.; Koch, S. W.; Prineas, J.; Stolz, H. (2004). "Excitonic Photoluminescence in Semiconductor Quantum Wells: Plasma versus Excitons". Physical Review Letters 92 (6). doi:10.1103/PhysRevLett.92.067402.
- [19.] Lakowicz, J. R. (1999). Principles of Fluorescence Spectroscopy. Kluwer Academic / Plenum Publishers
- [20.] Ashutosh Sharma; Stephen G. Schulman (21 May 1999). Introduction to Fluorescence Spectroscopy. Wiley. ISBN 978-0-471-11098-9.
- [21.] Elgrishi, Noémie; Rountree, Kelley J.; McCarthy, Brian D.; Rountree, Eric S.; Eisenhart, Thomas T.; Dempsey, Jillian L. (3 November 2017). "A Practical Beginner's Guide to Cyclic Voltammetry". Journal of Chemical Education. 95 (2): 197.
- [22.] Heinze, Jurgen (1984). "Cyclic Voltammetry-"Electrochemical Spectroscopy". New Analytical Methods (25)". Angewandte Chemie International Edition in English. 23 (11): 831–847. doi:10.1002/anie.198408313.

- [23.] Bott, Adrian W. (September 1999). "Characterization of Chemical Reactions Coupled to Electron Transfer Reactions Using Cyclic Voltammetry" (PDF). Current Separations. **18** (1)
- [24.] Nicholson, R.S. (1965). "Theory and Application of Cyclic Voltammetry for Measurement of Electrode Reaction Kinetics". Anal. Chem. **37** (11): 1351–1355. doi:10.1021/ac60230a016.
- [25.] Cohen, Edward; Lightfoot, E. J. (2011). "Coating Processes". Kirk- Othmer Encyclopedia of Chemical Technology. New York: John Wiley. doi:10.1002/0471238961.1921182203150805.a01.pub3. ISBN 978-0471238966.
- [26.] Emslie, A. G.; Bonner, F. T.; Peck, L. G. (1958). "Flow of a viscous liquid on a rotating disk". J. Appl. Phys. 29 (5): .
- [27.] Danglad-Flores, J.; Eickelmann, S.; Riegler, H. (2018). "Deposition of polymer films by spin casting: A quantitative analysis". Chem. Eng. Sci. 179: 257–264. doi:10.1016/j.ces.2018.01.012. hdl:21.11116/0000-0000-2D6C-6.
- [28.] "What Is Spin Coating?". Inseto. November 4, 2020. Retrieved 2023-05-2
- [29.] Höhne G, Breuer KH, Eysel W (October 1983). "Differential scanning calorimetry: Comparison of power compensated and heat flux instruments". Thermochimica Acta. **69** (1–2):145–151. Bibcode:1983TcAc...69..145H. doi:10.1016/0040-6031(83)85073-4,1983
- [30.] Gabbott, Paul (2008). Principles and applications of thermal analysis. Oxford:Blackwell Pub. ISBN 978-14-051-317,2008
- [31.] Brown, Michael E. (1998). Handbook of Thermal Analysis and Calorimetry, Volume 1 1st Edition. Elsevier Science. ISBN 978-00-805-3959-1,1998
- [32.] Coats, A. W.; Redfern, J. P. (1963). "Thermogravimetric Analysis: A Review". Analyst.88 (1053):906-924.Bibcode:1963Ana88..906C.
- [33.] Liu, X.; Yu, W. (2006). "Evaluating the Thermal Stability of High PerformanceFibers by TGA". Journal of Applied Polymer Science. 99 (3): 937–944. doi:10.1002/app.22305,2006

- [34.] What Is a Source Measure Unit (SMU)?, National Instruments, retrieved July 11, 2016
- [35.] Budmir, Miles (March 6, 2014), "Taking the Measure of Test Equipment", Test & Measurement Tips.
- [36.] Cejer, M.A., Choosing the Optimal Source Measurement Unit Instrument for Your Test and Measurement Application (PDF), Tektronix, retrieved July 22, 2016
- [37.] Ron Khormaei, et al., "High-Resolution Active Matrix Electroluminescent Display", Society for Information Display Digest, p. 137, 1994.
- [38.] M. Aguilera, L. Arbuthnot and T. Keyser, "First Generation VGA Electroluminescent Display for Head Mounted Applications", Proc. 10th Int. SPIE AeroSense Conf., (1996).
- [39.] M. Aguilera, B. Aitchison, D. Basham, S. Moehnke, K.Ping, R. Tuenge, W. Vetanen, C. King, "An RGB VGA Active Matrix EL Display", SID '96 Digest,p. 125, (1996).
- [40.] M. Leppänen, G. Härkönen, A. Pakkala, E. Soininen, R. Törnqvist, "Broadband Double Layer Phosphor for an Inverted Filtered RGB Electroluminescent Display", Proc. 93 EuroDisplay, p. 229, (1993).
- [41.] CIE (1932). Commission internationale de l'Eclairage proceedings, 1931.Cambridge: Cambridge University Press.
- [42.] Smith, Thomas; Guild, John (1931–32). "The C.I.E. colorimetric standards and their use". Transactions of the Optical Society. **33** (3): 73–134.
- [43.] Guild, J. (1932). "The colorimetric properties of the spectrum". Philosophical Transactions of the Royal Society of London. Series A, Containing Papers of a Mathematical or Physical Character. 230 (681–693): 149–187. Bibcode:1932 RSPTA.230..149G. doi:10.1098/rsta.1932.0005. JSTOR 91 229.
- [44.] Fairman, H. S.; Brill, M. H.; Hemmendinger, H. (February 1997). "How the CIE 1931 Color-Matching Functions Were Derived from the Wright-Guild Data".
 Color Research and Application. 22 (1): 11–23. doi:10.1002/(SICI)1520-

- 6378(199702)22:1<11::AID-COL4>3.0.CO;2-7.
- and Fairman, H. S.; Brill, M.H.; Hemmendinger, H. (August 1998). "Erratum: How the CIE 1931 Color- Matching Functions Were Derived from the Wright–Guild Data". Color Research and Application. 23 (4): 259. doi:10.1002/(SICI)1520-6378(199808)23:4<259::AID-COL18>3.0.CO;2-7.
- [45.] CIE (1926). Commission internationale de l'éclairage proceedings, 1924. Cambridge: Cambridge University Press. The 1924 luminous efficiency function seriously underestimates sensitivity at wavelengths below 460 nm, and has been supplemented with newer and more accurate luminosity curves; see Luminosity function#Improvements to the standard.
- [46.] "Understand color science to maximize success with LEDs part 2 LEDs Magazine, Issue 7/2012". 18 July 2012. Archived from the original on 2017-11-11.
- [47.] Speranskaya, N. I. (1959). "Determination of spectrum color co-ordinates for twenty seven normal observers". Optics and Spectroscopy. 7: 424–428.
- [48.] CIE1931 colour-matching functions, 2 degree observer,2019, doi:10.25039/CIE.DS.xvudnb9b, retrieved 6 February 2025
- [49.] CIE 1964 colour-matching functions, 10 degree observer,2019, doi:10.25039/CIE.DS.sqksu2n5, retrieved 6 February 2025
- [50.] Wyman, Chris; Sloan, Peter-Pike; Shirley, Peter (July 12, 2013). "Simple Analytic Approximations to the CIE XYZ Color Matching Functions". Journal of Computer Graphics Techniques. **2** (2): 1-11. ISSN 2331-7418.
- [51.] CIE 170-2:2015: Fundamental Chromaticity Diagram with Physiological Axes
 Part 2: Spectral Luminous Efficiency Functions and Chromaticity Diagrams.
 CIE. ISBN 978-3-902842-05-3. Archived from the original on Nov 19, 2023.
- [52.] "CIE functions". Colour & Vision Research Laboratory. Institute of Ophthalmology, University College London. Archived from the original on Nov 19, 2023.
- [53.] "Resolving Display Color Matching Issue" (PDF). KONICA MINOLTA.^

- Sumpner, W. E. (1892). "The diffusion of light". Proceedings of the Physical Society of London. 12 (1): 10–29. Bibcode: 1892 PPSL...12...10S. doi:10.1088/1478-7814/12/1/304.
- [54.] Ulbricht, R. (1900). "Die bestimmung der mittleren räumlichen Lichtintensität durch nur eine Messung". Elektrotechnische Zeit. (in German). **21**: 595–610.
- [55.] Sumpner, W. E. (1910). "The direct measurement of the total light emittedfrom a lamp". The Illuminating Engineer. **3**: 323.
- [56.] "Integrating Sphere Design and Applications" (PDF). Sphere Optics. SphereOptics LLC. Archived from the original (PDF) on 2009- 08-15.
- [57.] Rosa, E. B.; Taylor, A. H. (1916). "The integrating photometric sphere, its construction and use". Transactions of the Illumination Engineering Society. 11: 453.
- [58.] Taylor, A. H. (1920). "The Measurement of Diffuse Reflection Factors and a New Absolute Reflectometer". Journal of the Optical Society of America. 4(1): 9–23.
- [59.] Benford, Frank A. (1934). "A Reflectometer for All Types of Surfaces".

 Journal of the Optical Society of America. 24

 (7): 165–174. doi:10.1364/JOSA.24.000165. Retrieved 2021-10-12,1934
- [60.] Sharpe, C. H.; Little, W. F. (1920). "Measurements of Reflectance Factors". Transactions of the Illumination Engineering Society. **15**: 802,1920
- [61.] Karrer, Enoch (1921). "Use of the Ulbricht Sphere in measuring reflection and transmission factors". Scientific Papers of the Bureau of Standards. **17**: 203–225.,1921 doi:10.6028/nbsscipaper.092. Retrieved 2021-10-12.
- [62.] Hanssen, Leonard (2001-07-01). "Integrating-sphere system and method for absolute measurement of transmittance, reflectance, and absorptance of specular samples". Applied Optics. 40 (19): 3196–3204.
- [63.] Korte, H.; Schmidt, M. (1967). "Über Messungen des Leuchtdichtefaktors an beliebig reflektierenden Proben". Lichttechnik (in German). 19: 135A 137A,1967\

Chapter 5: Effect of growth temperatures on the structural and optical properties of bulk pristine tris-(8-hydroxy quino line) aluminium (III)

Abstract:

Bulk samples of Tris (8-hydroxyquinoline) aluminium (Alq₃) were prepared using wet synthesis method followed by annealing at 50 °C, 100 °C, 150 °C and 200 °C for 2 hours. X ray diffraction pattern showed the formation of Alq₃ crystal, which is constituted of Al atom, anions of 8-hydroxyquinoline (8-Hq) and porous Al₂O₃ - Al(OH)₃. structure. The spectra of FTIR (Fourier-transform infrared) reveals that annealing Alq₃ at 50 °C reduces the C=C peak to negligible but reappears when annealed at 150 °C. FESEM on as-prepared Alq₃ shows hexagonal rod-shaped stacked structures which on annealing at 50 °C changes to tetragonal agglomerated grains along with appearance of oval and circular shaped pores on it. From fluorescence spectroscopy it is found that the peak intensity changes non-monotonically with annealing temperatures followed by red shift and blue shift of peak maximum at 150 °C and 200 °C respectively. The temperature dependent change in the properties is mainly attributed to the onset of hydrolysis in Alq₃ and change in the electronic transition levels.

5.1. Introduction

Organic Light Emitting Diode (OLED) also known as organic electroluminescent is a solid-state device that is being used in multiple technological platforms like lighting industries, displays for television, mobile phones, cameras and many more [1-5]. In recent years, OLED has drawn huge attention for its longer durability, low driving voltage, wide range of color-mixing, higher optical luminous efficiency and easy fabrication technology [5-8].

Alq₃ or Tris–(8-hydroxy quinoline)aluminium is one of the intriguing electroluminescent electron transporting material which has built up a great interest among scientists for its

excellent electrical and optical characteristics [1, 3, 8, 9]. High electrical conductivity and bright effulgent luminescence property makes it a desirable candidate for making flexible OLEDs [8]. Moreover, functional antifouling coatings with Alq₃:TiO₂ has found to have an efficient inhibitory effect on the growth of algae, thus leading to promising antibacterial activity against unwanted bacteria [9]. Further, organic semiconductors based on Alq₃ when doped with tetracyanoquinodimethane, can behave as an organic photo detector as reported by Vergara et.al.[10]. Alq₃ is an organic polymeric semiconducting material wherein a heterocyclic octahedral organic chelate complex of quinoline ligand is coordinated with an aluminium metal atom [4,11]. The molecular structure represents MN₃O₃ type compound where M involves a trivalent metal, N signifies nitrogen atoms & O represents oxygen atoms [11]. On addition, Alq₃ has 2 isomeric polymorphs: facial (fac-Alq₃) and meridional (mer-Alq₃) which have C3 and C1 symmetry respectively. Interestingly, it can be tuned to have red or blue shift of green light when Alq₃ is mixed with other organic (PMMA matrix) or inorganic (SiO₂) semi conducting materials [11]. The energy of creation of excitons associated with Alq₃ green emission centers has been found to around 6.86 eV at 300 K and 6.78 eV at 10 K [12,13]. The temperature and wavelength dependent on tunable property can be heavily utilized in solar cell and OLEDs applications [8]. However, the device performance of Alq₃ is highly affected by thermal and structural instability when exposure to air, water and Joules heating due to electric field [14, 15]. The main reason behind the instability has still remained a subject of debatable. In our study, we fabricated bulk Alq₃ powder through wet synthesis process and annealed at different series of temperature [16]. The central idea is to carry out systematic study and recognize the changes in the optical and thermal properties in respective systems which are annealed at different temperatures during the process of synthesis [16].

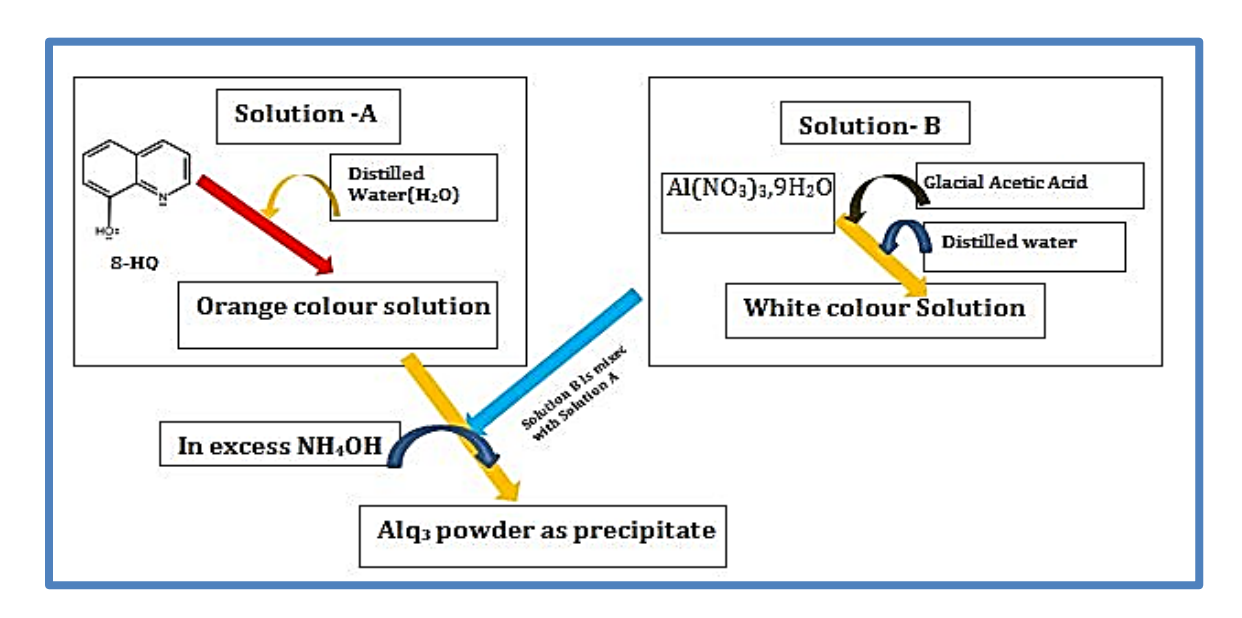
Degradation, instability and chemical failure are some of the crucial issues that limit Alq₃ as ETL or host material for OLED applications [14]. Chemical reactions such as hydrolysis and oxidation are mostly held responsible for its dynamic behavior. On exposure to atmospheric conditions, two remarkable changes are found to occur: (1) some amount of

moistures or trace water vapor hydrolyze Alq₃ and converts it into 8Hq(8-hydroxyquinoline) and instable hydroxylated aluminium quinolate (Alq₂OH) and (2) rest amount gets evaporated with the increase of annealing temperature losing moisture and as a result of further heating, destabilization of Alq₃ bond initiates and three quinolinate ligands set themselves free [14, 15]. There have been some reports on the study of properties of Alq₃ thin film and its derivatives which have been annealed in nitrogen, oxygen, humid air but very limited studies have been reported on Alq₃ amorphous bulk system [16, 17,18]. In our present study, the main aim is to find the changes that occurred in the optical properties, morphological and elemental changes of as synthesized mer-Alq₃ powder. This information can be used in order to design high performance OLED and offers excellent potential to improve the optical parameters of solid-state lighting technology and solar OPV cells operating in ambient conditions.

5.2. Experimental Methods:

1. Synthesis of Mer-Alq₃ powder and its aqueous solution:

Tris (8-hydroxyquinoline) aluminium (Alq₃) was synthesized by wet synthesis method as proposed by J.G. Mahakhode et al. with small changes in few steps but keeping the main procedure intact [17]. Firstly, 5 grams of 8-hydroxyquinoline (8-Hq) (C₉H₇NO) were dissolved in 25 mL of acetic acid and added 25 mL of double distilled water. The mixture was heated along with stirring at 50 °C for ½ h until a transparent orange solution (solution 1) was obtained. Secondly, 4.31 gm of Al(NO₃)₃, 9H₂O (LOBA) was of double distilled water and then the mixed solution was heated at 50 °C along with continuous stirring until a clear white transparent solution was formed (solution 2). Thereafter, solution 1 and solution 2 were mixed with constant stirring for 10 more minutes after which 25 mL of ammonium hydroxide (NH₄OH) was added dropwise to get a yellow-green precipitate of Alq₃ which was further filtered and washed 10 times



Scheme 5.1: Schematic diagram of wet-synthesis procedure of Alq₃

with warm double distilled water until the filtrate became colorless transparent solution. The residues on filter paper were collected and dried at around 60 °C for 2 hours to evaporate the dissolved moistures and finally yellow green powder of mer- Alq₃ (Al(C₉H₇NO)₃) was obtained [17-20]. The steps involved during the synthesis are clearly depicted in a schematic diagram represented as scheme 1

The chemical reaction that took place is as follows:

$$3(C_9H_7NO) + A1(NO_3)_3.9H_2O \rightarrow A1(C_9H_7NO)_3 + 9H_2O + 3(NO_2)$$
 (5.1)

The dried Alq₃ powder was grinded and converted into pellets of diameter 12 mm and thickness 1 mm by using 15 tons of hydraulic pressure on KBr die set. For systematic study, Alq₃ powder pellets were annealed at 50 °C, 100 °C, 150 °C and 200 °C in an hot air oven for 2 hrs. with a constant heating rate of 2 degrees per minute. Here, in the case of Scheme-2, 8-Hq molecules play a pivotal role in the presence of atmospheric hydrogen where 8-Hq molecules get deprotonated leading to lose its hydroxyl groups which corrode on the surface of Alq₃ [21-24]. On the other hand, 8-Hq molecules formed through hydrolysis of Alq₃ get oxidized with excess amount of oxygen, thus forming a non-emissive polymer: 8-hydoxy quinoline N oxide (NEP) [25]. The corroded Alq₃ molecules get direct contact with oxygen

and form a semi or meso-porous Al₂O₃ layer on Alq₃ which further reacts with humid air and forms Al(OH)₃.

Scheme 5.2: Conversion of Alq₃ to non-emissive polymer 8-hydroxy quinoline- N- oxide (NEP)

The aluminium hydroxide is found to decompose into Al₂O₃ and water molecules to some extent. As a result, a porous semi porous Al₂O₃-Al(OH)₃ hetero layer was formed on Alq₃ structure and during cooling the 3 freed atoms 8-Hq again recrystallized and agglomerated which increased the particle –sizes of porous Al₂O₃ [21-26] (Vide Scheme 2).

5.3. Results and discussions:

A. Morphological study:

1. X-ray Diffraction spectroscopy of Alq₃ pellet and its analysis:

Figure 1 shows the XRD spectroscopy analysis of as-prepared Alq₃ and the same annealed at different temperatures. It is observed that the Bragg reflections peaks of bulk as- prepared Alq₃ (sample A) are detected at 2θ = 10.7°, 12.8°, 13.6°, 15.2°, 15.9°, 17.1°, 18.3°, 21.3°, 22.4°, 23.2°, 24.4° (JCPDS card No. 26-1550). When pellet of Alq₃ is annealed at 50 °C (sample

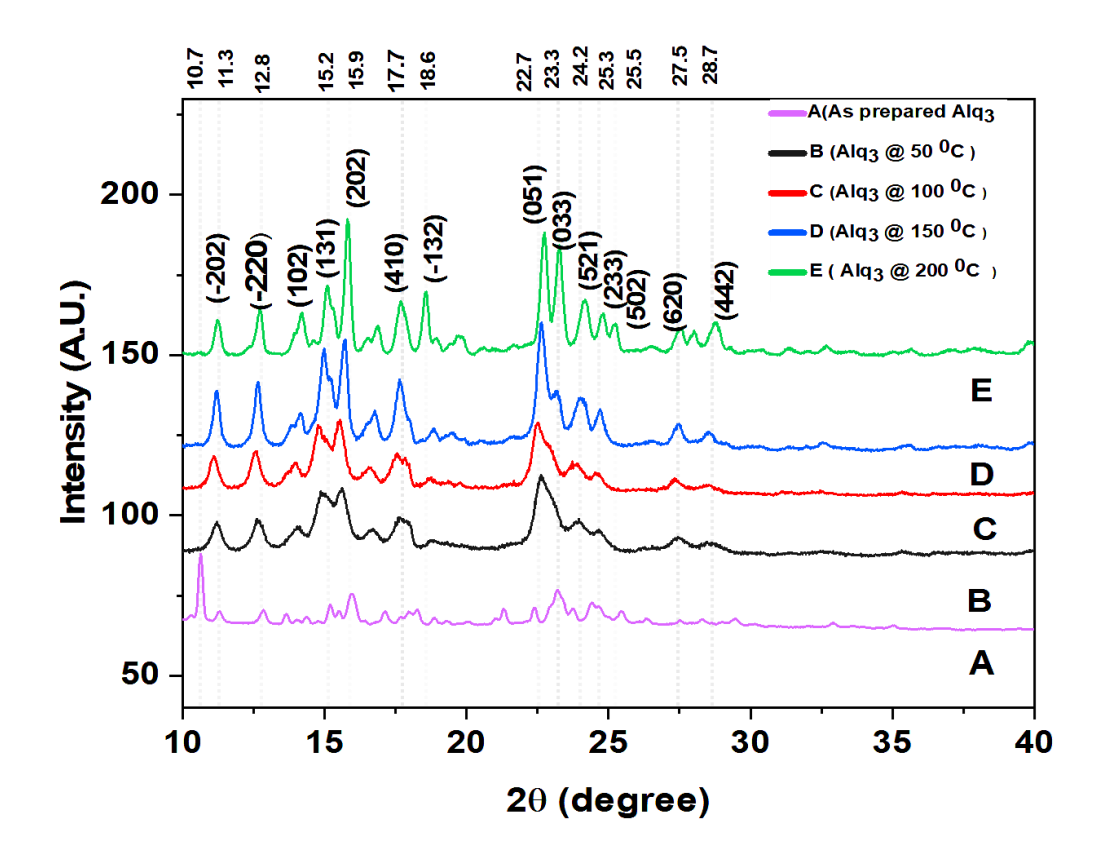


Figure 5.1: XRD spectra of as prepared bulk Alq₃ (Sample A) and Alq₃ pellets annealed at (1) 50 °C (Sample –B) (2) 100 °C (Sample-C) (3) 150 °C (Sample D) and (4) 200 °C (Sample-E)

B), the sharp peaks are found to appear at 2θ: 11.2°, 12.6°, 15.0°, 15.6°,22.6° which corresponds to crystalline planes (-202), (-220), (131), (202) and (051) respectively (PDF pattern 00-010-766]. For sample annealed at 100 °C, the intense sharp peaks are found at 2θ:11.0°, 12.6°, 14.8°, 15.5°, 22.5° which corresponds to (-202), (-220), (-112), (131), (202),(051) and (102) crystalline orientations (PDF pattern 01-076-1381). Whereas when Alq₃ pellet is annealed at 150 °C, more sharper peaks are found at 2θ: 11.2°, 12.6°, 14.9°, 15.7°,22.5° which corresponds to (-202), (-220), (-112), (131), (202), (051),(211), (221) and (460) crystalline planes (following PDF pattern 00-010-0789). Interestingly, when the sample is annealed at 200 °C, the diffraction peaks become highly intense and sharp as compared to 150 °C. The large peaks are found at 2θ: 11.2°, 12.7°, 15.1°, 15.8°, 22.7°

(following the PDF pattern 00-044-0696) which corresponds to the crystalline planes (-202), (-220), (-112),(131), (202), (051), (131), (202), (051) and (033).

From table 5. 1 and figure 5.1: it is well observed that the Bragg reflection peaks for B (at 50 °C) are broad peaks, and intensity is higher compared to as-prepared Alq₃ powder. The prominent sharp peaks of as-prepared bulk Alq₃ (A) at $2\theta = 10.7^{\circ}$ disappears in case of sample B, sample C and sample D and the peaks are of longer and broader in size and width respectively.

Table 5.1: The morphological details of bulk Alq₃ powder (Sample-A) and four annealed Sample-B, Sample-C, Sample-D and Sample-E

Sample	Annealing	Lattice	Lattice Parameter	Volume	Mol.wt.
Name	Temp(°C)		(A°)	(c.c.)	(gm/mol)
A	Room Temperature	Poly crystalline triclinic	a=10.3,b=13.74,c=8.2 2	386.72	459.4
В	50	tetragonal	a=b=4.9,c=19.4	479.4	137.7
С	100	tetragonal	a=b=21.1, c=19.4	3287.4	264.8
D	150	orthorhombic	a=19.7, b=35.7, c=7.3	5162.7	384.64
Е	200	orthorhombic	a=20.1, b=20.0, c=13.4	5373.4	60.08

This depicts the increase of crystallinity in the sample due to annealing. The sharp peaks found at 200 °C are attributed to (-202), (202), (200), (202),220), (411), (400), (111), (116), (442) and (620) crystalline phases which are formed due to porous Al₂O₃ on the surface of Alq₃. (JCPDS Card No 33-0018). (101), (110), (220), (1-10) &(102) crystalline phases are attributed to Alq₃; (110) is mostly attributed (to annealed Alq₃ whereas (311) & (110) crystalline phases are attributed to Al(OH)₃ (JCPDS Card No. 21- 1307 and JCPDS Card No. 24-1879]. (220), (400) and (040) crystalline phases are attributed to 8-hydroxy quinoline and it also proves that (400), (311), (110) and (220) depicts the formation of Alq₃ crystal (which is constituted by the Al atom), 8-Hq and porous Al₂O₃-Al(OH)₃ as per JCPDS Card No 33-0018 [27-32]

2. FESEM (scan electron microscopy) images and its analysis:

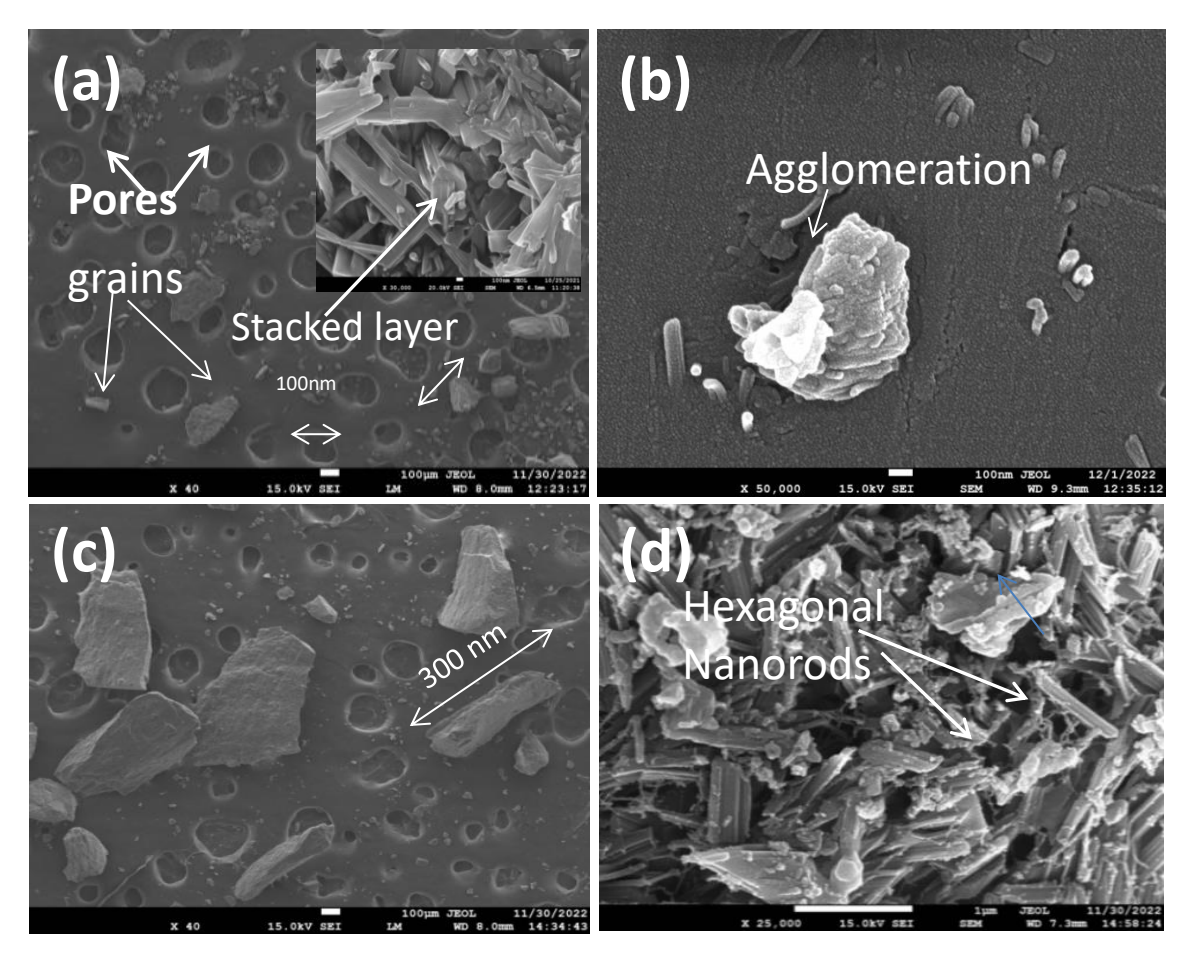


Figure 5.2(a): FESEM images of Alq₃ powder annealed 50 °C having 7500x and 50000x magnification. The inset shows the image for as -prepared Alq₃ without annealing, (b)FESEM images of Alq₃ annealed at 100 °C (40x & 50000x magnification), (c)FESEM images of Alq₃ annealed at 150 °C (15000x & 25000x magnification) (d)FESEM images of Alq₃ annealed at 200 °C (15000x & 25000x magnification)

Figure 5.2 (a) shows the FESEM images of Alq₃ pellet annealed at 50 °C where several tetragonal agglomerated grains of Alq₃ along with oval and circular pores are seen throughout the surface. The inset of fig. 2 (a) shows FESEM image of an as-prepared Alq₃ bulk which resembles stacked nanorods with discrete and clustered layered structure where no pores are found on the basal surface of the Alq₃ nano particles. The nano rod clusters as

found match well with the published report on Alq₃ nanoparticles. The average diameter of the pores is found to be of $\sim 250 \, \mu m$ and the tetragonal grains possess average length of ~ 300 µm along a-axis which further encounters phase transformation during its crystallization as moisture evaporated. On increasing the annealing temperature to 100 °C, no such remarkable changes appeared except the diameter of the grains increases to ~ 500 µm in length and decrease in number of pores as found from figure 2(b). Many small pores are found to overlap with each other to form big pores with porous diameter greater than 200 µm. But there are also several numbers of small pores having porous diameter less than 200 µm. At this stage, the grains possess a tetragonal shape with a length of around 600 nm and a wider diameter of 450 nm along a-axis. In figure 2(c), with the further increase of temperature to 150 °C, the porosity tends to decrease, and the pores tend to coalesce with each other. The defects found in the basal surface of Al₂O₃-Al(OH)₃ layer as seen in case of fig 2(d), are reducing gradually in the temperature range between 100 °C and 150 °C whereas the size of the orthorhombic granular agglomeration increases in length and width. At 200 °C, the porosity loses its shape completely and leads to agglomeration of stacked layers of hexagonal nanorod of non-emissive polymer 8hydroxyquinoline N-oxide with very few numbers of micro and semi pores as observed. Here, the porous Al₂O₃-Al(OH)₃ structural surface ceases to exist and tends to agglomerate in random orientation to form NEP of 8-Hq derivative [21-27].

B. Optical properties study:

1.UV-Visible Characteristics spectroscopy analysis:

Figure 5.3 describes the UV-VIS spectra of as-prepared Alq₃ (Sample-A) and synthesized Alq₃ pellets which were annealed at four different temperatures in a hot air oven namely at 50 °C (Sample-B), 100 °C (Sample-C), 150 °C (Sample-D) and 200 °C (Sample-E) Sample-B, 288 nm for Sample-C, 290 nm for Sample-D and 289 nm for Sample-E. As from the XRD analysis, it is confirmed that the lattice structure of as-prepared bulk Alq₃ Sample-A resembles polycrystalline triclinic at room temperature, some amounts

of moisture are vigorously absorbed into Alq₃ pellets which fill up the intermolecular gaps

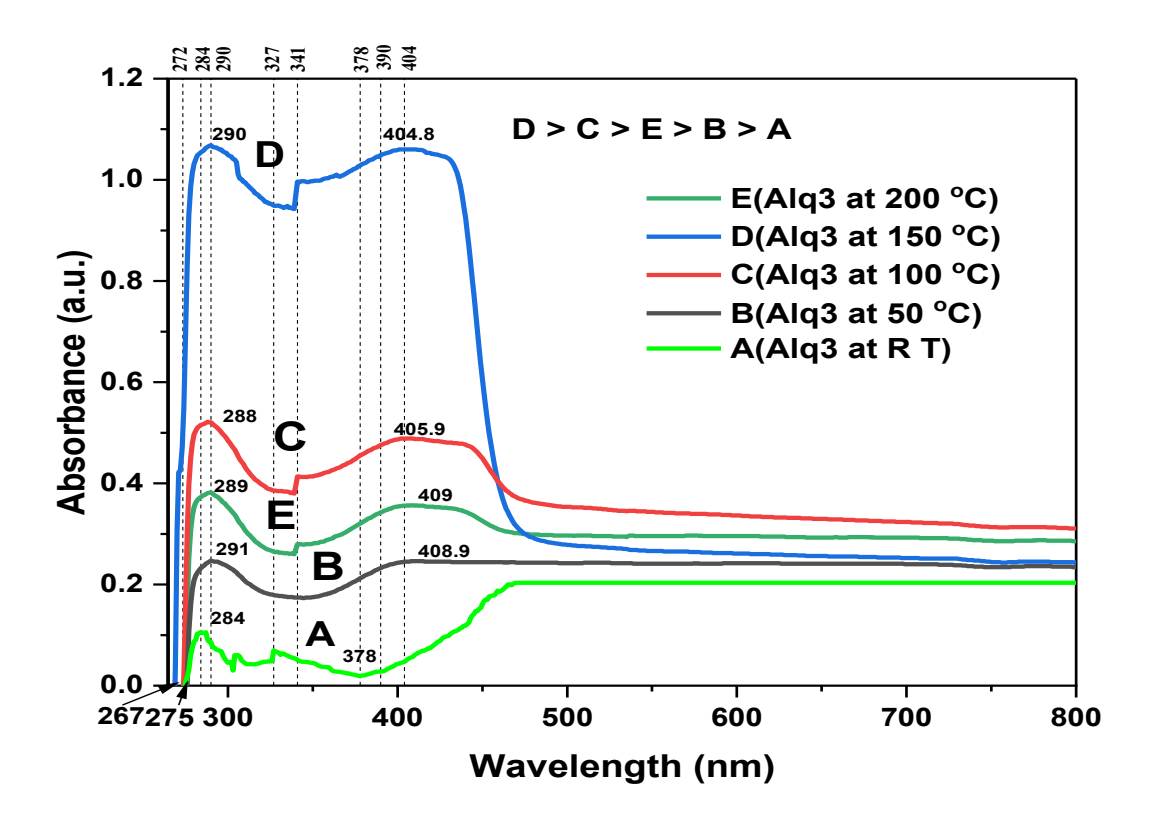


Figure 5.3: The plot shows UV-Visible spectroscopy of as-prepared bulk Alq₃ (Sample-A), Alq₃ pellet annealed at 50 °C (Sample-B), Alq₃ pellet annealed at 100 °C (Sample-C), Alq₃ pellet annealed at 150 °C (Sample-D) and Alq₃ pellet annealed at 200 °C (Sample-E)

and results in the smooth surface. During the application of heat, the moisture evaporated, and oxidation occurred which resulted in the formation of tetragonal lattice at 50 °C. Hence, there is a sign of slight variation in the UV light absorption spectra for bulk Sample-A as compared to Sample-B which was annealed at 50 °C. This is also in good agreement with the results as found from the XRD (Fig 5.1 and Table 5.1). Moreover, unlike in as-prepared Sample-A, an additional hump at higher wavelength is found at 408.94 nm for Sample-B, 405.9 nm for Sample-C, 404.8 nm for Sample-D and 409

nm for Sample-E which are mainly attributed to the formation of porous Al(OH)₃. Al₂O₃ layered structure on the Alq₃ surface [19,20]. Overall, the absorption edge of Alq₃ shows red-shift from 284 nm to 291 nm (RT to 50 °C), blue shift from 291 nm to 288 nm (50 °C to 100 °C), red shift from 288 nm to 290 nm (100 °C to 150 °C) and at the end blue shift is observed from 290 nm to 289 nm (150 °C to 200 °C).

With the increase in annealing temperature in the range of 50 °C to 90 °C, the moisture entrapped inside the Alq₃ pellets get dried. Moreover, destabilization and weakening of Al-O, Al-N, quinolate ligand anion (C₉H₆NO⁻) and Al³⁺ cation starts to kick in at the same temperature range. Between 100 °C and 150 °C, three molecules of hygroscopic volatile 8Hq get free due to breaking of the coordinate covalent bond between quinolate ligand anion (C₉H₆NO ⁻) and Al³⁺ cation. This leads to the acceptance of more oxygen atoms to fill up its two lone pairs. The free 8 Hq is mild luminescent in nature which further shows the highest absorbance intensity at 150 °C. Between 150 °C and 200 °C, these 3 molecules of free 8 Hq get oxidized in excess amount of oxygen to form non emissive chelated polymeric complex of 8-Hq i.e. [(8-hydroxyquinoline) N oxide] s annealed at 200 °C as found from the graph (NEP) [33-37]. This supports the quenching of absorbance-intensity for sample E that. These are interesting novel findings which may open new field of research field in the horizon of degraded annealed Alq₃ and non-emissive polymeric material can also be used for photoluminescent material and its allied all possible applications. We should also need to continue more in-depth study such that newer newer innovations come out and cater different spectra of thought, idea and futuristic and pluralistic possibilities

2.FTIR spectroscopy and its analysis:

From Figure 5.4, we get the Fourier transform infra-red spectroscopy images of asprepared Alq₃ powders and its thermally annealed modification for 50 °C (sample-B), 100 °C (Sample-C), 150 °C (Sample-D) and 200 °C (Sample-E) in hot air oven. The sharp and different stretching vibrations among 3 quinolinate ligand and central Al(III) atoms are witnessed due to C–N-C bond which are observed at 1495.7, 1464.7, 1376.7, 1326.1, 1280.5, 1228.2 cm⁻¹, C–O bond between benzene rings and deprotonated hydroxyl functional group (OH) of 8-Hq found at 1055.9, 1032.1 cm⁻¹, aromatic amine at 1499, 1384

cm⁻¹, aromatic C=C bond of pyridine and benzene ring observed at 1602.9 and 1604.0 cm⁻¹, C-H bond at 788.0, 742.5, 644.8, 576.2 cm⁻¹, Al– O–Al bond (short height less intense at 758 cm⁻¹), Al– O bond at 540.6, 644 cm⁻¹ and Al–N bond found at 454.3, 414.6 cm⁻¹. The weak intensity peaks due to vibrational stretching O-H are found at 3039 cm⁻¹ which is due to presence of minute amount of moisture of H₂O molecules in all the samples under measurement.

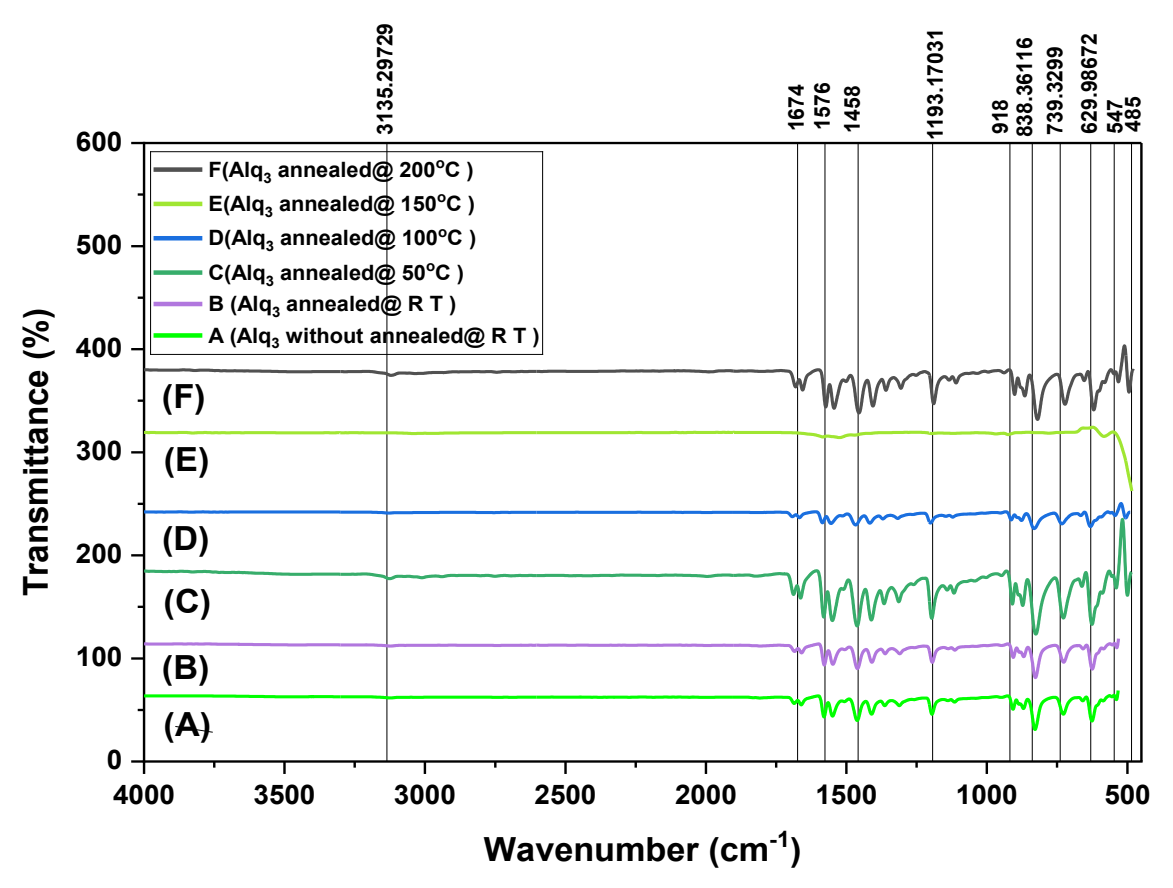


Fig 5.4: FTIR spectra of Alq₃ powder made pellet annealed at room temperature (Sample-A), 50 °C (Sample-B), 100 °C (Sample-C), 150 °C (Sample-D) and 200 °C (Sample-E)

When the as-prepared Alq₃ pellet was annealed at 50 °C, the moisture entrapped into the pellet started to evaporate which removes the defects of bulk powder resulting in higher crystallinity and strong intense IR peaks. Whereas in between 100 °C and 150 °C the C- C, C=C bond, C-N-C, C-O, Al-O-Al, Al-N, Al-O, C-C and C-H bonds of pyridine and benzene rings of Alq₃ break down due to the application of thermal annealing and evaporation of moisture.

This further leads to oxidation and destabilization which is mainly due to the breaking of bonds. It is also found that Alq₃ gets oxidized and some parts of Alq₃ react with condensed moisture present in the hot oven to form porous Al₂O₃- Al(OH)₃ structure layer over Alq₃. This contaminated layer causes weak intense peaks at 100 °C (C) and tends to show feeble intensity peaks at 150 °C(D). This occurred due to the formation of C=O bonds between the benzene ring and deprotonated hydroxyl group (tautomerism of 8-Hq) at 100 °C (C) which disappears at 150 °C (D) and again reappears at 200 °C (E). The intense peaks observed at 200 °C (E) are of sharp but less intense compared to the sample-B (50 °C). This ensures the restructuring of the C-C, C=C bond, C-N-C, C-O, Al-O-Al, Al-N, Al-O, C-C and C-H bonds of pyridine and benzene rings of Alq₃ which starts within 150 -200 °C due to excess oxidation of 8Hq to form non-emissive polymer, 8-hydroxyquinoline-N Oxide (NEP) which is amorphous in nature and restructured again to form agglomerated orthorhombic nanorods [37-44]. Interestingly,

3. The Photoluminescence (PL) spectra analysis:

To find the changes due to alteration of annealing temperatures, fluorescence spectra (FLR) is shown in Fig 5.5(a) and photoluminescence (PL) spectra is shown in fig 5.5(b) and 5.5(c) for the as prepared and annealed samples respectively. FLR spectra shows the decreasing order of fluorescent intensity which is found as 517.1 nm (E) > 522.8nm (B) > 533.1nm (D) > 528.4 nm (C). Fig 5.5(b) shows the maximum photoluminescence intensity at 518.6 nm for asprepared bulk Alq₃ powder which shows the highest peak intensity at 518.6 nm, which is in good agreement with the other reported studies that show strong PL peaks at ~519 nm. Moreover, from the figure 5(b) and 5(c), it clearly exhibits the shift in the peak position of the annealed state as compared to the as-prepared Alq₃. The excitation wavelength is kept fixed at 385 nm for each of the five samples whereas the emission wavelength is found to lie between 370 - 700 nm. The highest sharp peaks for each individual sample are found within the range 517.1 nm and 533.4 nm. With the increase in temperature, the FLR intensity of figure 5.5(a) increases

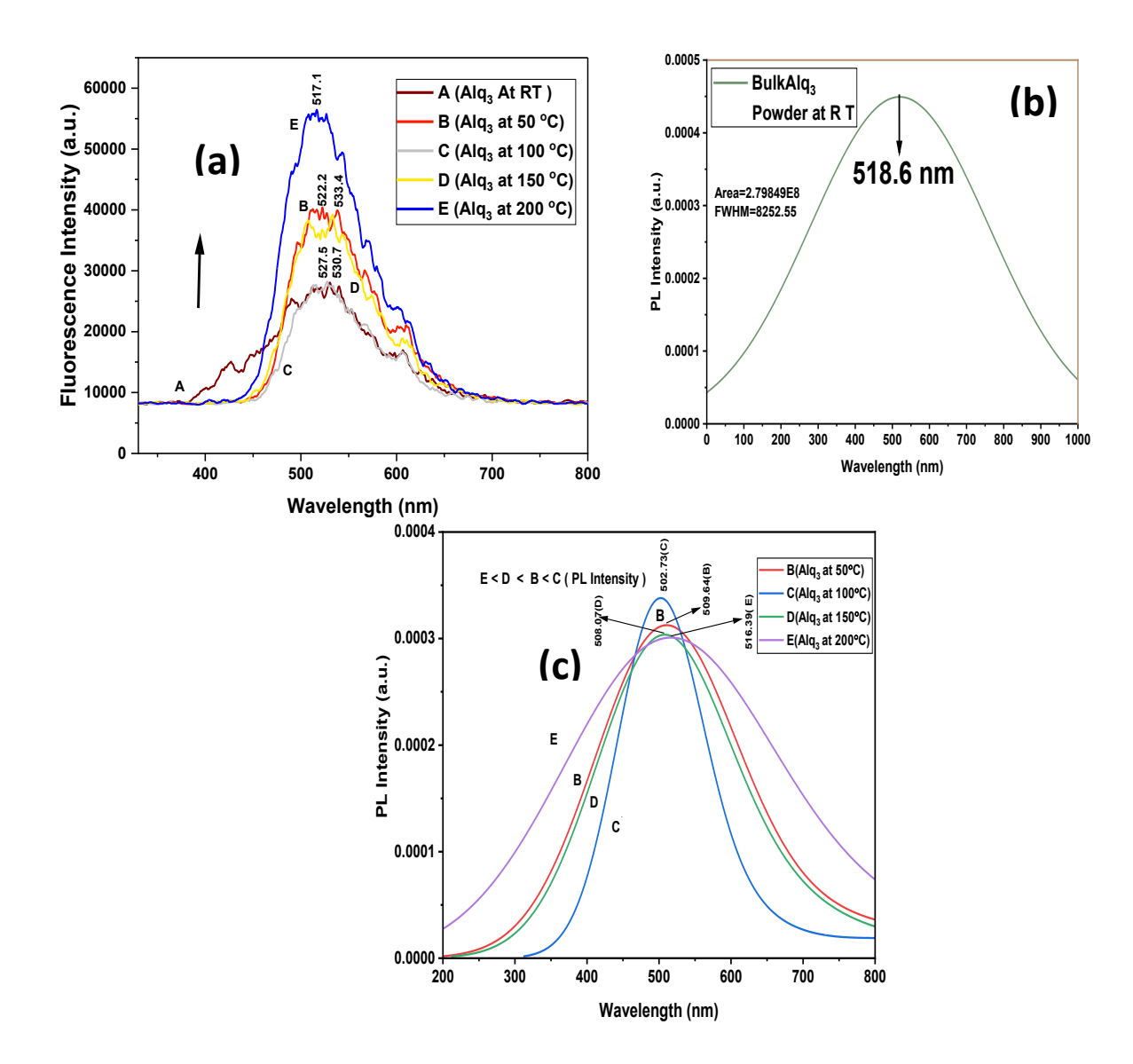


Figure 5.5:(a) Fluorescence spectra (b) normalized PL spectra of pure bulk Alq₃ at room temperature without annealed state and (c) normalized PL spectra of sample B to E

to 150 °C and reaches a maximum at 200 °C. FLR intensity is found to exhibit red shift below 150 °C whereas above 150 °C, it shows blue shift and continues until it reaches 200 °C. PL intensity as shown in fig. 5(c) is found to be in decreasing order of intensity with peaks at 502.73 nm (C) > 509.64 nm (B) > 508.07 nm (D) > 516.39 nm (E) as compared to Fig 5.5 (b) i.e., 518.6 nm. The decreasing order of FWHM (full width at half maximum) of the normalized PL are as follows: 101.72 (E) > 101.46 (B) > 100.64 (D)> 99.72 (C) which resembles with the fluorescence spectral performance. With an increase in annealing temperature, the PL intensity for Sample-E shows maximum FLR and PL intensity and Sample-A shows minimum which resembles with the reports of Papadimitakopoulos et al [22]. From Sample-B to Sample-C, increase in PL intensity shows red shift whereas blue shift has been observed for Sample-D and Sample-E compared to PL intensity of Sample-A in Figure 5.5(b) On thermal annealing at 50 °C, the entrapped moisture at first evaporated and the fluorescent Alq₃ pellet become dry, resulting in higher FLR intensity and PL intensity peaks. Between 50-100 °C, thin layer of porous hybrid A₁₂O₃-Al(OH)₃ layers is formed on Alq₃ surface on exposure to hot air removing sub-gap absorption and microstructure- surface defects. At 100 °C, breaking and weakening of C=C, C-N-C, C-O stretching, Al- O, Al-N bonds and isoindole deformation starts causing a cleavage of coordinate covalent bond between quinolate ligands and metallic aluminium phase change. Consequently, π - π * (pi-pi*) electronic transitions of hydroxyquinoline ring leads to electronic transitions of phenoxide and pyridine rings. Alq₃ hydrolyses and decomposes into free 8-Hq and instable ligand Alq₂OH. The freed and weak fluorophore 8-Hq starts to evaporate and get saturated quickly [33]. which causes a decrease in FLR intensity between 50 °C (B) and 100 °C (C) and a weak intensity at 100 °C. At 150 °C additional free weak fluorescent 8-Hgs are yielded which influences the increase in fluorescence intensity compared to 100 °C. Between 150 °C and 200 °C, maximum numbers of free molecule of 8-Hq reacts strongly with excess amount of oxygen and forms higher amount of aggregated NEP which causes strange increase in FLR intensity for polymeric aggregation which is in complete agreement with the finding as reported by Dhruba Chatterjee et al [44]. As more emissive excimers are formed in the aggregated

state, the greater emissive polymer face higher level of emission- quenching which causes its highest amount of fluorescence and PL emission [24,25,39,44]. Although 8-Hq derivative, 8-hydroxy N oxide, itself is a non-emissive polymer without having π – conjugation, still it is found to exhibit higher fluorescence at 200 °C which resembles with the report of Dhruba Chatterjee et al. [44]. This opens a new pathway of research on fluorescence property of non-emissive non-fluorescent material which can have promising applications in bio-medical and optical devices. [43-44].

5.4. Conclusion:

From the optical and morphological study of Alq₃ pellet, it is found that thermal annealing of Alq₃ bulk powder (pellet) in the presence of hot air from 50 °C to 200 °C shows remarkable changes which is mentioned worthy and it will open a new avenue of research. With the increasing annealing temperature of mer-Alq3 at 50 °C, the UV-VIS absorbance, Photoluminescence and FLR peak intensity increases rapidly and at 100 °C it shows reduction of intensity due to hydrolysis of Alq₃ and production of weak fluorogenic free 8-Hq molecules. On an annealing at 150 °C, the pellet shows an increase in UV-VIS absorbance and FTIR transmittance. FLR and PL intensity reveals that due to limited oxidation at 200 °C, all the peak intensities found to be strong compared to other annealing temperatures which form conjugated aggregated non emissive polymer (NEP) and its derivative after oxidation of 8- Hq. This is surprising and needs a lot of attention in this regard. Along with the optical measurements, the XRD spectra and FESEM images also explain the occurrence of phase shifting, change of structure, π - π * electronic transition, chemical degradation and instability of Alq₃ crystals and powder that occurred during the increase of annealing temperature from 150 °C to 200 °C. The chemical failure and degradation of optical efficiency and structural rigidity due to hot air exposure between 150 °C and 200 °C becomes precise and significant as new non emissive polymers are formed which again shows higher fluorescence. Despite chemical degradation, recrystallization of structure, chemical bonding also forms new 8-Hq derivative as non- emissive polymer which can give fluorescence more than as-prepared Alq₃. This result will broaden the aspects of using Alq₃ and its derivative in OLED application and solid-state lighting technology (SSL) and solar cell application and also reopens a new horizon of enthusiasm for fluorescence from non-emissive polymer and

its further applications. Henceforth, further investigation is required in this field in order to make bulk Alq3 useful for more versatile applications. This experimental work establishes all the base of our entire Ph.D research project. From these results we got Alq3-N-oxide a non-emissive polymer which enhances the optical, thermal, and structural properties of pristine bulk Alq3 powder and its thin film manifold which solves our first research objective to form a voltage tunable wide emission spectrum OLED. Here we at first stage find out the appropriate ETL and EML layer. In our next chapter we continue this study further and form a simple structured OLED with green luminescence.

References

- [1.] Dresner, J. (1969). Double injection electroluminescence in anthracene. $RCA\ REVIEW,\ 30(2),32\$
- [2.] Tang, C. W., & VanSlyke, S. A. (1987). Organic electroluminescent diodes. *Applied physics letters*, 51(12),
- [3.] Van Slyke, S. A., Chen, C. H., & Tang, C. W. (1996). Organic electroluminescent devices with improved stability. *Applied physics letters*, 69(15), 2Chen, Y., & Ma,D. (2012). Organic semiconductor heterojunctions as charge generation layers and their application in tandem organic light-emitting diodes for high power efficiency. *Journal of Materials Chemistry*, 22(36), 18718-18734.[4]
- [4.] Jiang, P., Zhu, W., Gan, Z., Huang, W., Li, J., Zeng, H., & Shi, J. (2009). Electron transport properties of an ethanol-soluble AlQ 3-based coordination polymer and its applications in OLED devices. *Journal of Materials Chemistry*, 19(26), 4551-4556.
- [5.] Burrows, P. E., Gu, G., Bulovic, V., Shen, Z., Forrest, S. R., & Thompson, M. E. (1997). Achieving full-color organic light-emitting devices for lightweight, flat-panel displays. *IEEE Transactions on electron devices*, 44(8), 1188-1203
- [6.] Rajeswaran, G., Itoh, M., Boroson, M., Barry, S., Hatwar, T. K., Kahen, K. B., ... & Takahashi, H. (2000, May). 40.1: Invited Paper: Active Matrix Low Temperature

- Poly-Si TFT/OLED Full Color Displays: Development Status. In *SID Symposium Digest of Technical Papers* (Vol. 31, No. 1, pp. 974-977). Oxford, UK: Blackwell Publishing Ltd.
- [7.] Hung, L. S., & Chen, C. H. (2002). Recent progress of molecular organic electroluminescent materials and devices. *Materials Science and Engineering: R: Reports*, 39(5-6), 143-222.
- [8.] Hou, J., Zhao, H., Zhang, Z., Yu, L., & Yan, X. (2023). The antifouling tris-(8-hydroxyquinoline) aluminum: Titanium dioxide coatings under visible light.

 Surface and CoatingsTechnology,468,129743

 https://doi.org/10.1016/j.surfcoat.2023.129743
- [9.] Sánchez Vergara ME, Cantera Cantera LA, Rios C, Salcedo R, Lozada Flores O, Dutt A(2023). Preparation of Hybrid Films Based in Aluminum 8-Hydroxyquinoline as Organic Semiconductor for Photoconductor Applications. Sensors.23(18):7708. https://doi.org/10.3390/s23187708
- [10.] Tang, C. W., VanSlyke, S. A., & Chen, C. H. (1989). Electroluminescence of doped organic thin films. *Journal of applied physics*, 65(9), 3610-3616..
- [11.] Salleh, M. M., Hasnan, T., Azis, T., Sepeai, S., & Yahaya, M. (2007). Fabrication of organic light emitting diodes (oleds) for flat panel displays. *Berkala Ilmiah MIPA*, 17(3).
- [12.] Popielarski, P., Mosinska, L., Zorenko, T., & Zorenko, Y. (2023). Luminescence of tris (8-hydroxyquinoline) aluminium thin films under synchrotron radiation excitation. *Journal of Luminescence*, *261* 119930. https://doi.org/10.1016/j.jlumin.2023.119930
- [13.] Cölle, M., & Brütting, W. (2004). Thermal, structural and photophysical properties of the organic semiconductor Alq3. *physica status solidi (a)*, 201(6), 1095-1115
- [14.] Aziz, H., Popovic, Z., Xie, S., Hor, A. M., Hu, N. X., Tripp, C., & Xu, G. (1998). Humidity induced crystallization of tris (8-hydroxyquinoline) aluminum layers in organic light-emitting devices. *Applied Physics Letters*, 72(7), 756-758. small molecule-based organic light-emitting devices. *Science*, 283(5409), 1900-

- 1902.
- [15.] Bi, H., Zhang, H., Zhang, Y., Gao, H., Su, Z., & Wang, Y. (2010). Fac-Alq3 and Mer-Alq3 Nano/Microcrystals with Different Emission and Charge-Transporting Properties. *Advanced Materials*, 22(14), 1631-1634.https://doi.org/10.1002/adma.200903094
- [16.] Mahakhode, J. G., Bahirwar, B. M., Dhoble, S. J., & Moharil, S. V. (2006). Tunable Photoluminescence from tris (8-hydroxyquinoline) aluminum (Alq3). *Proc of ASID, New Delhi*, 237-239.
- [17.] Debsharma, M., Pramanik, T., Daka, C., & Mukherjee, R. (2022, May). Recent advances in the electrical and optical properties of Alq3 and Alq3 derivatives based OLEDS. In *Journal of Physics: Conference Series* (Vol. 2267, No. 1, p. 012159). IOP Publishing
- [18.] T suboi, T., & Torii, Y. (2010). Selective synthesis of facial and meridianal isomers of Alq3. *Molecular Crystals and Liquid Crystals*, 529(1), 42-5299
- [19.] Aziz, H., Popovic, Z. D., Hu, N. X., Hor, A. M., & Xu, G. (1999). Degradation mechanism of properties. *Advanced Materials*, 22(14), 1631-1634.
- [20.] Tsuboi, T., & Torii, Y. (2010). Photoluminescence characteristics of green and blue emitting Alq3 organic molecules in crystals and thin films. *Journal of non-crystalline solids*, 356(37-40), 2066-2069.
- [21.] Higginson, K. A., Thomsen III, D. L., Yang, B., & Papadimitrakopoulos, F. (2004). Chemical Degradation and Physical Aging of Aluminum (III) 8-Hydroxyquinoline: Implications for Organic Light-Emitting Diodes and Materials Design. In Organic Light-Emitting Devices: A Survey (pp. 71-101). New York, NY: Springer New York.
- [22.] Higginson, K. A., Zhang, X. M., & Papadimitrakopoulos, F. (1998). Thermal and morphological effects on the hydrolytic stability of aluminum tris (8-hydroxyquinoline)(Alq3). *Chemistry of Materials*, *10*(4), 1017-1020
- [23.] Papadimitrakopoulos, F., Thomsen, D. L., & Higginson, K. (2000, March). The Nature of Chemical Impurities Formed during Degradation o Aluminum (III) 8-Hydroxyquinoline: Implications for Organic Light-Emitting Diodes. In APS

- March Meeting Abstracts (pp. E23-010).
- [24.] Knox, J. E., Halls, M. D., Hratchian, H. P., & Schlegel, H. B. (2006). Chemical failure modes of AlQ3-based OLEDs: AlQ3 hydrolysis. *Physical Chemistry Chemical Physics*, 8(12), 1371-1377.
- [25.] Panek, J. J., Błaziak, K., & Jezierska, A. (2016). Hydrogen bonds in quinoline Noxide derivatives: First-principle molecular dynamics and metadynamics ground state study. *Structural Chemistry*, 27, 65-75.
- [26.] Souza, A. D. V. D., Sousa, L. L. D., Fernandes, L., Cardoso, P. H. L., & Salomão, R. (2015). Al2O3–Al (OH) 3-Based castable porous structures. *Journal of the European Ceramic Society*, *35*(6), 1943-1954.
- [27.] El-Nahass, M. M., Farid, A. M., & Atta, A. A. (2010). Structural and optical properties of Tris (8-hydroxyquinoline) aluminum (III)(Alq3) thermal evaporated thin films. *Journal of alloys and compounds*, 507(1), 112-119.
- [28.] Fung, M. K., Ng, A. M. C., Djurišić, A. B., Chan, W. K., & Wang, H. (2012).Preparation of 8-hydroxyquinoline wires by decomposition of tris (8-hydroxyquinoline) aluminium. *Journal of Experimental Nanoscience*, 7(5), 578-585
- [29.] Goldman, M., & Wehry, E. L. (1970). Environmental effects upon fluorescence of 5-and 8-hydroxyquinoline. *Analytical Chemistry*, *42*(11), 1178-1185.
- [30.] Ansari, S. A., & Husain, Q. (2011). Immobilization of Kluyveromyces lactis β galactosidase on concanavalin A layered aluminium oxide nanoparticles—its future aspects in biosensor applications. *Journal of Molecular Catalysis B: Enzymatic*, 70(3-4), 119-126.
- [31.] Syarif, D. G., Yamin, M., & Pratiwi, Y. I. (2019, February). Self combustion synthesis of Al2O3 nanoparticles from bauxite utilizing sugar as fuel for nanofluids with enhanced CHF. In *Journal of Physics: Conference Series* (Vol. 1153, No. 1, p. 012068). IOP Publishing.
- [32.] Brinkmann, M., Gadret, G., Muccini, M., Taliani, C., Masciocchi, N., & Sironi, A. (2000). Correlation between molecular packing and optical properties in different crystalline polymorphs and amorphous thin films of mer-tris (8-

- hydroxyquinoline) aluminum (III). *Journal of the American Chemical Society*, 122(21), 5147-5157
- [33.] Muccini, M., Brinkmann, M., Gadret, G., Taliani, C., Masciocchi, N., & Sironi, A. (2001). Optical spectroscopy of unsolvated and solvated crystalline Alq3. *Synthetic metals*, 122(1), 31-35
- [34.] Brinkmann, M., Gadret, G., Taliani, C., Masciocchi, N., Sironi, A., & Muccini, M. (2001). Interplay between optical properties and molecular packing in novel isolated crystalline phases of tris-(8-hydroxyquinoline) Aluminium (III). *Synthetic metals*, 121(1-3), 1499-1500
- [35.] Cuba, M., & Muralidharan, G. (2015). Effect of thermal annealing on the structural and optical properties of tris-(8-hydroxyquinoline) aluminum (III)(Alq3) films *Luminescence*, 30(3), 352-357
- [36.] Park, S. Y., Ghosh, P., Park, S. O., Lee, Y. M., Kwak, S. K., & Kwon, O. H. (2016). Origin of ultraweak fluorescence of 8-hydroxyquinoline in water: photoinduced ultrafast proton transfer. *RSC advances*, 6(12), 9812-9821.
- [37] Kim, S., Kim, D. H., Choi, J., Lee, H., Kim, S. Y., Park, J. W., & Park, D. H. (2018). Growth and brilliant photo-emission of crystalline hexagonal column of Alq3 microwires. *Materials*, 11(4), 472.
- [38] Bulteau, Y., Tarrat, N., Pébère, N., & Lacaze-Dufaure, C. (2020). 8-Hydroxyquinoline complexes (Alq3) on Al (111): atomic scale structure, energetics and charge distribution. *New Journal of J Chemistry*, 44(35), 15209-15222.
- [39] Puschnig, P., & Ambrosch-Draxl, C. (2008). First-principles approach to the understanding of π-conjugated organic semiconductors. *Monatshefte für Chemie-Chemical Monthly*, 139, 389-399.
- [40] Djurišić, A. B., et al. "Influence of atmospheric exposure of tris (8-hydroxyquinoline) aluminum (Alq 3): a photoluminescence and absorption study." *Applied Physics A* 78 (2004): 375-380.
- [41] Garbuzov, D. Z., Bulović, V., Burrows, P. E., & Forrest, S. R. (1996). Photoluminescence efficiency and absorption of aluminum-tris-quinolate (Alq3)

- thin films. *Chemical Physics Letters*, 24 (1999). Metal— Alq3 complexes: the nature of the chemical bonding. *Journal of the American Chemical Society*, 121(36), 8216-8220
- [42] Nandiyanto, A. B. D., Oktiani, R., & Ragadhita, R. (2019). How to read and interpret FTIR spectroscope of organic material. *Indonesian Journal of Science and Technology*, 4(1), 97-118.
- [43] Chatterjee, D. P., Pakhira, M., & Nandi, A. K. (2020). Fluorescence in "nonfluorescent" polymers. *ACS omega*, 5(48), 30747-30766

Chapter 6: Influence of thermally annealed nanocrystalline Alq₃ thin film for flexible WOLED and Solid-State Lighting application

Abstract:

In this study, we have synthesized a polycrystalline thin film of meridional Tris (8hydroxyquinoline) aluminium (Alq₃) using wet synthesis and spin coating techniques. We annealed the nanorods of Alq₃ sequentially at RT (room temperatures), 50 °C, 100 °C, 150 °C, and 200 °C for 2 hours at a heating rate of 2°C/min before the measurement. We observed significant changes in the optical, thermal, and morphological properties of mer- Alq₃. XRD diffraction and FESEM images confirm that the polycrystalline triclinic nanorods of Alq₃ get shortened in length and become wider in diameter. These morphological changes are followed by a phase change to semi-porous stacked tetragonal agglomerated grains when dry and pure Alq₃ powder is annealed at 50 °C. Further, they transform and recrystallize into orthorhombic grains agglomerated on a less semi-porous matrix between 100°C and 150°C. We got the highest optical, surface morphological, and electrical performances of Alq₃ thin film when it was annealed at 150 °C. We also fabricated ITO/PEDOT: PSS/V₂O₅/Alq₃/LiF/Ag-based un-optimized OLED devices for respective temperatures ranging from RT (room temperature) -150°C. The synthesized OLED is found to have a turn-on voltage of around 2.84 volts at 1 cd/m², and a driving voltage of 4.3 V at 1000 cd/m². Low value of HOMO and LUMO (-5.94 eV and -3.08 eV respectively) energy level is found to further enable Alq₃ as a promising ETL (electron transport layer) or HBL (hole blocking layer). This opens an avenue for fabricating WOLEDs with simple architecture as well as at ambient atmospheric conditions

6.1. Introduction:

Organic Light Emitting Diode (OLED) is an organic solid-state electroluminescent

device that has multi-tasking hi-tech applications in small, large, flat, full-colored displays for television, mobile phones, computers, cameras, oscilloscope, traffic lighting, vehicle indicators [1-5]. Solid-state lighting (SSL) is the lighting technology where solid-state semiconductors emit light unlike filaments, glass bulbs, gases & plasmas that are used in the case of traditional fluorescent tubes, incandescent and halogen lamps. SSL is manufactured using LEDs (Light-emitting diodes) and OLEDs and are heavily used in space technology, medical field and interior lighting. Despite it, OLED-based SSL is still far behind LED as it is coping with difficulties in pluralistic commercial production and mass popularity due to their higher manufacturing cost, shorter lifetime, chemical degradation and absence of encapsulation. In contrast, flexibility, refresh rate, easy synthesis process, and thinner width, are the qualities for which OLED-based SSL are used in high-end car lights, decorative lighting, traffic lighting as well as in low curvature containing angular area lighting.

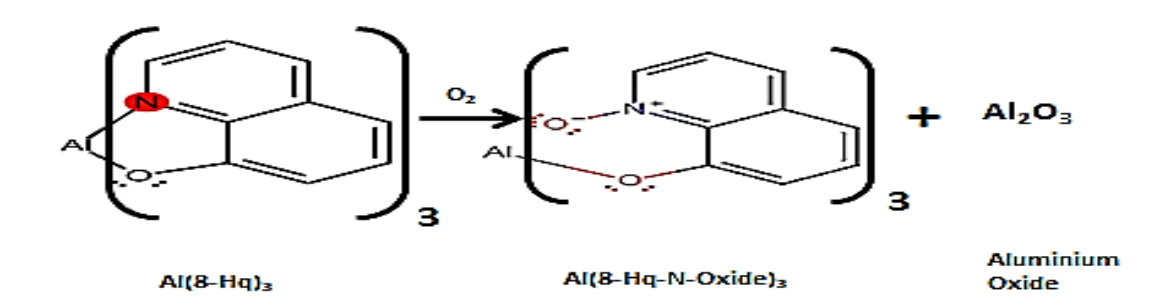
In 1987, C.W. Tang et al. [1,3] reported a bi-layered thin film of OLED using aromatic hole transport layer (HTL) layer diamine and organic ETL layer Alq3. Alq3 has achieved enormous popularity for its excellent blue-green bright luminescence, low cost, easy fabrication technique, less operational voltage, and fine-tuning ability of emission wavelength. Despite its multidimensional applicability, Alq₃ has encountered serious shortcomings in their operations such as smaller-span durability and severe deterioration in photoluminescence (PL) and electroluminescence (EL) efficiency over time. The novel OLED exhibited a brightness of luminance $> 1000 \text{ cd/m}^2$, high luminous efficacy = 1.5 lm/W, and EQE of 1% photon/electron. The constant effort to improve the efficiency of the Alq₃ based OLED has led to many interesting findings in the last couple of decades. Tang et.al. [1,3] also showed that the efficiency of an OLED can be optimized significantly by doping fluorescent organic dyes into the host organic Alq₃ matrix which caused enhancement in the energy transfer from the host layer to organic dye layers with a yield of higher EL and PL quantum efficiency. Armstrong and his co-researchers in 2003 reported a technique and performance of -SONR2, a strong electron-donating group at the C-5 position of phenoxide ring in Alq₃, that exhibited higher blue shift of green luminescence.

at 580 nm compared to 514 nm of parent Alq₃. In 2005 C.Y Kwong et al. reported OLED performance with three substituted Alq₃ derivatives: Al(Meq)₃,(tris(4- methyl-8hydroxyquinoline)aluminium, Al(Cl₂q)₃(tris(5,7-dichloro-8-hydroxyquino linato)aluminium and B(Alq) bis-(2-methyl-8-hydroxyguinolinato)-4-(phenylphenolato)aluminium(III)which exhibits maximum luminance of 31839 cd/m², 33714 cd/m² and 35256 cd/m² and current densities of 4.3 cd/A, 6.8 cd/A, and 8.7 cd/A respectively. In 2011, J.P. Heiskanen et al. [19] synthesized 11H-indolo[3,2-c]quinolin-4- ol complex, an Alq₃ derivative which shows 3.5 times better photoluminescence compared to parent Alq₃.In 2016 Paez-Sierra. B.A. et al. investigated the MEH-PPV(poly(2-methoxy-5-(2'-ethylhexyloxy)-(pphotoluminescence of phenylenevinylene)) doped Alq₃ matrix with varied concentration of MEH PPV with 2.19 eV work-function and energy band gap of 2.33 eV. In 2023 Jiayi Song et al reported Alq₃,MoO₃(molybdenum oxide) and NPB(N,N'-di(naphthalene-1-yl)-N,N'diphenyl-benzidine) based hetero-junction OLED exhibiting brightness of 46040 cd/m².[12-14]. In spite of the above-mentioned reports, the reason behind the degradations and limitations in the quantum efficiency has still remain debatable. Moreover, in attempt to improve the PL and EL efficiencies, researchers have made the synthesis process more cumbersome and expensive. Furthermore, only limited findings have been reported regarding the thermal analysis of Alq₃ such as sublimation degradation, thermal stability and specific heat capacity. For example, Colle et al. reported various temperaturedependent phases of Alq3 [12] whereas Xu et al. [14] has reported glass transition and crystallization of Alq₃ thin film at 130°C and 185°C respectively [14-16]. Investigation on morphology-dependent optical and transport properties in Alq₃ will help us to bridge the research gap for the development of efficient, durable and cost effective ETL layer. In this work, we have systematically investigated the altering structural, optical, electrical, and thermal properties of Alq₃ thin film by sequentially annealing at different temperatures ranging from room temperature (RT) to 200 °C. It is established that the variation of growth temperature from 150 °C to 200 °C leads to red and blue shifts in fluorescence maxima due to the recrystallization of 8-hydroxyquinoline(8-Hq) ligand and formation of non-emissive polymer 8-hydoxyquinoline-N-oxide. Although this is a non-emissive polymer emitter, its normalized PL and EL spectra show more intensity in photoluminescence as well as electroluminescence which is novel and interesting.

Based on it, our research also involved demonstrating an OLED device by stacking layers of PEDOT: PSS [poly(3,4-methylenedioxy thiophene), polystyrene sulphonate] and Alq₃ which is annealed at 150°C as this combination showed maximum electroluminescence (EL) and excellent photoluminescence (PL) with minimum chemical degradation, maximum current and high-power efficiency. Here, optical and electronic properties of grown annealed samples are performed to determine the energy levels and understand the mechanism of charge injection that leads to efficient optical properties of the fabricated OLED hetero structure.

6.2. Experimental Methods:

1. Synthesis of bulk polycrystalline mer-Alq3:



Schematic diagram 1: Conversion mechanism tris(8-hydroxyquinoline-N-xide)aluminium(III)[Al(q-N-oxide)₃], a non-emissive polymer (NEP) from tris(8-hydroxyquinoline)aluminium [Alq₃] in presence of excess oxygen(O₂) gas.

We synthesized Tris (8-hydroxyquinoline)aluminium (Alq₃) by wet synthesis method

as mentioned in our previous chapter number 3 by Mrinmoy Debsharma et al. [22]. The chemical reaction that took place is as follows (Schematic diagram 1 in Chapter 4). The dried 4.63 gm. synthesized Alq3 powder was ground and dissolved into 30 ml acetone (Merck, purity >99%) bought from the market along with 50 ml double distilled water (Anchiale technologies bought from market) with constant stirring at 50 °C temperature. The resultant solution was ultra-sonicated for ½ h with constant heating at 50°C. A yellowish-green homogenous solution was obtained and ready for spin coat fabrication [31- 36]. This yellowish -green solution was poured into five 10 ml test tubes. Then spin coated at 3000 rps for 30 s over pre-cleaned glass slides to form five individual thin films. These five uniform thin films of Alq3 were annealed at 50 °C, 100 °C, 150 °C, and 200 °C in a hot air oven for 2 hrs. with a constant heating rate of 2 degrees per minute [22-31]. Then the best performing Alq3 thin film was spin -coated on pre-cleaned ITO-coated PET sheet for our OLED device fabrication.

2. Preparation of PEDOT: PSS solution for thin film formation:

PEDOT: PSS is a dark, blue-colored organic dye obtained from Sigma Aldrich with 3-4%(w/v) in H₂O and was not purified further. As the dye is insoluble in water, to make it a homogeneous solution for the application of spin coating, PEDOT: PSS was dissolved in ethylene glycol in the volumetric ratio 9:1 along with constant stirring for $\frac{1}{2}$ h in a magnetic stirrer. The resultant bluish emulsion was ultrasonicated for another $\frac{1}{2}$ hr. after which the yielded bluish solution was filtered using filter paper having a diameter of 0.45 μ m until bluish transparent precipitate was obtained.[35]

3. Preparation of Alq₃ solution for thin film formation:

At first, the ITO-coated PET sheet (purchased from Techinstro, India) with a resistance of $10\Omega/\text{sq}$) was cleaned using a detergent solution, acetone, and ethanol (bought from the market having purity > 99% for solutions) in succession for several times. It was allowed to dry at room temperature using a hot plate at 27 °C under the ambient atmosphere. The solution of PEDOT: PSS was subsequently spin-coated for the HTL layer on the PET (polyethylene terephthalate)-coated sheet. A 15-minute drying period was followed by the vacuum-assisted spin-coater machine depositing a thin film of

tris(8-hydroxyquinolinilato)aluminium (III). This process helped us to fabricate an OLED device where the stacked layers were constructed like: ITO (175 nm)/PEDOT: PSS(48 nm)/ $V_2O_5(12 nm)$ /Alq₃(83 nm)/LiF(3 nm)Ag(100 nm). In this hetero-structure, ITO (Indium tin oxide) acts as a transparent anode, PEDOT: PSS is an organic dye that acts as a transparent bulk hole transport layer (HTL), Alq₃, an ETL layer acts as a green emissive layer and silver-paste used at the perimeter of the Alq₃ layer acts as a metallic cathode. A bi-layer un-optimized device (II) was fabricated to exhibit electron transport and emitting character with the device configuration: ITO coated PET sheet (175 nm)/PEDOT: PSS (48nm)/ $V_2O_5(12 nm)$ /Alq₃ (83 nm)/LiF(3 nm)/Ag (100 nm) where PEDOT: PSS acts as hole transport layer (HTL) as well as HIL. All the measurements of the constructed OLED were performed without any encapsulation and subjected to experimental measurement at room temperature. [35,36-39]

6.3. Results and discussion:

A. Morphological study:

(a)X-ray Diffraction spectroscopy of Alq3 pellet and its analysis:

XRD spectroscopy analysis of Figure 6.1 of a thin film of polycrystalline Alq3 reveals that the Bragg reflections peaks of Alq3 annealed at 25°C (sample A) are detected respectively XRD spectroscopy analysis of Figure 6.1 of a thin film of polycrystalline Alq3 reveals that the Bragg reflections peaks of Alq3 annealed at 25°C (sample A) are detected respectively at $2\theta = 10.7^{\circ}$, 12.8° , 13.6° , 15.2° , 15.9° , 17° , 18.3° , 21.3° , 22.4° , 23.2° , 24.4° (following JCPDS card No. 26-1550). For Alq3 annealed at 50 °C (sample B), the intense peaks are seen at $2\theta = 11.2^{\circ}$, 12.6° , 15.0° , 15.6° , 22.6° which signifies crystal planes of (-202), (-220), (131), (202) and (051) respectively (as per PDF pattern 00-010-766). For sample C annealed at 100° C, the intense peaks are visible at $2\theta = 11^{\circ}$, 12.6° , 14.8° , 15.5° , 22.5° for crystalline phases (-202), (-220), (-112), (131), (202), (051) and (102) crystalline orientations (PDF pattern 01-076-1381). Whereas when the Alq3 pellet is annealed at 150° C, sharper peaks are found at $2\theta = 11.2^{\circ}$, 12.6° , 14.9° , 15.7° , 22.5° which attributes to (- 202), (-220), (-112), (131), (202), (051), (211),(221) and (460) crystalline planes. On annealing at 200° C, strong intense

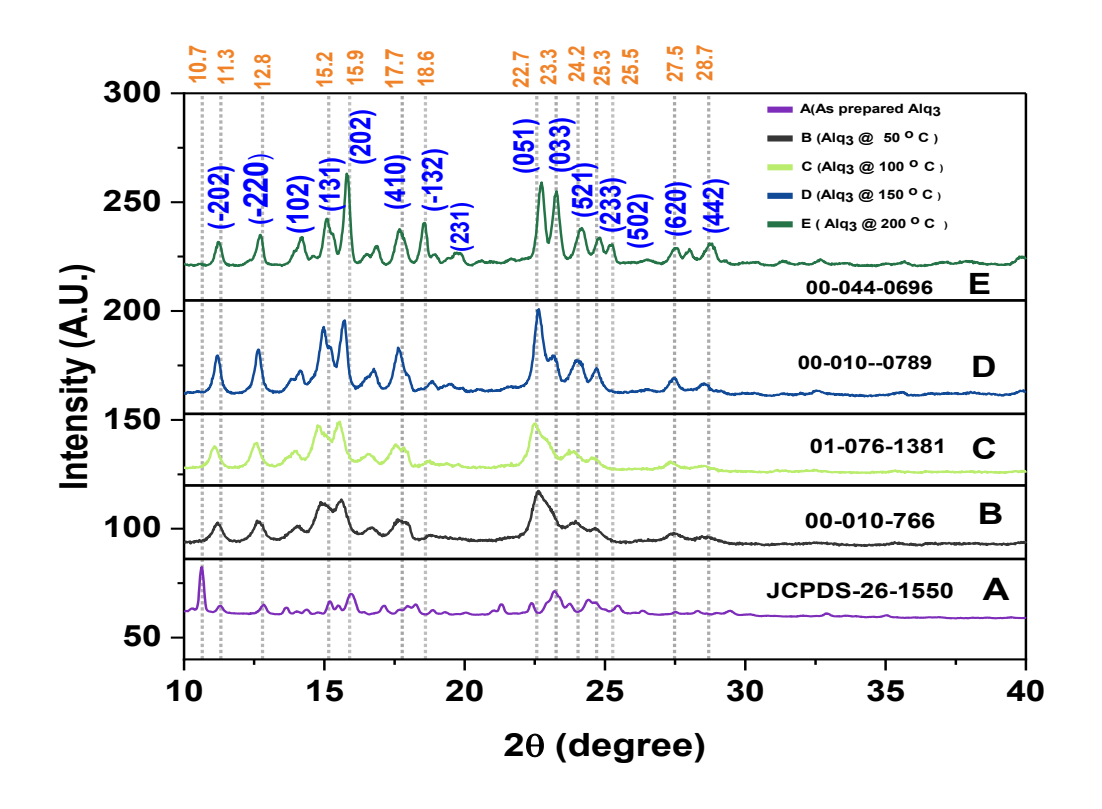


Figure 6.1: XRD spectra of as prepared bulk Alq₃ annealed at room temperature (Sample A) and Alq₃ pellets annealed at (1) 50 °C (Sample B) (2) 100 °C (Sample C) (3) 150 °C (Sample D) and (4) 200 °C (Sample E)

peaks appeared at 2θ = 11.2°, 12.7°, 15.1°, 15.8°, 22.7° (following the PDF pattern 00-044-0696) which corresponds to the crystalline planes (- 202), (-220), (-112), (131), (202),(051), (131), (202), (051) and (033) planes (following PDF pattern 00-010-0789). The sample annealed at 200 °C is found to have intense diffraction peaks sharper than that that appeared for a sample at 150 °C. In the plot, the intense peaks shown by curve (E) are the highest in intensity compared to other curves. From curves (A) to (E) all curves confirm the crystalline character of the annealed Alq₃ at a different temperature ranging from RT to 200 °C. Also, from our previous work (Mrinmoy Debsharma et.al.) [22] it can be concluded that on annealing from room temperature to high temperature,

the triclinic crystal plane changes its crystalline characteristics and phase changes to tetragonal and retains it till 100°C. But on annealing beyond 100 °C, the crystal structure transforms into the ortho-rhombic structure. The XRD diffractogram and the intensity of the curve (E) are attributed to the re- emergence of the crystalline structure due to the evolution of a non-emissive polymer [28]. The Curves (B) and (C) and their peaks describe the evaporation of moisture and breaking of Al-O, Al-N, and C-N bonds. In contrast, the curves (D) and (E) signify the hydrolysis of Alq₃ and oxidation of 8-Hq molecules to form 8-Hq-N-oxide [22-31].

(b)FESEM (Field Emission Scanning electron microscopy) image analysis:

From FESEM images of Figure 6.2(A) -6.2(C) it is clear that the polycrystalline nanorod (250 nm) structure of thin film Alq₃ gets shortened and wider in diameter on annealing at RT and further annealing at 50 °C, those grains start to disappear but oval and semi-circular pores are found to appear in a major portion of the sample's surface which may be due to the evaporation of moistures. In contrast to Alq₃ being annealed at 50°C as shown in the figure, the diameter of oval and circular pores reduces and becomes very few in numbers at 100°C. This Pattern may be caused by the hydrolysis of Alq₃ molecules which results in the creation of Alq₂-OH and 8-Hq molecules. The pore's size begins to shrink between 100 and 150 degrees (Fig. 6.2(D) and(E)) Celsius, losing its oval and circular shape. Furthermore, the semi-porous Al(OH)₃-Al₂O₃ structure on the Alq₃ base is lost as a result of the restructuring of the crystal size, which causes the diameter and length of orthorhombic grains to rise. The orthorhombic structure as shown in fig. 2F changes into a multi-stacked polycrystalline nanorod structure between 150 and 200 degrees Celsius, which is different from the un-annealed, state of the mer-Alq₃ sample at room

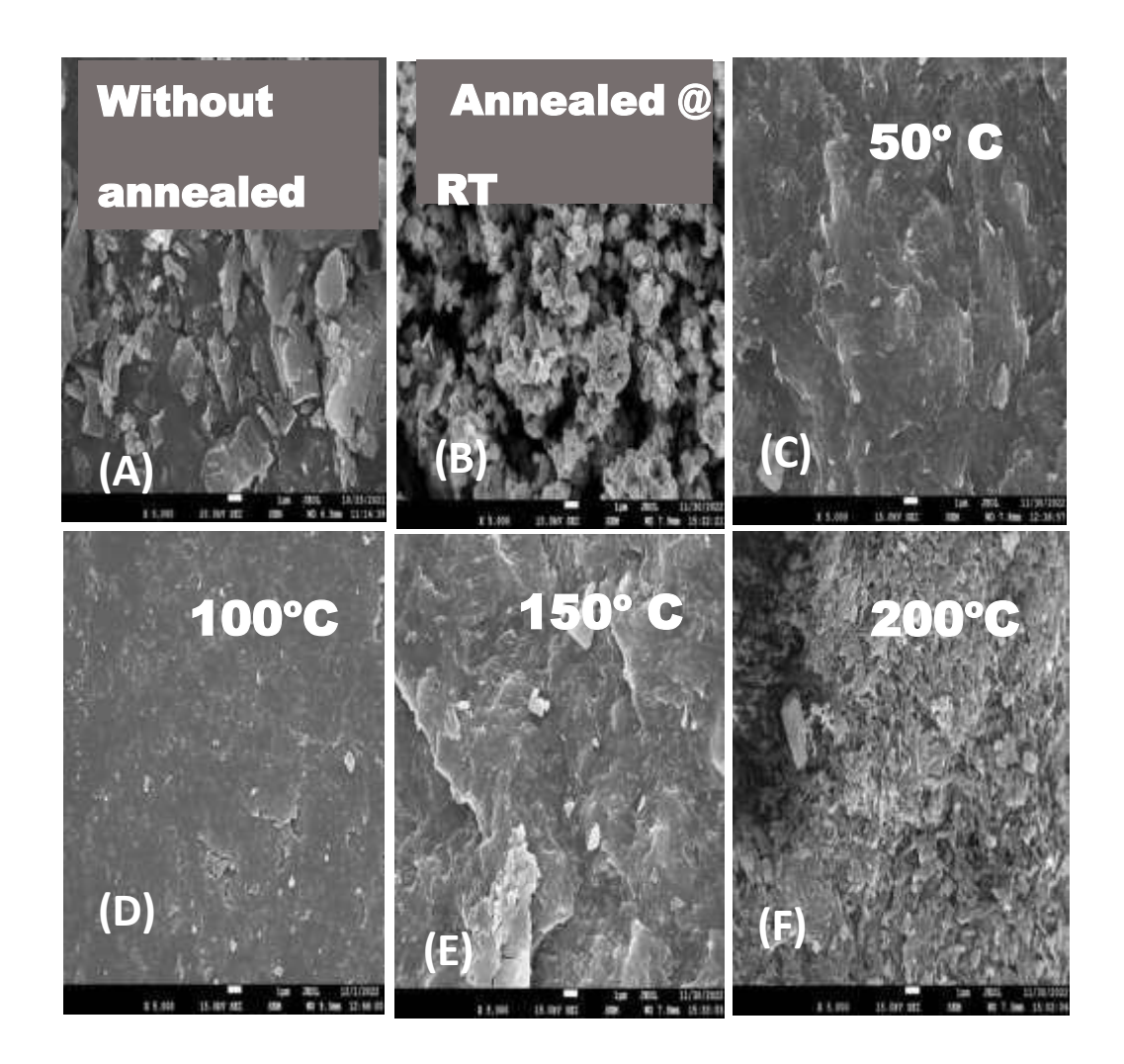


Figure 6.2: FESEM images of (A) without annealed bulk Alq₃ and bulk Alq₃ powder annealed at (B) room temperature (C) 50°C (D)100°C (E)150°C (F) 200°C based on 5000X amplification

temperature. This occurs due to the formation of the non-emissive polymer, Al(8-Hq-N-Oxide)₃[tris(8-hydroxyquinoline-N-oxide)aluminium(III) and Al₂O₃. This results in the reappearance of semi-porous structures, big agglomerated grains of Al₂O₃, over Al(8-Hq-N-Oxide)₃ surface as we have explained in detail through FTIR, XRD and FESEM characterization in our previous published research article(Mrinmoy Debsharma et al.). These results conform with the result of XRD analysis. [22-31]

B. Thermal Properties analysis:

(1) Differential Scanning Calorimetry (DSC) Analysis:

Figure 6.3 describes the comparative DSC (Differential Scan Calorimetric) analysis of bulk polycrystalline Alq₃ powder where the heating rate is 10 °C/min. From the Figure, it is clear that a negligible phase transition has been observed. Alq₃ annealed at (a) RT (b) 50 °C and 100 °C (c) 150 °C. (d) 200 °C exhibits the maximum intense endothermic melting peak at 414 °C, 414.6 °C, 414.3 °C, and 413.3 °C respectively [38-39]. The phase transitions around the melting point of Alq₃ annealed at 50 °C and 100 °C result in a minor rightward shift and immediate left shift from 100 °C to 200 °C. The specific heat of bulk Alq₃ powder annealed

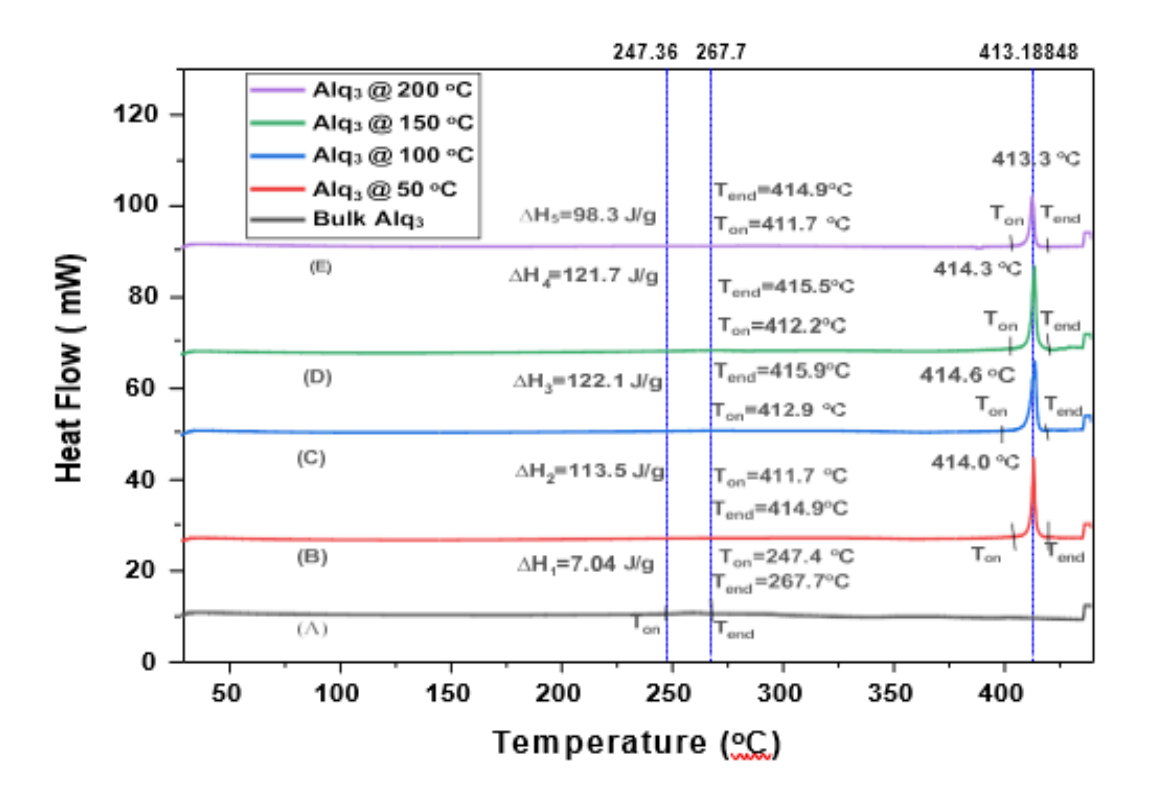


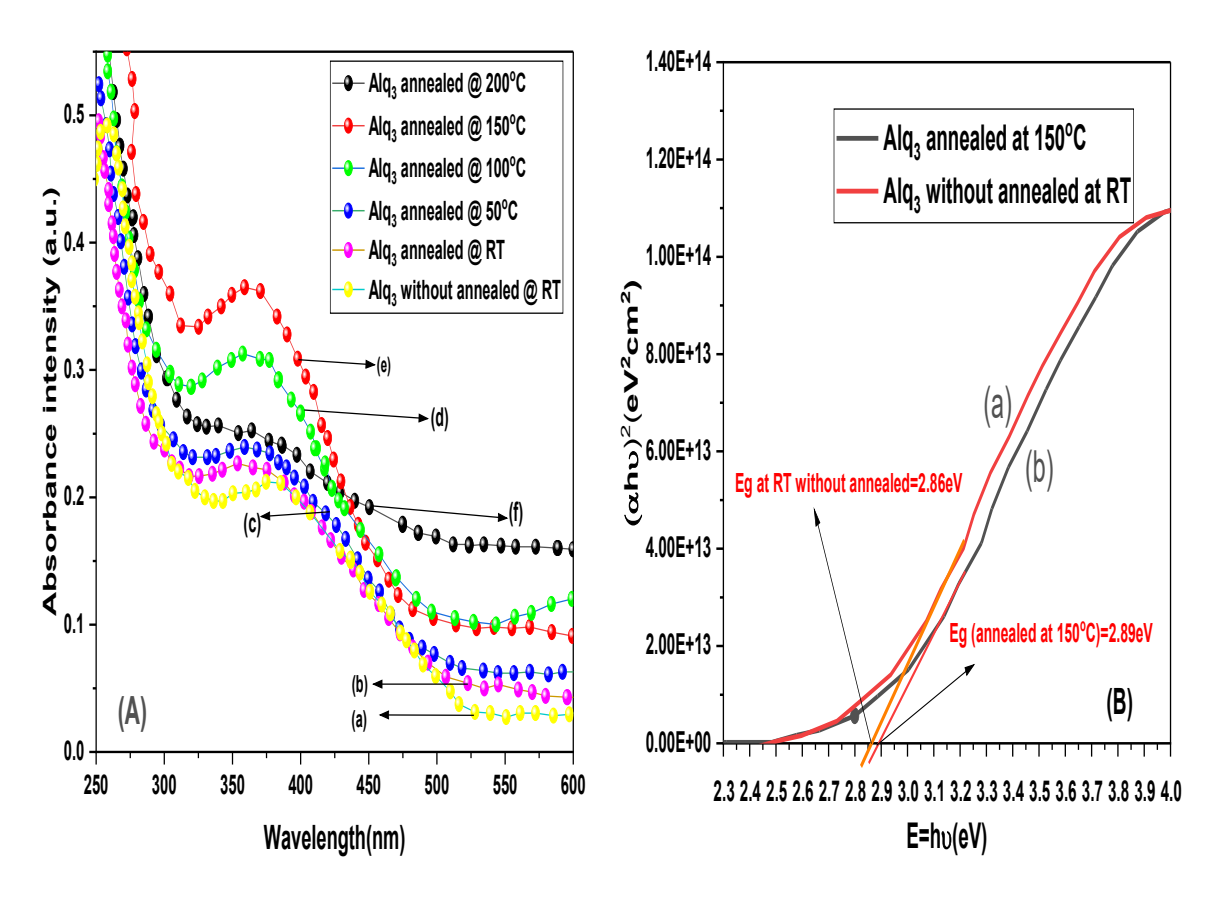
Figure 6.3: DSC curves of bulk Alq₃ powder annealed at (a) room temperature (b) 50 °C (c) 100 °C (d) 150 °C and (e) 200 °C.

at (a) room temperature (b) 50 °C and 100 °C (c) 150 °C (d) 200 °C are found to be as

 Δ H1=7.04 J/g, Δ H2=113.5 J/g, Δ H3=122.1 J/g, Δ H4=121.7 J/g and Δ H5=98.3 J/g respectively. The specific heat (ΔH) reaches its maximum value at 100 °C and then decreases to 98.3 J/g at 200 °C. The most significant aspect is that all DSC curves maintain phase. Broad shorter endothermic peaks for all five samples of annealed Alq₃ powder are seen at 436°C. The endothermic melting points are seen around 414.4°C which is in good agreement with the other published report. The specific heat (ΔH) reaches its maximum value at 100°C and then decreases to 98.3 J/g at 200°C a stable linear nature till 387.8 °C. The DSC curves (e) exhibit a weak exothermic crystallization peak at 387.9°C. A weak and wide exothermic crystallization peak was detected between 248.7°C and 258.5°C in the curve (a) which is because of transition occurred from α -Alq₃ to γ -Alq₃ [36]. All five annealed samples possess the γ -Alq₃ phase during their crystalline phase. Broad shorter endothermic peaks for all five samples of annealed Alq₃ powder are seen at 436°C. The endothermic melting points are seen around 414.4°C which is in good agreement with the other published report. The specific heat (ΔH) reaches its maximum value at 100°C and then decreases to 98.3 J/g at 200 °C.

C. Optical properties and Photoluminescence (PL) properties study:

Figure 6.4(A) [(a)-(f)] depict the normalized UV-Vis absorption spectra of as prepared without annealed Alq3 thin film at room temperature(curve-(a)) and Alq3 thin film annealed at room Temperature (RT) (curve-(b)), 50 °C(curve-(c)), 100 °C(curve-(d)), 150 °C (curve-(e)) and 200 °C (curve-(f)), From figure 6.4(A) it is clearly observed that curve -(e) exhibit the highest broad absorbance intensity at 359.4 nm whereas curve- (a) show the lowest broad absorbance peaks at 385.4 nm. The maximum intense peaks for curve-(b) curve- (c), curve-(d), and curve- (f) are seen at 353.1 nm,360.4nm,356.9 nm and 339.6 nm. We have explained all changes in absorbance intensity w.r.t. the change in annealing temperature of bulk mer-Alq3 powder clearly in our previous published work [2]. As absorbance intensity Alq3 thin film annealed at 150°C is the highest absorbance intensity which decreases at 200°C. The higher amount of absorbance intensity for an OLED emitter can emit higher

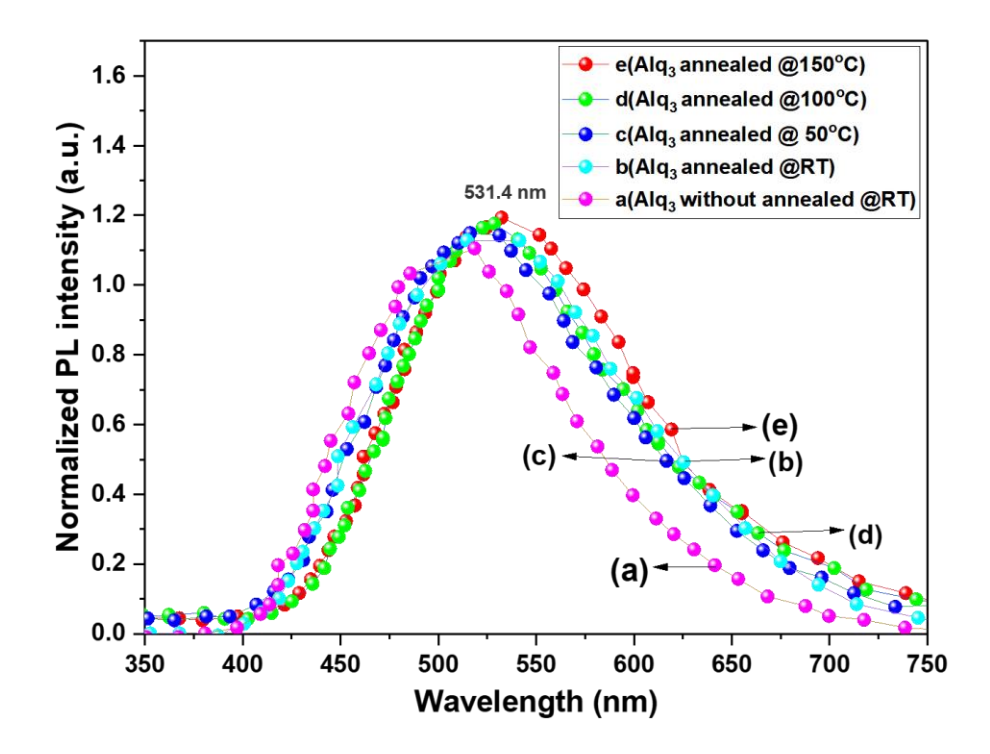


we do not consider 200°C and all other annealing temperatures except

Figure 6.4(A)[(a)-(f)]: UV-Vis absorption spectra of Alq₃ thin film of (a) without annealed at room temperature (RT) & of [(b)-(f)] annealed at (b) varied temperature from room temperature (RT) to 200 °C. **Figure 6.4(B):** the Tauc plot of the Alq₃ thin film(a) without annealed at room temperature (RT) (b) annealed at 150°C

10°C for the rest of all measurements. So, we plotted the Tauc-plot of Alq₃ thin film annealed at 150 °C only for their highest absorbance intensity. We observe a high broad UV-Vis absorbance peak at the wavelength 359.4 nm for Alq₃ thin film annealed at 150°C and a sharper intense peak at 257.4nm. When we move forward from curve (a) to curve (f) absorbance intensity at first blue shifts from 385.4 nm to 353 nm then we

observe a consecutive red shift, a blue shift, a red shift and again a blue shift starting from the curve(b) to curve(f) within the visible region. In organic semi-conductor, $\sigma \rightarrow \sigma^*$, $n \rightarrow \pi$ and $\pi \rightarrow \pi^*$ molecular orbital electronic transitions are found to occur due to absorption in the visible as well as UV region. A quinolinolate storage devices



are just a few examples of materials that can be created

Figure 6.5: Normalized photoluminescence (PL) spectra of Alq₃ thin film without annealed at RT & annealed at (b)RT (c)50 °C (d) 100 °C and e) 150 °C

molecular orbitals. [38]. $\pi \to d$ and $d \to \pi^*$ molecular orbital electronic transitions, due to the high energetic absorbance band, occur between 210 and 288 nm [39]. The optical energy band-gap (Eg) of the organic semiconductor material is determined by UV-Vis absorption spectra followed by a Tauc plot of the same spectra. The value of the Tauc plot is the value of the optical band gap of Alq₃ organic semi-conductor and is given as:

$$(\alpha\hbar\gamma) = (\hbar\gamma - Eg)^n \tag{6.4}$$

where n is 1/2 for allowed direct transitions and n=2 for allowed indirect transition, Eg is the energy band-gap, α denotes absorbance co-efficient which is also equal to 2.303(A/d) where d= sample thickness, A is the absorbance of the thin film, b is the Planck's constant and ν is the frequency of the absorbed radiation [38,39] Figure 4 (B) clearly shows that the UV-Vis spectra of Alq₃ thin film till $(\alpha hv)^2 = 0$ are extrapolated to give the optical energy gap (Eg) of the Alq₃ thin film.

From Figure 6.4(B), the direct optical bandgap of Alq3 thin film is 2.89 eV, which is in good agreement with other published experimental results [19,38, 39]. For PEDOT: PSS, optical band gap Eg is found to be 1.44 eV at room temperature. [[38,39] during the rest of all our characterization measurements. The peak intensity of green color emission increased gradually with the regular rise in temperature from room temperature to 150°C. The emission wavelength red-shifted from 6.5(a) to 6.5 (b),6.5(b) to 6.5(c),6.5(c) to 6.5(d), and 6.5(d) to 6.5(e) respectively compared to their respective previous temperatures. The highest intense peak of the 6.5(e) PL curve is found at 531.4 nm for Alq3 thin film annealed at 150°C. [9,13,16,19,35-39]. When the excitation energy is more than thin film emission energy PL spectra undergo a distinct red shift by following Frank Condon's transition principle. [13,16,19,39].

D. Electrical properties study and device performance of the fabricated ITO/PEDOT: PSS/V₂O₅/Alq₃/LiF/Ag structure-based OLED device.

1. Electrochemical properties study through cyclic voltammogram analysis:

The most acceptable technique to characterize the electrochemical properties of organic materials is measurement through cyclic voltammetry [4,13,14,40,41,42]. The highest occupied molecular orbital (HOMO) and the lowest unoccupied molecular orbital (LUMO) of organic semiconductors is the energy level needed for extracting

required to introduce an electron to an atom (i.e., reduction) respectively [5]. The HOMO and LUMO can be evaluated through redox potential i.e., Ered and Eox derived from the cyclic-voltammogram of cyclic voltammetry. We used ferrocene as our known reference an electron from an atom of a molecule (i.e., oxidation) and the energy with a reference value of -4.8 eV for the calculation of HOMO and LUMO energy levels. We used the following formula given by J L Bredas et al. [40] to estimate them as follows:

$$E_{\text{HOMO}} = [-4.8 - \text{Eox onset}] \tag{6.5}$$

$$E_{LUMO} = [-4.8-Ered onset]$$
 (6.6)

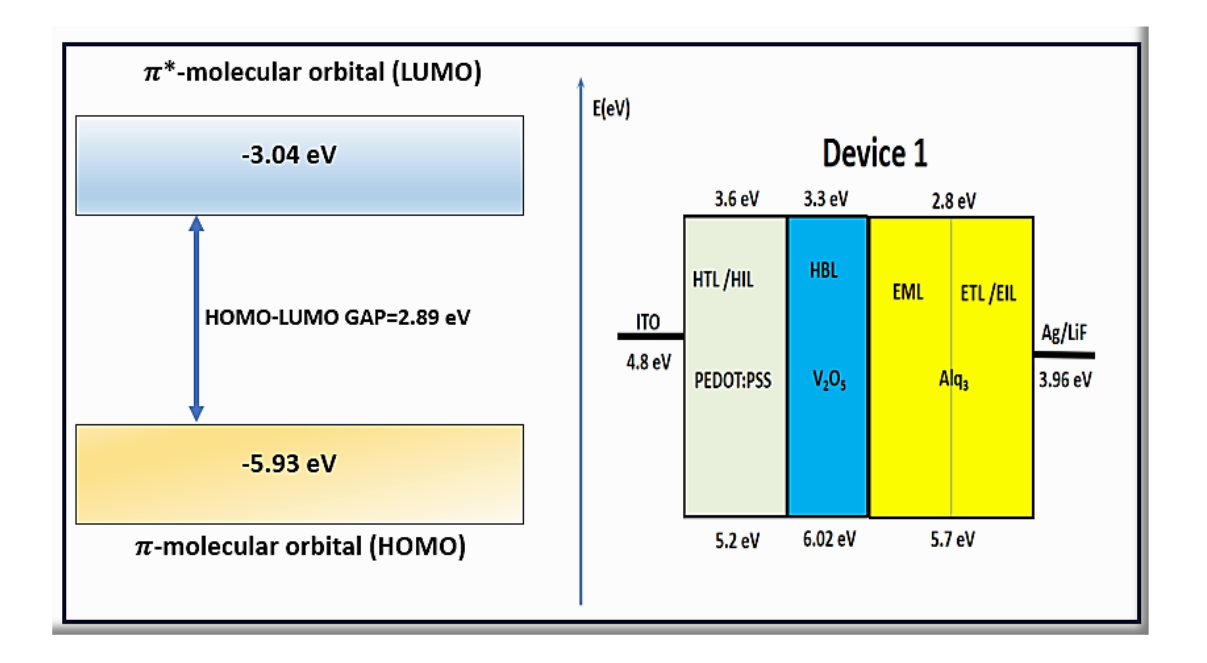
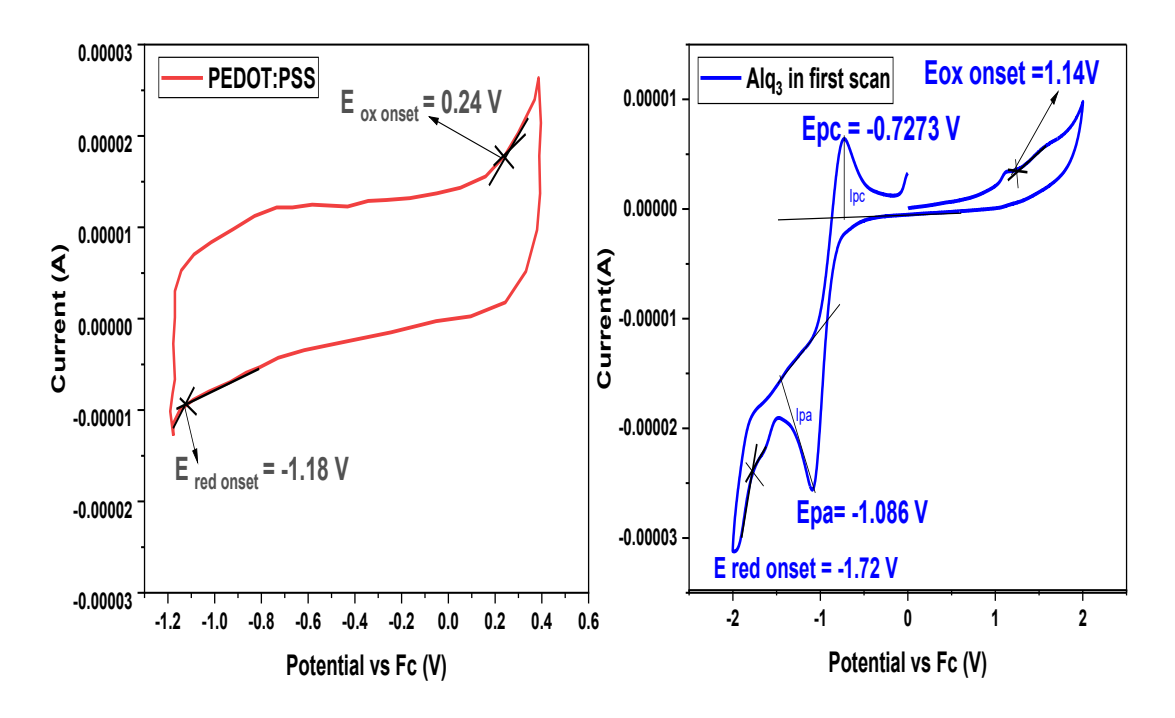


Figure 6.6: HOMO –LUMO energy level band gap of Alq 3 and PEDOT: PSS based OLED

The anodic and cathodic scans of the Alq₃ and PEDOT show the quasi-reversible waves at the onset of oxidation potential between 0.24 to 1.14 volt vs. Ag/AgNO₃ (for oxidation) and reduction potential lies between -1.18 to -1.72 volts vs

Ag/AgNO₃ (for reduction). In this case, the 4.8 eV denotes the onset potential of Ferrocene in a vacuum. From figure 6 and 7, the HOMO and LUMO energy level diagram of the HTL PEDOT: PSS and ETL Alq₃ are found and are mentioned in the tabular form as shown below. From the energy diagram of Alq₃ thin film, the HOMO and LUMO level are found as 5.04 eV and 3.18 eV respectively [41,42]. Based on cyclic-voltammetry, we see the E(HOMO) and E(LUMO) of PEDOT: PSS are as follows: E_{HOMO} = -5.04 eV and E_{LUMO} =-3.62 eV and E_{gap} =1.42 eV. In the case of Alq₃, E_{HOMO} =-5.94 eV and E_{LUMO} =-3.08 eV, and E_{gap} =2.86 eV. The work function of the Ag cathode and the transparent anode ITO fulfill the requisite energy level for constructing a single junction bi–layered OLED using organic materials. (Figure 6.6, Figure 6.7, and Table 6.2). The optical band gap from UV-VIS spectra and CV estimated energy band gap conforms with the other reported



experimental data. The HOMO-LUMO energy level difference

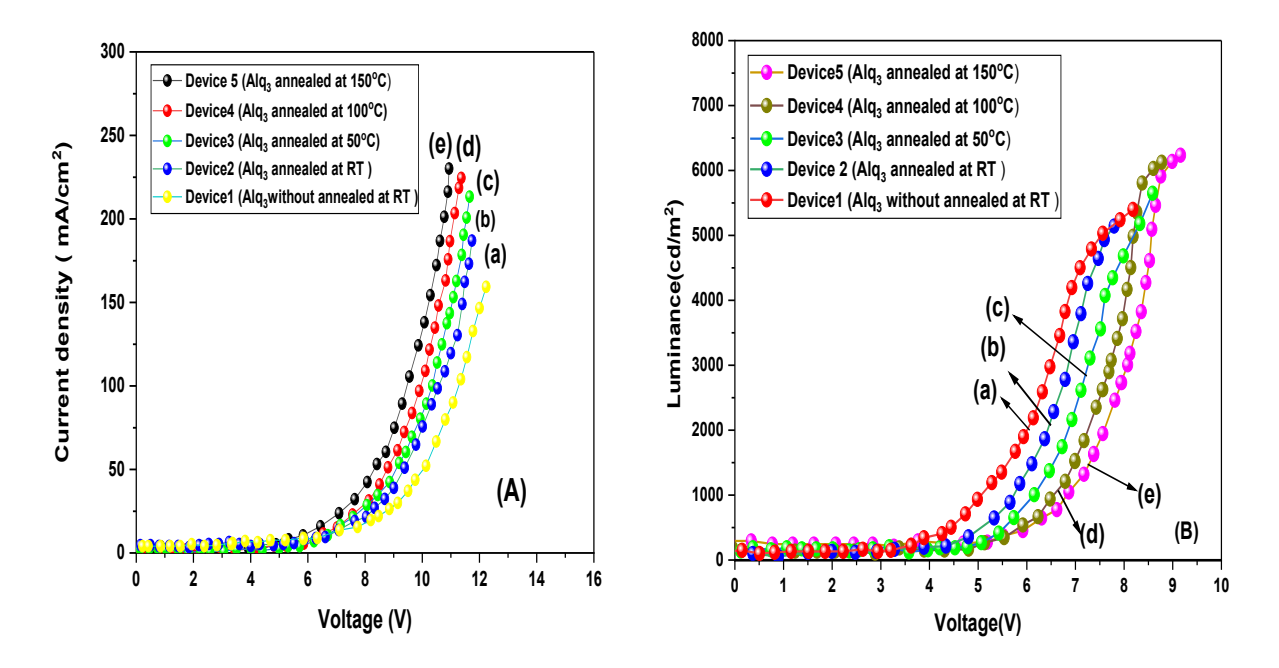
Figure 6.7: Cyclic voltammogram of the (a) PEDOT: PSS and (b) Alq₃ 167

Table 6.1: Comparison table between HOMO-LUMO value of PEDOT: PSS and Alq₃

Compound	Eox onset vs	Ered onset	НОМО	LUMO	Eg(LUMO
	EFc (V)	EFc (V)	(eV)	(eV)	- НОМО)
PEDOT: PSS	0.24	-1.18	-5.04	-3.62	1.42
Alq ₃ RT without annealed	1.14	-1.72	-5.94	-3.08	2.86
Alq ₃ annealed @ RT	1.16	-1.74	-5.96	-3.06	2.90
Alq ₃ 50°C	1.19	-1.73	-5.99	-3.07	2.92
Alq ₃ 100°C	1.14	-1.77	-5.94	-3.03	2.91
Alq ₃ 150°C	1.13	-1.76	-5.93	-3.04	2.89

2. Electroluminescence properties and OLED device performance analysis

To investigate the OLED's device performance as a single top-emitting transparent OLED, the architecture of ITO/PEDOT: PSS/V₂O₅/Alq₃/LiF/Ag was fabricated. Here, Ag acts as a low-work function metallic cathode, ITO-coated PET sheet acts as a transparent high-work function anode, Alq₃ as ETL, and PEDOT: PSS as HTL of our fabricated OLED. Figure 8(A) (a)-(e) shows current density vs. voltage (J-V) characteristics of single-layered OLED where ETL layers i.e. Alq₃ thin films of device1 to device5 layers were fabricated (a) as-prepared Alq₃ thin film [device1] and function metallic cathode, ITO-coated PET sheet acts as a transparent high work function anode, Alq₃ as ETL and PEDOT:PSS as HTL of our fabricated OLED. Figure 6.8(A) (a)-shows current density vs. voltage (J-V) characteristics of single-layered OLED where ETL layers i.e. Alq₃ thin films of device1 to device5 layers were fabricated (a) as-prepared Alq₃ thin film [device1] and annealed at (b) RT (room temperature) [device2] (c)50°C [device3] (d)100°C [device4] and (e)150°C [device5].



PEDOT: PSS cathode, A) Currentvoltage) ITO/PEDOT: PSS/V₂O₅/Alq₃/LiF/Ag PEDOT: PSSfabricated found that from 0-2 volts, all OLED devices show a very weak current density which is around 0.064 mA/cm². Around 2.46 V all five devices show a significant rise in corresponding current density of 3.15 mA/cm². The five devices achieve their respective maximum current density of 163.4mA/cm², 190.8mA/cm², 216.8mA/cm², 229.9 mA/cm² and 234.1mA/cm² at 12.4V, 11.9V, 11.7V, 11.4V and 10.9V respectively. From figure 8(B) it is seen that Device 1 to Device 5 exhibit significantly low turn-on voltage i.e., 2.81 V, 2.84 V, 2.89 V, 2.91 V and 3.10 V. Around 4.16 V all five devices show a significant rise in corresponding luminance. The Driving voltages of five devices are found to be 8.29V, 7.90V, 8.71V, 8.86V and 9.26V which indicates that the OLED can be operational even after 10 volts. The five devices exhibit the highest luminance of 5413.4cd/m²,5259.8 cd/m², 5760.2cd/m², 6223.7cd/m² and 6338.6cd/m² respectively. characteristicsdepictPE, CE, QE, and EL vs. wavelength characteristics plot we confirm that device 5 is the best OLED device compared with the performances of the rest four OLED devices. From this result, it is clear that our emissive material Alq₃ powder annealed at 150 °C is a promising electron transport material or hole-blocking material which should enhance the PL and EL properties of

WOLED as well as green OLED for possible applications in solid-state the highest EL intense peak at 530.8 nm which is also in agreement with the result obtained from the CIE coordinates of the Chromaticity diagram. (Figure 10A and Table 3). We also find that there are no significant changes occurring in the EL spectral peaks and shapes of the EL spectral curve on account of voltage variation. Therefore, Alq3 powder annealed at 150°C exhibits excellent electrical properties as well as OLED device performances. PE, CE, QE, and EL vs. wavelength characteristics plot we confirm that device 5 is the best OLED device compared with the performances of the rest of the four OLED devices. From this result, it is clear that our emissive material Alq₃ powder annealed at 150 °C is a promising electron transport material or hole-blocking material which should enhance the PL and EL properties of WOLED as well as green OLED for possible applications in solid-state the highest EL intense peak at 530.8 nm which is also in agreement with the result obtained from the CIE coordinates of the Chromaticity diagram. (Figure 10A and Table 3). We also find that there are no significant changes occurring in the EL spectral peaks and shapes of the EL spectral curve on account of voltage variation. Therefore, Alq₃ powder annealed at 150°C exhibits excellent electrical properties as well as OLED device performances. ITO/PEDOT: PSS/V₂O₅/Alq₃/LiF/Ag-basedMoreover, the current density- voltage- luminance (J-L-V) characteristics depict the diode characteristics of the ITO/PEDOT: PSS/V₂O₅/Alq₃ /LiF/Ag-based OLED device. Working of OLED is based on forward bias that's why reverse bias is not considered for our measurement. Within the limit of 2.46 volts and 4.6 volts, the current density as well as luminance starts to increase gradually with the increase of voltage and follows a nonlinear curve. Figure 9.6(A)[(a)-(e)] depicts the values of EQE for device 1 to device 5 as 1.003%,1.061%,1.190%,1.336% and 1.488%. The possible reason for the low EQE% is that Alq₃ is an excellent fluorescent material that uses only singlet excitons for its radiative recombination. From the power efficiency versus luminance (ηp-L) plot of Figure: 6.9(B)[(a)-(e)], we get the maximum power efficiency at 100 cd/m² luminance for the five devices i.e., from device 1 to device 5 as 28.18 lm/W,29.33 lm/W, 31.52 lm/W, 32.87 lm/W and 34.24 lm/W. From current efficiency (CE) versus current density(nc-J) plot of Figure 6.9(C)[(a)-(e)] gives the maximum current efficiency for

100 cd/m² current density of device 1 to device 5 as 3.96cd/A,4.43 cd/A,5.15 cd/A,5.79 cd/A and 6.24 cd/A. The EL intensity –wavelength plot for a constant applied voltage of 9 V of Figure 9(E)[(a)-(e)] shows the highest EL intense peaks of device 1 to device 5 at 517.3 nm,519.5 nm,522 nm,528.6 nm, and 530.8 nm. The EL intensity –wavelength plot for varied applied voltage from 3V to 9 V of Figure 9(D) gives the maximum EL intensity at 530.8 nm for device 5 while the inset gives lighting. The EL spectra of Figure 9(d) exhibits greenish-white light illumination with the highest EL peaks at 517.3 nm for device 1. After a critical comparison regarding PE, CE, QE, and EL vs. wavelength characteristics plot we confirm that device 5 is the best OLED device compared with the performances of the rest four OLED devices. From this result, it is clear that our emissive material Alq₃ powder annealed at 150 °C is a promising electron transport material or hole- blocking material which should enhance the PL and EL properties of WOLED as well as green OLED for possible applications in solid-state the highest EL intense peak at 530.8 nm which is also in agreement with the result obtained from the CIE coordinates of the Chromaticity diagram. (Figure 10A and peaks and shapes of the EL spectral curve on account of voltage variation. Table3). We also find that there are no significant changes occurring in the EL spectral characteristics

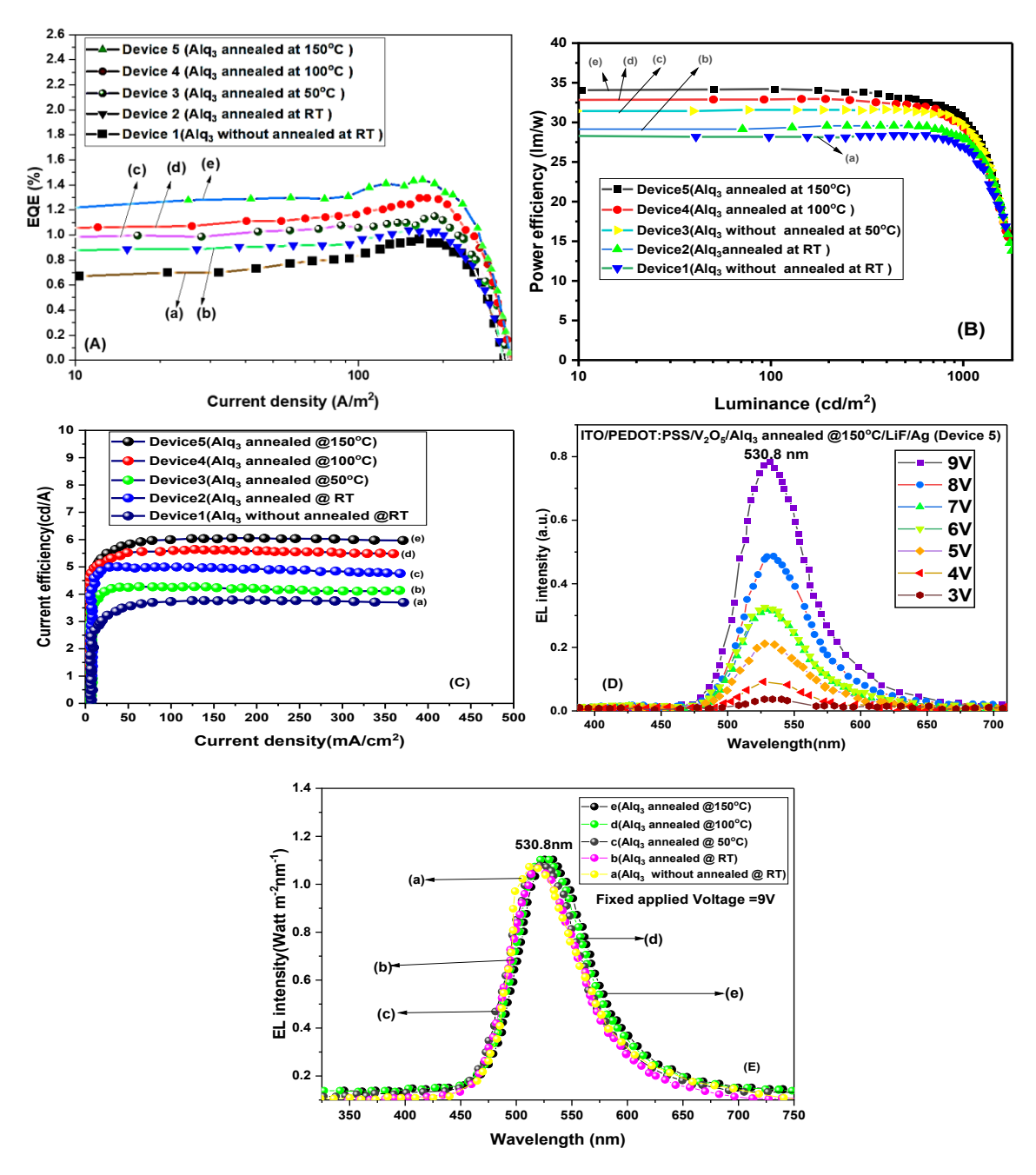


Figure 6.9(A): External quantum efficiency (EQE)a vs. current density(ηext-J) characteristics plot(B)Power efficiency vs. luminance plot(C)Current efficiency vs. current density plot and (D EL intensity vs. wavelength plot for varying applied voltage from 3-9V and Figure 6.9(E): EL intensity vs, wavelength plot for devices 1 to devices 5 at constant wavelength of 9V

Therefore, Alq₃ powder annealed at 150°C exhibits excellent electrical properties as well as OLED device performances.

Table 6.2: EL properties and device performance related to summarized data of the the result obtained from the CIE coordinates of the Chromaticity diagram. (Figure 10A and Table 3).

Cmpd.	Turn	Driving	Voltage	Voltage	Max.	Max.	CE @ V	PE	EQE
	on	voltage	at	at 1000	Luminance	Curr.	(Max. CE @	(lm/W)	(%)
	voltag		1cd/m ²	cd/m ²	at voltage	Densit	Max. J)		
	e					y			
						(J _{max})			
Alq ₃ thin	2.81V	8.29 V	3.16 V	5.21V	5413.4	163	3.96 cd/A	28.18	1.003
film					cd/m ²	mA/cm ²	for	lm/w	
without					@8.29 V	@12.4V	100mA/cm^2	@100	
annealed							current	cd/m^2	
at RT							density		
Alq ₃ thin	2.84V	7.90 V	2.93V	5.87V	5259.8	190.8	4.43cd/A	29.33	1.061
film					cd/m ²	mA/cm ²	for	lm/w	
annealed					@7.92 V	@11.9V	100mA/cm^2	@100	
at RT							current density	cd/m ²	
Alq ₃ thin	2.89V	8.71 V	2.89 V	6.12V	5760.2	216.6	5.15 cd/A	31.52	1.190
film					cd/m ²	mA/cm ²	@8.84volt	lm/w	
annealed					@8.71 V	@11.7V	for 100	@100	
at 50°C							mA/cm^2	cd/m^2	
							current density		
Alq ₃ thin	2.93V	8.86 V	2.84 V	6.45 V	6223.7	226.9	5.79 cd/A	32.87	1.336
film					cd/m ²	mA/cm ²	for 100mA/cm	lm/w	
annealed					@8.86 V	@11.4V	current density	@100	
at 100°C								cd/m ²	
Alq ₃ thin	3.10V	9.26 V	2.81V	6.88 V	6338.6	234.1	6.24 cd/A	34.24	1.488
film					cd/m ²	mA/cm ²	for	lm/w	
annealed					@9.26 V	@10.9V	100mA/cm^2	@100	
at 150°C							current density	cd/m ²	

We also find that there is no significant changes occurring in the EL spectral based five OLED devices i.e., device1 to device enhancement in the emitting character as well as in its electron transport character., with greenish-white light emission. E. Chromaticity diagram analysis (based on CIE 1931):

The CIE coordinates have further helped to find out the material efficiency or performance of any electroluminescent or luminescent materials. The main goal is to compare the emission color of the emitting materials using CIE color coordinates. The chromaticity diagrams and CIE coordinates of without annealed Alq₃ thin film at room temperature (RT) and Alq₃ thin films annealed at room temperature (RT), 50°C, 100°C are 150°C are demonstrated in Figure 6.10[a)-(e)] and Table 6.4 respectively. The PL spectrum or emission spectrum of Alq₃ thin films annealed at RT -150°C were excited at 385 nm. Based on it, The value of CIE coordinates of the Alq₃ thin films are evaluated as (0.2989,0.3262), (0.3262,0.4348), (0.3474,0.4099) (0.3196,0.4555) and (0.3050,0.3828). The obtained CIE-coordinates are found to be located in proximity of the white, light green, and yellow- green region of the elliptic CIE chromaticity region which is the requisite condition for making green, yellow, and white OLED. If we substitute different functional groups at the different positions of phenoxy groups of the pyridine group or tuning the chemical The value of CIE coordinates of the Alq₃ thin films are evaluated as (0.2989, 0.3262),(0.3262, 0.4348),(0.3474, 0.4099)(0.3196, 0.4555)and(0.3050,0.3828). The obtained CIE-coordinates are found to be located in the proximity of the white, light green, and yellow- green region of the elliptic CIE chromaticity region which is the requisite condition for making green, yellow, and white OLED. If we substitute different functional groups at the different positions of phenoxy groups of the pyridine group or tuning the chemical molecular structure or atomic packing the CIE coordinates may change the position of the CIE coordinate. From analyzing the CIE coordinates of the five devices it is determined that the annealed Alq₃ thin film annealed at 150°C is the potential emissive material for the fabrication of green or white OLEDs or solid-state lights. The highest color rendering index (CRI) of device

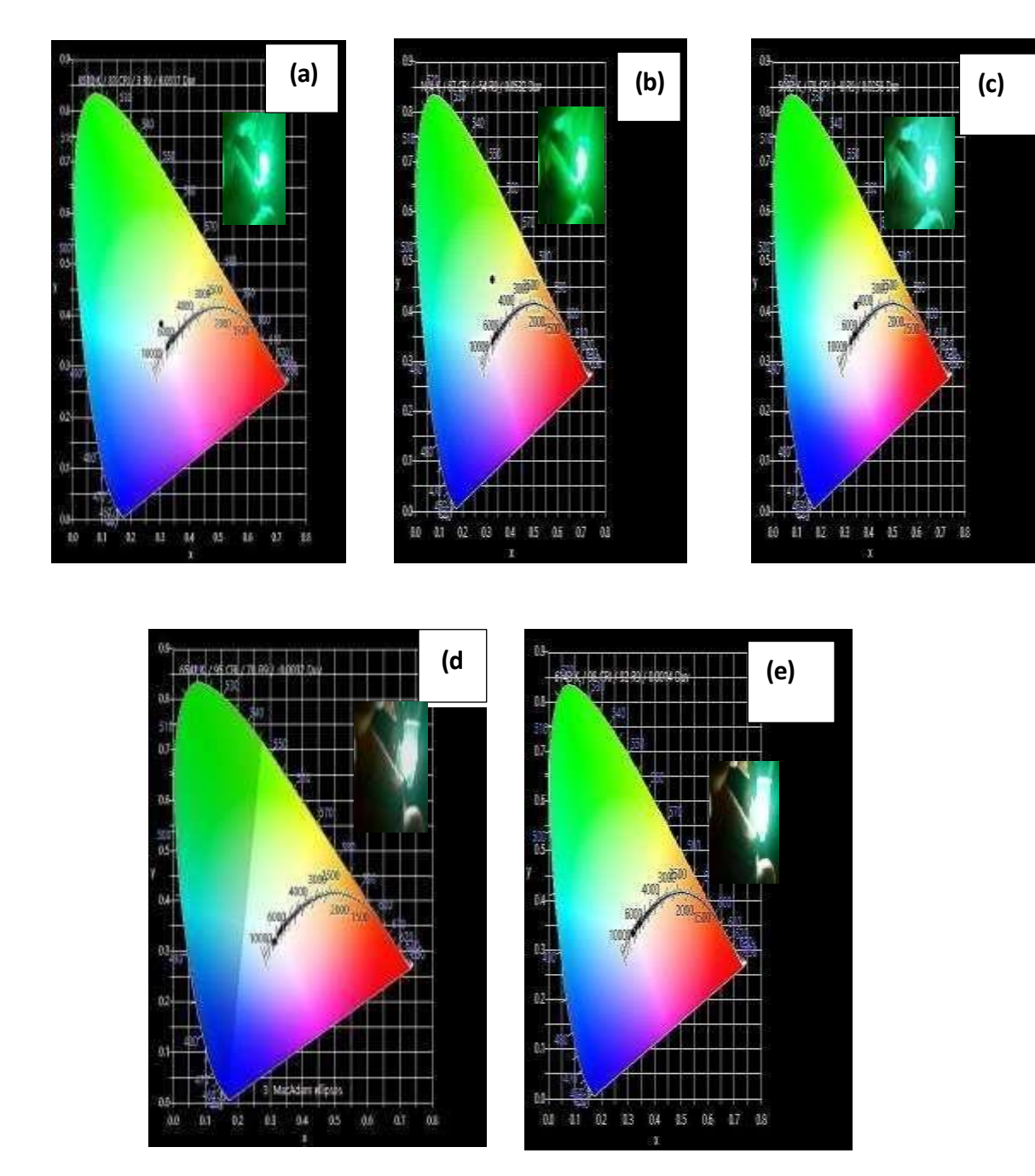


Figure 6.10[(a)-(e)]: Chromaticity diagram of Alq₃ thin film emitter layer of ITO/PEDOT: PSS/V₂O₅/Alq₃/LiF/Ag-based five OLED devices i.e., device1 to device5, with greenish-white light emission

1 is the lowest i.e., 81 which reduces to 67 for device 2. After that, the CRI value increases significantly with the rise in annealing temperature and reaches the value of 98

at 150°C. Between 150°C and 200°C no structural change occurs that's why CIE chromaticity measurement was not considered for our measurement. Similar changes happened in the case of the correlated color temperature (CCT) value. The CCT values of device1 to device5 are 6513 K, 5845 K, 5688 K, 6541 K, and 6143 K whereas the CRI values for device 1 to device 5 are 81,67,78,95 and 98, and R9 values are found to be 3,57,-27,78,92 respectively.

Table 6.3: Chromaticity diagram data of Alq₃ thin film emitter layer of ITO/PEDOT: PSS/V₂O₅/Alq₃/LiF/Ag-based five OLED devices i.e., device1 to device 5, with greenish-white light emission

Compound	CCT	CRI	R9	X	y	CIE coordinates	λemissi
							on
Alq ₃ thin film annealed at	6143 K	98	92	0.29891	0.32621	(0.2989, 0.3262)	0.8 nm
150 °C							
Alq ₃ thin film annealed	6541 K	95	78	0.3262	0.4348	(0.3262,0.4348)	28.6 nm
at 100°C							
Alq ₃ thin film annealed at 50°C	5688 K	78	-27	0.3474	0.4099	(0.3474,0.4099)	21.4nm
Alq ₃ thin film annealed at	5845 K	67	-57	0.3196	0.4555	(0.3196,0.4555)	0.6 nm
RT							
Alq ₃ thin film without annealed at RT	6513	81	3	0.3050	0.3828	(0.3050,0.3828)	9.2 nm

From this result, it is confirmed that Alq₃ thin film as well as bulk powder annealed at 150 °C is a solid-state lighting material or fluorescent electroluminescent emitter that gives cool white light which can be utilized in multidimensional practical applications. From the five pictures of CIE chromaticity diagram, it is clearly shown that due to growth of annealing temperature at first the green luminescence of without annealed Alq₃ sample changes its colour to greenish yellow then it turns into yellowish white and at 150°C it turns into whitish yellow where the tint of yellow is low and colour of white light is more. This is impressive findings that without using any

vacuum atmosphere proper encapsulation and sophisticated fabrication infrastructure still WOLED and all green and yellow OLED can be obtained varying concentration of dopants into pure and annealed Alq₃ sample.

6.3. Conclusion:

In this work, we have systematically studied structural dependent optical, electrical, and thermal properties of Alq₃ thin film by annealing it from room temperature to 200 °C. On thermal annealing from RT to 200°C, the Alq₃ changes its mer-isomeric phase from α to γ- phase. Between 100 and 150°C crystal size transforms from tetragonal to orthorhombic due to excess oxidation of 8Hq molecules and formation of oxide of 8Hq i.e., tris(8-hydroxy- N-oxide)aluminium(III), thus resulting in restructuring of the crystal size and losing the semi-porous structure of Al(OH)₃-Al₂O₃ structure on Alq₃ base and leads to the formation of non–emissive polymer, i.e.,8-hydoxyquinoline-Noxide (NEP) which exhibit excellent photoluminescence. The DSC curves confirm that the annealed Alq₃ maintains stability till 345 °C. The variation of growth temperature from 150 °C to 200 °C was found to exhibit red and blue shifts in fluorescence maxima. Based on this fact, an OLED device is demonstrated by stacking layers of PEDOT: PSS and Alq₃ which is annealed at 150 °C as this showed maximum luminescence with minimum chemical degradation and exhibiting maximum enthalpy change due to recrystallization and structure regaining 8-Hq ligand.

The fabricated OLED is found to perform well with EQE=1.488%. At 2.84 volts, our fabricated OLED exhibits the maximum current efficiency value of 3.89 cd/A. It shows a turn-on voltage of around 2.84 V for a luminance of 1cd/m² volt and the driving voltage for 1000 cd/m² is found to be around 4.3 volt. The performance of bi-layered ITO/PEDOT:PSS/V₂O₅/Alq₃/LiF/Ag-based OLED device opens an avenue where a WOLED as well as green OLED with simple architecture that can deliver stable photoluminescence and electroluminescence even in ambient atmospheric conditions. The device is found to exhibit greenish white luminance of 9689.2 cd/m² with CRI value=98, CCT value=6143 K., R9 value=92 and CIE coordinate (0.29891,0.32621) along with low turn-on voltage of 2.48 V, driving voltage of 7.92V, and low value of

HOMO and LUMO energy level which further enables the components as a promising ETL (electron transport layer) or HBL(hole blocking layer). All these properties and features suggest that this annealed Alq₃ polymer at 150°C is a very promising candidate as a solid-state WOLED or green OLED (organic light-emitting diodes) devices suitable for space, medical and optical communication applications. In this experiment we achieved our first research goal forming and fabricating a voltage tunable low voltage driven green whitish luminescence emitting OLED with annealed Alq₃ emitter, ETL, and PEDOT: PSS HTL. Ag (silver paste) cathode and ITO as anode. These OLEDs can be used in different devices.

References:

- [1] Tang, C. W., & VanSlyke, S. A. (1987). Organic electroluminescent diodes. *Applied physics letters*, 51(12), 913-915.
- [2] Chen, Y., & Ma, D. (2012). Organic semiconductor heterojunctions as charge generation layers and their application in tandem organic light-emitting diodes for high power efficiency. *Journal of Materials Chemistry*, 22(36), 18718-18734
- [3] Van Slyke, S.A., Chen, C.H., & Tang, C. W. (1996). Organic electroluminescent devices with improved stability. *Applied physics letters*, 69(15), 2160-2162...
- [4] Tang, C. W., VanSlyke, S. A., & Chen, C. H. (1989). Electroluminescence of doped organic thin films. *Journal of applied physics*, 65(9), 3610-3616..
- [5] Burrows, P. E., Gu, G., Bulovic, V., Shen, Z., Forrest, S. R., & Thompson, M. E. (1997). Achieving full-color organic light-emitting devices for lightweight, flat- panel displays. *IEEE Transactions on electron devices*, 44(8), 1188-1203.
- [6] Kim, S., Kim, D. H., Choi, J., Lee, H., Kim, S. Y., Park, J. W., & Park, D. H. (2018). Growth and brilliant photo-emission of crystalline hexagonal column of Alq3 microwires. *Materials*, 11(4), 472.

- [7] **Ki**m TS, Kim DH, Im H-J, Shimada K, Kawajiri R, Okubo T, Murata H, Mitani T (2004) Improved lifetime of an OLED using aluminum(III) tris (8-hydroxyquinolate).
- [8] Salleh, M. M., Hasnan, T., Azis, T., Sepeai, S., & Yahaya, M. (2007). Fabrication of organic light emitting diodes (oleds) for flat panel displays. *Berkala Ilmiah MIPA*, 17(3).
- [9] Debsharma, M., Pramanik, T., Daka, C., & Mukherjee, R. (2022, May). Recent advances in the electrical and optical properties of Alq3 and Alq3 derivatives based OLEDS. In *Journal of Physics: Conference Series* (Vol. 2267, No. 1, p. 012159). IOP Publishing.
- [10] Rajeswaran, G., Itoh, M., Boroson, M., Barry, S., Hatwar, T. K., Kahen, K. B., ... & Takahashi, H. (2000, May). 40.1: Invited Paper: Active Matrix Low Temperature Poly-Si TFT/OLED Full Color Displays: Development Status. In SID Symposium Digest of Technical Papers (Vol. 31, No. 1, pp. 974-977). Oxford, UK: Blackwell Publishing Ltd.
- [11] Thangaraju K, Kumar J, Amaladass P, Mohanakrishnan AK, Narayanan V (2006) Study on photoluminescence from tris-8-hydroxyquinoline aluminium thin films and influence of light. *Appl Phys Lett* 89:082106–3
- [12] Colle M, Gmeiner J, Miliu W, Hillebrecht H, Brutting W (2003) Preparation and characterization of blue-luminescent Tris(8-hydroxyquinoline)- aluminum (Alq3). *Adv. Funct. Mater.13(2)*, 108–112 (2003).
- [13] Cölle, M., & Brütting, W. (2004). Thermal, structural and photophysical properties of the organic semiconductor Alq3. *physica status solidi (a)*, 201(6), 1095-1115.
- [14] Xu MS, Xu JB (2005) Visualization of thermally activated degradation pathways of tris(8- hydroxyquinoline) aluminum thin films for electroluminescence application. *Thin Solid Films* 49:317–22
- [15] Kong H J, Park JW, Kim YM (2013) Integration of organic LEDs with

- inorganic LEDs for a hybrid lighting system. Semicond SciTechnol 28:015011
- [16] Wang M-H, Konya T, Yahata M, Sawada Y, Kishi A, Uchida T, Lei H, Hoshi Y, Sun L-X (2010) Thermal change of organic light emitting Alq3 thin films. *J Therm Anal Calorim* 99:117–2
- [17] Cölle, M., & Brütting, W. (2004). Thermal, structural and photophysical properties of the organic semiconductor Alq3. *physica status solidi (a)*, 201(6), 1095-1115.
- [18] Aziz, H., Popovic, Z., Xie, S., Hor, A. M., Hu, N. X., Tripp, C., & Xu, G. (1998). Humidity induced crystallization of tris (8-hydroxyquinoline) aluminum layers in organic light-emitting devices. *Applied Physics Letters*, 72(7), 756-758. small molecule-based organic light-emitting devices. *Science*, 283(5409), 1900-1902.
- [19] Bi, H., Zhang, H., Zhang, Y., Gao, H., Su, Z., & Wang, Y. (2010). Fac-Alq3 and Mer-Alq3 Nano/Microcrystals with Different Emission and Charge-Transporting Properties. *Advanced Materials*, 22(14),1631-1634https://doi.org/10.1002/adma.200903094
- [20] Cuba, M., & Muralidharan, G. (2015). Effect of thermal annealing on the structural and optical properties of tris-(8-hydroxyquinoline) aluminum (III)(Alq3) films. *Luminescence*, 30(3), 352-357
- [21] Mahakhode, J. G., Bahirwar, B. M., Dhoble, S. J., & Moharil, S. V. (2006). Tunable Photoluminescence from tris (8-hydroxyquinoline) aluminum (Alq3). *Proc of ASID, New Delhi*, 237-239.
- [22] Debsharma, M., Pramanik, T., Pramanik, G., Maity, A. R., Jain, A., & Mukherjee, R. (2024). Effect of growth temperatures on the structural and optical properties of bulk tris-(8-hydroxyquinoline) aluminium (III). *Applied Physics A*, 130(5), 281
- [23] Aziz, H., Popovic, Z. D., Hu, N. X., Hor, A. M., & Xu, G. (1999). Degradation mechanism of properties. *Advanced Materials*, 22(14), 1631-1634..

- [24] Higginson, K. A., Thomsen III, D. L., Yang, B., & Papadimitrakopoulos, F. (2004). Chemical Degradation and Physical Aging of Aluminum (III) 8-Hydroxyquinoline: Implications for Organic Light-Emitting Diodes and Materials Design. In *Organic Light-Emitting Devices: A Survey* (pp. 71-101). New York, NY: Springer New York.
- [25] Higginson, K. A., Zhang, X. M., & Papadimitrakopoulos, F. (1998). Thermal and morphological effects on the hydrolytic stability of aluminum tris (8-hydroxyquinoline)(Alq3). *Chemistry of Materials*, 10(4), 1017-1020
- [26] Papadimitrakopoulos, F., Thomsen, D. L., & Higginson, K. (2000, March). The Nature of Chemical Impurities Formed during Degradation o Aluminum (III)
 8- Hydroxyquinoline: Implications for Organic Light-Emitting Diodes. In APS March Meeting Abstracts (pp. E23-010).
- [27] Knox, J. E., Halls, M. D., Hratchian, H. P., & Schlegel, H. B. (2006). Chemical failure modes of AlQ3-based OLEDs: AlQ3 hydrolysis. *Physical Chemistry Chemical Physics*, 8(12), 1371-1377.
- [28] Panek, J. J., Błaziak, K., & Jezierska, A. (2016). Hydrogen bonds in quinoline N- oxide derivatives: First-principle molecular dynamics and metadynamics ground state study. *Structural Chemistry*, 27, 65-75.
- [29] Souza, A. D. V. D., Sousa, L. L. D., Fernandes, L., Cardoso, P. H. L., & Salomão, R. (2015). Al2O3–Al (OH) 3-Based castable porous structures. *Journal of the European Ceramic Society*, 35(6), 1943-1954.
- [30] El-Nahass, M. M., Farid, A. M., & Atta, A. A. (2010). Structural and optical properties of Tris (8-hydroxyquinoline) aluminum (III)(Alq3) thermal evaporated thin films. *Journal of alloys and compounds*, 507(1), 112-119.
- [31] Goldman, M., & Wehry, E. L. (1970). Environmental effects upon fluorescence of 5-and 8-hydroxyquinoline. *Analytical Chemistry*, 42(11), 1178-1185..
- [32] Brinkmann, M., Gadret, G., Muccini, M., Taliani, C., Masciocchi, N., & Sironi, A. (2000). Correlation between molecular packing and optical properties in

- different crystalline polymorphs and amorphous thin films of mer-tris (8-hydroxyquinoline) aluminum (III). *Journal of the American Chemical Society*, 122(21), 5147-5157
- [33] WangM-H, Konya T, Yahata M, Sawada Y, Kishi A, Uchida T, Lei H, Hoshi Y, Sun L-X (2010) Thermal change of organic light emitting Alq3 thin films. J Therm Anal Calorim 99:117–2
- [34] Kim, S., Kim, D. H., Choi, J., Lee, H., Kim, S. Y., Park, J. W., & Park, D. H. (2018). Growth and brilliant photo-emission of crystalline hexagonal column of Alq3 microwires. *Materials*, 11(4), 472.
- [35] Djurišić, A. B., et al. "Influence of atmospheric exposure of tris (8-hydroxyquinoline) aluminum (Alq 3): a photoluminescence and absorption study." *Applied Physics A* 78 (2004): 375-380.
- [36] Chatterjee, D. P., Pakhira, M., & Nandi, A. K. (2020). Fluorescence in "nonfluorescent" polymers. *ACS omega*, 5(48), 30747-30766
- [37] Wang MH, Sawada Y, Saito K, Horie S, Uchida T, OhtsukaM, Seki S, Kobayashi S, Arii T, Kishi A, Takahashi T, Nishimoto Y, Wakimoto T, Monzen K, Kashima I, Nishikiori T, Sun LX, Ozao R (2007) Thermal change of Alq3, tris(8- hydroxyquinolinato)aluminum(III) studied by Tg and XRD-DSC. J Therm Anal Calorim 89:363–66
- [38] Debsharma, M., Pramanik, T., Pramanik, G., Maity, A. R., Jain, A., & Mukherjee, R. (2024). Effect of growth temperatures on the structural and optical properties of bulk tris-(8-hydroxyquinoline) aluminium (III). *Applied Physics A*, 130(5), 281.
- [39] Saeed, A., Al-Buriahi, M. S., Razvi, M. A. N., Salah, N., & Al-Hazmi, F. E. (2021). Electrical and dielectric properties of meridional and facial Alq₃ nanorods powders. *Journal of Materials Science: Materials in Electronics*, 32, 2075-2087.
- [40] Bredas, J. L., Silbey, R., Boudreaux, D. S., & Chance, R. R. (1983). Chain-length dependence of electronic and electrochemical properties of conjugated

- systems:polyacetylene, polyphenylene, polythiophene, and polypyrrole. Journal of the American Chemical Society, 105(22), 6555-6559.
- [41] Shafiee, A., Salleh, M. M., & Yahaya, M. (2011). Determination of HOMO and LUMO of [6, 6]-phenyl C61-butyric acid 3-ethylthiophene ester and poly (3-octyl-thiophene-2, 5-diyl) through voltametry characterization. *Sains Malaysiana*, 40(2), 173-176.
- [42] Leonat, L., Sbarcea, G., & Branzoi, I. V. (2013). Cyclic voltammetry for energy levelsestimation of organic materials. *UPB Sci Bull Ser*

Chapter 7: Effect of ZnO nanoparticle on morphology and optical properties of polycrystalline yellow emissive Alq₃ for OLED application

Abstract:

We observe a distinct red shift of the electronic absorption band in a composite nanoparticle system consisting of wide band gap semiconductor ZnO grains embedded into tris(8-hydroxyquinolinato)aluminium (Alq₃) matrix and calcined at 50 °C. To investigate the morphology and optical properties, we prepared coordination complex Alq₃ by using wet synthesis method, with the absorption peak found to be at 358 nm at room temperature. For ZnO:Alq3 composites, it exhibits a lower energy band gap of 2.85 eV as compared to wide band gap ZnO nanoparticle (3.37 eV) and as-prepared bulk Alq₃ (2.89 eV). On illuminating with excitation wavelength of 385 nm, as-prepared Alq₃ shows a fluorescence band peaking at around 520 nm but with the increasing concentration of ZnO nanoparticles, it exhibits broad peaks which are found to be shifted to higher wavelengths. The composites show yellow colored emission at 548.7 nm wavelength which is an essential requisite condition for white colored OLEDs. Further, XRD, FESEM confirms the rod shaped ZnO nanoparticle get embedded and agglomerated onto Alq₃ surface resulting in an increase in structural volume (662.8 c.c.) compared to that of individual constituents 47.6 c.c for ZnO and 386.72 c.c. for Alq₃ powder. Experimental analysis suggests that incorporation of ZnO filler into Alq₃ matrix causes a significant improvement in the optical & structural properties as compared to pristine Alq₃, thus opening a room for futuristic OLED applications.

7.1 Introduction:

Organic Light Emitting Diodes (OLEDs) have become the center of attention among

researchers for developing next generation lighting and flat panel display appliances owing to their distinctive advantages like thin, transparent, roll-able, flexible and low-cost electronic gadgets. OLEDs have surpassed inorganic LEDs far away for their low cost, easy fabrication procedure, low operating voltage, tunable emission wavelength, higher thermal stability, excellent flexibility, low electricity consumption and excellent eco-friendly material properties [1,2,3,4,5].

The most desired electroluminescent organometallic compound used for optoelectronic materials is Tris(8-hydroxyquinolinato)aluminium (Alq₃) which has a vast application in areas of white light emitting diodes, solid state lighting, organic photovoltaic solar cells, organic light emitting transistors (OLETs) and many more [4,6,7]. Alq₃ is an organometallic n-type semiconducting chelate which has exquisite electron transport ability, blue-green luminescence, relatively longer stability and easy synthesis procedure compared to its inorganic counterparts [6,7,8]. Alq₃ possesses five crystalline phases namely α , β , γ . δ and ϵ , where α and γ are responsible for blue luminescence and rest of three phases are responsible for green luminescence under ultraviolet excitation on Alq₃ complexes [9,10,11,12,13,14].

VanSlyke and Tang [2] for the first time have reported their novel Alq₃ based OLED in 1987, and the demand towards the versatile application of Alq₃ in optoelectronic and electroluminescent devices has been increasing till today.[2] Although Alq₃ acts as ETL layer as well as an emissive layer of an OLED, research group of So and Fong [15] in 2006 have exhibited the hole transport properties of Alq₃ with low mobility under an applied field of approximately 1 MV cm⁻¹. On the other hand, in 2017, Derkowska and Zielinska reported that Alq₃ possesses two absorbance band i.e,. band-A and band-B which causes ligand oriented electronic shift in Alq₃[16,17]. Within the spectral range of 350-450 nm, A-band is found when firstly electronic transitions originate from ground energy state to excited energy state and secondly when charges are transferred from the oxygen containing quinolinolate ring to the nitrogen containing pyridyl ring that causes a π - π * transition of the qH₂⁺. The band-B can be visible within the spectral range between 210 nm and 280 nm. This is due to the central metal aluminium (Al) atom-containing p-band facilitates strong p- π * transitions and at the same time electrons

are shifted from 3p electronic orbital to π^* molecular orbitals [16,17]. However, the major shortcoming of Alq₃ and its derivatives are its lower chemical stability and often prone to photo-oxidation, thus leading to loss of consistent photoluminescence as well as electroluminescence on direct exposure to moisture, water-splash and atmospheric gases like oxygen, hydrogen, nitrogen. This limits the materials longevity and uncontrollably alters the properties in organic electroluminescent appliances like OLEDs, OLETs and solar OPV cells [18,19,20,21,22,23]. To overcome these hurdles, research groups have been focusing on hybrid Nanocomposite which consists of organometallic/inorganic hybrid structure. Interestingly, it is found to exhibit comparatively improved performance compared to pristine Alq₃ alone in charge mobility, mechanical stability, chemical stability along with their electroluminescence and photoluminescence efficacy etc. [7,8,9,10,11]. Moreover, inorganic /organometallic hybrid nano-composites is found to deliver an enhanced charge-carrier transportation which further improves the electro-optical properties and electronic properties of OLEDs and other opto-electronic devices[24,25,26,27,28]. Zinc oxide (ZnO) is a potential biocompatible inorganic n-type semiconducting metallic oxide for its outstanding electrical, optical, spintronic and photonic properties and promising applications in optoelectronics devices such as photodiodes, light emitting diode (LED), piezoelectric devices and ultra-violet lasers [29,30,31,32]. Further, non-toxic ZnO exhibits higher optical transmittance, excellent electron mobility, higher exciton binding energy of near about ~60 MeV and also exhibits direct band gap of ~3.37 eV at room temperature [29,30,31,32]

In our study, our goal is to develop flexible, lightweight, low-cost and wide range temperature-based hybrid or Nanocomposites that deliver an enhanced charge-carrier transportation which improves the electro-optical properties and electronic properties of OLEDs and opto-electronic devices. Here, we synthesized ZnO Nano-particles,

and ZnO/Alq₃ Nanocomposite in bulk form and characterized the samples at room temperature and normal atmospheric condition. It is found that when ZnO Nanoparticles are incorporated into as-prepared Alq₃, then the ZnO/Alq₃ Nano-composite shows a red shift in fluorescence spectra and slight blue shift in UV-Vis absorption

spectra along with reduced energy band gap as found from Tauc plot method when compared to pure ZnO Nano-particles and Alq₃, thus proves to exhibit better performance with respect to existing OLED materials. Through ZnO/Alq₃ Nanocomposite, we can further modify the electrical properties of ZnO incorporated Alq₃. We can convert the wide band gap semiconductor to narrow band gap semiconductor thus regulating the electroluminescence and photoluminescence on the basis of electron hole recombination rate in emissive layer of an OLED. This feature can be used to tune the colour of the emitted radiation from the emissive layer of an OLED. In this study we get yellow colored emission at 548.7 nm (yellow colour generally visible within 500-570 nm wavelength. [9,16,23,29,30] From our study on composites, we found that Alq₃ emits green photoluminescence at wavelength of 520.1 nm. Moreover, it is established that the fabrication of polymers like Alq₃ on ZnO NP or vice-versa improves the characteristics of a ZnO/Alq₃ Nanocomposites [29,30,31,32,33]. This suggests that if we attach electron donating or electron accepting substituents to quinolinolate ligand of Alq₃ we can maneuver the emission wavelength, optical band gap as well as color-tuning of emitted light from Alq3 and its complexes using chemical methods like doping, co-precipitation, sol-gel and wet exfoliation method [33,34].

7.2 Experimental Methods:

1. Synthesis of Zinc Oxide nanoparticles:

ZnO Nano-particles are synthesized through aqueous sol- gel method following Bolla G Rao et al (2017) [33]. At first 12.00 gm NaOH pellet were dissolved in 150 ml of distilled water and stirred for 5 minutes (Solution-A). Then 16.5 gm of zinc acetate di hydrate [Zn(CHCO)_{2.,2}H₂O] was dissolved in 100 ml distilled water and stirred for 5 minutes (solution-B). Then solution-A was mixed with solution-B to get solution-C. After that 150 ml of aqueous ethanol (C₂H₅OH) solution was added drop wise to the solution-C and heated at 80°C with continuous stirring for 15 minutes. After the complete reaction the white precipitate of zinc oxide (ZnO) Nanoparticle were obtained. This white precipitate was collected using filter paper and washed in distilled

water for 6 to 8 times and then allowed to be dried at room temperature. Then that white-coloured dried powder was scintillated at 450°C in an oven for 5 hrs. Finally, the scintillated ZnO Nano-particle powder was crushed into fine powder using mortar and pestle. Later on, that fine ZnO NP powder was utilized for our ZnO-Alq₃ composite-fabrication [33,34,35].

2. Synthesis of tris(8-hydroxyquinolinato) aluminium (Alq₃):

Electroluminescent material Alq₃ is synthesized through wet-synthesis method using the procedure reported by J.G. Mahakhode, et al. [35] where we deviated some steps keeping the original synthetic procedure intact on the basis of experimental needs as discussed earlier in the Chapter 4 & Chapter-6. Then that yellow precipitate of mer- Alq₃ was filtered and washed 8-10 times with warm water. Then, the yellow green precipitate was heated to 60°C for 2 hours. The dried yellow –green colored Alq₃ powder was then crushed into fine powder using a mortar pestle and a crucible pot. That fine yellow green powder of Alq₃ was used for our ZnO/Alq₃ Nano-composite formation.

3. Fabrication of Alq₃/ZnO Nanocomposites:

Zno/Alq₃ Nanocomposites were fabricated through a novel and low-cost easy procedure via solution intercalation and exfoliation adsorption method [30,31,32]. At first, 0.50 gm of Zinc oxide Nanoparticle (ZnO NP) was added in the mixed solution of 10 ml distilled water and 10 ml ethanol (C₂H₅OH) solution (taken in 1:1 volumetric ratio) with stirring for 20 minutes and was thereafter ultra-sonicated for 30 minutes. An opaque white solution was formed (solution -G). Then 0.50 gm of Alq₃ powder was mixed with 10 ml of ethanol (C₂H₅OH) and 10 ml of distilled water and stirred for 20 minutes and then ultra-sonicated for 30 minutes. A yellow-green opaque solution (solution-H) was obtained. After that, solution-G was added into Solution-H and the resulting mixture (solution-I) was then again ultra-sonicated in sonication bath for 4 hours. A light white mixed green-yellow precipitate was obtained at the bottom of the transparent colorless solution. The excess liquid was decanted and then allowed the viscous yellow white solution in a water-bath with heating at 50 °C for 8 hours and then

left it in open air at room temperature over-night to settle down and to dry. Then dried yellow ZnO/Alq₃ (1wt%:1wt% ratio) Nano-composite powder is finally formed which were collected and crushed into fine powder with the help of crucible pot and a mortar and pestle. In another attempt we filtered the yellow-white solution using filter paper and the yellow-white precipitate was collected over filter paper. The yellow precipitate was collected in a petri dish and allowed to be dried overnight. Then the dried powder was heated at 50 °C for 2 hours to remove moisture absorbed in it. Finally, the dried powder was collected and crushed into fine powder using mortar and pestle. [30,31,32]

7.3 Results and discussion:

A. Structural and morphological Study:

1. X-Ray Diffraction spectroscopy:

From the XRD spectroscopy aided by Bruker Xray Diffraction Spectrometer, it is namely (100), (102),(110) at 2θ =30.1°, 45.2°, 53.2° (PDF pattern 01-080-7100). Along with it, two sharp peaks are found in the XRD of the bulk Alq₃ having crystallographic plane at (011) (121) at 2θ =10.6°, 18.3° (PDF pattern 26-1550) while intense sharp peaks are found having crystallographic plane of (100), (102), (110) and (011), (121) at clearly observed that ZnO Nano-particle has distinct sharp intense peaks namely (100), 2θ =11.1°, 17.6° 19.2° and 2θ = 24.1°, 26.1° (PDF pattern 00-049-2409) respectively which clearly convince the incorporation of ZnO Nano-particle into Alq₃, thus

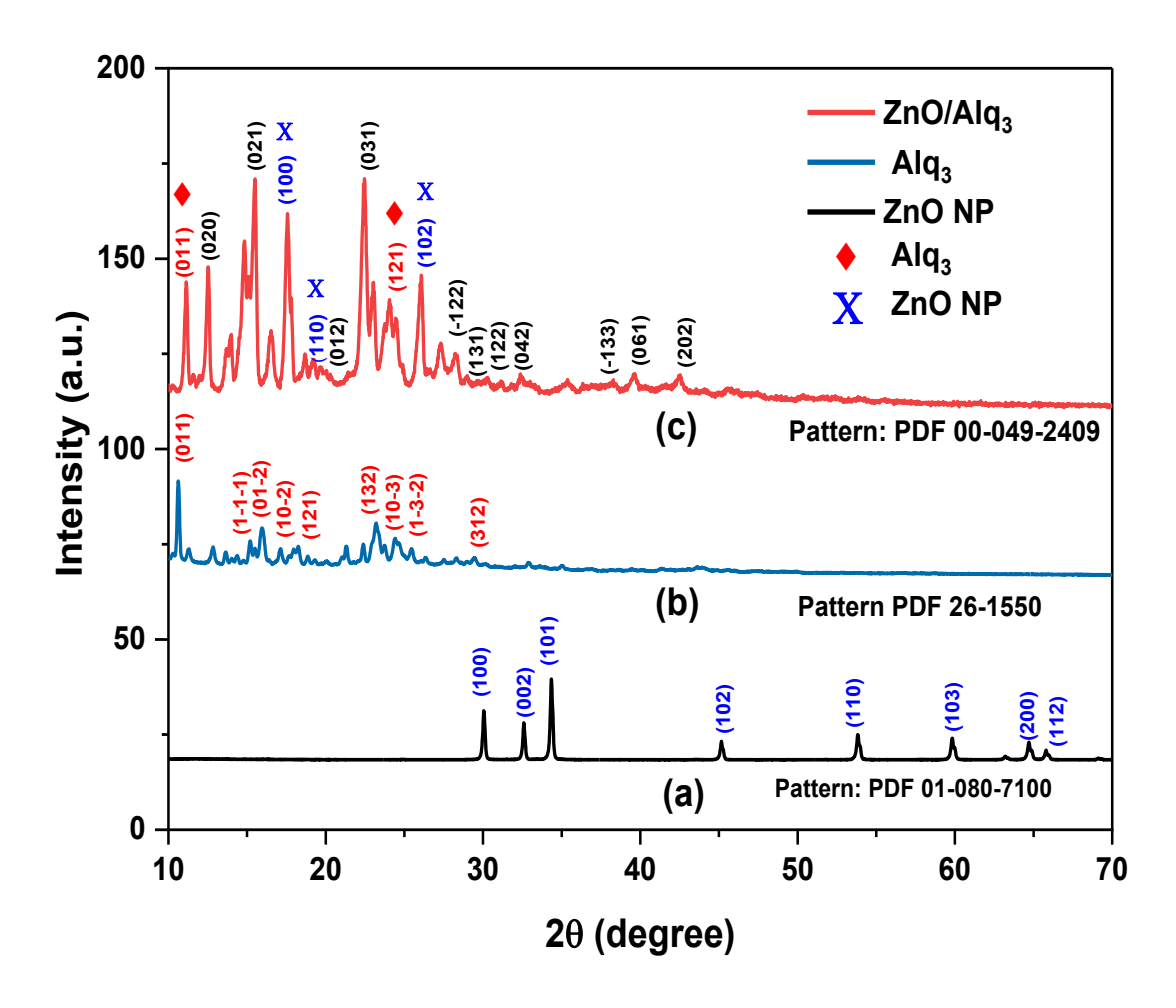


Figure7.1: XRD spectroscopy of (a) ZnO nanoparticles (b) Bulk Alq₃ powder and (c)ZnO:Alq₃

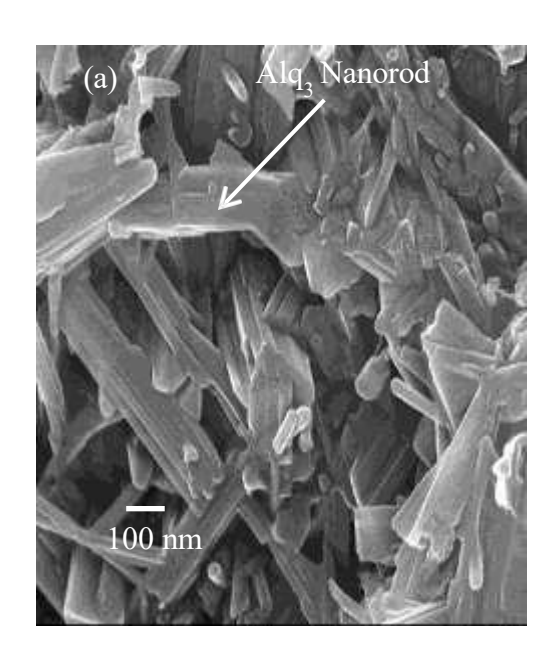
 2θ =11.1°,17.6° 19.2° and 2θ = 24.1°, 26.1° (PDF pattern 00-049-2409) respectively which clearly convince the incorporation of ZnO Nano-particle into Alq₃, thus formation of ZnO:Alq₃ Nano-composite system. The intensity of sharp peaks explains the newly formed Nano-composite system which exhibits different physical and chemical properties compared to its individual components, i.e., Alq₃ and ZnO Nano-particles. [22,29,30,31,32].

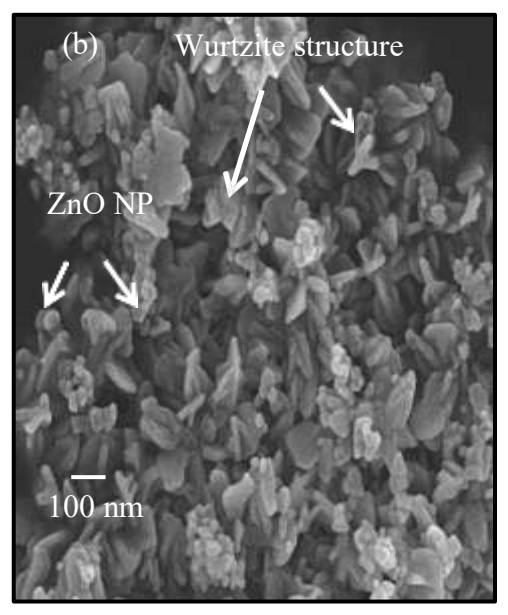
Table 7.1: Structural comparison table for Alq₃, ZnO NP, ZnO /Alq₃ Nanocomposites

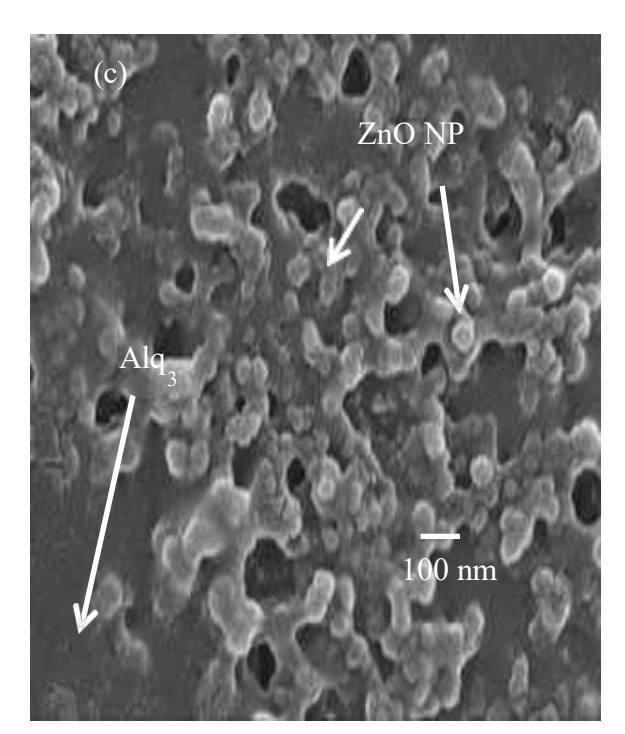
Sample Name	Lattice	Lattice Parameter	Volume	Mol. wt.
		(A°)	(c.c.)	(gm/mol)
Alq ₃	polycrystalline	a=10.3, b=13.7, c=8.2	386.72	459. 4
	triclinic			
ZnO NP	Hexagonal	a=3.2, b=13.9, c =5.2	47.6	81.4
	Wurtzite			
ZnO/Alq ₃	Monoclinic	a= 5.1, b=13.9, c=9.44	662.8	142.2
Nano- composites				

3.FESEM (Field Emission Scan Electron Microscopy) spectroscopy:

From FESEM image aided by JEOL Field Emission Scan electron microscope of Figure 7.2(a) it is clearly observed that bulk Alq $_3$ powder possesses semi-porous polycrystalline triclinic lattice and hexagonal stacked Nano-rod like layers. Figure 7.2(b) also confirms the hexagonal and spherical wurtzite structure of ZnO Nano-particles where two hexagonal planes are intersected with each other having a=3.2 A $^{\circ}$, b=13.9 A $^{\circ}$, c=5.2 A $^{\circ}$. From figure 7.2(c) it is clear that hexagonal monoclinic layered structures are formed when spherical ZnO nanoparticles are incorporated into the base of Alq $_3$. The FESEM images thus show the conformity with the XRD spectral images and peaks [22,29,30,31,32]. In figure 7.2 (a) we clearly observe the fine hexagonal nanorod structure of pure bulk mer-Alq $_3$ powder , but when hexagonal wurtzite structure of zinc oxide nanoparticle is doped into Alq $_3$ host matrix the whole structure becomes monoclinic From figure 7..2(C) it is clearly seen that ZnO nanoparticles lose their wurtzite structure and granular partially semi hemispherical or capsule like structure remain embedded into the diffused Alq $_3$ structure. Incorporation of ZnO nanoparticles are distinctly proves about the making of ZnO/Alq $_3$ nanocomposites







0.1 **Figure 7.2:** FESEM images of (a) Pure Alq₃ Nanorod powder (b) ZnO Nanoparticle (c)

 $0.2~wt~\%~ZnO~/Alq_3~nanocomposites$

B.Optical property study:

1. Ultra-Violet Visible (UV-VIS) absorbance spectroscopy:

The absorption spectra of ZnO Nano-particles, as-prepared Alq₃ and ZnO/Alq₃ nano-composites are illustrated in Figure 7.3.

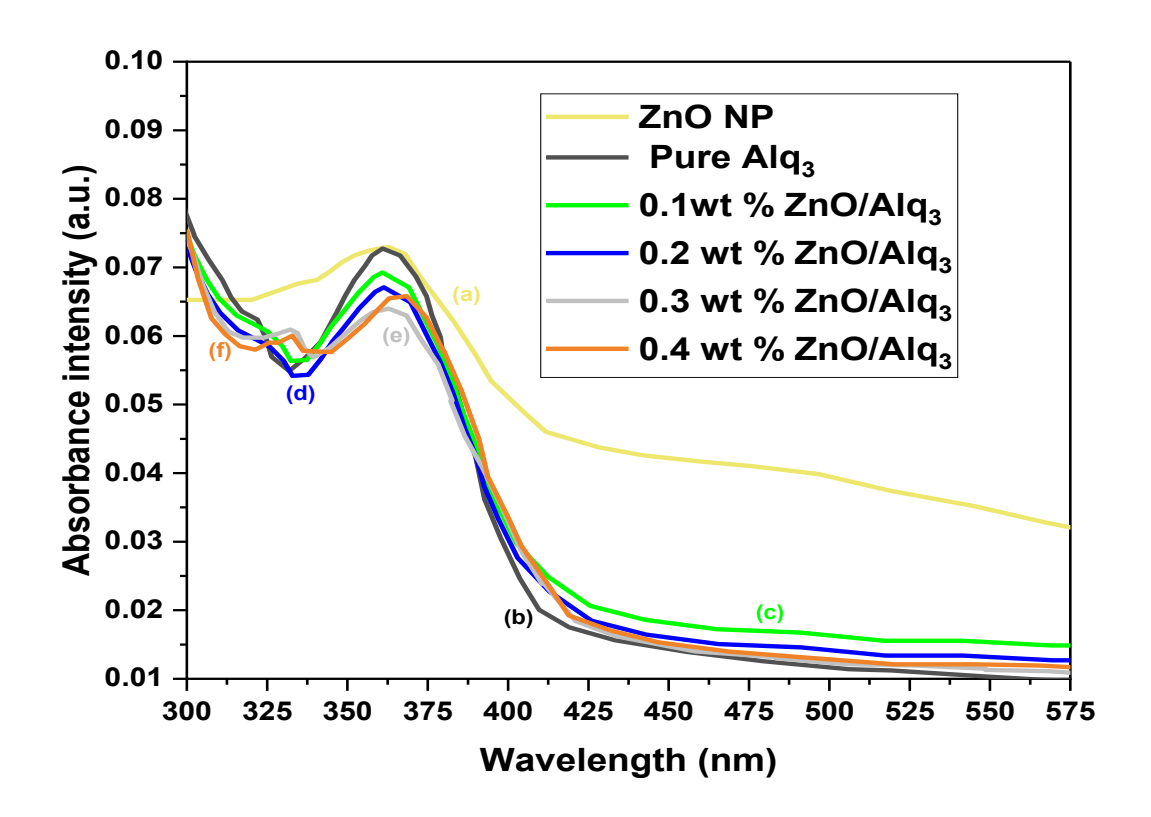


Figure 7.3: UV–Vis spectroscopy of (a) ZnO-NP (b) Alq₃ powder (c) 0.1wt % ZnO/Alq₃ Nanocomposites (d) 0.2wt % ZnO/Alq₃ Nano-composites (e) 0.3wt % ZnO/Alq₃ Nanocomposites (f) 0.4 wt % ZnO/Alq₃ Nanocomposites

The highest and strongest peaks of the absorption spectrum of ZnO Nano-particles, Alq₃ and 0.1 wt % ZnO/Alq₃ Nanocomposites are seen at the wavelength of 362.7nm, 361.0 nm and 360.9 nm respectively. The absorption peaks at 362.7 nm and all peaks within the range of 330 nm and 400 nm are formed due to the π - π * transitions of quinolinolate ligands of Alq₃[22,29,30]. When ZnO incorporates into Alq₃, it is clearly seen that the

intense peaks of ZnO NP at 362.7 nm blue shifts to 360.9 nm and intense peaks of Alq₃ at 361.0 nm blue shifts to 361.0 nm. But this comparison spectra validates that ZnO Nano-particles have indeed embedded into the host Alq₃ matrix... The other possible reason for this peak-shift is the alteration of direct energy band—gap that takes place on the Alq₃ surface that results in blue shifts for both ZnO NP and pure Alq₃;

This energy band gap of the materials can further be ascertained by Tauc plot method and by applying the under mentioned equation:

$$(\alpha h v) = (h v - Eg)^n \tag{7.1}$$

Where n is $\frac{1}{2}$ for allowed direct transitions, and n=2 for allowed indirect transitions α =absorbance coefficient, h=Planc's constant, ν =frequency of absorbed radiation, E_g =energy band gap [29,30]..

The direct band gap of pure Alq₃ powder at room temperature is 2.89 eV which is consistent with the erstwhile reported work whereas the direct and wide energy band gap for ZnO Nano-particle is found to be 3.37 eV. Nevertheless, when ZnO is incorporated into pure Alq₃, the wide band gap of the ZnO in the composite system is reduced from 3.37 eV to 2.85 eV and from 2.89 eV to 2.85 eV for pure Alq₃ Hence, the energy band gap of Alq₃ or ZnO can be tuned by incorporation of ZnO into pure Alq₃ powder. From figure 3, we can analyze the change in absorbance intensity due to the increase in ZnO NP wt% concentration compared to the absorbance intensity of pure Alq₃, pure ZnO NP and hybrid 0.1 - 0.4 wt% ZnO/Alq₃ Nanocomposites. The intense absorption peaks are red shifted from 360.9 nm (for 0.1 wt% ZnO/Alq₃) to 361.3 nm (for 0.2 wt% ZnO/Alq₃) and then it started to increase in absorbance intensity as it red shifted from 361.3 nm (0.2 wt% ZnO/Alq₃) nm to 362.9 nm (0.3 wt% ZnO/Alq₃) and then again red shifted for the increase in the absorbance intensity from 362.9 nm(0.3 wt% ZnO/Alq₃) to 368.5 nm (0.4 wt% ZnO/Alq₃). From Tauc plot of Figure 7.4 B we can observe that the wide Optical band gap of ZnO (3.37 eV) and Alq₃ (2.89 eV) are lowered to 2.85 eV. This confirms that the incorporation of ZnO NP can tune the band gap of Alq₃ by making hybrid Nanocomposite of ZnO NP and Alq₃ molecules.

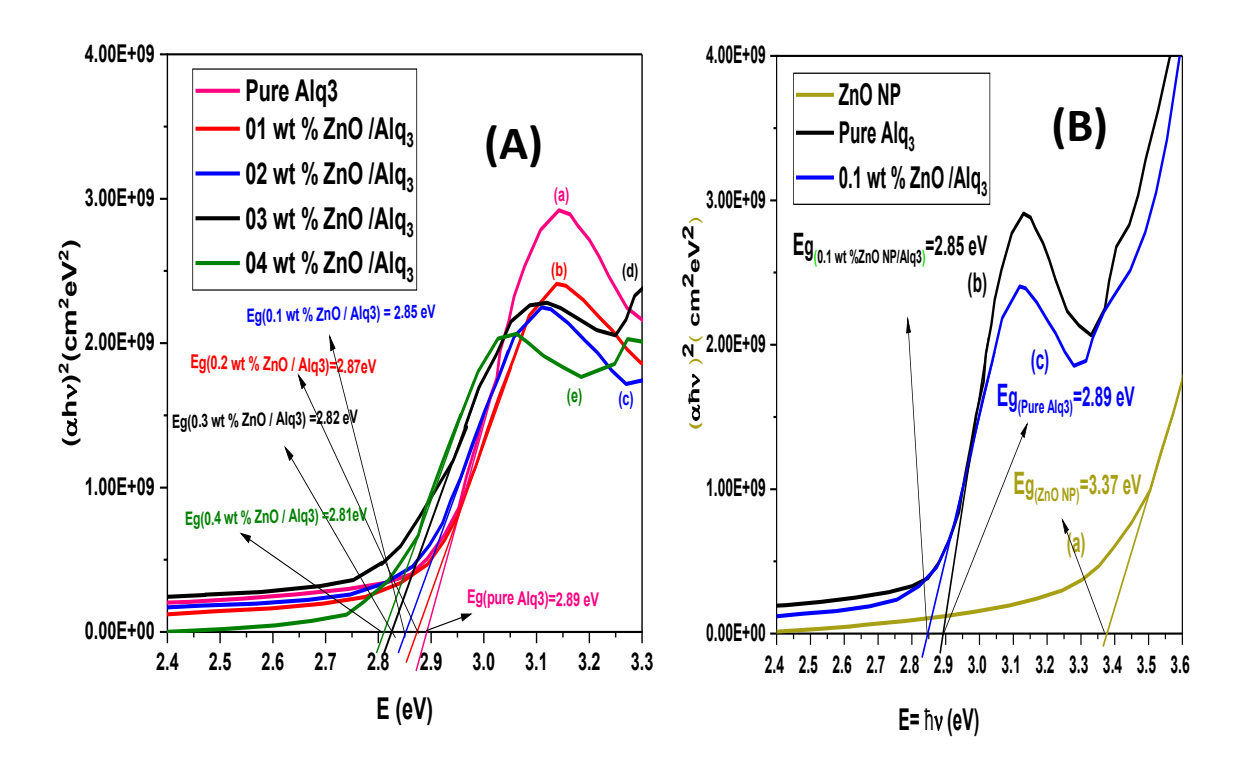


Figure 7.4:(A) Tauc plot of (a) Alq₃ powder (b) 0.1wt % ZnO/Alq₃ Nanocomposites (c) 0.2wt % ZnO/Alq₃ Nanocomposites (d) 0.3wt % ZnO/Alq₃ Nanocomposites (e) 0.4 wt % ZnO/Alq₃ Nanocomposites (B) Tauc Plot of (a) ZnO Nano-particles (b) pure Alq₃ powder (c) 0.1 wt % ZnO/Alq₃ Nanocomposites

From the absorbance spectra of Figure 7.4(A), Tauc plot of 7.4(B) and Table 7.2, it is clear that when ZnO concentration weight % are increased from 0.1% to 0.2% the optical band gap (Eg) increased to 2.87 eV but it drastically starts to lowering down to 2.82 eV for 0.3 wt% and it reduces to the lowest optical band gap value of 2.81 eV for 0.4 wt% of ZnO NP. These results prove that composite can maneuver the optical properties, especially the can be controlled with variable concentrations of inorganic semiconductor ZnO NP into another wide band-gap organic semiconductor Alq₃ and yielded a comparatively narrow bandgap containing ZnO/Alq₃ Nanocomposites [22,29,30]

.

Table 7.2: comparative study of optical band gap with respect to concentration increase of Zno NP within Alq₃

Sl. No.	Name of the samples	Maximum absorption peaks found at	Optical band gap Eg (in eV)
1.	ZnO NP	362.7 nm	3.37 eV
2.	Alq ₃	361.0 nm	2.89 eV
3.	0.1 wt% ZnO/Alq ₃ nano composites	360.9 nm	2.85eV
4.	0.2 wt% ZnO/Alq ₃ nano composites	361.3 nm	2.87 eV
5.	0.3 wt% ZnO/Alq ₃ nano composites	362.9 nm	2.82 eV
6.	0.4 wt% ZnO/Alq ₃ nano composites	368.5nm	2.81 eV

2. Fluorescence spectroscopy:

From the fluorescence spectroscopy aided by PERKIN EILMER fluorescence-spectrometer, we can distinctly determine that ZnO Nano-particle exhibits highest intense peaks at 512.3 nm. The intense green photoluminescence intense peak of Alq₃ is seen at the wavelength of 520.1 nm which is in agreement with the result of mostly published reports so far (~520 nm). Thus, for ZnO NP, the blue shift of green

photoluminescence is observed. The higher intense peaks for 0.1 wt % ZnO/Alq₃ is obtained at 538.1 nm which results in red shift of green photoluminescence of Alq₃[22,39,30].

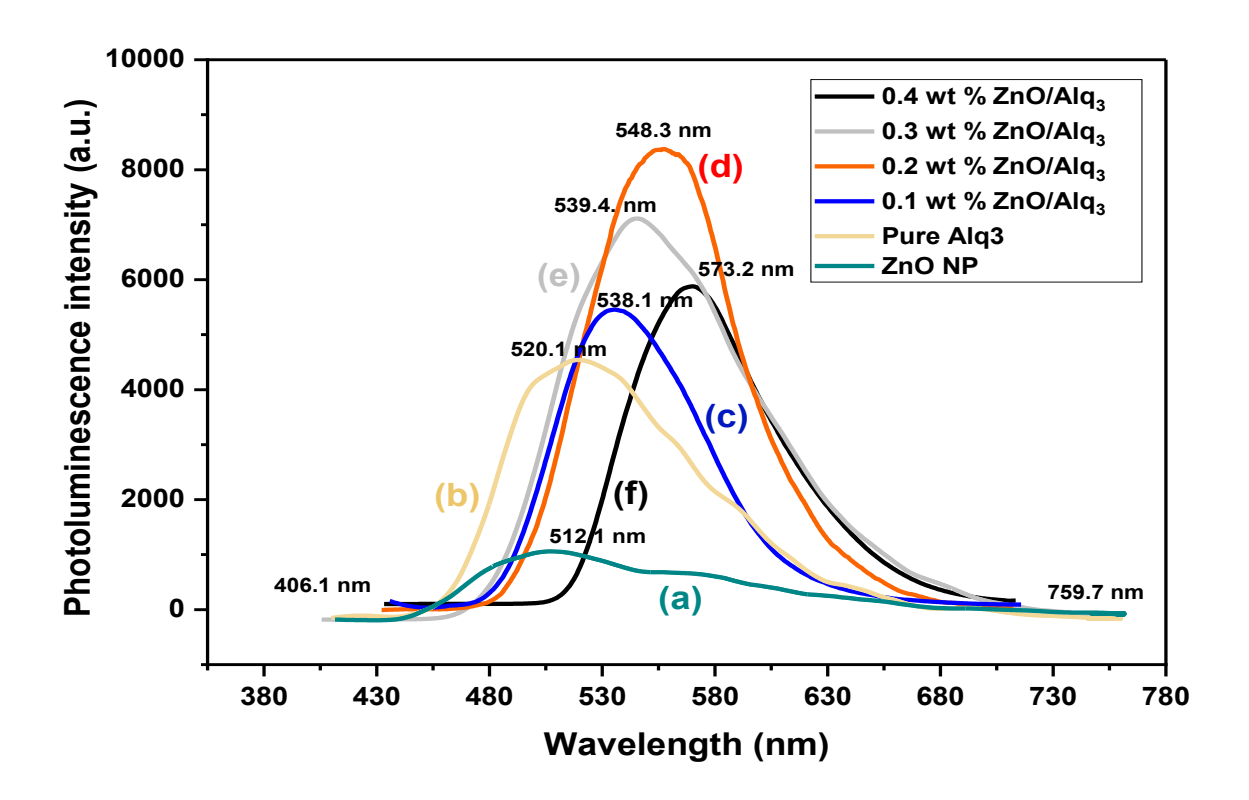


Figure 7.5: Fluorescence spectroscopy of (a) ZnO Nano-particle (b) Alq₃ and (c) 0.1 wt% ZnO/Alq₃ Nanocomposites (d) 0.2 wt% ZnO/Alq₃ Nanocomposites(e)0.3 wt% ZnO/Alq₃ Nanocomposites(c) 0.4 wt% ZnO/Alq₃ Nanocomposites

The other intense peaks are 548.3 nm for 0.2 wt% ZnO/Alq₃ Nanocomposites ,539.4 nm for 0.3 wt% ZnO/Alq₃ Nanocomposites and 573.2 nm for 0.4 wt% ZnO/Alq₃ Nanocomposites. The highest peaks are 548.3 nm. Above of this range red shifting and lower than this blue shift of absorbance intensity occurs.

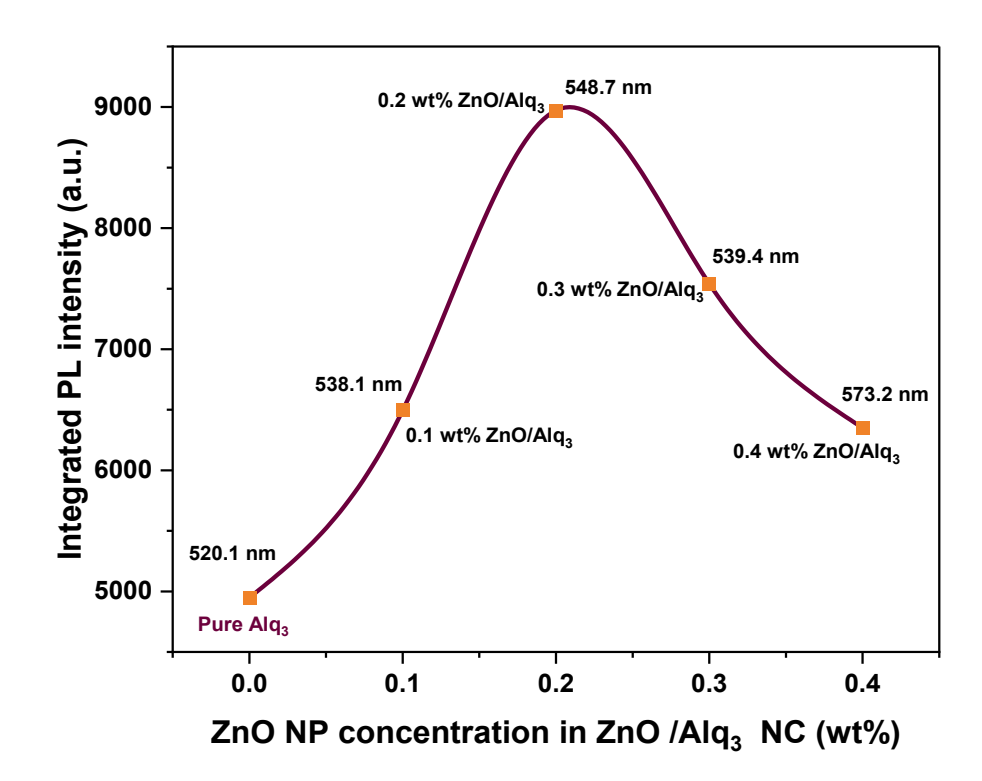


Figure 7.6: Integrated PL peak- intensity variation curve (λ_{ex} =385 nm) for variable ZnO NP concentration (weight percentage or wt%) incorporated over Alq₃ molecules in ZnO/Alq₃ Nanocomposites

In figure 7.6 the changes in integrated PL intensity with respect to different weight percentages of ZnO NP concentration are clearly described in a nutshell. The integrated PL intensity curves are seen within the wavelength beginning from 520.1 nm to 573.2 nm. The emission intensity increases firstly from 520.1 nm (for pure Alq₃) to 538.1 nm (for 0.1 wt % ZnO /Alq₃) and then it reaches its maximum intensity at 548.7 nm (for 0.2 wt % ZnO /Alq₃). Thereafter, the integrated PL intensity starts to lower down drastically at the wavelength 539.4 nm (for 0.3 wt % ZnO /Alq₃) and then reaches 573.2 nm (for 0.4 wt % ZnO /Alq₃). This result proves that up to 0.2 wt % ZnO concentration integrated PL intensity results in higher photoluminescence whereas in between 0.2 wt % and 0.4 wt % integrated PL intensity begins to quench [22,29,30].

3. Fourier Transform Infrared Spectroscopy:

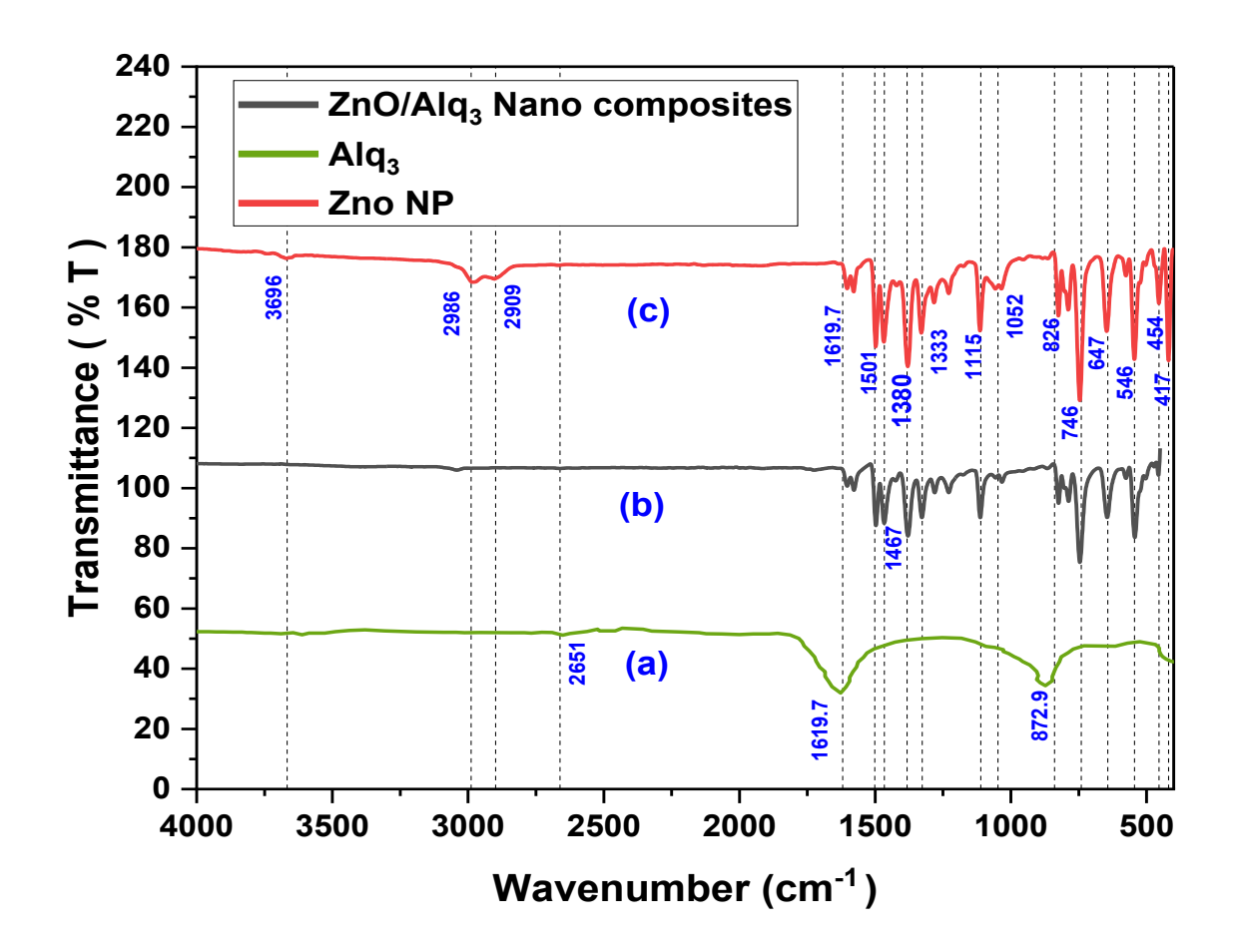


Figure 7.7: FTIR spectroscopy image of (a) ZnO NP (b) Alq₃ powder (c) ZnO/Alq₃ Nano composites

From the FTIR spectroscopy aided by PERKIN EILMER IR spectrometer as shown in figure 7.7, it is clear that most of the intense peaks are found within the range between 417 cm⁻¹ and 1619.7 cm⁻¹. The FTIR characteristics peaks are due to vibration modes of Alq₃, ZnO NP and ZnO/Alq₃ NPs which are observed within 400-800 cm⁻¹. Vibrations of aromatic quinoline rings are detected within 400-600 cm⁻¹ and vibration of quinolinolate ligand and Al³⁺ cation (Al-O bond stretching) are seen within 600-800 cm⁻¹. The weak

intensity peaks due to vibrational stretching non bonded O-H stretch for hydroxyl functional group are found at 3696 cm⁻¹ which is due to presence of moisture or H₂O molecules in the samples under experiment. Moreover, C-C bonding of aromatic rings and pyridine and benzene ring or quinolinolate ligands are also found at 2986 and 2909 cm⁻¹ respectively. Different stretching vibrations of (i) C-N-C bond among central Al(III) atoms and three quinolinolate ligands are observed at 1501, 1467, 1380 and 1333 cm⁻¹(ii) C-O bond between benzene rings and deprotonated hydroxyl functional group (OH) of 8-Hq are found at 1115 and 1052 cm⁻¹, (iii) aromatic amines are seen at 1467 and 1380 cm⁻¹ (iv) aromatic C=C bond of pyridine and benzene ring are observed at 1619.7 and 1611 cm⁻¹, (v) C-H bond at 826 and 746 cm⁻¹, (vi) short height Al-O-Al bond are seen at 748 cm⁻¹, (vii) Al-O bond are witnessed at 546, 647 cm⁻¹. and (viii) Al-N bonds are found at 454 and 417 cm⁻¹. The weak intensity peaks at 2986 and 2909 cm⁻¹ are due to vibrational stretching of O-H bond which in turn is due to presence of minute amount of moisture of H₂O molecules in all the samples under measurement. Lu et al [36] reported that Zn-O vibration bands are found within the region between 400 cm⁻¹ and 500 cm⁻¹. The stretching vibrations at 417 and 454 cm⁻¹ are obtained due to vibration of Al³⁺ cation, quinolinolate (C₆H₅NO⁻) anion, Al-N bonds and Zn-O bonds of metal oxides which is in conformity with the report of Xia Lu et al [36]. Al-O bond of metal oxides is found at 546, 647 cm⁻¹ and Al-O-Al bonds are visible at 748 cm⁻¹. These peaks confirm the existence of Alq₃ and ZnO NPs within the ZnO/Alq₃ Nanocomposites. The intense peaks of ZnO NP at 1619.7 cm⁻¹ and intense peaks of Alq₃ at 826 cm⁻¹ are clearly witnessed in FTIR of ZnO/Alq₃ which signifies that ZnO NP remain embedded into the Alq₃ surface, which is also accords with the result of XRD, FESEM. The higher peaks of ZnO/Alq₃ nanocomposites compared to pure Alq₃ are also due to nanocomposite surface where semi spherical ZnO NP remains embedded and erected from Alq₃ surface from where higher intensity transmittance occurs [22,29,30,36].

B. Electroluminescence and device performance study:

Based on the result obtained from previous chapter I also tried to fabricate a ZnO nanoparticle incorporated Alq₃ emitter matrix-based OLED and characterize its electric properties, especially electroluminescence and device performance. The noteworthy

matter is I used 0.3 wt% ZnO nanoparticle for doping into Alq₃ emitter matrix. The reason was Alq₃ annealed at 150°C and 0.3 :1 wt% ratio of ZnO /Alq₃ nanocomposites exhibit the

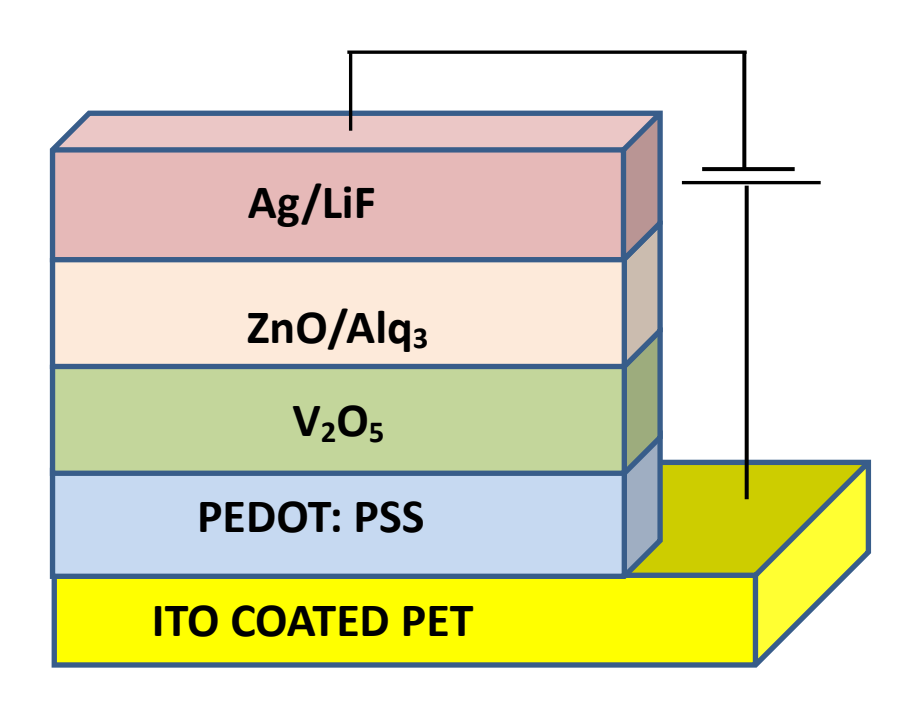
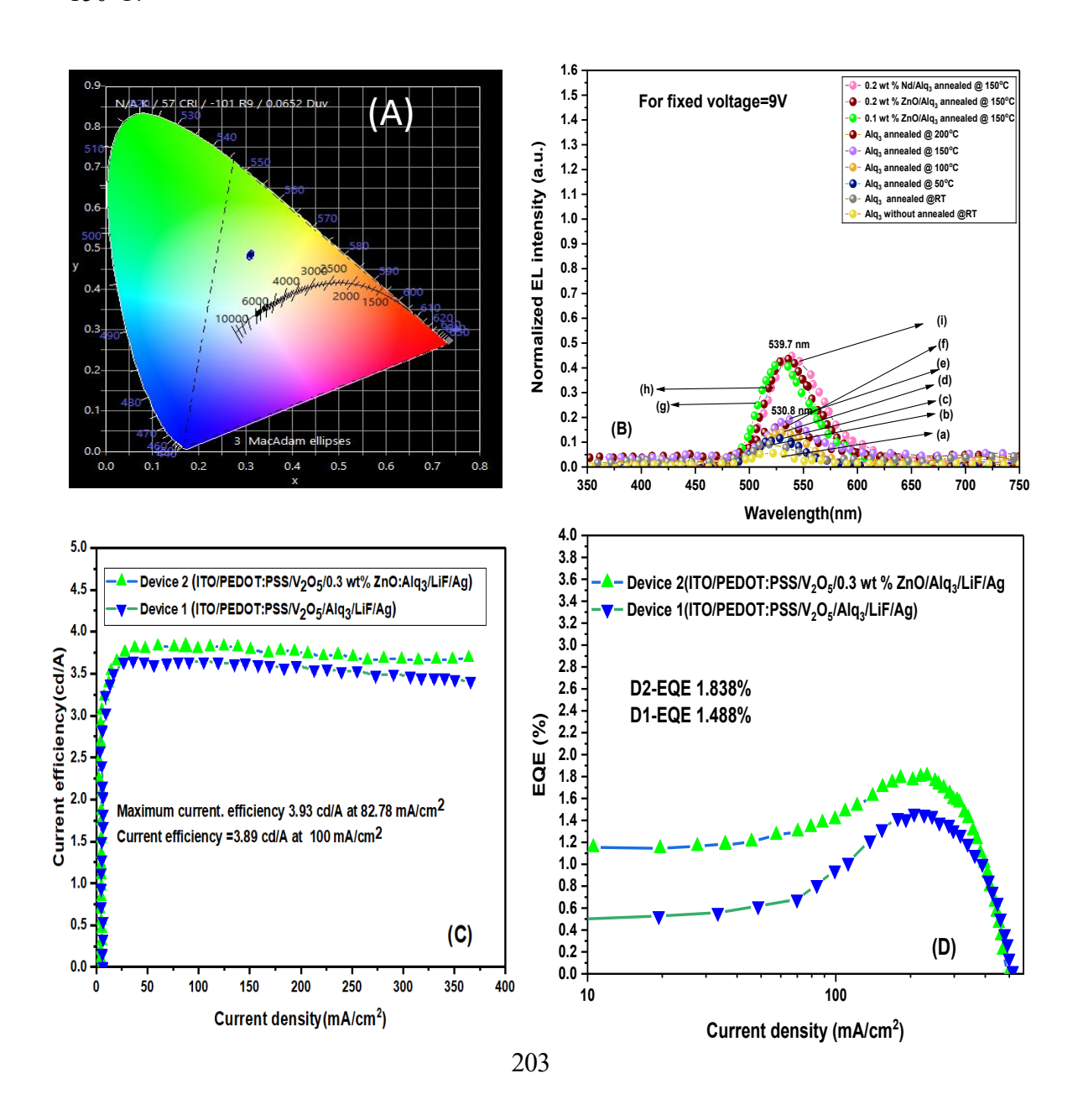


Figure 7.8: Stacked architecture of ZnO/Alq₃ nanocomposites- based OLED

highest magnitude of Absorbance intensity and Alq₃ both acted as ETL and HTL of OLED gives maximum photoluminescence when it is annealed at 150°C under ambient condition in a hot air oven ranging from room temperature to 200°C. We also fabricated an un optimized OLED without employing any sophisticated instruments such as vacuum, argon or nitrogen gas driven atmosphere, robust encapsulation. Our aim was to form a high temperature and high voltage or high current compatible which can be operational at low turn-on voltage as well as would be economical, rollable, durable, stable, longer lifespan and less prone to luminous quenching due to chemical failure, ageing, higher current, corrosion etc. We found that our fabricated device performed excellent exhibiting a low turn -on voltage, higher current efficiency, power efficiency. As Alq₃ itself is a highly fluorescent, it uses emissive singlet exciton mostly for photon

generation. This results in low EQE %. From date obtained table 7.3 and 7.3, we found that our unoptimized 0.3 wt % ZnO/Alq₃ nanocomposites emitter based OLED exhibit a higher current efficiency 3.93 higher cd/A, EQE % of 1.838 % compared to 1.488% of annealed Alq₃ and higher power efficiency of 31.1 lm/W, higher current density of 365.3 A/m² which is along with low turn-on voltage of 2.81 volt and driving voltage is 5.93V and higher luminance of 10956 cd/m² at 10.9 volt. Which is more enhanced device performance compared to the OLED formed with Alq₃ powder emitter annealed at 150°C.



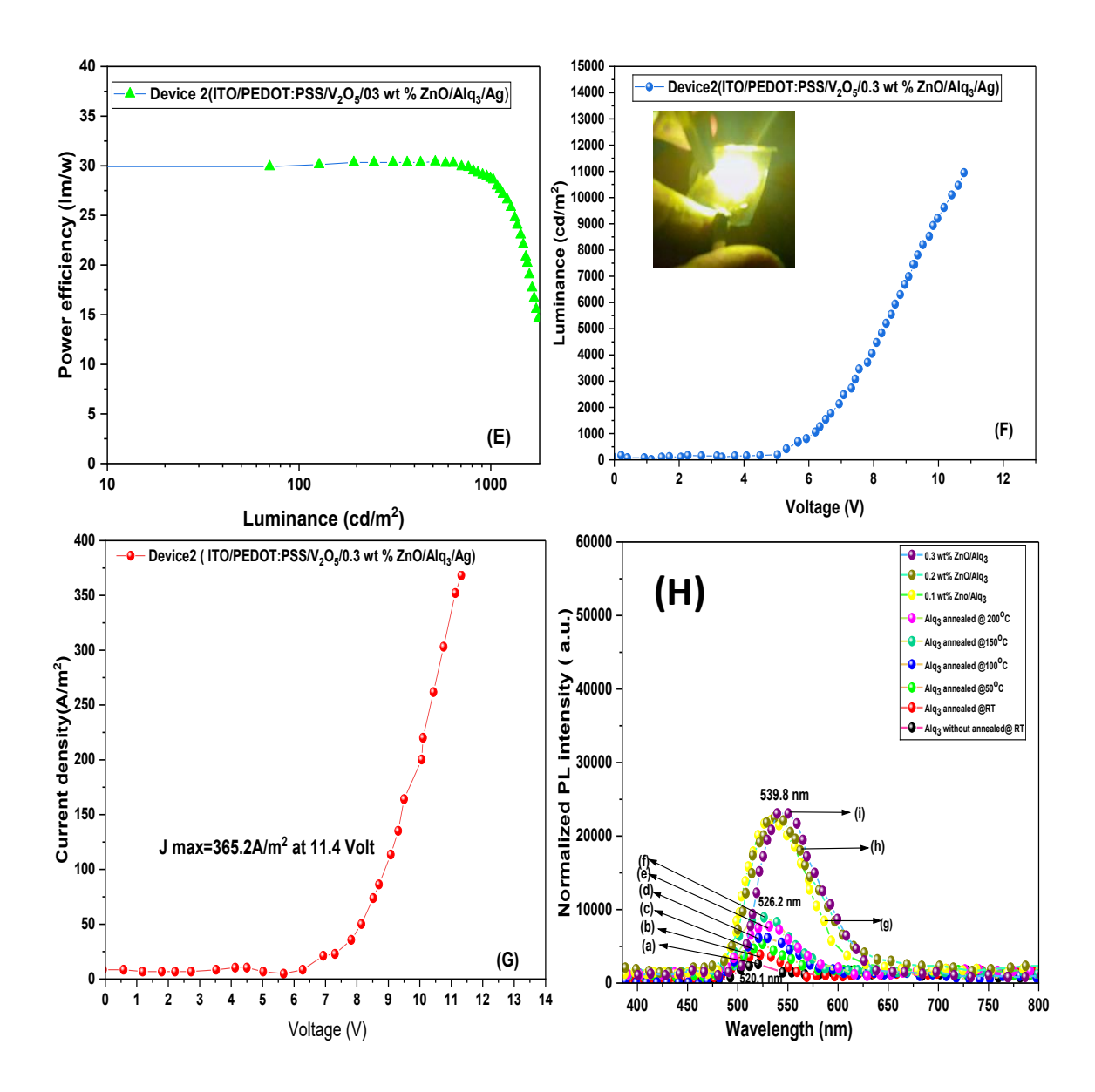


Figure 7.9: (A)chromaticity diagram (B)normalized EL intensity -wavelength plot) (C)Current efficiency vs. current density (η_{c} -J) plot (D) External quantum efficiency vs. current density (η_{ext} -J) plot (E)Power efficiency vs. Luminance (η_{p} -L) plot (F) Luminance vs-voltage(L-V) plot (G) Current density vs voltage (J-V) plot and (H) normalized PL intensity vs wavelength plot for ITO/PEDOT:PSS/V₂O₅/0.3wt% ZnO:Alq₃/LiF/Ag (device2)

Table 7.3: Comparative chromaticity data of Alq₃ powder annealed at 150°C ITO/PEDOT: PSS/V₂O₅/Alq₃/LiF/Ag (device1) and 0.3 wt % ZnO nanoparticle incorporated Alq₃ nanocomposites- based OLED devices ITO/PEDOT: PSS/V₂O₅/0.3wt% ZnO:Alq₃/LiF/Ag (device2)

Compound	CCT	CR	R9	X	y	CIE	λemission
		I				coordinates	
Alq ₃ powder	5592K	98	91	0.3078	0.4453	(0.3078,	520.6
annealed at 150 °C						0.4453)	nm
0.3 wt%	6019 K	57	101	0.3110	0.4832	(0.3110,	539.8
ZnO(II)/Alq ₃						0.4832)	nm

Table 7.4: Comparative electroluminescence and device performance-oriented data of Alq₃ powder annealed at 150°C ITO nanocomposites- based OLED devices ITO/PEDOT: PSS/V₂O₅/0.3wt% ZnO:Alq₃/PEDOT: PSS/V₂O₅/Alq₃/LiF/Ag (device1) and 0.3 wt % ZnO nanoparticle incorporated Alq₃ /LiF/Ag (device2)

Device	Turn	Driving	Voltage	Voltage	EQE	CE	PE	Maximum
name	on	voltage	at	at	(%)	(cd/A)	(lm/W)	luminance
	voltage		1	1000				at
			cd/m ²	cd/m²				maximum
								Voltage
Device	3.1	9.26	2.87	6.88	1.488	3.89	34.2	6338.6
1								(9.6)
Device	2.81	5.8	2.816	6.32	1.838	3.925	35.1	10956
2			•					(10.9)

7.6. Conclusions:

A whitish-yellow colored ZnO/Alq₃ nanocomposites were synthesized by doping ZnO NP with Alq₃ bulk powder through solution intercalation and exfoliation adsorption method. The synthesized ZnO/Alq₃ nanocomposite exhibits a lower energy band gap of

2.85 eV compared to wide band gap ZnO NP (3.37 eV) and Alq₃(2.89 eV). The composite also exhibits red shift of fluorescence spectra while excitation wavelength is 385 nm. It also displays yellow colored emission at 348.7 nm wavelength which is an essential requisite condition for white colored OLEDs. FESEM images of prepared ZnO/Alq₃ nano- composites reveal that it has spherical granular structure of ZnO NP on smooth surface of Alq3. This structure results in strong and higher intense FTIR peaks and causes blue shifts of absorption peaks of ZnO NP (362.7 nm) and Alg₃(361.0 nm) at 360.9 nm. Hence the tuning of photoluminescence and colour in wide band gap semiconductor Alq₃ was observed by replacing with comparatively smaller energy gap semiconducting ZnO/Alq₃ nanocomposites. Our unoptimized 0.3 wt % ZnO/Alq₃ nanocomposites emitter- based OLED exhibits a higher current efficiency 3.93 higher cd/A, EQE % of 6.57 % and higher power efficiency of 31.1 lm/W, higher current density of 365.3 A/m² which is along with low turn-on voltage of 2.81 volt and driving voltage is 5.93V and higher luminance of 11956 cd/m² at 10.9 volt. Which is more enhanced device performance compared to the OLED formed with Alq₃ powder emitter annealed at 150°C. Therefore, ZnO/Alq₃ Nano- composite can indeed be utilized as an excellent transparent emissive layer (EML) and electron transport layer (ETL) for futuristic white and vellow electroluminescent OLETs and OLEDs. In this research work we tried to tune the optical band gap of Alq₃ emissive by incorporating ZnO Nano particle into Alq₃ matrix to improve optical properties and electroluminescence and recombination rate of electron-hole pair within the EML layer, which fulfils our second research objective. It also obtained that the fabricated OLED could emit yellowish white luminescence which is required for WOLED and solid-state lighting application which is our fourth research objective.

References:

- [1.] Zou, S. J., Shen, Y., Xie, F. M., Chen, J. D., Li, Y. Q., & Tang, J. X. (2020). Recent advances in organic light-emitting diodes: toward smart lighting and displays. Materials Chemistry Frontiers, 4(3), 788-820.
- [2.] Tang, C. W., & Van Slyke, S. A. (1987). Organic electroluminesecnt

- diodes. Appt. Phys. Leu, 51(12), 913-915.
- [3.] Park, J., Heo, S., Park, K., Song, M. H., Kim, J. Y., Kyung, G., ... & Bien, F. (2017). Research on flexible display at Ulsan National Institute of Science and Technology. *npj Flexible Electronics*, *1*(1), 9.
- [4.] Cui, S., Hu, Y., Lou, Z., Yi, R., Hou, Y., & Teng, F. (2015). Light emitting field-effect transistors with vertical heterojunctions based on pentacene and tris-(8-hydroxyquinolinato) aluminum. *Organic Electronics*, 22, 51-55. https://doi.org/10.1016/j.orgel.2015.03.029
- [5.] Jeong, E. G., Kwon, J. H., Kang, K. S., Jeong, S. Y., & Choi, K. C. (2020). A review of highly reliable flexible encapsulation technologies towards rollable and foldable OLEDs. *Journal of Information Display*, *21*(1), 19-32.
- [6.] Will, P. A., & Reineke, S. (2019). Organic light-emitting diodes. In *Handbook* of Organic Materials for Electronic and Photonic Devices (pp. 695-726). Woodhead Publishing.
- [7.] Pérez-Bolívar, C., Takizawa, S. Y., Nishimura, G., Montes, V. A., & Anzenbacher Jr, P. (2011). High-Efficiency Tris (8-hydroxyquinoline) aluminum (Alq3) Complexes for Organic White-Light-Emitting Diodes and Solid-State Lighting. *Chemistry—A European Journal*, 17(33), 9076-9082
- [8.] Zawadzka, A., Płóciennik, P., Strzelecki, J., Łukasiak, Z., & Sahraoui, B. (2013). Photophysical properties of Alq3 thin films. *Optical Materials*, 36(1), 91-97.
- [9.] Fukushima, T., & Kaji, H. (2012). Green-and blue-emitting tris (8-hydroxyquinoline) aluminum (III)(Alq3) crystalline polymorphs: Preparation and application to organic light-emitting diodes. *Organic Electronics*, *13*(12), 2985-2990
- [10.] Cölle, M., & Brütting, W. (2004). Thermal, structural and photophysical properties of the organic semiconductor Alq3. *physica status solidi* (a), 201(6), 1095-1115.
- [11.] 0 Painuly, D., Mogha, N. K., Masram, D. T., Singhal, R., Gedam, R. S., & Nagpure, I. M. (2018). Phase stability and transformation of the α to ε-phase of

- Alq3 phosphor after thermal treatment and their photo-physical properties. Journal of Physics and Chemistry of Solids, 121, 396-408.
- [12.] Rajeswaran, M., Blanton, T. N., Tang, C. W., Lenhart, W. C., Switalski, S. C., Giesen, D. J., ... & Young, R. H. (2009). Structural, thermal, and spectral characterization of the different crystalline forms of Alq3, tris (quinolin-8-olato) aluminum (III), an electroluminescent material in OLED technology. *Polyhedron*, 28(4), 835-843
- [13.] Debsharma, M., Pramanik, T., Daka, C., & Mukherjee, R. (2022, May). Recent advances in the electrical and optical properties of Alq3 and Alq3 derivatives based OLEDS. In *Journal of Physics: Conference Series* (Vol. 2267, No. 1, p. 012159). IOP Publishing.
- [14.] El-Nahass, M. M., Farid, A. M., & Atta, A. A. (2010). Structural and optical properties of Tris (8-hydroxyquinoline) aluminum (III)(Alq3) thermal evaporated thin films. *Journal of alloys and compounds*, 507(1), 112-119.
- [15.] Fong, H. H., & So, S. K. (2006). Hole transporting properties of tris (8-hydroxyquinoline) aluminum (Alq3). *Journal of applied physics*, 100(9).
- [16.] Dalasiński, P., Łukasiak, Z., Wojdyła, M., Re, M., & Bała, W. (2006). Study of optical properties of TRIS (8-hydroxyquinoline) aluminum (III). *Optical Materials*, 28(1-2), 98-101.
- [17.] Derkowska-Zielinska, B. (2017). Enhancement of third-order nonlinear optical susceptibility of Alq 3 in polar aprotic solvents. *Optics Letters*, 42(3), 567-570.
- [18.] Higginson, K. A., Thomsen III, D. L., Yang, B., & Papadimitrakopoulos, F. (2004). Chemical Degradation and Physical Aging of Aluminum (III) 8-Hydroxyquinoline: Implications for Organic Light-Emitting Diodes and Materials Design. In *Organic Light-Emitting Devices: A Survey* (pp. 71-101). New York, NY: Springer New York.
- [19.] Knox, J. E., Halls, M. D., Hratchian, H. P., & Schlegel, H. B. (2006). Chemical failure modes of AlQ3-based OLEDs: AlQ3 hydrolysis. *Physical Chemistry Chemical Physics*, 8(12), 1371-1377.
- [20.] Aziz, H., Popovic, Z. D., Hu, N. X., Hor, A. M., & Xu, G. (1999). Degradation

- mechanism of properties. Advanced Materials, 22(14), 1631-1634
- [21.] Duvenhage, M. M., Ntwaeaborwa, O. M., & Swart, H. C. (2012). UV exposure and photon degradation of Alq3 powders. *Physica B: Condensed Matter*, 407(10), 1521-1524.
- [22.] Debsharma, M., Pramanik, T., Pramanik, G., Maity, A. R., Jain, A., & Mukherjee, R. (2024). Effect of growth temperatures on the structural and optical properties of bulk tris-(8-hydroxyquinoline) aluminium (III). *Applied Physics A*, 130(5), 281.
- [23.] Duvenhage, M. M., Ntwaeaborwa, M., Vis Khantham, S., Tunhoo, B., Onlaor, K., Thiwawong, T., & Nukeaw, J. (2012). Electrical properties of dye-doped colour tunable organic light emitting diode. *The Canadian Journal of Chemical Engineering*, 90(4), 903-908.
- [24.] Cuba, M., & Muralidharan, G. (2015). Effect of thermal annealing on the structural and optical properties of tris-(8-hydroxyquinoline) aluminum (III)(Alq3) films. *Luminescence*, 30(3), 352-357
- [25.] Sanchez, C., Julián, B., Belleville, P., & Popall, M. (2005). Applications of hybrid organic–inorganic nanocomposites. *Journal of materials chemistry*, 15(35-36), 3559-3592
- [26.] Boeckler, C., Feldhoff, A., & Oekermann, T. (2007). Electrodeposited Zinc Oxide/Phthalocyanine Films—An Inorganic/Organic Hybrid System with Highly Variable Composition. *Advanced Functional Materials*, *17*(18), 3864-3869.
- [27.] H. G., Swarts, P. J., Swarts, J. C., & Swart, H. C. (2015). Determination of the optical band gap of Alq3 and its derivatives for the use in two-layer OLEDs. *Optical Materials*, 42, 193-198.
- [28.] Duvenhage, M. M., Ntwaeaborwa, M., Visser, H. G., Swarts, P. J., Swarts, J. C.,
 & Swart, H. C. (2015). Determination of the optical band gap of Alq3 and its derivatives for the use in two-layer OLEDs. *Optical Materials*, 42, 193-198
- [29.] Cuba, M., & Muralidharan, G. (2014). Enhanced luminescence properties of hybrid Alq3/ZnO (organic/inorganic) composite films. *Journal of luminescence*, 156, 1-7.

- [30.] Makki, A. H., & Park, S. H. (2021). Yellow emissive tris (8-hydroxyquinoline) aluminum by the incorporation of ZnO quantum dots for OLED applications. *Micromachines*, *12*(10), 1173.
- [31.] Sypniewska, M., Szczesny, R., Popielarski, P., Strzalkowski, K., & Derkowska-Zielinska, B. (2020). Structural, morphological and photoluminescent properties of annealed ZnO thin layers obtained by the rapid sol-gel spin-coating method. *Opto-Electronics Review*, 28(4)
- [32.] Kapustianyk, V., Turko, B., Kostruba, A., Sofiani, Z., Derkowska, B., Dabos-Seignon, S., ... & Sahraoui, B. (2007). Influence of size effect and sputtering uconditions on the crystallinity and optical properties of ZnO thin films. *Optics Communications*, 269(2), 346-350.
- [33.] Rao, B. G., Mukherjee, D., & Reddy, B. M. (2017). Novel approaches for preparation of nanoparticles. In *Nanostructures for novel therapy* (pp. 1-36). Elsevier.
- [34.] Daka, C., & Mukherjee, R. (2022). Synthesis and Characterization of ZnO Nanoparticles and Alq3 for Fabrication of Alq3/ZnO Nanocomposites.120-133,
- [35.] Mahakhode, J. G., Bahirwar, B. M., Dhoble, S. J., & Moharil, S. V. (2006). Tunable Photoluminescence from tris (8-hydroxyquinoline) aluminum (Alq3). *Proc of ASID, New Delhi*, 237-239.
- [36.] Lu, J. G., Ye, Z. Z., Zhang, Y. Z., Liang, Q. L., Fujita, S., & Wang, Z. L. (2006). Self-assembled ZnO quantum dots with tunable optical properties. *Applied physics letters*, 89(2).

Chapter 8: To Study the Structural, Optical and Electrical Properties of Rare Earth Europium(III) and Neodymium(III) Ion Doped Alq₃ Based Emissive Layer for OLED Application and Solid State Lighting Application

Abstract:

In this research work we synthesized mer-Alq₃ [tris(8-hydroxy quinolinato)aluminium(III) powder and its solution, europium nitrate Eu(NO₃)₃ and neodymium nitrate [Nd(NO₃)₃] solution, vanadium pentoxide(V₂O₅) solution and PEDOT: PSS (poly(3,4-ethylenedioxy thiophene), polystyrene sulphonate) solution in lab for stack layer OLED fabrication. We annealed synthesized Alq₃ powder from room temperature to 200°C in a hot air oven. We found the best performance of mer-Alq₃ powder when it was annealed at 150°C. Thus, we took Alq₃ powder annealed at 150°C for our material under investigation. Rare. These ions and rare earth complexes based emissive layers exhibit excellent photoluminescence or electroluminescence properties. Those proven or reported results also motivated us to study the EL and PL properties of rare earth ions in the case of europium (III) ion doped and neodymium(III) doped mer-Alq₃ powder, We also fabricated three kinds of devices (device 1 ,device 2 and device 3) having architectures: ITO-coated PET sheet $(175 \text{nm})/\text{PEDOT:PSS}(48 \text{nm})/\text{V}_2\text{O}_5(12 \text{nm})/\text{Alq}_3(83 \text{nm})/\text{LiF}(3 \text{nm})/\text{Ag}(100 \text{ nm})[\text{device1}],$ ITO- coated PET sheet(175nm)/PEDOT:PSS(48nm)/V₂O₅(12nm)/Nd:Alq₃(83nm) /LiF(3 nm)/Ag(100nm)[device2]and ITO-coated PET sheet (175nm)/PEDOT:PSS(48nm)/V₂O₅ (12nm)/Eu:Alq₃ (83nm)/LiF(3 nm)/Ag (100 nm)[device 3] respectively. Our central aim was to construct voltage tunable cost effective, inexpensive transparent flexible OLED (Organic Light Emitting Diode) having wide emission spectrum using Alq₃ thin film (ETL layer plus EML or Emissive layer), PEDOT: PSS thin film(HTL or Hole Transport Layer),ITO coated PET (Poly Ethylene Terephthalate)sheet(transparent anode) and Ag silver paste(cathode) Here multi layered thin films are spin coated one after another on the transparent anode as well as transparent substrate ITO (Indium Tin Oxide) coated PET utilizing the spin coating method. After construction the electroluminescence (EL) and photoluminescence (PL) properties and device efficiency of the Alq3 –based bi – layered single junction OLED device was examined using PL spectroscopy, UV-VIS spectroscopy, Cyclic voltammetry, XRD and FESEM EDS analysis, EL and PL intensity vs wavelength plot analysis and J-L-V plot analysis, TG and DSC curve and chromaticity diagram. We find that device 3 has exhibited the best SSL OLED performances compared to other two OLEDs with 2.56V turn on voltage, driven voltage of 5.8V ,0.95% EQE, current efficiency of 4.69 cd/A and power efficiency of 34.48lm/W and maximum luminance at 11.9 Volt is 11589.2 cd/m². This Solid state OLED has potential applications specially for all kinds of illumination, full-colour HD flexible displays and OLED lamps etc.

8.1. Introduction:

There are 17 elements in the family of rare –earth elements (RRE) of the periodic table. Of them 13 rare earth or lanthanide elements (cerium to ytterbium i.e., atomic no. 58-70) possess incompletely packed 4f outer shells curtained by $5s^25p^6$ outermost subshells, excluding the four rare earth elements having atomic numbers 21,39,57 and 71. The 4f shell of these four RRE elements are completely filled with their maximum strength of 14 electrons. But the 4f shells of the remaining 13 RREs are partially filled and totally curtained by the completely filled $5s^25p^6$ outer subshells. Because of this partially filled outermost 4f shell those 13 RREs exhibit higher electronic levels and show excellent electromagnetic and optical properties. These delimited energies of those higher electronic levels have remained unaffected from the outer chemical influence. Hence tri positive RRE cations exhibit luminescence because of energy-level shift within the outer 4f shell which is usually not allowed according to spin & parity prohibition rule of quantum mechanics. (Figure 1) But when these RRE cations do not possess any central symmetric positions in its crystal lattice they show luminescence efficiently. [1-5]

Researchers worldwide involved with this field of research are continuously innovating and developing new methodology and processing techniques for longer durability, low operating voltages, higher transparency and higher flexibility, higher external and internal efficiency (EQE and IQE) using various suitable materials to enhance PL and EL efficiency of OLED displays and OLED lights. [6-16]

The manufacturing cost of LED based SSL is comparatively low and gives bright colourful luminescence at low voltage that's why mass production of Solid-state LED lamps is obvious consequences and get extreme popularity among the users. But still due to rigid structural form SSL using LED cannot be applied to acute angular plane as well as in flexible surface. That's why thin flexible low voltage driven brighter flickering free displays and SSL using OLED would be a real solution for multi-dimensional full colour HD displays and bright lighting applications. Solid state lights can be used in every application where OLED and LEDs are used. On the other hand, continuous R&D has lowered the manufacturing cost of OLED displays as well as OLED SSLs, But OLED SSL are still many steps far behind than LED SSLs on account of higher chemical cost, device manufacturing cost, chemical degradation, shorter life span etc. [14-20]

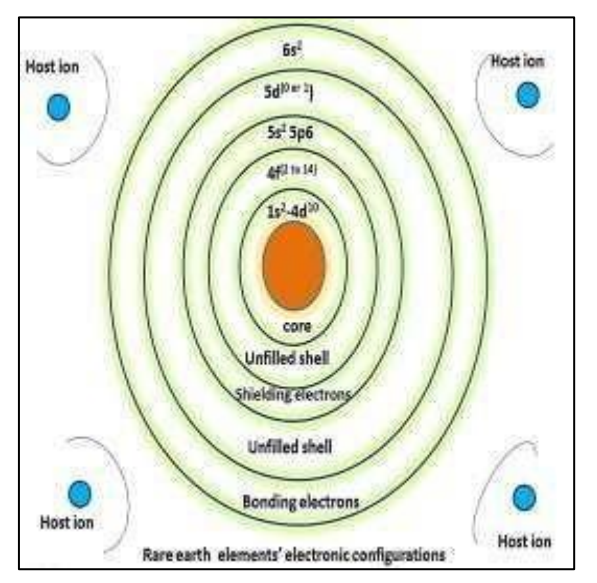
8.2. What are the major differences between OLED display and OLED lighting?

OLED displays send messages videos and images which refresh at higher image-data and display-data sending rate more than 120Hz which needs costly TFT substrates to control those pixels to give high resolution videos and images. But OLED display consists of a number of small pixels. OLED display emits a fractional part of brightness and can address RGB pixels individually which results in shorter lifespan of an OLED display. Thats why OLED displays have been converted into an ideal device for exquisite means of messaging and showing videos and images on television screens and smart phone-screens. While OLED lights are the light-engines which create ambiance, functional illumination and sometime helps to communicate like indicators. The large OLED lighting segments are 1000 times bigger in size compared to those RGB small pixels of OLED displays. OLED lights can address large OLED light segments which refresh at slower data rate and thus it

does not require costly TFT screen. OLED lights act as a functional light source as they can emit natural white spectra, uniform illumination with higher brightness and can work on large surface area lighting. The lifespan of OLED lights is generally more than 10 years. OLED light panels are considered as "single big pixel "or an array of large OLED lighting segments. [24-27]

8.3. How lanthanides or rare earth complexes affect in photoluminescence and electroluminescence of OLEDs:

When lanthanide complexes, i.e rare earth complexes (RRE complexes) are used as emissive materials of OLEDs, lanthanides exhibit excellent colour-saturation as well as higher PL and EL efficiency in those OLEDs. The rare earth ions of the RRE complexes exhibit excellent luminescence for their unusual electronic structures. The electronic configuration of the rare earth ion is $4f^x5s^25p^6(x=0 \text{ to } 14)$ where each rare earth ions



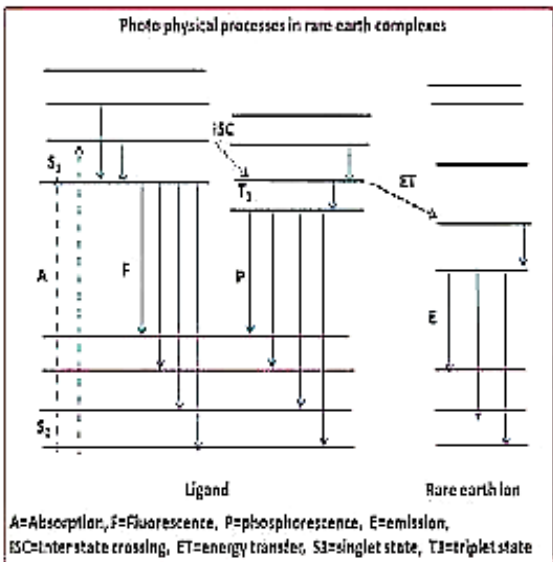


Figure 8.1A: Photophysical processes of rare earth complexes

contains an incompletely filled 4f shell. Due to the screening effect of 5s orbital electrons and 5p orbital electrons, the energies of their electronic levels remain unaffected against the

external chemical atmosphere. This leads to the emission of sharp line-like spectra (FWHM <10nm), excellent color-purity, emission of 30,000 spectral lines within the range UV (ultra-violet) and NIR (near infra-red) due to magnificent energy transitions of electronic levels. It has been well proven that the energy levels of ligand singlets (S1) present in RRE metallic chelates are converted into higher efficiency yielding triplet energy levels (T1) through intra-energy state conversion (ISC) method [Figure 8.1A]. These ligand singlet energies are also converted into the excited state of the metal ion present at the center of the RRE chelates. The electrons present in the 4f inner orbital associated with the RRE central metal ion causes 5Dx → 7Fx energy transition resulting in a band of sharp spectral lines and 20-95% photoluminescence (PL) efficiency and electroluminescence (EL) efficiency compared to common phosphorescent and fluorescent compounds.

There are three processes involved with the energy transfer procedure:

- (1) Each ligand absorbs excited energy and forms a singlet state(S1) on itself.
- (2) Singlet states (S1) of each ligand transfer its energy to the corresponding triplet state (T1) of the ligand by the method of intersystem crossing (ISC)
- (3) Triplet state (T1) of ligands transfers its energy to the central RE ion and excites 4f electrons using resonance coupling method and thus energy transfer occurs between triplet state (T1) of ligand and 4f excited state of RRE ion generating light by radiative –decay method. (Fig. 8.1A)

RRE complexes play decisive roles for light emission from those RRE complexes. When lanthanides are incorporated into the emissive layer of OLEDs it eliminates the 25% efficiency limitations of spin statistics of efficiency as both or either of the excited singlet and triplet ligands transfer their excitation energy to the lanthanide ion.

The unique photoluminescence and electroluminescence characteristics use of rare earth complexes as emissive materials of OLEDs provide an effective means to produce highly efficient low-voltage driven OLEDs having excellent color-purity. For this reason, RRE complexes are the best choice for the optical communication application like upconversion emitters, fiber amplifiers etc. Since the first published report of electroluminescence properties from RRE complex, researchers from every corner of the world have shown great interest in the EL properties of rare earth elements and rare earth

complexes due to their outstanding color purity and excellent luminescent characteristics and higher PL and EL efficiency. Even in recent times there has been continuous research going on the study of EL phenomenon, molecular structure device performance of RRE and RRE complexes. [27-36]

8.4. Advantages of wide band gap semiconductors:

Wide band-gap semiconducting materials (WBGSC) usually possess an energy bandgap more than 2 electron-volt(eV). E.g. Sic, RRE complexes, ZnO nanoparticles, GaN, Alq₃, Alq₃-RRE complex nano composites are the best choice material for solid state lighting (SSL). The wide band gap semiconducting materials have many advantages compared to narrow band gap materials for their higher efficiency, small former wavelength, shorter wavelength, higher luminescence properties and ability to handle high

temperature, high frequency, high power functionality and supports faster switching over to higher temperature dependent functions. WBGSCs. enable LED or OLEDs to emit high quality brighter energy efficient white light and emit visible and UV electromagnetic radiation.

Table 8.1: Comparative data analysis of Eu(III) and Nd(III) ion's electronic configuration

Element	Electronic configuration	Rare Earth (III) ion configuration (RE ³⁺)	Crystal structure	E.S. transitions	G.S. transitions	Emission Energy levels
Neodymium (Nd-60)	[Xe]4f ⁴ 6s ²	4f ³	Dhcp	⁴ G _{5/2}	⁴ I _{9/2}	⁴ F _{3/2}
Europium (Eu- 63)	[Xe]4f ⁷ 6s ²	4f ⁶	Всс	⁷ F ₂	⁷ F ₁	⁵ D ₀

Eu³⁺ cation activated complexes are successfully used in colour television as its redcomponent. Rare earth doped phosphors are used to yield considerable increase in luminescence of energy-saving luminescent SSL lamps along with X-ray influencing screens etc. The first rare-earth complex used as emissive material in fluorescent lamp and CRT lamp was Y₂O₃: Eu(III). In 1964 neodymium yttrium aluminium garnet lasers (YAG lasers) were discovered, after 1987 RRE complex-dependent OLEDs or RRE coordination compound-based OLEDs became extremely popular among researchers. [27-37]

The energy level structure or electronic configuration of Europium trivalent cation (Eu³⁺) is [Xe]4f⁶ which consists of 60 electrons. Out of 60 electrons 54 electrons occupy identical confined shells like a Xenon atom does. The remaining 6 electrons exist inside the 4f-shell. The confined 5s² & 5p⁶ exterior shells completely protect that 4f shell well from its surrounding environment. The six electrons of 4f shell can be introduced into different seven (7) 4f orbitals in 3003 ways. [27-36]

 Nd^{3+} ion is a trivalent rare earth ion which has $4f^3$ RE^{3+} configuration. This causes absorption peaks from G.S. (ground state) $^{11}I_{9/2}$ to various excited energy states in UV-Vis spectral region [110,111]. Europium (III) ion is a very popular emitter used for red luminescence. Europium (III) ions usually doped into different host crystal lattices. Eu^{3+} ions doped phosphors create sharp spectral emission lines because of transitions from 5DX to 7FX (where X=0,1,2,3,4,5,6) for excitation wavelength ranging from 395 to 398 nm. [27-37]

Therefore, our materials of interest were tri positive trivalent Nd³+(atomic no 60) and Eu³+(atomic no 63) cations and their complex show efficient luminescence depending upon the number of electrons present in its 4f outermost shell. Trivalent RRE ion activated complexes have attracted many researchers' interests to introduce RRE complexes as emissive materials of organic light emitting diodes (OLED) for higher quantum efficiency, line-like emission, easy synthesis process and higher luminescent efficiency. Rare earth ions can be used as luminescent materials. These ideas have caused path breaking development in the field of luminescence and solid-state lighting and general illumination. [22,27-37]

In our present work we studied the morphological, optical and electrical properties of Eu(III) ion and neodymium ion in tris(8-hydroxyquinoline)aluminium(III) (Alq₃) -based OLED application and possible solid state lighting application. We also studied the photoluminescence and electroluminescence characteristics and device performance of fabricated device made by pure Alq₃ ,0.3 wt %[sample-(a)], Eu/Alq₃ nano composites[sample-(b)] and 0.3wt % Nd/Alq₃ nano composites. We used three varied

concentrations during making of both Eu/Alq3 and Nd/Alq3 nano composites respectively :0.1:1, 0.2:1 and 0.3:1. We found 0.3:1 is the best concentration which gives best result. From the PL spectra it is clear 0.3 wt%\$/Eu(III) nano composite based OLED device (device 3)exhibit highest EL and PL characteristics compared to the other two device (device 1 and device 2).For morphological study we analyzed XRD diffractogram , FTIR spectra, FESEM images of the three powder i.e., pure Alq3, 0.3 wt % Eu/Alq3 and 0.3wt % Nd/Alq3. We used UV-VIS, PL spectra for optical study and used cyclic voltammetry (CV) plot, J-L-V plot, power efficiency -L plot, EQE-J plot for electrical property and OLED performance of the fabricate three devices.

In our experiment our host and principal material of interest is Alq₃ and its novel derivatives. Though tris(8-hydroxyquinolinato)aluminium(III) or Alq₃ [Al(C₉H₆NO)₃] itself is not a ligand but it is basically an organic semiconducting metal chelated coordination complex which contains three 8- Hq (8-hydroxyquinoline) ligands. These three 8-hydroxyquinolineligands form bonds with a central metallic aluminium atom and coordinate complex chelate. [22;27-37]

For stack layered OLEDs, transitional metal oxides like MoOx, V₂O₅, ReO₃ and WO₃, WO₃, and ReO₃ are commonly used as HTL and HIL for enhancement of device performance. These transitional metal oxides act as HTL or HIL (or electron acceptor) dopant for the fabrication of p-doped devices as well as buffer layer between HTL and EML respectively resulting significant improvement in the device performance of OLEDs. We used V₂O₅ as our HIL as well as our buffer layer which protects back tracking of holes towards PEDOT: PSS(HTL) of our fabricated OLEDs. V₂O₅ also protects the PEDOT: PSS layer from chemical degradation. We got significant improvement in EL and PL characteristics using V₂O₅ as HIL compared to device performance of OLEDs without V₂O₅ layer. Here we spin coated V₂O₅ layer over PEDOT: PSS layer instead of doping for better performance of V₂O₅ layer in hole injection and electron blocking characteristics needed for our OLED [38-43].

OLED lighting and display technologies have left behind their other counterpart for low cost, high resolution, higher brightness, full-color, flexible, fast refresh rate, low voltage—driven high quality multitasking display screens and pluralistic variety of efficient OLED

lamps. But organic molecules exhibit broad emission spectrum and lower efficiency which limit OLEDs to achieve the yardstick of high-class displays and energy —saving, bright, flickering-free cool lighting market. These shortcomings of OLED motivate all the researchers worldwide who are working continuously in this specific field to innovate and develop emissive novel material and their synthesis and fabrication techniques

8.5. Experimental Methods:

A. Synthesis of bulk polycrystalline mer-Alq3 and thermal annealing at different temperatures:

We performed the synthesis of mer- Alq₃ powder in lab via wet-synthesis method as reported by J.G. Mahakhode, et al and Debsharma et al. [22,44], keeping the original synthesis unchanged we made small changes in the synthetic (as discussed in page 85). The 4.598 gm dried Alq₃ powder was grinded and dissolved into 20 ml acetone (Sigma Aldrich, purity 99%) along with 10 ml double distilled water with constant stirring at 50 °C temperature. The resultant solution was ultrasonicated for ½ h with constant heating at 50 °C. A yellowish green homogenous solution was obtained and ready to be used for spin coat fabrication [36]. The thin film of Alq₃ was annealed at 50 °C, 100 °C, 150 °C and 200 °C in a hot air oven for 2 hrs. with the constant heating rate of 2 degrees per minute]. as mentioned in our previous report by Debsharma et al. [22]. We got better optical luminescence from thin films of Alq₃ were annealed at 150 °C compared to without pure Alq₃ powder at RT. This is due to formation of 8 –hydroxyquinoline-N-oxide, a non-emissive polymer, which gives better fluorescence and photoluminescence. [22,43,44] The chemical reaction that took place is as follows as mentioned by Debsharma. M. et al. [22]:

$$3(C_9H_7NO) + Al(NO_3)_{3,,9}H_2O \rightarrow Al(C_9H_7NO)_3 + 9H_2O + 3(NO_2)$$
 (8.1)

$$Alq_3 + H_2O \longrightarrow Alq_2OH + 8-Hq$$
 (8.2)

$$8-Hq+O_2 \longrightarrow 8-Hq-N \text{ oxide (NEP)}$$
 (8.3)

B. Preparation of PEDOT: PSS solution and V₂O₅ solution for thin film formation:

PEDOT: PSS is an organic dye which was obtained from Sigma Aldrich and was not purified further. As the dye is insoluble in water, to make it a homogeneous solution for the application of spin coating, PEDOT: PSS was dissolved in ethylene glycol in the volumetric ratio 9:1 along with constant stirring for ½ h in a magnetic stirrer. The resultant bluish emulsion was ultrasonicated for another ½ hr. after which the yielded bluish solution was filtered using filter paper having a diameter of 0.45 μm until bluish transparent precipitate was obtained. [38-41]

At first 0.542 gmV₂O₅ powder, bought from market (Sigma Aldrich) was dissolved in 10 ml of monoethylamine (99.8% purity, Sigma Aldrich and 20 ml of ethanol (98% pure), Sigma Aldrich) dilute hydrogen peroxide (H₂O₂) (15 mol%, Sigma Aldrich) solution resulting a whitish pink transparent solution which was then ultrasonicated for 45 minutes in a ultra sonicator bath at room temperature. As a result, pinkish white transparent solution was produced. This yielded solution was used for our OLED fabrication [38-41]

C. Preparation of Alq₃ solution for thin film formation:

1. Fabrication technique:

At first the ITO coated PET sheet was cleaned with acetone and ethanol alternately several times. It was dried at room temperature by using a hot plate at 27 °C under an ambient atmosphere. The solution of PEDOT: PSS was then spin-coated for HTL layer on the PET coated sheet. Afte drying it for 15 minutes, thin film of tris(8-hydroxy quinolinilato(aluminium (III) was deposited through spin coater machine under vacuum condition. This process helped us to fabricate an OLED device where the stacked layers are constructed like: ITO/PEDOT: PSS/V₂O₅/Alq₃/LiF/Ag. In this hetero structure, ITO (Indium tin oxide) acts as a transparent anode, PEDOT: PSS is an organic dye acts as a transparent bulk hole transport layer (HTL), Alq₃, an ETL layer acts as a green emissive layer and silver-paste used at the perimeter of the Alq₃ layer acts as metallic cathode. The thickness of Alq₃ and PEDOT: PSS layers are 83 nm and 12 nm, respectively. All the measurements of the constructed OLED were performed without any encapsulation and subjected to experimental measurement at room temperature.

D. Synthesis of Europium Nitrate from Europium oxide(Eu₂O₃):

At first 2.14 gm. europium oxide bought from market (Sigma Aldrich) was dissolved in 5 ml distilled water and the resultant opaque milky white solution was treated with conc. HNO₃ (1:6 volumetric ratio) to yield soluble europium nitrate [Eu(NO₃)₃] which showed pH value 3 which confirmed that the resultant solution was acidic. The yielded white solution was heated at 60°C for ½ hr. with constant stirring. As a result, a white translucent solution of europium nitrate was obtained which was allowed to settle down. The white precipitate was filtered and collected after drying at 50°C for 15 minutes. [45-47]

E. Synthesis of Eu³⁺ doped Alq₃ nanocomposites.:

At first 100 mg europium nitrate as prepared powder is dissolved in double distilled water on which Alq₃ powder was added with different wt% ratios: 1:0.1.1:02 and 1:0.3. The resultant solutions are individually ultrasonicated for 4 hrs. Then the mixture was heated to 50°C for 8 hrs. to get dried Eu³⁺ doped Alq₃ nanocomposites powder.[47]

F.Synthesis of Nd³⁺ doped Alq₃ nanocomposites.:

At first 0.186 gm neodymium nitrate [Nd(NO₃)₃](Sigma Aldrich) as prepared powder was dissolved in the 5 5 ml acetone and 10 ml double distilled water on which 0.502 gm. Alq₃ powder dissolved in 10 ml was added with different wt% ratios: 1:0.1.1:02 and 1:03. The resultant solutions are individually ultrasonicated for 4 hrs. Then the mixture was heated to 50°C for 8 hrs. to get dried Nd³⁺ doped Alq₃ nanocomposites powder.[47]

$$Eu_2O_3 + 6HNO_3 \rightarrow 2Eu(NO_3)_3 + 3H_2O$$
 (8.4)

$$Al(C_9H_7NO)_3 + Eu(NO_3)_3 \rightarrow Eu(C_9H_7NO)_3 + Al_2O_3$$
 (8.5)

$$Al(C_9H_7NO)_3+Nd(NO_3)_3 \rightarrow Nd(C_9H_7NO)_3+Al(NO_3)_3$$
 (8.6)

8.6. Results and discussions:

A. Structural and morphological properties study:

1. X-Ray Diffraction spectroscopy analysis:

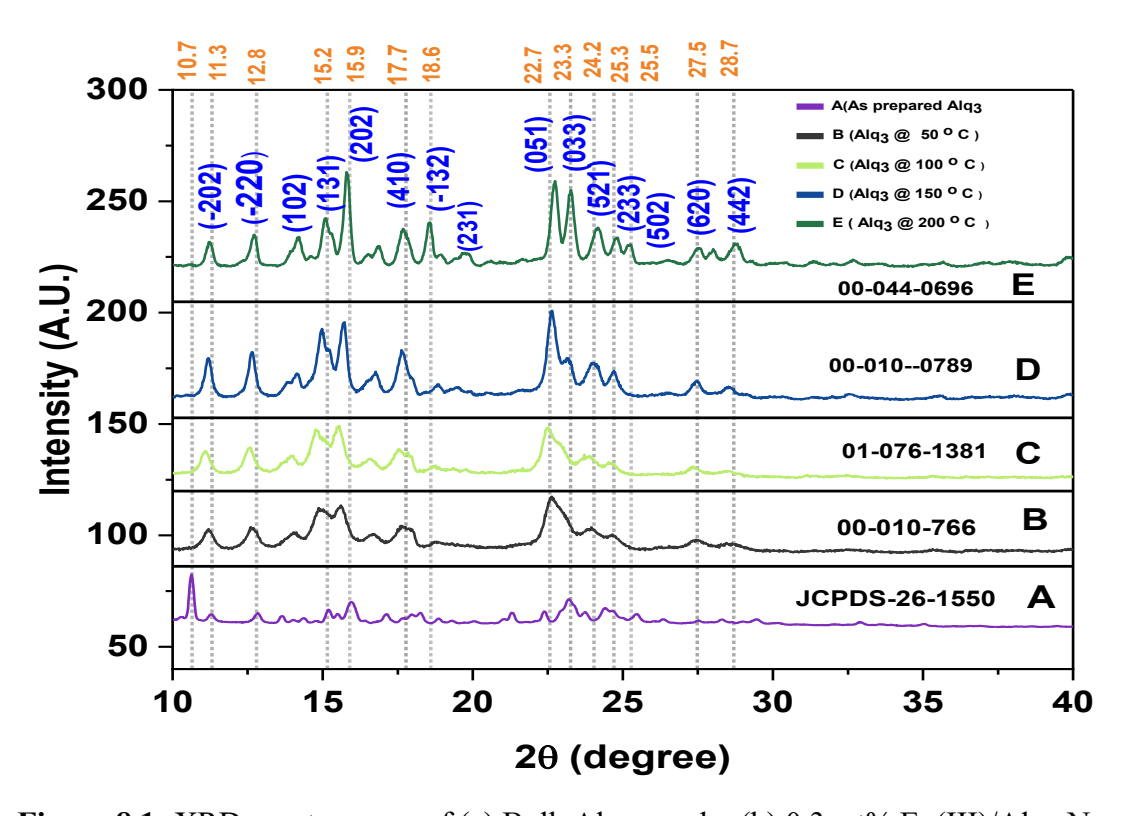


Figure 8.1: XRD spectroscopy of (a) Bulk Alq₃ powder (b) 0.3 wt% Eu(III)/Alq₃ Nanocomposites(c) 0.3 wt% Nd(III)/Alq₃ Nanocomposites

From the XRD spectroscopy produced by BRUKER X-Ray Diffractometer, sharp peaks are found in the XRD of the bulk Alq₃ annealed at 150°C [sample-(a)] having crystallographic plane corresponds to (1-10), (-202), (-220), (0-11), (110), (1-1-1), (01-2), (10-2), (020), (100), (121), (220), (10-3), (031), (132), (2-22), (1-3-2) and (-2-2)31) are clearly visible at $2\theta = 10.6^{\circ}, 11.2^{\circ}, 12.8^{\circ}, 13.7^{\circ}, 14.3^{\circ}, 15.1^{\circ}, 15.9^{\circ}, 17.1^{\circ}, 18.2^{\circ}, 21.4^{\circ},$ 22.3°, 23.1°, 24.5, 25.4°, 26.3°, 28.3°, 29.5° and 32.9° (JCPDS 26-1550). It is observed that 0.3 wt % Nd(III)/Alq₃ Nano-composites[sample-(b)] show distinctive sharp peaks (1-10), (020), (031), (2-20),(121),(340),(400), (2-12), (3-30), (1-21) and (202) crystalline planes at $2\theta = 11.1^{\circ}, 11.3^{\circ}, 12.7^{\circ}, 15.1^{\circ}, 15.7^{\circ}, 16.7^{\circ}, 17.9^{\circ}, 22.6^{\circ}, 23.2^{\circ}$ and 27.5° (PDF pattern 00-033-1759) The intense sharp peaks of 0.3 wt % Eu(III)/Alq₃ Nanocomposites[sample(c)] correspond to the crystalline planes (002), (101), (-103), (220), (-204), (-202), (-212), (-303), (-115)(311)and clearly visible are at θ=11.6°,12.9°,15.1°,15.9°,17.8°,20.0°,22.8°,23.5°, 26..4°, 27.6°, 28.7° (PDF pattern 00-058-1656)...After analysis of Figure 1(a),(b) and (c) we can clearly detect the existence of sharp intense peaks of pure Alq₃ namely (1-10)(031)(020)&(121) within the XRD diffractogram of 0.3 wt % Nd(III)/Alq₃ Nanocomposites and (220), 132) &&(-202) within the XRD diffractogram of 0.3 wt % Eu(III)/Alq₃ Nanocomposites. The rest of the peaks found in the XRD diffractogram of sample(b) and (c) are due to incorporation of Nd(III) and Eu(III) ions and ions into the sample(b) and sample(c)Nanocomposites respectively.

Table 8.2: Structural comparison table and crystallographic details of Alq₃, 0.3 wt % Eu(III)/Alq₃ and 0.3 wt % Nd(III)/Alq₃ nanocomposites respectively

Sample Name	Lattice	Lattice	Volum	Mol. wt.
		Paramete	e	(gm/mol)
		r (Å)	(c.c.)	
Alq ₃	polycrystalline	a=10.3, b=13.7, c=8.2	386.72	459. 4
	triclinic			
0.3wt% Nd/Alq ₃	Monoclinic	a=13.1,b=20.63, c=8.36	2191.66	1269.84
0.3 wt% Eu/Alq ₃	Monoclinic	a=11.17,b=5.62,c=20.13	1263.63	241.22

From table 8.1, we can decide that polycrystalline Alq₃ powder converts into monoclinic 0.3 wt % Eu(III)/Alq₃ and monoclinic 0.3 wt % Nd(III)/Alq₃ Nanocomposites powder respectively. During this conversion volume of pure Alq₃ powder increases from 386.72 c.c. to 1263.63 c.c. (0.3 wt % Eu(III)/Alq₃) and 2191.66 c.c. (for 0.3 wt % Nd(III)/Alq₃)

respectively. The lattice constants of Alq₃, Eu(III)/Alq₃ and 0.3 wt % Nd(III)/Alq₃ Nanocomposites respectively are a=10.3 Å, b=13.7 Å, c=8.2 Å; a=11.17 Å, b=5.62 Å, c=20.13 Å and a= 13.1 Å, b=20.63 Å, c=8.36Å. The molecular weight of pure Alq₃ powder is 459..4 gm/mole which decreases to 241.22 gm/mole (for 0.3 wt % Eu(III)/Alq₃) and increases to 1269.84 gm/mole (for 0.3 wt % Nd(III)/Alq₃). Sharp intense peaks describes about the formed new Nano-composites which exhibit altered chemical and physical properties in comparison to their specific components, i.e., Alq₃ and 0.3 wt % Eu(III)/Alq₃) and 0.3 wt % Nd(III)/Alq₃). Nanoparticles [22,39,43,44,].

2. Field Emission Scan Electron Microscopy (FESEM) spectroscopy and energy dispersive spectroscopy (EDS) analysis:

From images of 8.2(a), 8.2(b) and 8.2(c) given by JEOL Field Emission Scan electron microscope we observe that the bulk polycrystalline Alq₃ powder possesses triclinic lattice

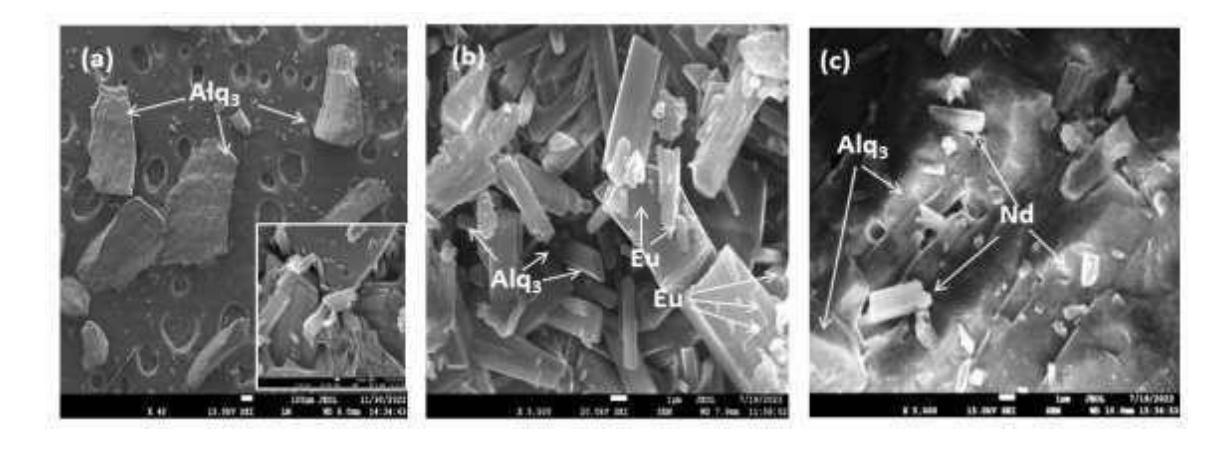


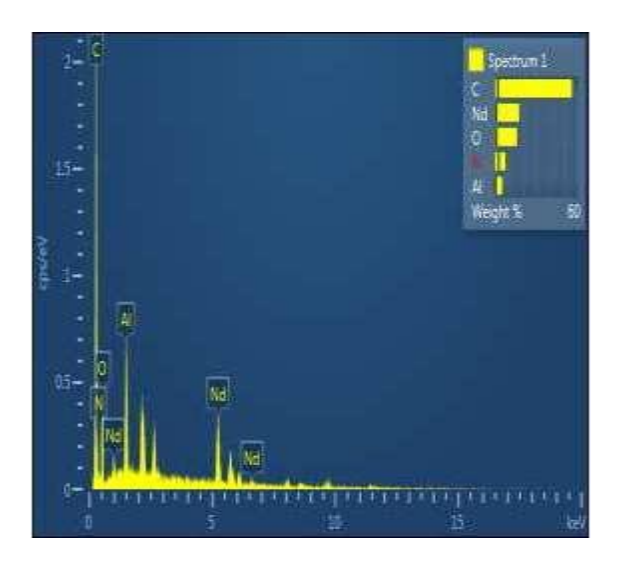
Figure 8.2: FESEM images of (a) Pure Alq₃ Nano-rod powder annealed at 150°C (inset pure Alq₃ powder) (b) 0.3 wt% Eu(III)/Alq₃ Nanoparticle (c) 0.3 wt % Nd(III) /Alq₃ Na

as well as hexagonal stacked Nano-rod like semiporous vertical layers. From the figure 8.2(b) and 8.2(c), we observe the distinctive triclinic structure of the structure of .3 wt%

Eu(III)/Alq₃ Nanoparticle and 0.3 wt % Nd(III) /Alq₃ Nanocomposites respectively amidst the hexagonal and orthorhombic nanorod of mer-Alq₃ which confirms that Eu(III) composite system with the help of both ions. The FESEM image confirms the findings of XRD diffractogram and crystallographic data illustrated by table 1 table 8.1A and EDS spectrum of Figure 8.2A.[22,39,43,44].

Table 8.3: Comparative data of EDS spectrum of 0.3 wt% Neodymium /Alq₃ nano composites and EDS Spectrum 2 for 0.3 wt% Europium/Alq₃/nanocomposites nocomposites

Compound	%	C	N	0	Al	Eu/Nd	Total
0.3wt% Nd/Alq ₃	Wt%	55.19	7.20	15.55	4.92	17.14(Nd)	100.00
0.3wt% Nd/Alq ₃	Atomic	72.00	8.06	15.23	2.86	1.86 (Nd)	100.00
	%						
0.2wt0/. Eu/Ala	Wt%	65.09	5.25	12.65	8.8	9 21 (Eu)	100.00
0.3wt% Eu/Alq ₃	VV 170	03.09	3.23	12.03	8.8	8.21 (Eu)	100.00
0.3wt% Eu/Alq ₃	Atomic	75.48	3.01	13.44	4.33	1.74 (Eu)	100.00
	%						



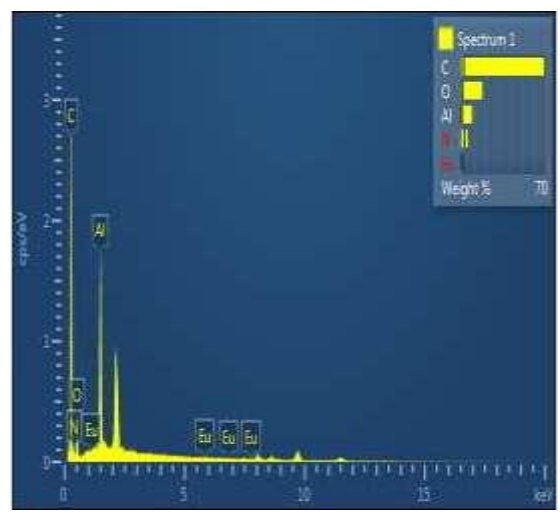


Figure 8.2A: EDS Spectrum 1(left image) for 0.3 wt% Neodymium /Alq₃ nano composites and EDS Spectrum 2 (right image for 0.3 wt% Europium/Alq₃/nanocomposite

B. Thermal properties study:

1. Thermo gravimetric Analysis (TGA):

Figure 8.3(a),(b) and (c) demonstrate the thermo gravimetric analysis (TGA) curve of sample-(a), sample-(b) and sample-(c). The Thermo gravimetric analysis of the three plotted curves were studied between 25°C (room temperature) and 575°C at a heating rate of 10°C/min where holding time at 575°C was 1 minute. We observed distinct crystal defects due to the hydrolysis of 8-Hq ligand molecules. The sample weight of for sample (a), sample (b) and sample(c) are 3.022 mg,3.568 mg, 3.843 mg. Here we can find maximum weight loss% for three samples are $\Delta Y_{a,=}58.7\%$, $\Delta Y_{b}=45.6\%$, and $\Delta Y_{c}=26.7\%$ respectively within temperature range 343.4-477.4°C,343.3-475.7°C and 169.2-398.7°C. The possible cause is partial sublimation of melting of its polymorphic phases and degradation of Alq₃, Between, 25°C and 175°C the small weight loss occurred due to the elimination of water (H₂O) molecules from three samples. The second stages between 176°C and 375°C,

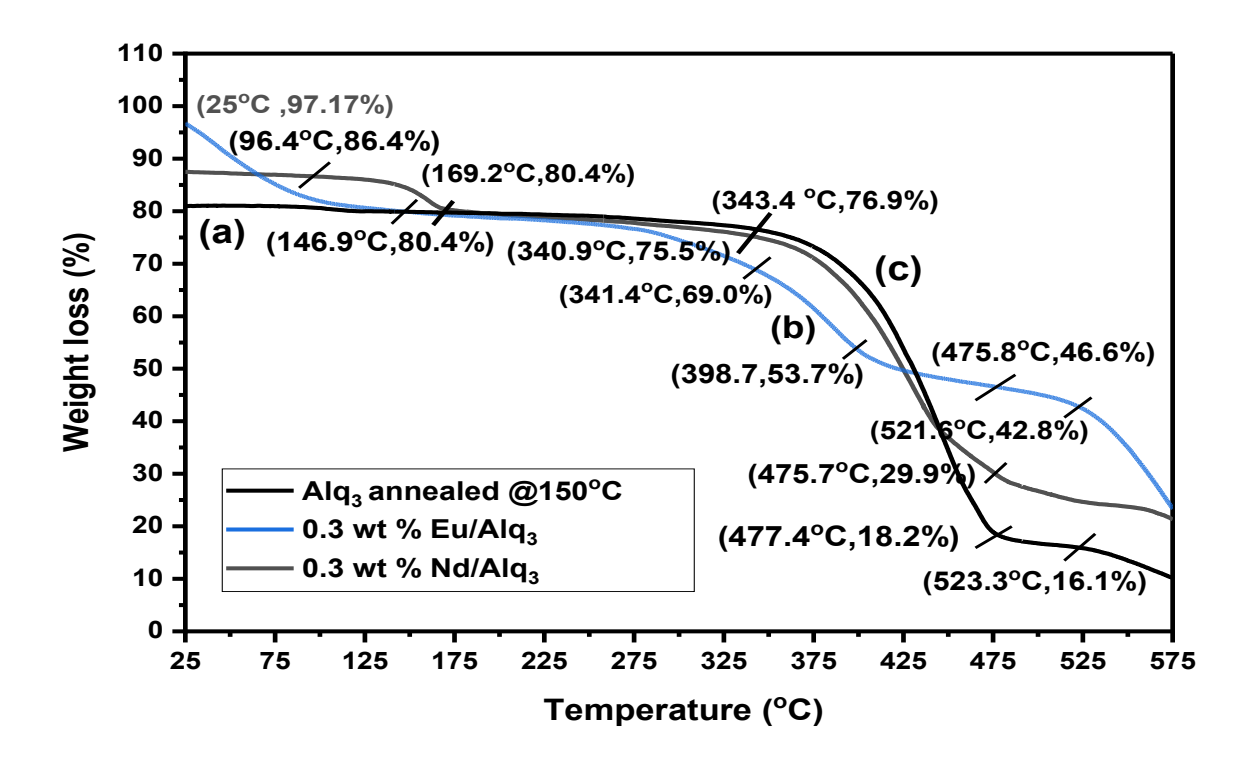


Figure 8.3: TG curve of (a) Pure Alq₃ Nano-rod powder annealed at 150°C(b) 0.3 wt % Nd(III) /Alq₃ Nanocomposites and (c) 0.3 wt% Eu(III)/Alq₃ Nanoparticle

small weight loss % happens because of phase modification of amorphous samples into crystalline materials [39]. The right most stages of weight loss% within 475°C and 575°C take place on account of chemical decomposition of 8-hydroxyquinoline ligand molecules. Here we clearly find from three TG curves that three samples remain thermally stable till 343.4 °C but in between 344°C and 523.3 °C three materials drastically undergo maximum amount of weight loss% resulting loss of stability. From this result, we can say that these three materials can be used as OLED emitters for higher temperature stability which is utmost important for OLED formation. [22,26,39,43,44].

2. Differential Scanning Calorimetry (DSC) Analysis:

From Figure 4 we analyze the DSC (Differential Scan Calorimetric) curves of the three samples: (a) Pure Alq₃ Nano-rod powder (b) 0.3 wt % Nd(III) /Alq₃ Nanocomposites

and(c) 0.3 wt% Eu (III)/Alq₃ Nanoparticle. In these cases, we took heating rate of the materials as 10 °C/min. We clearly find that Alq₃ powder annealed at 150°C sample-a) has the highest endothermic sharp peaks of crystallization at 387.3°C and 413.4 °C. The sample (b)

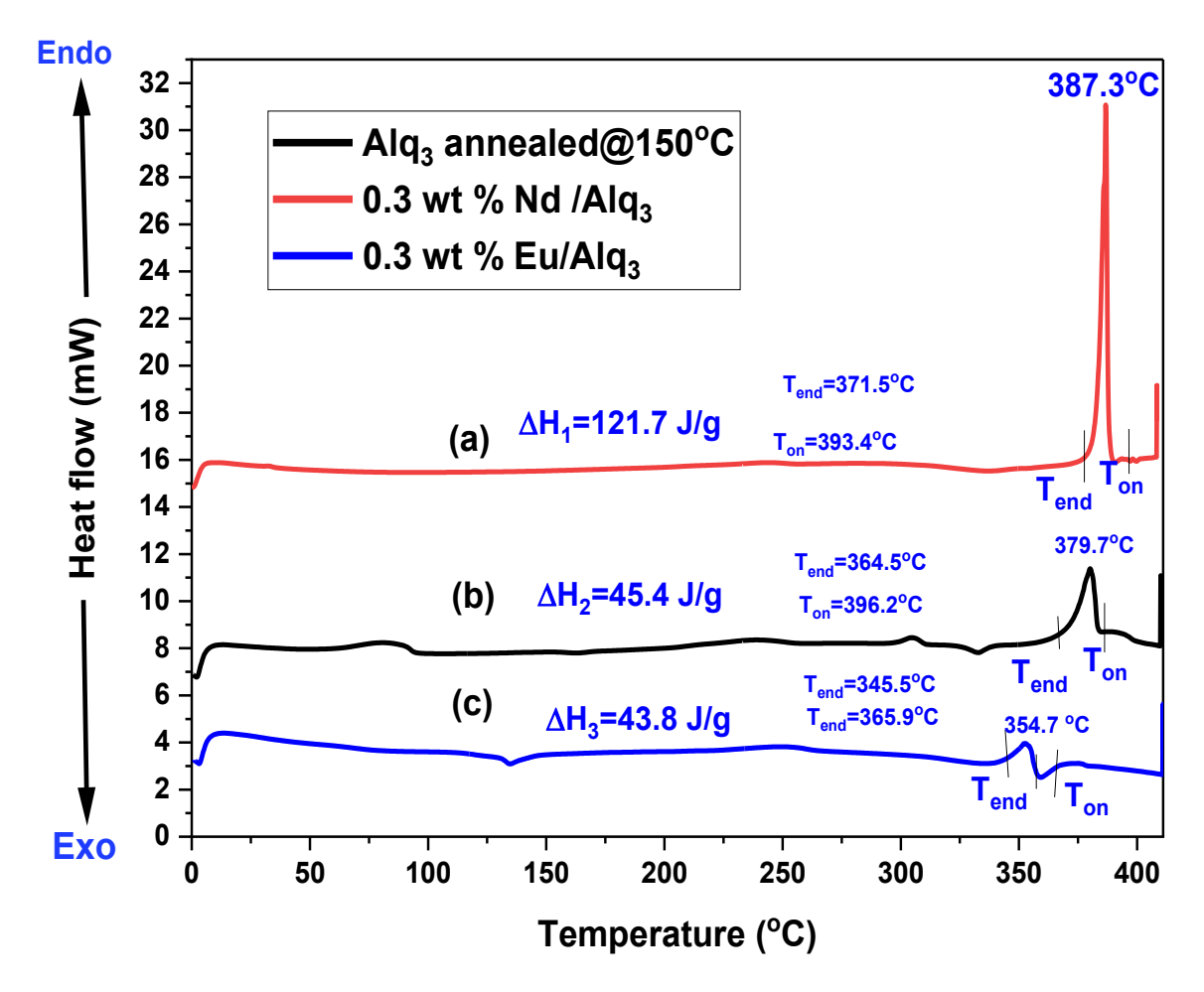


Figure 8.4: DSC curves of (a)bulk Alq₃ powder annealed at 150 °C (b) 0.3 wt % Nd(III) /Alq₃ Nanocomposites and(c) 0.3 wt% Eu(III)/Alq₃ Nanoparticle.

exhibits short endothermic peaks of crystallization at 379.7°C and 414°C while sample (c) 0.3 wt% Eu(III)/Alq₃ Nanoparticle shows one endothermic peak at 354.7 °C and an exothermic peak of melting at 357.1°C which exist adjacent to each other. and ΔH_3 =43.8 J/g, respectively. The specific heat of sample-(a), sample-(b), and sample-(c) 0 are obtained as: ΔH_1 =121.7 J/g, ΔH_2 =45.4 J/g [22,26,39,43,44]

Table 8.4. Comparative analysis of TG and DSC curves of three samples

Compound	Maximu	Temperatu	Endother	Maximu	T <i>e</i> mperat	
	m	re mic		m specific	ure	
	weight	range (from	Melting	heat(J/g)	range	
	loss	°C to °C)	point (°C)/	(ΔH)	(from	
	(%)				°C to °C)	
	$(\Delta \mathbf{Y}_1)$					
Alq ₃ annealed@	76.9-	343.4 to	387.3	121.7	371.5 to	
150°C	18.2=58.7	477.4			393.4	
0.3 wt% Nd/Alq ₃	75.5-	343.3 to	379.7	45.4	364.5 to	
	29.9=45.6	475.7			396.2	
0.3 wt% Eu/Alq ₃	80.4-	169.2 to	354.7	43.8	345.5 to	
	53.7=26.7	398.7			365.9	

C. Optical properties and photoluminescence (PL) properties:

1. Ultra-violet Visible (UV-vis) spectra analysis:

From figure 3(A)we can see the absorbance intensity vs wavelength plot which clearly shows that the maximum absorbance intensity of bulk Alq3 powder is 349.9 nm which blue shifts to 383.5 nm for 0.3 wt% Nd(III)/Alq3 nanocomposites and blue shift to 398.6 for 0.3 wt% Eu(III) nano composites. The peaks for both Alq3 and 0.3 wt% Nd(III) Alq3 nanocomposites are intense and broad whereas for 0.3 wt% Nd(III)/Alq3 nanocomposite is sharp and intense. The absorbance intensity is lowest for bulk powder but maximum value for 0.3 wt% Eu(III)/Alq3 nano- composites. Absorbance intensity peaks seen in between 300 nm and 600 nm wavelengths are produced because of the π - π * transitions of 8-hydroxyquinoline or quinolinolate ligands of host Emitting material Alq3[22,23,26,29,30,43,44].

As Eu(III) ions and Nd(III) ions incorporate into the Alq₃ matrix the intense peaks of Alq₃ at 349.9 nm resulting in a blue shift to 383.5 nm for 0.3 wt% Nd(III)/Alq₃ Nanoparticle and again blue shifts to 398.6 nm for 0.3 wt % Eu(III) /Alq₃ Nanocomposites. After

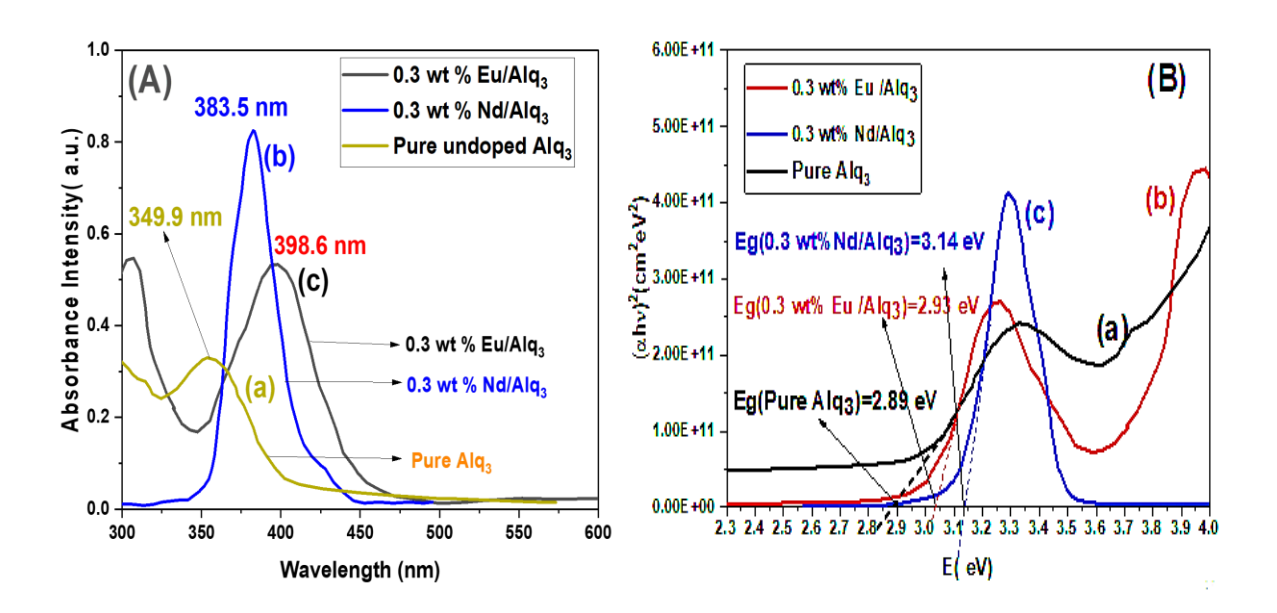


Figure 8.5: (A) UV Vis absorption spectra of (a) Pure Alq₃ Nano-rod powder (b) 0.3 wt% Nd(III)/Alq₃ Nanoparticle (c) 0.3 wt % Eu(III) /Alq₃ Nanocomposites and (B) Tauc plot of (a) Pure Alq₃ Nano-rod powder (b) 0.3 wt % Nd(III) /Alq₃ Nanocomposites and (c) 0.3 wt% Eu(III)/Alq₃ Nanoparticle

analyzing the comparison spectra of these three compounds we validate that rare-earth Eu(III) and Nd(III) ions have certainly embedded into the host Alq₃ matrix resulting in blue shifts for both 0.3 wt% Nd(III)/Alq₃ Nanoparticle and 0.3 wt % Eu(III) /Alq₃ Nanocomposites. The shift of intense peaks are observed also due to the modification of direct Eg (energy bandgaps) of host Alq₃ matrix after the incorporation of Eu(III) and Nd(III) ions into pure Alq₃ matrix. We can ascertain the value of energy bandgap of these three materials using Tauc plot method and obeying the following equation:

$$(\alpha h v) = (h v - Eg)^n \tag{8.7}$$

Where n=2 for allowed indirect transitions and n = $\frac{1}{2}$ for allowed direct transitions, and E_g=energy band gap, α =absorbance coefficient, ν =frequency of absorbed radiation and h=Planc's constant [22,23,29,30],

From Tauc plot of figure 3B, it is noticed that the wide and direct optical band gap of pure Alq₃ powder (2.89 eV) gets elevated to 2.93 eV for 0.3 wt% Nd (III)/Alq₃ Nanoparticle and to 3.14 eV for 0.3 wt % Eu(III) /Alq₃ Nanocomposites. These results confirm that the energy band gap of Alq₃ can be tuned by incorporation of Eu(III) and Nd(III) ions into pure Alq₃ matrix. Here we able to tune the optical energy band gap of emissive layer of Alq₃. Here the produced Eu(III) and Nd(III) embedded Alq₃ possess wide band gap which is pre-requisite for solid state lighting and its allied applications. To maneuver the optical band gap is utmost essential properties of OLEDs., OLETs and solid state lights for its photoluminescence(PL) and electroluminescence(EL). The optical band gap can be tuned easily implementing the variation in doping concentration of rare earth ions into the organic emissive Alq₃ matrix which results in significant improvement of the electron-hole pair recombination rate .[22,23,27,29,30].

2. Photoluminescence (PL) spectra analysis:

Here figure 4 describes normalized PL spectra of Alq3 powder,0.3 wt % Eu(III)/Alq3 and 0.3 wt % Eu(III)/Alq3 nanocomposites. From figure 4 we clearly observe that the Photoluminescence spectral maximum intensities are 520.1 nm,541.3 nm, and 544.5 nm for pure Alq3 powder,0.3 wt% Nd(III)/Alq3 nano composites and 0.3 wt% Eu(III)/Alq3. The 0.3 wt% Eu(III)/Alq3 exhibit highest photoluminescence intensity of 544.5 nm red shifts compared to lowest intensity 520.1 nm of pure Alq3 powder. The 0.3 wt% Nd(III) /Alq3 show PL peaks of intensity 541.3 nm also red –shifts compared to 520.1 nm PL intensity of pure Alq3. The PL intensity of these three material can be expressed in the increasing order of PL intensity as: pure Alq3< 0.3 wt% Nd(III)/Alq3 < 0.3 wt% Eu(III)/Alq3 This results confirms that doping of Eu(III) and Nd(III) ions into Alq3 powder gives better luminescence performance which can be used successfully for the OLED fabrication or solid-state lighting application as a promising emitting material [22,23,26,27,29,43,44]

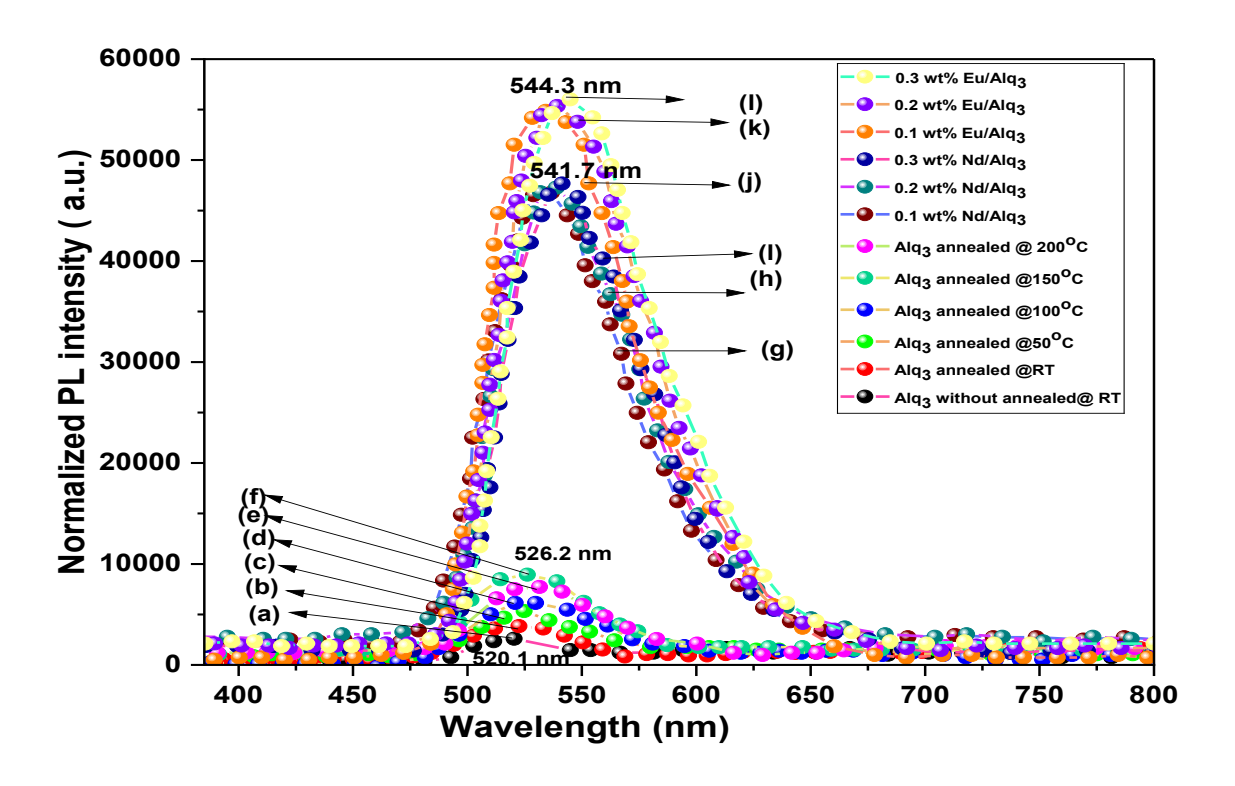


Figure 8.6: Normalized photoluminescence (PL)spectra of (a) Pure Alq₃ Nano-rod powder (b) 0.3 wt% Nd(III)/Alq₃ Nanoparticle (c) 0.3 wt% Eu(III) /Alq₃ Nanocomposites

3. FTIR (Fourier Transform Infra –Red) spectra analysis:

The FTIR spectroscopy of figure 4(a),(b)and(c) given by PERKIN EILMER IR spectrometer, exhibits that maximum number of intense and sharp FTIR characteristic downward peaks are found within the range between 468 cm⁻¹ and 1663 cm⁻¹. The intense FTIR characteristics peaks of pure Alq₃ Nano-rod powder, 0.3 wt% Eu(III)/Alq₃ Nanoparticle and 0.3 wt % Nd(III) /Alq₃ Nanocomposites, within wavenumber 400-800 cm⁻¹, are formed because of vibration modes of the aforementioned materials. The weak FTIR intensity peaks are seen at 3672 cm⁻¹ due to non-bonded O-H vibrational stretch of hydroxyl functional groups. The aromatic C-C bonding of pyridine ring, quinolinolate ligands benzene ring are also seen at 3044.3 and 2909 cm⁻¹ respectively. The C–N-C bond among three 8-hydroxy quinoline or quinolinolate ligands and central metallic Al(III)

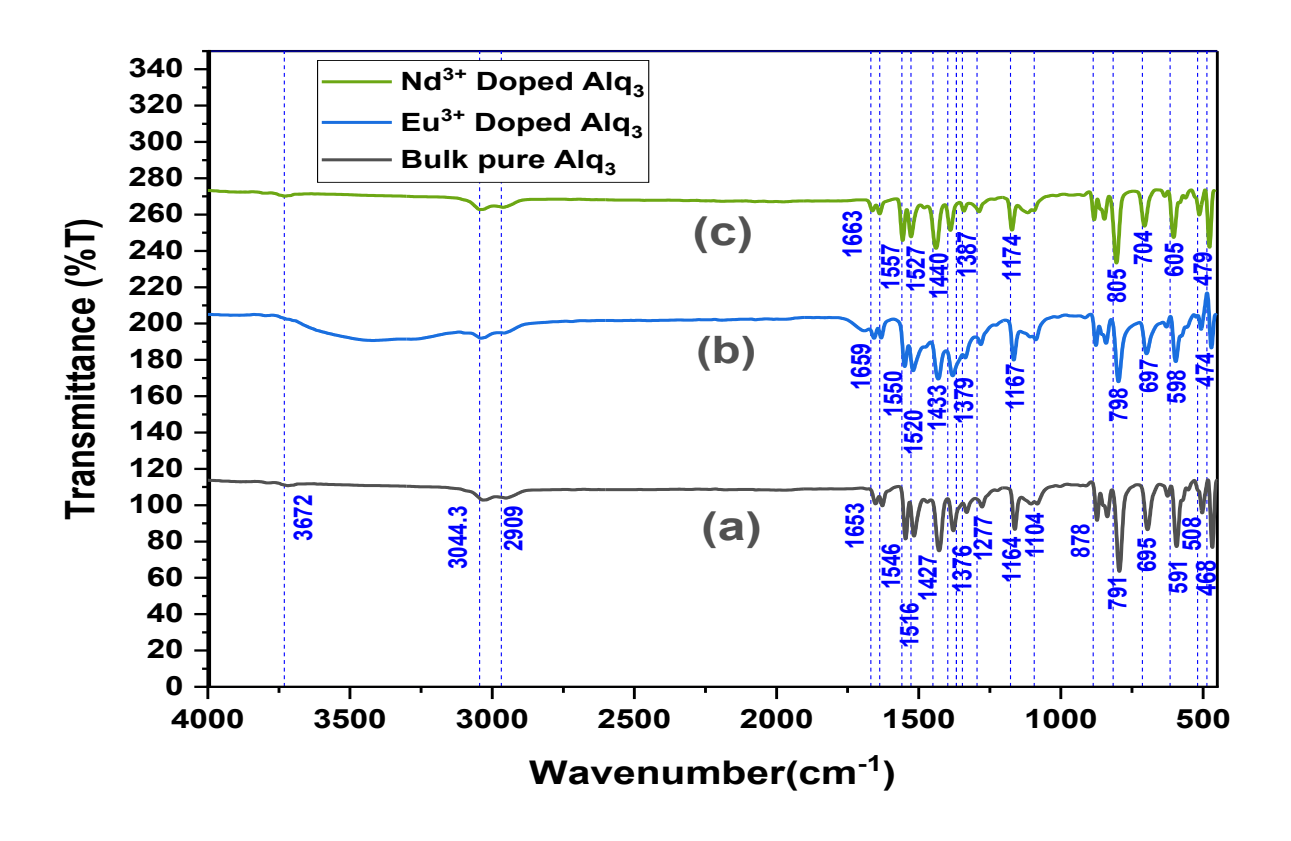


Figure 8.7: FTIR spectroscopy of a) Pure Alq₃ Nano-rod powder (b) 0.3 wt% Eu(III)/Alq₃ Nanoparticle (c) 0.3 wt % Nd(III) /Alq₃ Nanocomposites

atoms, Eu(III) or Nd(III) atoms are visible at 1653,1546, 1516, 1427, 1376 and 1277 cm⁻¹. The C–O bond between deprotonated hydroxyl functional group (OH) of 8-Hq ligands and benzene rings are seen at 1164 and 1104 cm⁻¹, the aromatic amines are found at 1427 and 1376 cm⁻¹ aromatic C=C bond of pyridine and benzene ring are observed at 1653 and 1611 cm⁻¹, C-H bonds are visible at 878 and 791 cm⁻¹, short length Al–O–Al bond are seen at 791 cm⁻¹, Al–O bonds appear at 591 and 695 cm⁻¹. and Al–N bonds are detected at 468 cm⁻¹. Eu-O bonds are found at 474 cm⁻¹.and Nd-O bonds are found at 478 cm⁻¹.Due to stretching vibration mode of Al³⁺ or Eu³⁺or Nd³⁺ cation, quinolinolate (C₆H₅NO⁻) anion, Al-N bonds or Eu-N or Nd-N bonds and Al-O bonds or Eu-O bonds or Nd-O bonds of metal oxides are found at 417 cm⁻¹ and 454 cm⁻¹ which is in agreement with the result as reported Xia Lu et al[36], .These FTIR characterizing peaks validates the existence of Pure

Alq₃ Nano-rod powder ,0.3 wt% Eu(III)/Alq₃ Nanoparticle and 0.3 wt % Nd(III) /Alq₃ Nano-composites. It also confirms that europium nitrate [Eu(NO₃)₃] and neodymium nitrate [Nd(NO₃)₃] nanoparticles incorporate into the Alq₃ matrix. this results also match the results we get from XRD and FESEM analysis. [22-27,41,42,43,44-47]

D. Electrical properties, electrochemical properties and electroluminescence properties study:

1. Electrochemical properties analysis:

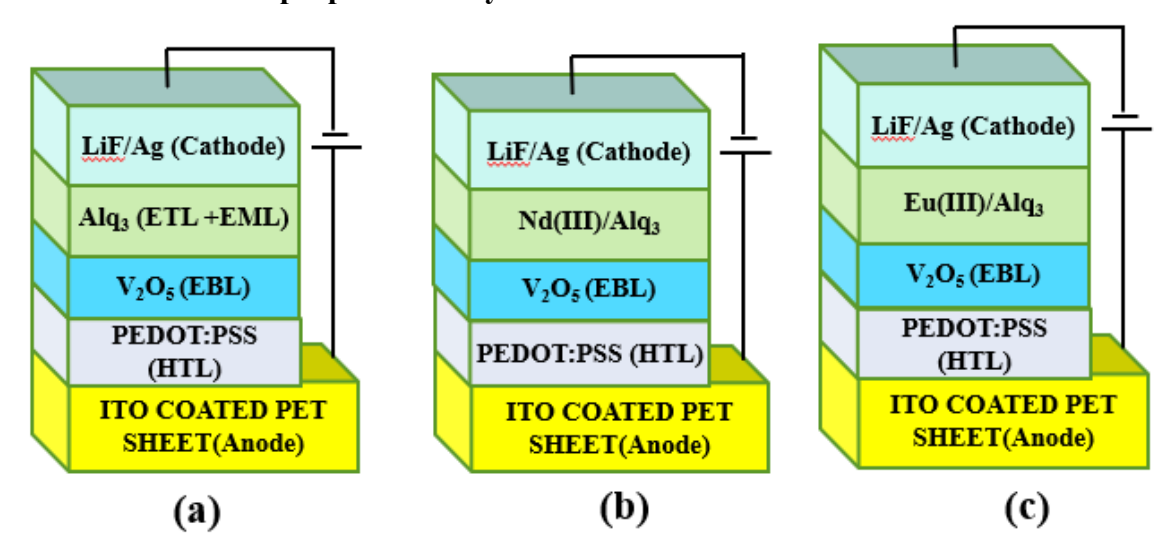


Figure 8.8: Schematic architecture of (a) Device1: ITO/PEDOT:PSS/ V₂O₅/Alq₃/LiF/Ag -based OLED (b) Device2: ITO/PEDOT: PSS/ V₂O₅/0.3wt%Nd(III)/Alq₃/LiF/Ag- based OLED and (c) Device3: ITO/PEDOT: PSS/V₂O₅/0.3 wt % Eu(III)/Alq₃/LIF/Ag- based OLED

We have performed three electrodes containing cell system based cyclic voltammetric measurement aided by AUTOLAB PGSTAT-30 electrochemical analyzer with scanning rate of 10 mV/s keeping the whole system at room temperature. We took 0.1 M acetonitrile solution (tetrabutyl ammonium hexafluoro phosphate solution) as our supporting electrolyte [24],Ag/AgNO₃ as reference electrode submerged in 0.1 M acetonitrile electrolyte solution and Pt(platinum)-metal as our counter electrode in addition to our working electrode. We purged each solution that was used for our experiment with ultrapure N₂ gas for 15 minutes before its use in the cell and a N₂ blanket was utilized during

our experiment.

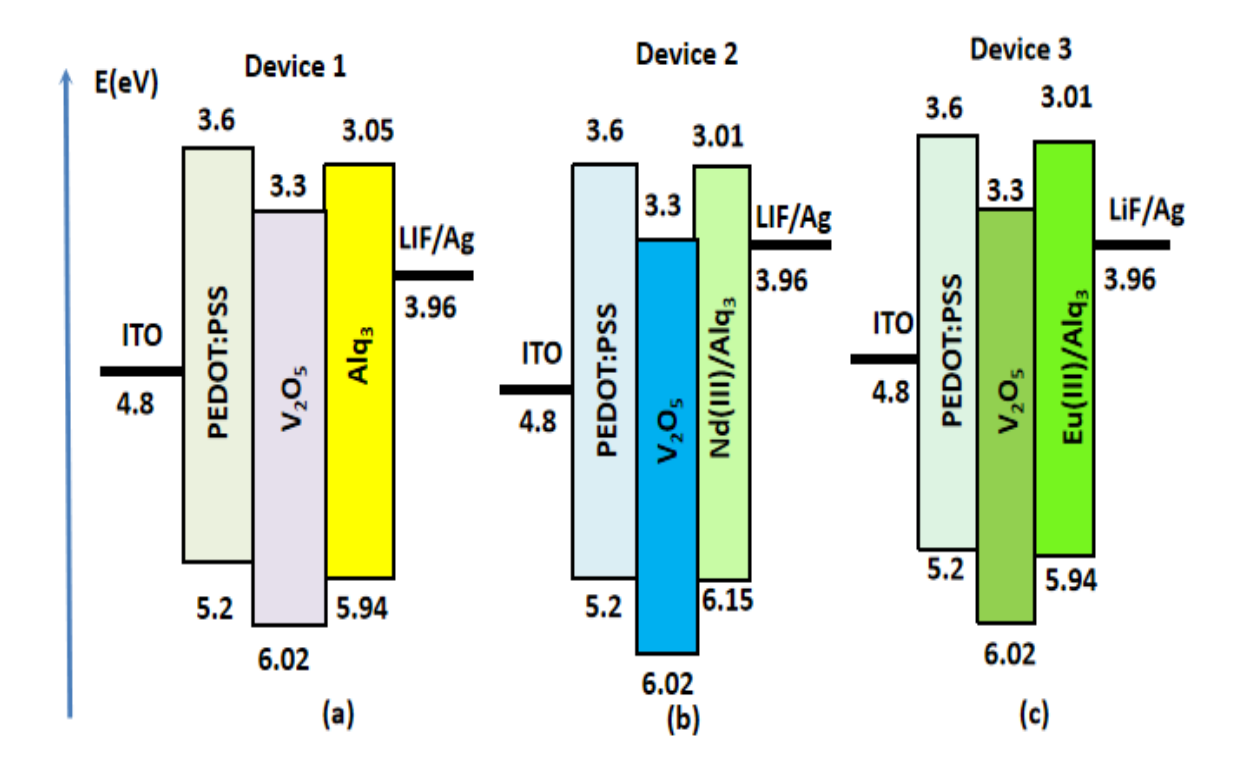


Figure 8.9: Schematic energy level of (a) Device1: ITO/PEDOT: PSS/ V₂O₅/Alq₃/LiF/Ag based OLED (b) Device2: ITO/PEDOT: PSS/ V₂O₅/0.3wt%Nd(III)/Alq₃/LiF/Ag based OLED and (c) Device3: ITO/PEDOT: PSS/V₂O₅/0.3 wt % Eu(III)/Alq₃/LIF/Ag based OLED

We have found out the HOMO energy levels LUMO energy levels as well as the charge – injection capacities of the a) Pure Alq₃ Nano-rod powder (b) 0.3 wt% Eu(III)/Alq₃ Nanoparticle (c) 0.3 wt % Nd(III) /Alq₃ Nanocomposites respectively. The onset oxidation potentials, the reduction potentials, HOMO –LUMO energy level and the energy bandgap of the above-mentioned three materials are clearly depicted in Fig.6 & Figure 7 and in table 2. The free hydroxyl functional group the Alq₃ and its derivatives which make hydrogen

Table 8.5: Comparison table for device HOMO LUMO energy levels of each constituent charge carrier conducting and emissive layer materials of OLED device 1, OLED device 2 and OLED device 3

Compound	Eox onset VS	Ered onset VS	НОМО	LUMO	Eg (LUMO -
	$\mathbf{E_{Fc}}$ (V)	E _{Fc}	(eV)	(eV)	НОМО)
		(V)			(eV)
PEDOT:PSS	0.44	-1.18	-5.24	-3.62	1.62
V_2O_5	1.22	-1.52	-6.02	-3.28	2.74
Alq ₃	1.14	-1.75	-5.94	-3.05	2.89
0.3wt% Nd/Alq ₃	1.35	1.79	-6.15	-3.01	3.14
0.3 wt% Eu/Alq ₃	1.14	-1.79	-5.94	-3.01	2.93

bonds with the CV solvent used for CV measurement. For cathodic scans the $E_{\text{red onset}}$ (onset reduction potentials) of 1.18 V to 1.79 V versus Ag/AgNO₃ having quasi-reversible reduction waves are observed whereas irreversible oxidation waves having $E_{\text{ox onset}}$ (onset oxidation potentials) of 0.44 to 1.35 V versus Ag/AgNO₃ are found in the case of anodic scans. The energy levels of those three compounds can be determined compared with the reference onset potentials i.e.,4.8 eV vs. vacuum of the fferrocene [8]. The energy levels of HOMO and LUMO can be evaluated putting the $E_{\text{ox onset}}$ and $E_{\text{red onset}}$ values in the following two equations:

$$E_{HOMO} = [-4.8 - E_{ox \text{ onset}}] \tag{8.2}$$

$$E_{LUMO} = [-4.8 - E_{red onset}]$$
 (8.3)

Using these two formulae we get the value of HOMO energy level of the oxidation waves within the range of 5.24-6.15 V while the value of LUMO energy levels lies within 3.01-3.62 V (lower than vacuum). The energy gap values of HOMO–LUMO energy levels of the Alq₃ and its two nanocomposites lies within the range 1.62–3.14 eV. It is noteworthy that the band gap values evaluated through electrochemical cyclic voltammetry match with the value of optical band gap we have found from Tauc plot method of UV-VIS absorbance

spectra. Here LUMO energy levels of the Alq₃ and its two derivatives exhibit low values comparable to relatively higher value containing HOMO energy levels resulting in higher electron affinities in those three compounds under experiment. Hence these three materials can be chosen for their promising green and yellow emitting properties and as excellent n-type electron transporting characteristics or hole blocking characteristics for solid state lights, LEDs and OLEDs and their applications. [48.51,52-55]

C. Chromaticity diagram analysis (on the basis of CIE 1931):

The CIE coordinates of sample (a), (b),(c) and (d) are (0.3297,0.3526),(0.3078,0.4453), (0.3860,0.5334) and (0.3828,0.5447). The CIE- coordinates of (a), (b), (c) and (d) are located in the greenish white region, white region, greenish yellow region and greenish yellow region. We can regulate the location of CIE coordinates by substituting diversified functional groups or atoms at the different corners of phenoxy ligand of aromatic ring containing pyridine group. The locations of CIE coordinate of the sample (a), (b), (c) and (d) confirm that these four samples are excellent electroluminescent emitters which can be used as emissive layer in solid state lights and OLED displays and lights and other OLED applications. Sample (a) can be used as WOLED, green OLED emitters. Sample (b) can be used as pure WOLED emitters and sample (c) and sample(d) can be used as greenish yellow, green and yellow SSL and OLED emitters. The sample(a) shows correlated color temperature (CCT) is 6143 K, color rendering index (CRI)value = 98 and R9 value= 92 and sample (b) has CCT value=5592K, CRI value=91, R9 value=91, while sample (c) possesses CCT value=7352K, CRI value=59, R9 value = -86, and sample (d) has CCT=8935,CRI=63 and R9 value =-69 negative value of R9 value denotes lower content of red light in the mixture of emitted colour. The high CRI value and CCT value confirm the brighter cool white light emission. After comparative analysis of the four samples, it is confirmed that all four samples are potential OLED emitters. The first two can be used in cool brighter WOLED application and the last two can be used in WOLED with green or yellow tint, along with green and yellow OLED light [52-55]

CIE 1931

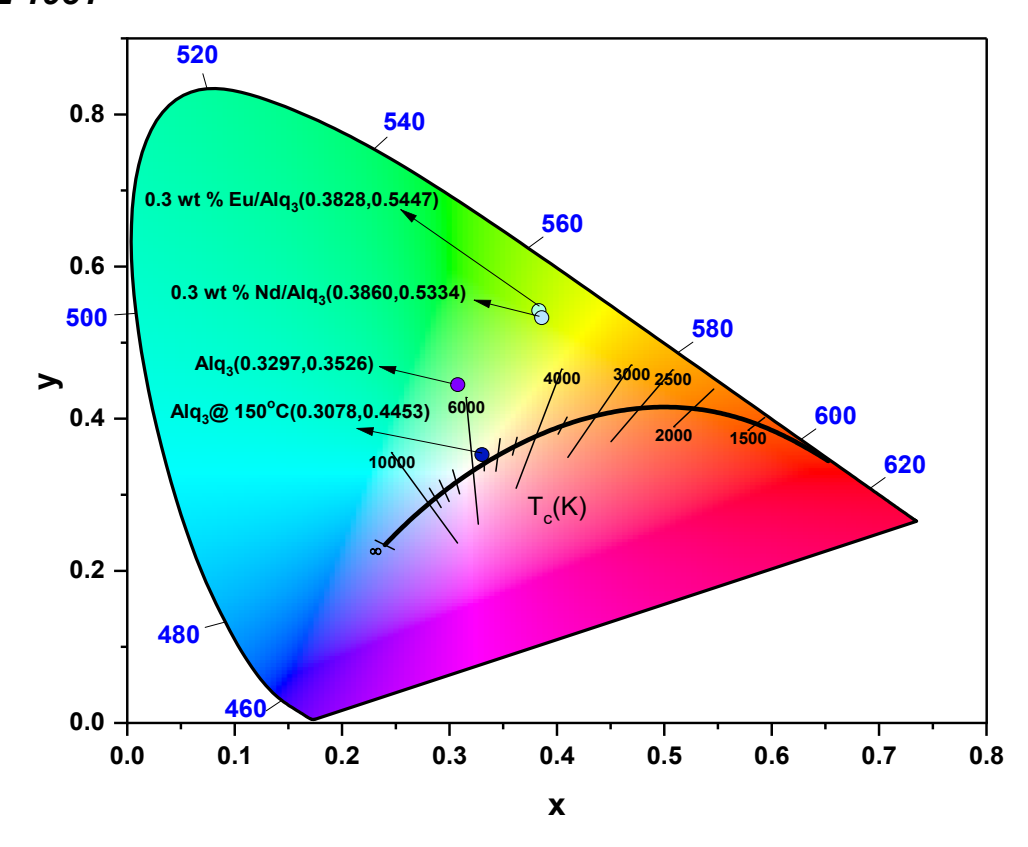


Figure 8.10: Chromaticity diagram of pure Alq₃ powder-based ITO/PEDOT: PSS/V₂O₅/Alq₃/LiF/Ag based and its annealed sample at 150°C and 0.3 wt% Neodymium(III) ion and 0.3 wt% Europium (III) ion doped Alq₃ nanocomposites and OLED made by them.

We find out CIE coordinates in Figure 7 and table 3 to detect the material efficiency and EL performance of our three electroluminescent materials i.e., (a) pure Alq₃ Nano-rod powder (b)Pure Alq₃ Nano-rod powder annealed at 150°C (c) 0.3 wt% Eu(III)/Alq₃ Nanoparticle (d) 0.3 wt % Nd(III) /Alq₃ Nanocomposites. We compare four CIE color coordinates to know the emission colour emitted by those electroluminescent materials individually through Origin software. The PL spectrum of the abovementioned four samples was excited at 355 nm.

Table 8.6: Comparative chromaticity data analysis of four samples (a) (b) (c) and (d)

Compound	CCT	CRI	R9	X	y	CIE	$\lambda_{emission}$
						coordinates	
Alq ₃ powder	6143 K	98	92	0.3297	0.3526	(0.3297, 0.3526)	517.6
without annealed							nm
Alq ₃ powder	5592K	98	91	0.3078	0.4453	(0.3078, 0.4453)	520.6
annealed at 150							nm
°C							
0.3 wt%	7352 K	59	-86	0.3860	0.5334	(0.3860,0.5334)	541.3
Nd(III)/Alq ₃							nm
0.3 wt % Eu(III)	8935K	63	-69	0.3828	0.5447	(0.3828, 0.5447)	544.5
/Alq ₃							nm

D. Electroluminescence properties study:

1. Current density –voltage and Luminance- voltage plot analysis:

To investigate the electroluminescent properties of Alq₃ and rare earth ion Eu(III) ion and neodymium Nd(III) ion doped Alq₃ nano composites w fabricated un-optimized three OLED devices. We fabricated these three devices without using any vacuum condition without any proper encapsulation and thus these OLED devices are exposed to a normal optimum atmospheric environment i.e. at normal temperature (R.T i.e 27°C or 300K) and pressure. We illustrated the HOMO energy levels and LUMO energy levels of the trilayered OLED materials used for construction of these three OLED devices. namely, ITO-coated PET sheet (175nm)/PEDOT:PSS(48nm)/V₂O₅ (12nm)/Alq₃ (83 nm)/LiF(3 nm)/Ag (100 nm)[device1], ITO-coated PET sheet (175nm)/PEDOT:PSS(48nm)/V₂O₅ (12nm)/Nd:Alq₃ (83 nm)/LiF(3 nm)/Ag(100nm)[device2]and ITO-coated PET sheet (175nm)/ PEDOT:PSS(48nm)/V₂O₅ (12nm)/Eu:Alq₃ (85 nm)/Ag (100 nm)[device respectively. Where ITO acts as a transparent anode, PET sheet as substrate, PEDOT: PSS as HTL V₂O₅ as hole blocking layer. Alq₃ acts ETL and EML and Metallic Ag was used

3]device1, device 2 and device 3. The architectural configuration of these three tri-layered OLED devices are as follows:

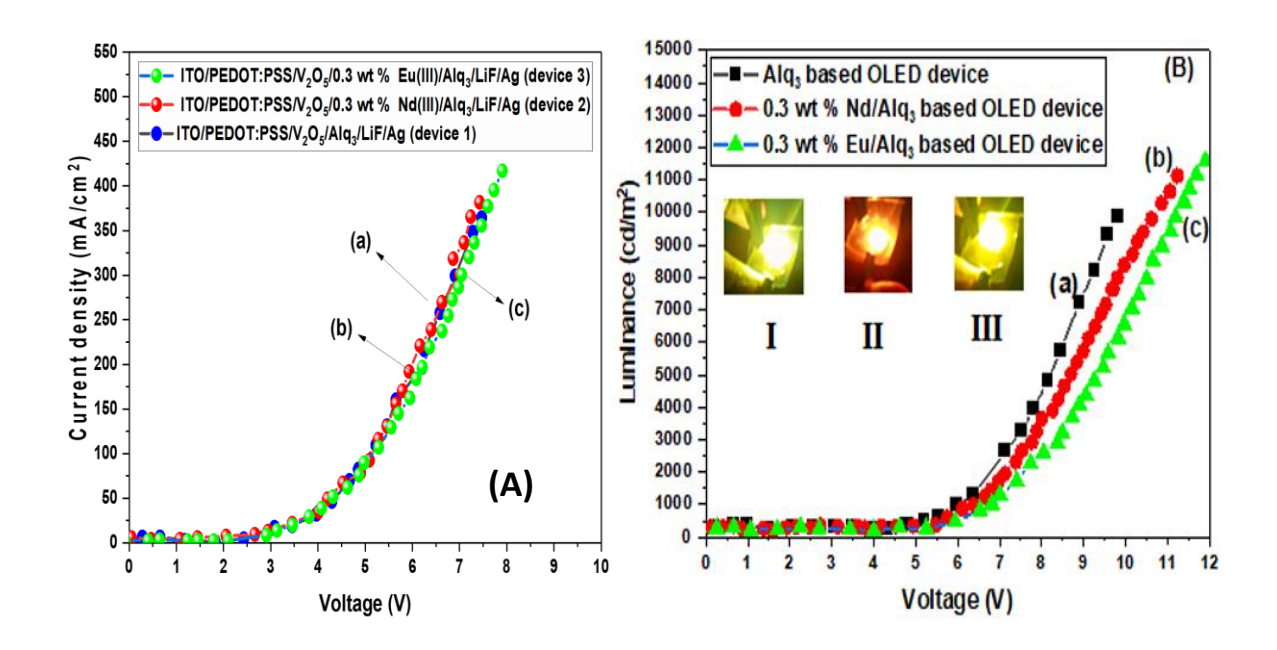


Figure 8.11 :(A) Current density vs voltage (J-V) plot (B) Luminance vs-voltage(L-V) plot for(a)ITO/PEDOT:PSS/V₂O₅/Alq₃/LiF/Ag(device1)(b) ITO/PEDOT:PSS/ V₂O₅/0.3wt% Nd(III):Alq₃/LiF/Ag(device2)and(c)ITO/PEDOT:PSS/V₂O₅/0.3wt%Eu(III):Alq₃/LiF/Ag (device 3)

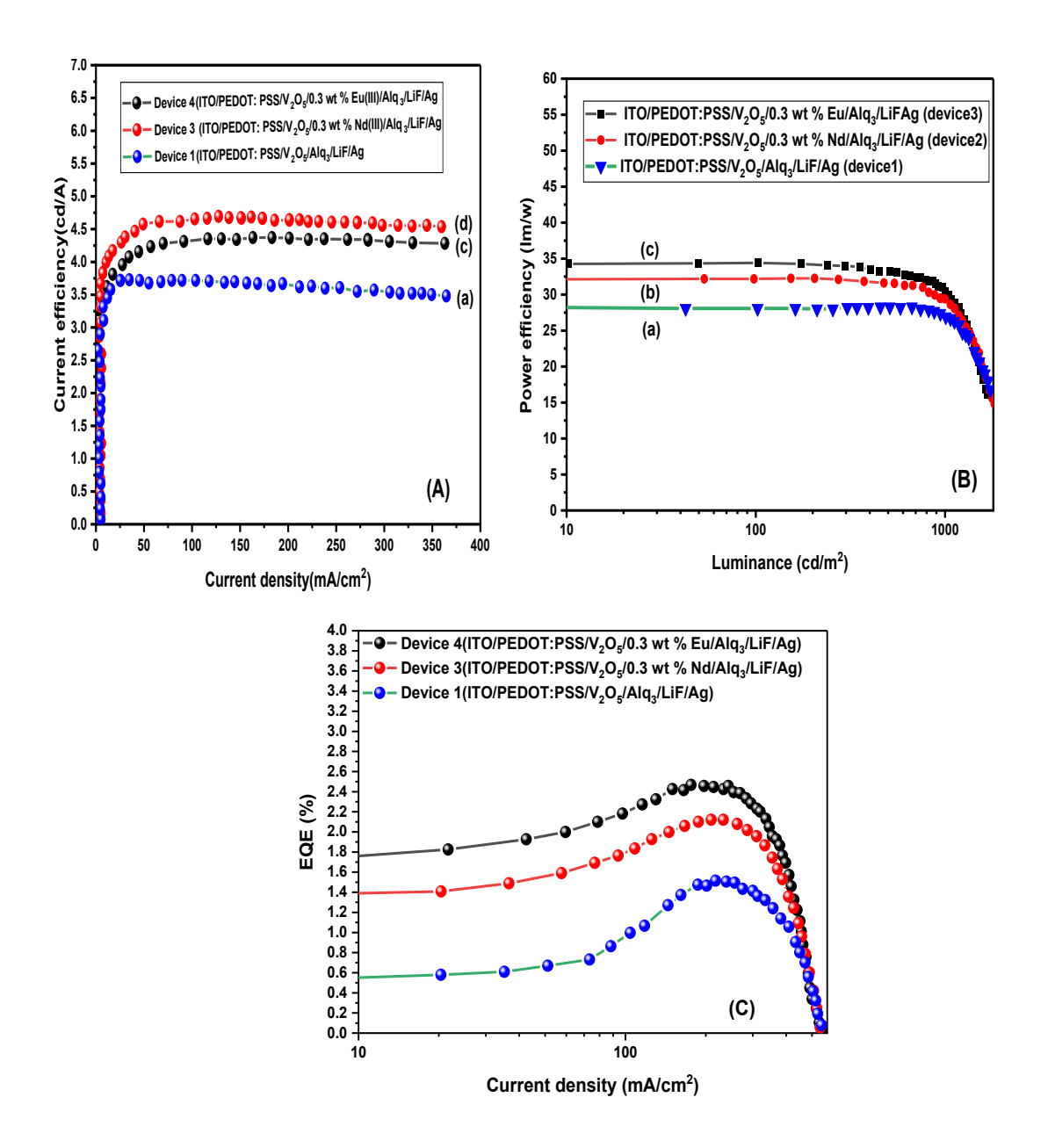
as low work function cathode as well as EIL respectively. From the plot of figure 8(A) we can compare the current density-voltage(J-V) characteristics of (a) ITO/PEDOT: PSS/V₂O₅/Alq₃/LiF/Ag (device1) (b) ITO/PEDOT: PSS/V₂O₅/0.3 wt% Nd(III):Alq₃/LiF/Ag(device2) and (c) ITO/PEDOT: PSS/V₂O₅/0.3wt%Eu(III):Alq₃/LiF/Ag (device 3).

We see the current density versus applied voltage curve of (a),(b) and (c) are almost identical in shape but curve (c) shows highest current density of 413.3 A/m² at 7.48 volt and for (a) current density 387.2 A/m² at 7.13 volt and (b)current density 367.8A/m² at 7.38 volt.[55]

From luminance-voltage(L-V) plot of figure 8(B) we observe three distinct curves. Figure

8.8B(a) shows maximum luminance of 9862.7 cd/m² at 9.8 volt, turn on voltage=2.87 volt at 1 cd/m² luminance and driving voltage =6.3v for 1000 cd/m² luminance. Curve (b) gives maximum luminance 11210.2 cd/m² at 11.2 volt, turn on voltage=2.56 volt at 1 cd/m² luminance and driving voltage =6.1v for 1000 cd/m² luminance while curve (c) exhibits maximum luminance of 11586.2 cd/m² at 11.9 volt, turn on voltage=2.48 volt at 1 cd/m² luminance and driving voltage =5.8v for 1000 cd/m² luminance. The device 3 exhibits best current density and luminance compared to the other two devices i.e., device 1 and device 2. The inset picture III also shows bright yellowish green luminescence for device 3 which is brightest among the three devices where I, II and III denote device1, device 2 and device 3.

From Figure 8.9(A),8.9(B) and 8.9(C) we demonstrate the electron transport properties the current efficiency vs. current density (η_c -J) plot, power efficiency vs. Luminance (η_p -L) plot and external quantum efficiency vs. current density (next-J) plot for three fabricated OLED devices. Our fabricated three devices are as follows: (a) ITO/PEDOT: $ITO/PEDOT: PSS/V_2O_5/0.3wt\%$ PSS/V₂O₅/Alq₃/LiF/Ag (device1) (b) Nd(III):Alq₃/LiF/Ag(device2)and(c) ITO/PEDOT:PSS/V₂O₅/0.3wt%Eu(III):Alq₃ /LiF/Ag (device 3). From figure 9(A)(a)(b) and (c) we get device 1 shows maximum current efficiency of 3.89 cd/A at 123.8 mA/cm² while device 2 exhibits maximum current efficiency of 4.14 cd/A at 167.6 mA/cm² and device 3 shows maximum current efficiency of 4.69 cd/A at 130.0 mA/cm². Therefore device 1 and device 3 exhibit the lowest and the highest current efficiency. From figure 9(B)(a)(b) and (c) we get device 1 shows maximum power efficiency of 28.74 lm/W at 9.78 cd/m² while device 2 exhibits maximum power efficiency of 32.35 lm/W at 9.78 cd/m² and and theice 3 shows maximum power efficiency of 34.48 lm/W at 9.78 cd/m². Therefore device 1 and device 3 exhibit the lowest and highest power efficiency. From Figure 9(A),9(B)and9(C) we demonstrate the current efficiency vs. current density (η_c -J) plot power efficiency vs. Luminance (η_p -L) plot and a) ITO/PEDOT:PSS/V₂O₅/Alq₃/LiF/Ag(device1)(b)ITO/PEDOT:PSS/V₂O₅/0.3wt%Nd(III) :Alq₃/LiF/Ag(device2) and (c)ITO/PEDOT:PSS /V₂O₅/0.3wt%Eu(III):Alq₃/LiF/Ag (device 3)



-Figure 8. 12 :(A) Current efficiency vs. current density (η_c -J) plot (B)Power efficiency vs. Luminance (η_p -L) plot for (C) External quantum efficiency vs. current density (η_{ext} -J) plot for (a) ITO/PEDOT:PSS/V₂O₅/Alq₃/LiF/Ag(device1)(b)ITO /PEDOT:PSS /V₂O₅/0.3wt%Nd(III):Alq₃/LiF/Ag(device2) and (c)ITO/PEDOT:PSS /V₂O₅/0.3wt%Eu(III):Alq₃/LiF/Ag (device 3)

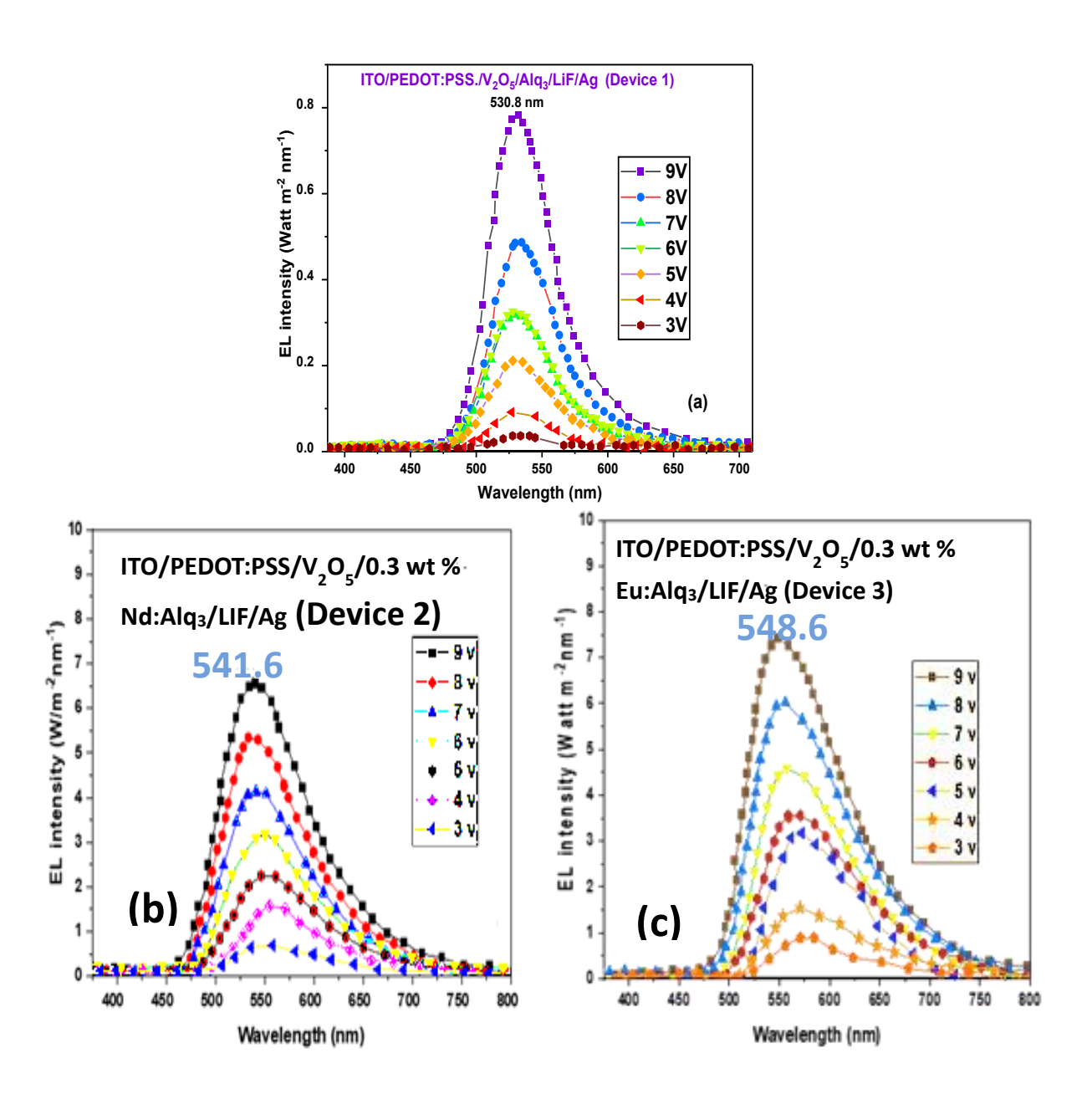


Figure 8.13: Electroluminescence intensity versus wavelength(EL - λ) plot for different voltage ranging from 3V to 9V for (a) ITO/PEDOT:PSS/V₂O₅/0.3wt% Alq₃/LiF/Ag(device1) (b) ITO/PEDOT:PSS/V₂O₅/0.3wt% Nd(III):Alq₃/LiF/Ag(device2) and(c)ITO/PEDOT:PSS/V₂O₅/0.3wt%Eu(III):Alq₃/LiF/Ag (device 3)

cd/A at 123.8 mA/cm² while device 2 exhibits maximum current efficiency of 4.14 cd/A at 167.6 mA/cm² and

Table 8.7: Comparative analysis of device performances of three OLED devices

Device	Turn-		Voltage	Voltage	EQE	CE	PE	Maximum
name	on	Driving	at	at	(%)	(cd/A)	(lm/W)	luminance
	Voltage	voltage	1 cd/m ²	1000				at
				cd/m²				maximum
								Voltage
Device 1	2.86	6.3	2.87	6.3	1.488	3.89	28.74	9852.7
								(9.8)
Device 2	2.61	6.1	2.56	6.1	2.142	4.14	32.35	11210.2
								(11.2)
Device3	2.56	5.8	2.4.8	5.8	2.471	4.69	34.48	11586.2
								(11.9)

device 3 shows maximum current efficiency of 4.69 cd/A at 130.0 mA/cm². Therefore device 1 and device 3 exhibit the lowest and the highest current efficiency. 3). From figure 9(B)(a)(b) and (c) we get device 1 shows maximum power efficiency of 28.74 lm/W at 9.78 cd/m² while device 2 exhibits maximum power efficiency of 32.35 lm/W at 9.78 cd/m² and device 3 shows maximum power efficiency of 34.48 lm/W at 9.78 cd/m². Therefore device 1 and device 3 exhibit the lowest and the highest power efficiency. From figure 9(C)(a)(b) and (c) we get device 1 shows maximum external quantum efficiency of 1.488% at current density of 202.3 mA/cm² while device 2 exhibits maximum external quantum efficiency of 2.142 % at current density of 240.1 mA/cm² and device 3 shows maximum external quantum efficiency 2.471 % at current density of 276.0 mA/cm². Therefore device 1 and device 3 exhibit the lowest and the highest external quantum efficiency. [52-55]

From figure 8.10(A)(B) and (C) we find the change of EL- λ spectra for different operating

voltage starting from 3V to 9V of device 1, device 2 and device 3 at room temperature respectively. The highest EL peaks for device1, device2 and device 3 are found at 530.8 nm ,541.6 nm and 548.6 nm which are almost alike when we compare with the highest peaks of PL intensity. The only difference we found for annealed Alq₃ at 150°C [Figure8.10. (a)].[52-55]

8.7. Conclusion:

In this research work we have studied the surface morphology, electrochemical properties, thermal properties, optical properties as well as electrical properties of bulk Alq₃ powder annealed at 150°C, 0.3 wt% Nd (III): Alg₃ Nano composites and 0.3 wt% Eu(III): Alg₃ Nano composites. At first, we synthesized mer-Alq₃ powder in lab then annealed from room temperature to 200°C. We observe that the mer Alq₃ powder annealed at 150°C exhibits the best optical and electrical properties needed for solid state lighting and OLED application. Then we fabricate three unoptimized OLED devices: (a) ITO/PEDOT: PSS/V₂O₅/Alq₃/LiF/Ag (device1) (b) ITO/PEDOT: PSS/V₂O₅/0.3wt% Nd(III):Alq₃/LiF/Ag(device2) and (c) ITO/PEDOT: PSS/ V₂O₅/0.3wt%Eu(III):Alq₃/Ag (device 3 device 1, device 2 and device 3. To investigate the influence of rare earth ion and rare earth complexes of Alq₃ we found that out of three OLED devices, device 3 performs bitter than its other two counter parts i.e., device 1 and device 2.the chemical and molecular structures were determined through XRD analysis, FESEM and FTIR analysis. Alq₃ and its annealed form at 150°C. The analysis of photo-physical properties through PL spectra and chromaticity diagram, CIE coordinates CCT value, CRI value and R9 confirmed that sample (a) ,sample (b) and sample (c) emit greenish white or white and greenish yellow and yellow photoluminescence respectively with higher chromaticity value and significant Stoke shifts. The thermal properties through TGA and DSC analysis confirmed the excellent molecular stability of those three samples. The electrochemical properties study through cyclic voltammetry indicates the low values of HOMO and LUMO energy levels of all three samples. Thus, they all possess excellent hole-blocking or electron transport capabilities. The three penta-layered unoptimized OLED devices with (a)bulk Alq₃ powder annealed at 150°C(b) 0.3 wt% Nd (III):Alq₃ Nano composites and (c)0.3 wt% Eu(III):Alq₃ Nano composites. Sample (a)showed a CE of 3.89 cd/A, PE of 28.74 lm/W

and EQE of 1.488% CCT of 5592 and CRI of 97,Sample (b) showed a CE of 4.14 cd/A,PE of 32.35 lm/W and EQE of 2.142 %, CCT of 7352 and CRI of 59 and sample(c) exhibited a CE of 4.69 cd/A,PE of 34.48 lm/W and EQE of 2.471%. CCT of 8935K and CRI of 63. From these results we can infer that Alq3 annealed at 150°C and their rare-earth doped nanocomposites are excellent emissive material and can surely be used for solid state lighting, OLED displays, OLED lights and their other possible applications. We also achieve our third and fourth research objectives through this experimental study discussed in this chapter. To achieve our goal, we incorporated rare earth metallic ion Eu³⁺ and Nd³⁺ into annealed Alq3 matrix-based OLED devices to tune recombination rate, optical band gap tuning, interstate crossing (IS), higher durability along with higher photoluminescence and electronic devices which are 3 times and 4 times better than pristine Alq3 emitter-based OLED. device. The green luminescence of pure Alq3 changes to greenish yellow. Our obtained results successfully have achieved our research objective number 3 and 4.

References:

- [1.] Curry, R. J., & Gillin, W. P. (2001). Electroluminescence of organolanthanide based organic light emitting diodes. *Current Opinion in Solid State and Materials Science*, *5*(6), 481-486.
- [2.] Eliseeva, S. V., & Bünzli, J. C. G. (2010). Lanthanide luminescence for
- [3.] Carnall, W. T., Goodman, G. L., Rajnak, K., & Rana, R. S. (1989). A systematic analysis of the spectra of the lanthanides doped into single crystal LaF3. *The Journal of chemical physics*, 90(7), 3443-3457.
- [4.] de Bettencourt-Dias, A. (2007). Lanthanide-based emitting materials inlightemitting diodes. *Dalton Transactions*, (22), 2229-2241.
- [5.] Geusic, J. E., Marcos, H. M., & Van Uitert, L. (1964). Laser oscillations in Nd- doped yttrium aluminum, yttrium gallium and gadolinium garnets. *Applied Physics Letters*, 4(10), 182-184.
- [6.] Tang, C. W., & VanSlyke, S. A. (1987). Organic electroluminescent diodes.

- *Applied physics letters*, *51*(12), 913-915.
- [7.] Chen, Y., & Ma, D. (2012). Organic semiconductor heterojunctions as charge generation layers and their application in tandem organic light-emitting diodes for high power efficiency. *Journal of Materials Chemistry*, 22(36), 18718-18734
- [8.] Van Slyke, S.A., Chen, C.H., & Tang, C. W. (1996). Organic electroluminescent devices with improved stability. *Applied physics letters*, 69(15), 2160-2162...
- [9.] Tang, C. W., VanSlyke, S. A., & Chen, C. H. (1989). Electroluminescence of doped organic thin films. *Journal of applied physics*, 65(9), 3610-3616..
- [10.] Burrows, P. E., Gu, G., Bulovic, V., Shen, Z., Forrest, S. R., & Thompson, M.E. (1997). Achieving full-color organic light-emitting devices for lightweight, flat-panel displays. *IEEE Transactions on electron devices*, 44(8), 1188-1203.
- [11.] Kim TS, Kim DH, Im H-J, Shimada K, Kawajiri R, Okubo T, Murata H, Mitani T (2004) Improved lifetime of an OLED using aluminum(III) tris (8-hydroxyquinolate).
- [12.] Salleh, M. M., Hasnan, T., Azis, T., Sepeai, S., & Yahaya, M. (2007). Fabrication of organic light emitting diodes (oleds) for flat panel displays. *Berkala Ilmiah MIPA*, 17(3).
- [13.] Kim, J. S., & Song, C. K. (2019). Textile display with AMOLED using a stacked-pixel structure on a polyethylene terephthalate fabric substrate. *Materials*, *12*(12), 2000.
- [14.] Thangaraju K, Kumar J, Amaladass P, Mohanakrishnan AK, Narayanan V (2006) Study on photoluminescence from tris-8-hydroxyquinoline aluminium thin films and influence of light. *Appl Phys Lett* 89:082106–3
- [15.] Colle M, Gmeiner J, Miliu W, Hillebrecht H, Brutting W (2003) Preparation and characterization of blue-luminescent Tris(8-hydroxyquinoline)-aluminum (Alq₃). *Adv. Funct. Mater.13(2)*, 108–112 (2003).

- [16.] Jou, J. H., Kumar, S., Agrawal, A., Li, T. H., & Sahoo, S. (2015). Approaches for fabricating high efficiency organic light emitting diodes. *Journal of Materials Chemistry C*, 3(13), 2974-3002.
- [17.] Craford, M. G. (2005, September). LEDs for solid state lighting and other emerging applications: status, trends, and challenges. In *Fifth International Conference on Solid State Lighting* (Vol. 5941, p. 594101). SPIE
- [18.] Arik, M., Petroski, J., & Weaver, S. (2002, May). Thermal challenges in the future generation solid state lighting applications: light emitting diodes. In *ITherm 2002. Eighth Intersociety Conference on Thermal and Thermomechanical Phenomena in Electronic Systems (Cat. No. 02CH37258)* (pp. 113-120). IEEE..
- [19.] Gessmann, T., & Schubert, E. F. (2004). High-efficiency AlGaInP light-emitting diodes for solid-state lighting applications. *Journal of applied physics*, 95(5), 2203-2216.
- [20.] Schubert, E. F., Kim, J. K., Luo, H., & Xi, J. Q. (2006). Solid-state lighting—a benevolent technology. *Reports on Progress in Physics*, 69(12), 3069.
- [21.] Sudheendran Swayamprabha, S., Dubey, D. K., Shahnawaz, Yadav, R. A. K., Nagar, M. R., Sharma, A., ... & Jou, J. H. (2021). Approaches for long lifetime organic light emitting diodes. *Advanced Science*, 8(1), 2002254.
- [22.] Debsharma, M., Pramanik, T., Daka, C., & Mukherjee, R. (2022, May). Recent advances in the electrical and optical properties of Alq3 and Alq3 derivatives based OLEDS. In *Journal of Physics: Conference Series* (Vol. 2267, No. 1, p. 012159). IOP Publishing
- [23.] Debsharma, M., Pramanik, T., Maji, P. S., Maity, A. R., Jain, A., & Mukherjee, R. (2024). Effect of ZnO nanoparticle on morphology and optical properties of yellow emissive bulk Alq3 for OLED application. *Optical Materials*, 115768.
- [24.] Murawski, C., Leo, K., & Gather, M. C. (2013). Efficiency roll-off in organic light-emitting diodes. *Advanced Materials*, 25(47), 6801-6827.

- [25.] Rajeswaran, G., Itoh, M., Boroson, M., Barry, S., Hatwar, T. K., Kahen, K. B., ... & Takahashi, H. (2000, May). 40.1: Invited Paper: Active Matrix Low Temperature Poly-Si TFT/OLED Full Color Displays: Development Status. In *SID Symposium Digest of Technical Papers* (Vol. 31, No. 1, pp. 974-977). Oxford, UK: Blackwell Publishing Ltd.
- [26.] Cölle, M., & Brütting, W. (2004). Thermal, structural and photophysical properties of the organic semiconductor Alq3. *physica status solidi (a)*, 201(6), 1095-1115.
- [27.] Xu MS, Xu JB (2005) Visualization of thermally-activated degradation pathways of tris(8- hydroxyquinoline) aluminum thin films for electroluminescence application. *Thin Solid Films* 49:317–22
- [28.] So, F., Kido, J., & Burrows, P. (2008). Organic light-emitting devices for solid-state lighting. *MRS bulletin*, *33*(7), 663-669.
- [29.] Khreis, O. M., Curry, R. J., Somerton, M., & Gillin, W. P. (2000). Infrared organic light emitting diodes using neodymium tris-(8- hydroxyquinoline). *Journal of Applied Physics*, 88(2), 777-780.
- [30.] He, P., Wang, H., Liu, S., Hu, W., Shi, J., Wang, G., & Gong, M. (2008). An efficient europium (III) organic complex as red phosphor applied in LED. *Journal of the Electrochemical Society*, 156(2), E46.
- [31.] Wei, C., Ma, L., Wei, H., Liu, Z., Bian, Z., & Huang, C. (2018). Advances in luminescent lanthanide complexes and applications. *Science China Technological Sciences*, *61*, 1265-1285.
- [32.] Wang, L., Zhao, Z., Wei, C., Wei, H., Liu, Z., Bian, Z., & Huang, C. (2019). Review on the electroluminescence study of lanthanide complexes. *Advanced Optical Materials*, 7(11), 1801256.
- [33.] Gorai, T., Schmitt, W., & Gunnlaugsson, T. (2021). Highlights of the development and application of luminescent lanthanide based coordination polymers, MOFs and functional nanomaterials. *Dalton Transactions*, 50(3), 770-784.

- [34.] Evans, R. C., Douglas, P., & Winscom, C. J. (2006). Coordination complexes exhibiting room-temperature phosphorescence: Evaluation of their suitability as triplet emitters in organic light emitting diodes. *Coordination chemistry reviews*, 250(15-16), 2093-2126.
- [35.] Weissman, S. I. (1942). Intramolecular energy transfer the fluorescence of complexes of europium. *The Journal of Chemical Physics*, 10(4), 214-217.
- [36.] Fangfang, C., Zuqiang, B., & Huang, C. (2009). Progresses in electroluminescence based on europium (III) complexes. *Journal of rare* earths, 27(3), 345-355
- [37.] Xu, H., Sun, Q., An, Z., Wei, Y., & Liu, X. (2015). Electroluminescence from europium (III) complexes. *Coordination Chemistry Reviews*, 293, 228-249.
- [38.] Zhang, H., Zhu, W., Wu, M., Feng, Z., Huang, L., Chen, Y., ... & Yang, Y. (2024). A step-wise bi-layered hole-injection layer composed of vanadium oxide and PEDOT: PSS for simultaneously enhancing efficiency and stability of organic light-emitting diodes. *Optical Materials*, 152, 115509.
- [39.] Debsharma, M., Pramanik, T., Pramanik, G., Maity, A. R., Jain, A., & Mukherjee, R. (2024). Effect of growth temperatures on the structural and optical properties of bulk tris-(8-hydroxyquinoline) aluminium (III). *Applied Physics A*, 130(5), 281
- [40.] Lee, H., Kim, Y. K., & Lee, C. (2012, June). Improved Performances in Phosphorescent Organic Light-emitting Diodes using Solution-processed Vanadium Pentoxide as a Hole Injection Layer. In SID Symposium Digest of Technical Papers (Vol. 43, No. 1).
- [41.] B. Sharma, R. Sharma, Simrandeep Kour, M. D. Sharma, O. Amin, A. R. Maity,and R. Mukherjee. "Fractional exponents of electrical and thermal conductivity of vanadium intercalated layered 2H-NbS2 bulk crystal." Indian Journal of Physics 96,no. 5 (2022): 1335-1339. https://doi.org/10.1007/s12648-021-02045-w

- [42.] Ma, C. G., Brik, M. G., Liu, D. X., Feng, B., Tian, Y., & Suchocki, A. (2016). Energy level schemes of fN electronic configurations for the di-, tri-, and tetravalent lanthanides and actinides in a free state. *Journal of Luminescence*, 170, 369-374.
- [43.] Cuba, M., & Muralidharan, G. (2015). Effect of thermal annealing on the structural and optical properties of tris-(8-hydroxyquinoline) aluminum (III)(Alq₃) films. *Luminescence*, 30(3), 352-357
- [44.] Mahakhode, J. G., Bahirwar, B. M., Dhoble, S. J., & Moharil, S. V. (2006). Tunable Photoluminescence from tris (8-hydroxyquinoline) aluminum (Alq3). *Proc of ASID, New Delhi*, 237-239.
- [45.] El-Nahass, M. M., Farid, A. M., & Atta, A. A. (2010). Structural and optical properties of Tris (8-hydroxyquinoline) aluminum (III)(Alq3) thermal evaporated thin films. *Journal of alloys and compounds*, 507(1), 112-119.
- [46.] Bi, H., Zhang, H., Zhang, Y., Gao, H., Su, Z., & Wang, Y. (2010). Fac-Alq3 and Mer-Alq3 Nano/Microcrystals with Different Emission and Charge-Transporting Properties. *Advanced Materials*, 22(14), 1631-1634. https://doi.org/10.1002/adma.200903094
- [47.] López-Romero, S., García-Hipólito, M., & Aguilar-Castillo, A. (2013). Bright green luminescence from zirconium oxide stabilized with Tb 3+ ions synthesized by solution combustion technique. *World Journal of Condensed Matter Physics*, 2013.
- [48.] Tauc, J., & Abraham, A. (1969). The fundamental absorption band of amorphous germanium. *Czechoslovak Journal of Physics B*, 19(10), 1246-1254.
- [49.] Panek, J. J., Błaziak, K., & Jezierska, A. (2016). Hydrogen bonds in quinoline N-oxide derivatives: First-principle molecular dynamics and metadynamics ground state study. *Structural Chemistry*, 27, 65-75.

- [50.] Chatterjee, D. P., Pakhira, M., & Nandi, A. K. (2020). Fluorescence in "nonfluorescent" polymers. *ACS omega*, 5(48), 30747-30766
- [51.] Souza, A. D. V. D., Sousa, L. L. D., Fernandes, L., Cardoso, P. H. L., & Salomão, R. (2015). Al2O3–Al (OH) 3-Based castable porous structures. *Journal of the European Ceramic Society*, 35(6), 1943-1954.
- [52.] Ohno, Y. (2000, January). CIE fundamentals for color measurements. In *NIP* & *Digital Fabrication Conference* (Vol. 16, pp. 540-545). Society of Imaging Science and Technology.
- [53.] Bredas, J. L., Silbey, R., Boudreaux, D. S., & Chance, R. R. (1983). Chain-length dependence of electronic and electrochemical properties of conjugated systems: polyacetylene, polyphenylene, polythiophene, and polypyrrole. *Journal of the American Chemical Society*, 105(22), 6555-6559.
- [54.] Leonat, L., Sbarcea, G., & Branzoi, I. V. (2013). Cyclic voltammetry for energy levelsestimation of organic materials. *UPB Sci Bull Ser B*, 75(3), 111-118.
- [55.] Seino, Y., Inomata, S., Sasabe, H., Pu, Y. J., & Kido, J. (2016). High-performance green OLEDs using thermally activated delayed fluorescence with a power efficiency of over 100 lm W-1. *Advanced Materials*, 28(13), 2638-2643.

Chapter 9: Conclusion and Scope for Future Work

9.1 Summary:

Conclusion and scope for future work is a summary of the research work that has been described in the previous chapters of this thesis. In this thesis, many research gaps and shortcomings of bulk Alq3 powder have been met through this experimental research work. Different experimental works such as synthetic procedures, doping, fabrications of different stacked layers of different voltage tunable OLED devices, with wide wavelength of emission spectrum, have been performed during this research work. The" *Introduction*" Chapter i.e starting chapter of our thesis provides an overview of organic electroluminescence, including its history, the role of organic semiconductors in organic electroluminescence, OLED architecture, OLED operation, key factors influencing OLED functionality, OLED physics, degradation of OLED materials, their causes, benefits and drawbacks, and real-world OLED.

In "Literary review, Researchgap and Research objective" research gaps and objectives are discussed in the second chapter, along with the literature reviews of the chosen research papers, journals, articles, and books from the same field that are referred to for in-depth study of this research work. There are more than 13000 plus published research articles and papers there relating directly or partially interconnected to this particular research field. We mentioned 28 such research papers as our reference which were very close to our study. and help us to choose the best and right route, steps, measurements, synthesis, fabrication techniques and characterization techniques we should follow. These papers also help us to compare our derived outcome with those research papers.

"The Materials, method of synthesis and fabrication techniques" chapter lists all the materials we used in this study, including their chemical names, organic polymeric materials, metallic or inorganic semi-conducting materials, and metallic cathodes, transparent anodes, transparent substrates, and EML, HTL, ETL, and HIL materials. It also discusses all of the essential synthesis and fabrication methods, including spin-coating.

"The Characterization techniques to determine electro-optical, electro- chemical and structural properties of OLED materials "i.e, fourth chapter covers various characterization techniques, the application of those instruments for specific types of characterization, the advantages and disadvantages of those instruments, the working principles of various measuring devices and their functionalities, characterization techniques, related laws and physics principles, and the precautionary measures that should be taken during characterization in order to obtain accurate measurements.

"The Effect of growth temperatures on the structural and optical properties of bulk pristine tris-(8-hydroxy quino line) aluminium (III) "i.e., Chapter 5 presents new findings that show that Alq3 decomposes and forms a semi-porous layer of Alq2(OH) and Al(OH)₃-Al₂O₃ on base material Alq₃ when annealed bulk Alq₃ powder and thin film are heated from room temperature to 200°C in a hot air oven under ambient conditions. The 8-Hq (8-hydroxy quinoline) ligands, however, recrystallize at 150 and 200 degrees Celsius to form the 8-Hq-N-oxide salt of aluminium, a non-emissive polymer that exhibits significantly better fluorescence and photoluminescence than unannealed Alq₃. What's interesting is that chemically oxidized Alq3 can still fluoresce after degradation, opening up new research opportunities. Each of the annealed bulk Alq₃ powder and thin film's temperature-dependent structural, optical, and thermal characteristics was examined separately. We also looked for chemical reactions that took place and the byproducts of those reactions when Alq3 reacted with oxygen gas and moisture. When exposed to atmospheric oxygen, we have also discovered the chemical formula of the degraded Alq₃. At 150°C, Mer-Alq₃ shows the highest PL efficiency, reduced susceptibility to degradation, optimal-absorbance and thermal-stability.

In the Chapter six i.e.," *Influence of thermally annealed nano- crystalline Alq3 thin film for flexible WOLED and solid-state lighting app*lication", the most significant stage of this research project was described. The ITO/PEDOT: PSS/V₂O₅ /Alq3/LiF/Ag-based green electroluminescent OLED device was made using a straightforward, unoptimized structure. ITO-coated PET sheet as a transparent anode or transparent substrate, mer-Alq3 as ETL and EML, and PEDOT: PSS layer as HTL, along with a shadow-masked

cathode created by silver paste solution, are used to build that OLED device. Mer-Alq₃ sample, the best-performing EML material, was used in this instance to form the ETL and EML layers after it was annealed at 150 degrees Celsius. This annealed emitter Alq₃ at 150°C-based OLED has a low turn voltage of 2.84 volts, a higher greenish-white luminance of 9689.2 cd/m² with a CRI value of 98, and a maximum current efficiency of 3.89 cd/A. These characteristics explain why using an annealed Alq₃-based emitter will behave like a great WOLED and can be used for transparent flexible slide-state lighting and display applications. It also fulfils our first research objective for making a voltage tunable OLED having wide emission spectrum.

In "Effect of ZnO nanoparticle on morphology and optical properties of poly-crystalline yellow emissive Alq₃ for OLED application "named chapter i.e., chapter seven we tried to tune the optical band gap of Alq₃ emissive by incorporating ZnO Nano particle into Alq₃ matrix to improve optical properties and electroluminescence and recombination rate of electron-hole pair within the EML layer. which fulfils our second research objective. It also obtained that the fabricated OLED could emit yellowish white luminescence which is required for WOLED and solid-state lighting application which is our fourth research objective.

In "To Study the Structural, Optical and Electrical Properties of Rare Earth Europium(III) and Neodymium(III) Ion Doped Alq₃ Based Emissive Layer for OLED Application and Solid State Lighting Application" chapter i.e. Chapter 8, we have also achieved our third and fourth research objectives through this experimental study discussed in this chapter. To achieve our goal we have incorporated rare earth metallic ion Eu³⁺ and Nd³⁺ into annealed Alq₃ matrix-based OLED devices to tune recombination rate, optical band gap tuning, interstate crossing (ISC), and higher durability along with higher photoluminescence and electronic devices which is 3 times and 4 times better than pristine Alq₃ emitter based OLED. device. The green luminescence of pure Alq₃ changes to greenish yellow. Our obtained results successfully have achieved our research objective number 3 and 4.

9.1. Scope for future work:

OLED research and technology is a rapidly expanding, potentially futuristic technology with a wide range of potential applications. The limitations of this technology have expanded beyond its current range of applications. Its applications are not limited to TVs, laptops, or smartphones; instead, it extends to solid-state lighting and flexible, rollable, and transparent displays. Even now, researchers are developing new OLED materials, innovative synthetic processes, and innovative dopants and doping methods. OLED and solid-state lighting applications have the following potential futures and a significant research gap:

- (1) The potential for further research to improve the colour purity, brightness, life span, energy efficiency, green synthesis, external quantum efficiency, and internal quantum efficiency of Alq₃ and its derivatives is enormous. The current work may guide numerous studies in this area.
- (2) Fourth-generation OLED technology often uses rare earth ions to assist with intersystem crossing (ISC) and reverse inter-system crossing (RISC) in thermally activated

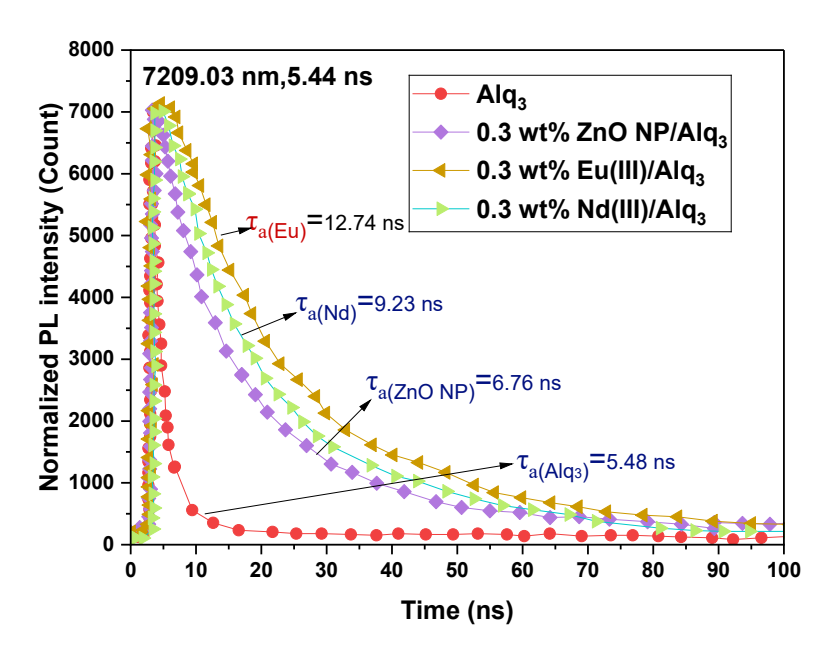


Figure 9.1: PL intensity decay or fluorescence average lifetime plot

delayed fluorescence (TADF) and hyperfluorescence (TADF + fluorescence) OLEDs. In these situations, all triplet excitons are harvested, and further work can be done using this method. Our current work can create fourth-generation OLEDs with narrow emission bands that are highly efficient. neodymium(III) and europium(III) doped Alq₃ may be a flexible, and affordable substitute.

This normalized PL intensity vs. time plot of Figure 9.1 clearly proves that Alq₃ has higher optical band band gap 2.89 eV and ZnO NP has 3.53 eV. For this reason, Alq₃ and ZnO cannot exhibit TADF and their average lifetime is low. But when Alq₃ is doped with 0.3 wt %ZnO NP and 0.3 wt % europium(III) and neodymium(III) they all support TADF where average life times are 6.76ns, 9.23ns,12.74 ns. Theses results can open different way of interests in this field.

- (3) Our work revealed the existence of a novel non-emissive polymer, namely the oxide advancements. of Alq₃, which exhibits superior fluorescence and electroluminescence compared to pristine Alq₃, thereby offering a promising avenue for future research. Non-emissive polymers provide improved electroluminescence and fluorescence, which will pave the way for future
- (4) Our inexpensive, effective, rollable, simple-structured OLED that uses ZnO/Alq₃, Eu/Alq₃, and neodymium may serve as the basis for numerous future research projects.

As a result, we are quite optimistic that our current work will serve as the appropriate reference for many future studies. We believe that our results will encourage other researchers in the same field to explore the atomic structures of Alq₃, its advanced doped versions, and its new hybrid nanocomposites that include other rare earth elements like terbium, as well as other transition metals like vanadium, silver, and cadmium, or alkali metals like lithium, potassium, and sodium.

9.2. Concise distillation of the thesis's main contributions:

If I summarize the thesis's main contribution in simple words. It will be as follows:

- (1) The degraded and oxidized Alq₃ due to thermal annealing in hot air forms a non-emissive polymer(NEP) which gives 3-4 times higher electroluminescence (EL) and higher photoluminescence(PL) intensity compared to pristine bulk Alq₃.
- (2) At 150°C, due to thermal annealing under ambient condition forms aluminium salt of 8-Hq-N-oxide, a non-emissive polymer, which shows more thermal stability compared to pure Alq₃ when it is used as electroluminescent emitters for an OLED.
- (3) Doping ZnO nanoparticle into host Alq₃ matrix, as 0.3:1 wt% concentration performed as the best doping concentration to exhibit the highest EL and PL intensity compared to pure Alq₃.It also lowers the optical band gap to 2.82 eV,and turn-on voltage of 2.81 V, EQE of 1.838 % CCT of 6019k CRI of 57 and gives whitish green emission of 539.8 nm.
- (4) Rare earth ion europium and neodymium ion doped Alq₃ nanocomposites exhibit higher EL and PL intensity compared to ZnO NP doped Alq₃ nanocomposites and pristine bulk Alq₃ powder
- (5) Europium doped Alq₃ nanocomposite-based OLED device shows the highest EL and PL intensity and as low turn on voltage as 2.56V and higher EQE of 2.47% CCT of 8935k and CRI of 63 and gives yellowish green photoluminescence of 544.5 nm
- (6)0.3 wt% Eu(III) doped Alq₃ emitter-based OLED is an excellent alternatives for all OLED Solid-State Lighting applications and is a better option for constructing yellow OLED,green OLED and also white OLED (WOLED)

Bibliography/Abbreviations.

A ampere

AC alternate current

Alq3 aluminum (III) tris-(8-quinolinolate)

BCP 2,9-dimethyl-4,7-diphenyl-1,10-henanthroline

cd candela

CIE Commission Internationale d'Éclairage

cm centimeter

C concentration

CE current efficiency

CV cyclic voltammetry

DC direct current

DFT density functional theory

E energy

EL electroluminescence

EML emissive layer

EQE external quantum efficiency

ETL electron-transport layer

Eu europium

eV electron-volt

fac facial

HBL hole-blocking layer

HOMO highest occupied molecular orbital

IQE internal quantum efficiency

ITO indium tin oxide

 Λ wavelength

lm/W lumen/watt

LUMO lowest occupied molecular orbital

m meter

M molar (mol/lt)

 μm micron (10⁻⁶ m)

mer meridionnal

nm nanometer

OLED organic light-emitting diode

PEDOT poly ethylene oxy thiophene

PE power efficiency

PL photoluminescence

PET poly ethylene tri ethylene terapthalate

PLED polymer light-emitting diode

PMMA poly(methyl methacrylate

PMOLED polymer matrix OLED

PSS polystyrene sulfonate

RE rare earth element

s second

SMOLED small-molecule organic light-emitting diode

TFT thin film transistor

TV television

UV ultra violet

V volt

ZnO NP zinc oxide nano particle